THE IONOSPHERIC Z RAY RETURN MECHANISM

by

John Warwick
J.W.Hudspeth,B.Sc.(Hons.)

submitted in fulfilment
of the requirements for the degree of
Doctor of Philosophy

UNIVERSITY OF TASMANIA
HOBART

MARCH 1982
Conferred March 1983

This thesis contains no material which has been accepted for the award of any other degree or diploma in any university.

To the best of my knowledge and belief, the thesis contains no copy or paraphrase of material previously published or written by another person, except where due reference is made in the text.

CONTENTS

ACKNOWLEDGEMENTS

This research was conducted over several years, part time and without financial assistance. I therefore thank not only the many people who assisted in various ways with the research work but also those assisting with part time and temporary full time employment.

In particular I thank the following people and organisations

- my supervisor Prof.G.R.A.Ellis for encouragement, for stimulating discussions and for critical evaluation of my work.
- Mr.G.T.Goldstone, OIC of the Hobart Ionospheric Station, for assistance with electronics, logistics, ionospheric records and scaling.
- the staff and students of the Physics Dept. (especially Mr.B.T.Wilson).
- the University Computing Centre, the University Library, the University Photographic and Printing Sections.
- the Ionospheric Prediction Service (especially Dr.L.McNamara).
- my friends, my parents, my wife's parents and especially my wife for their willing support.

SUMMARY

Two alternative mechanisms, backscattering and tilt/wedge, for return of the ionospheric Z ray are examined. It is found that further experimental information is required in order to choose between them. Experimental tests of the mechanisms are proposed. The Llanherne HF radio-telescope was used as a narrow beam ionospheric sounder to obtain angle of arrival information on the O, X and Z echoes. From the results of these experiments together with examination of h'f ionograms showing Z echoes it is concluded that neither mechanism satisfactorily explains the return of the Z echo in an overwhelming majority of cases. A third mechanism is proposed which returns the Z ray by trapping in an ionospheric duct. This mechanism is able to explain many features of the Z echo and computer ray tracing of the model together with evidence from the existing literature suggests that this mechanism is the one operating in almost all cases of Z echo, except perhaps for those occurring at very high magnetic latitudes close to the Dip Pole.

CHAPTER ONE

INTRODUCTION

Magnetoionic triple splitting of F region ionospheric echoes was first reported in the 1930's by Eckersley in 1933, Toshniwal in 1935 and Harang in 1936. Harang's evidence demonstrated conclusively that the third or Z echo was magnetoionic in origin and furthermore established some now familiar attributes of the Z echo, namely: a critical frequency approximately one half the electron gyro frequency below the O-mode critical frequency; a virtual reflection height above that of the O-mode at the same frequency (provided the ionogram is not complicated by significant F1 or lower layer effects); a low signal strength compared with O and X echoes.

It appeared likely that Z echoes were reflections from the $X = 1+Y$ reflection level of the Appleton-Hartree magnetoionic theory. However, there was a major difficulty in that the theory does not allow a vertical incidence, ground generated, radio signal to reach this $X = 1+Y$ level, the signal being reflected at the lower levels of $X = 1-Y$ if of extraordinary type polarisation or $X = 1$ if of ordinary type polarisation for wave frequencies above the electron

gyro frequency.

Mary Taylor in 1933 proposed that partial quasi-transverse vertical propagation (with some non-zero collision frequency) of the extraordinary mode may occur between the $X = 1-Y$ and $X = (1-Y^2)/(1-Y_L^2)$ levels such that the extraordinary wave reaches the otherwise inaccessible extraordinary branch and is reflected at $X = 1+Y$. Successful propagation to and from this reflection level depended on the presence of an extremely rapid variation of electron density above the $X = 1-Y$ level. No new Z-mode theory appeared until 1950 when Eckersley (1950) and Rydbeck (1950) independently proposed the possibility of coupling at the $X = 1$ level between the ordinary wave and the upper extraordinary wave branches, the Z wave propagating as an ordinary wave below this level and as an extraordinary wave above it. The theory effectively limited Z reflections to high geomagnetic latitudes within a few degrees of the Dip Pole and thus could not explain observations at mid-latitudes, such as those by Toshniwal (1935) at Allahabad and Newstead (1948) at Hobart. In 1949 Dieminger and Moller suggested that oblique incidence coupling might produce the Z echo and in 1950 Scott independently made a similar suggestion in more detail. Neither of these theories provided a complete and satisfactory explanation.

Experiments carried out by Hogarth (1951) in Canada and Landmark (1952) in Norway demonstrated conclusively that the Z echo was of ordinary type polarisation, thus verifying and

explaining Eckersley's (1933) triplet polarisation measurements. This evidence together with calculations by Banerji (1952) showing that the extraordinary ray had no practical possibility of penetrating to its higher reflection level, made it appear that the Z echo originated from the O-mode via a coupling process. However, clarification of the theory and concomitant confirming experimental results had yet to be achieved.

The question was finally resolved by the experiments and theory of Ellis (1953a,b;1956) at Hobart. Ellis had independently demonstrated the O-mode polarisation of the Z echo and further showed that its angle of return is in the magnetic meridian and inclined at about 9^{o} to the zenith for frequencies around 5 MHz, the dip angle at Hobart being 72^{o}. Ellis showed that an ordinary wave transmitted at the measured arrival angle would have its wave normal aligned with the magnetic field by the time it reached the $X = 1$ reflection level and thus significant coupling to the upper extraordinary mode would be expected even for negligible collision frequency. The wave transmitted through the $X = 1$ level would be reflected at the $X = 1+Y$ level and returned to the transmitter along the same path, coupling to an ordinary mode on transmission back through the $X = 1$ level. The only difficulty with this theory is that in a smooth plane stratified ionosphere the Z wave would approach its reflection level obliquely such that it would return to earth roughly perpendicular to the magnetic field, would fail to couple back to an ordinary wave at the $X = 1$ level and

would terminate its downward path at the $X = (1-Y^2)/(1-Y_L^2)$ level. The experiments carried out by Ellis showed that the Z echo did in fact return to the transmitter from the expected coupling region and so he concluded that the F region Z echo is observed due to the Z wave being scattered back along its path by small scale irregularities (i.e. a rough reflection layer) in the vicinity of the X = 1+Y level. An experiment carried out by Ellis (1954) showed a qualitative correlation between increased ionospheric roughness and Z echo occurrence.

Bowman (1960) suggested an alternative mechanism for the return of the Z ray. He postulated that the occurrence of Z mode was closely related to that of spread-F and that tilts and ripples in the ionization contours could be responsible for both phenomena, the Z ray becoming normal to the tilted ionization contours in the vicinity of its reflection level and therefore being returned along its path by specular reflection. Papagiannis (1965) made a similar proposal, suggesting that Ellis's results were made at a time when the zenith angle of the sun would have produced ionospheric layers tilted at such an angle as to be normal to the magnetic field direction. Papagiannis and Miller (1969) produced more detail on the alternative mechanism by ray tracing the Z ray through tilted parallel and tilted wedge-like layers.

Chapter 3 is a detailed critical review of these alternative theories and an experiment capable of choosing

between them is proposed. The following chapters give an account of an investigation carried out to determine the mechanism(s) appropriate to the return of the Z ray. Chapter 2 provides a brief description of background theory relevant to the problem.

CHAPTER TWO
BACKGROUND THEORY

2.1 Introduction

The following sections comprise brief descriptions of the Appleton-Hartree formula, the Booker quartic equation and the graphical method of Poeverlein. The content of these sections is mainly drawn directly from the works of Ratcliffe (1962) and Budden (1961,1964) and the original papers by Booker (1936,1938) and Poeverlein (1948,1949,1950). No attempt is made to describe the general features of the magnetoionic theory or wave propagation in the ionosphere and formulae are quoted without derivation. Interested readers are referred to the treatises by Ratcliffe and Budden.

The following notation has been adopted and is employed throughout this and the subsequent chapters.

c = free space velocity of electromagnetic waves

e = charge on electron (when numerical values are inserted this will be negative)

H_0 = magnitude of the imposed magnetic field

k = angular wave number ($=2\pi/\lambda$)

m = mass of electron

n = complex refractive index ($=\mu-i\chi$)

N = number density of electrons

ω = angular wave frequency

μ = refractive index (=real part of n)

κ = absorption coefficient

$\chi = \kappa c/\omega$ = absorption index = negative imaginary part of n

μ_o = magnetic permittivity of free space

ϵ_o = electric permittivity of free space

θ = angle the wave normal makes with the vertical (z direction)

Θ = angle the wave normal k makes with the magnetic field H

ν = frequency of collisions of electrons with heavy particles

$\omega_o^2 = 4\pi Ne^2/\epsilon_o m$

$\omega_H = \mu_o H_o |e|/m$

$X = \omega_o^2/\omega^2$

$Y = \omega_H/\omega$

$Z = \nu/\omega$

$U = 1 - iZ$

$Y_T = Y \sin\Theta$

$Y_L = Y \cos\Theta$

$\underline{Y} = \mu_o \underline{H_o} e/m\omega$

l_1, m_1, n_1 = direction cosines of vector Y (anti-parallel to $\underline{H_o}$ since e is negative)

2.2 The Appleton-Hartree Formula

The refractive index of a medium containing free

electrons, with a superimposed steady magnetic field is given by

$$n^2 = 1 - \frac{X}{1-iZ - \frac{1/2.Y_T^2}{1-X-iZ} + \left\{ \frac{1/4.Y_T^4}{(1-X-iZ)^2} + Y_L^2 \right\}^{1/2}}$$

This is the Appleton-Hartree formula.

It can be shown from this formula that one value of n^2 is zero when

$$X + iZ = 1 \qquad 2.1$$

$$X + iZ = 1 + Y \qquad 2.2$$

$$X + iZ = 1 - Y \qquad 2.3$$

and one value of n^2 is infinite when

$$X = (1-iZ).\frac{(1-iZ)^2 - Y^2}{(1-iZ)^2 - Y_L^2} \qquad 2.4$$

At frequencies greater than 1 MHz it is usually a satisfactory approximation to neglect collisions so that Z=Ø and the Appleton-Hartree formula becomes

$$n^2 = 1 - \frac{X}{1 - \frac{Y_T^2}{2(1-X) - \left\{ \frac{Y_T^4}{4(1-X)^2} + Y_L^2 \right\}^{1/2}}} \qquad 2.5$$

such that n^2 is always real.

The zeroes of n^2 (2.1,2.2,2.3) occur when

$$X = 1, \quad X = 1 + Y, \quad X = 1 - Y \qquad 2.6$$

and the infinity (2.4) occurs when

$$X = \frac{1 - Y^2}{1 - Y_L^2} \qquad 2.7$$

Furthermore, when X=1, one of the values of n^2 is unity.

The F-region gyro frequency at Hobart is about 1.4 MHz at ionospheric heights and as radio sounding of the Hobart F-layer rarely drops below this frequency we shall consider only the case for $Y < 1$. For a medium such as the ionosphere, the generally most useful way to consider refractive index variation is to plot curves showing the dependence of n^2 upon X, Y being relatively constant at a given location. If the wave normal is parallel or anti-parallel to the earth's magnetic field, $Y = \emptyset$ and we have purely longitudinal propagation, the variation of n^2 with X being shown in Fig.2.1. If the wave normal is perpendicular to the earth's magnetic field, $Y = \emptyset$ and we have purely transverse propagation as shown in Fig.2.2. The variation of n^2 with X for the case when the angle between the earth's magnetic field and the wave normal is intermediate between the purely transverse and purely longitudinal cases is shown by the shaded regions of Fig.2.3, the thick lines representing typical curves. The dotted lines show the limiting positions for purely transverse and purely longitudinal propagation and together with the line $X = 1$ form the boundaries within which the curves for an intermediate case must always lie. For the intermediate case n^2 has an infinity when X is given by 2.7 and this infinity lies between $1-Y^2$ and 1.

FIG.2.1

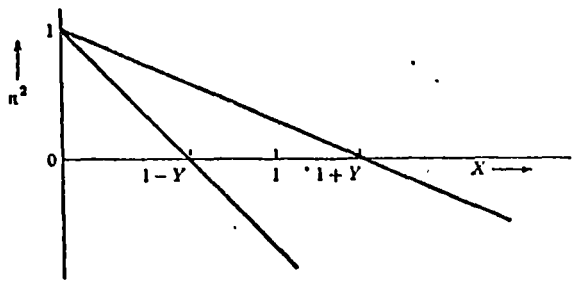

Variation of n^2 with X for purely longitudinal propagation, when $Y < 1$.

FIG.2.2

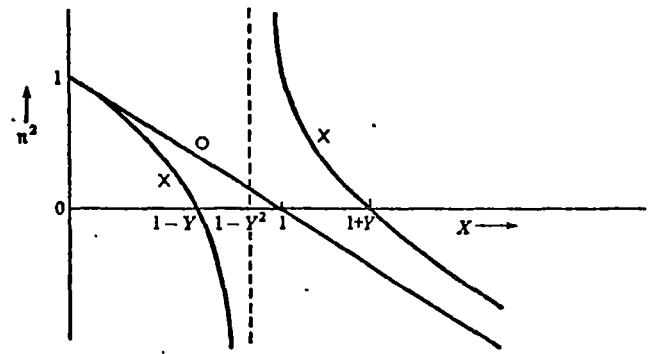

Variation of n^2 with X for purely transverse propagation when $Y < 1$.

FIG.2.3

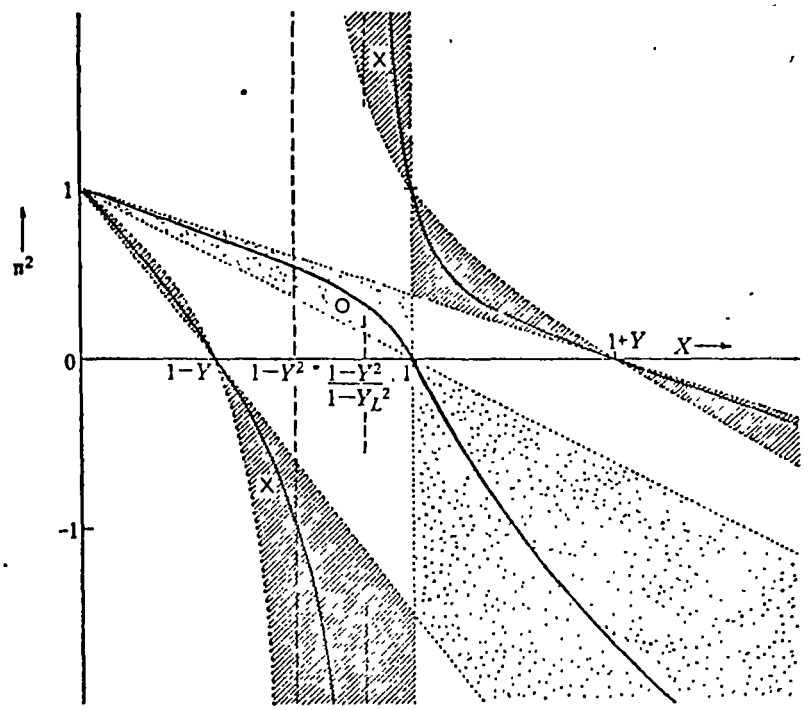

Variation of n^2 with X for intermediate inclination of the earth's magnetic field, when $Y < 1$. Electron collisions are neglected.

(Figs.6.1 to 6.3 of Budden, 1961)

Fig.2.4 shows the curves of n^2 with X for the case where the wave normal is almost but not quite parallel to the magnetic field. The infinity occurs at an X value just less than 1 and the O curve and upper X curve approach each other through having sharp bends close to the X = 1 line. For X < 1 the ordinary wave curve corresponds to a polarisation value close to -i but on traversing the almost vertical part of the curve near X = 1 the polarisation value changes rapidly over to a value close to +i and holds this value for X > 1. Budden (1961) has shown that this rapid change of polarisation is associated with strong coupling between the ordinary and extraordinary waves and this is the mechanism for high frequency (Y < 1) production of the Z-mode for vertical incidence sounding at very high dip latitudes. If an ordinary wave enters a medium of increasing electron density (increasing X) under the conditions of Fig.2.4 it will cause some of the upper extraordinary wave to be generated near X = 1. This extraordinary wave will be reflected at the X = 1+Y level and on its return path will generate some of the ordinary ray near X = 1. In the limit when the propagation is entirely longitudinal, the extraordinary wave takes over completely from the ordinary wave at X = 1, and for X > 1 the only wave present would be the extraordinary wave. This explains how the curves of Fig.2.4 go over, in the limit, into the curves of Fig.2.1.

Consider a horizontally stratified ionosphere and a

linearly polarised radiowave normally incident from below. As the ionosphere is a birefringent medium, there will be two transmitted waves and the quantities which refer to them will be distinguished by subscripts a and b respectively. The two waves will have polarisations ρ_a and ρ_b and refractive indices n_a and n_b given by the Appleton-Hartree formula. Since the wave normal of the incident wave is initially vertical, Snell's law shows that the wave normals of both the ordinary and extrordinary waves in the ionosphere are, and remain, normal (though this is not generally true of the ray direction). It is therefore possible to determine the propagation paths of the waves through the layers and to calculate the reflection and transmission coefficients at each boundary.

However the case for oblique incidence raises some difficulties. Consider a plane wave incident upon the ionosphere from below with its wave normal at an angle θ_I to the vertical and let for the two transmitted waves the refractive indices be n_a and n_b and the wave normal angles to the vertical be θ_a and θ_b respectively. As Snell's law applies for both waves

$$\sin\theta_I = n_a \sin\theta_a = n_b \sin\theta_b \qquad 2.8$$

If n_a and n_b were known then the unknown angles θ_a and θ_b could be determined but the values of n_a and n_b depend upon Y_L, Y_T which in turn depend upon θ_a and θ_b. Equation 2.8 therefore cannot be used directly to find θ_a and θ_b and herein lies the

problem of determining propagation paths at oblique incidence. The Booker quartic equation, as described in the following section, is normally used to overcome this obstacle.

2.3 The Booker Quartic Equation

Consider again a wave incident upon the ionosphere from below and consider one transmitted component only, as the following applies equally to both. As before, from Snell's law

$$\sin\theta_I = n.\sin\theta$$

where n and θ are both unknown but $n.\sin\theta$ is known and we may define the quantity q, first introduced into magnetoionic theory by Booker (1936,1939), as

$$q = n.\cos\theta$$

If we treat the refractive index n as though it were a vector inclined at an angle θ to the vertical then q is its vertical component and $\sin\theta_I$ its horizontal component (Fig.2.5). If q is known, n and θ follow from the relations

$$n^2 = q^2 + \sin^2\theta_I \quad , \quad \tan\theta = \sin\theta_I/q$$

q is the root of the quartic equation known as the Booker quartic. The following argument is a more general case which reduces to the preceding argument when $S_2=\emptyset$.

Consider a wave incident obliquely from below upon a horizontally stratified, slowly varying ionosphere such that in free space below the plasma its wave normal has direction

(Fig.6.4 of Budden, 1961)

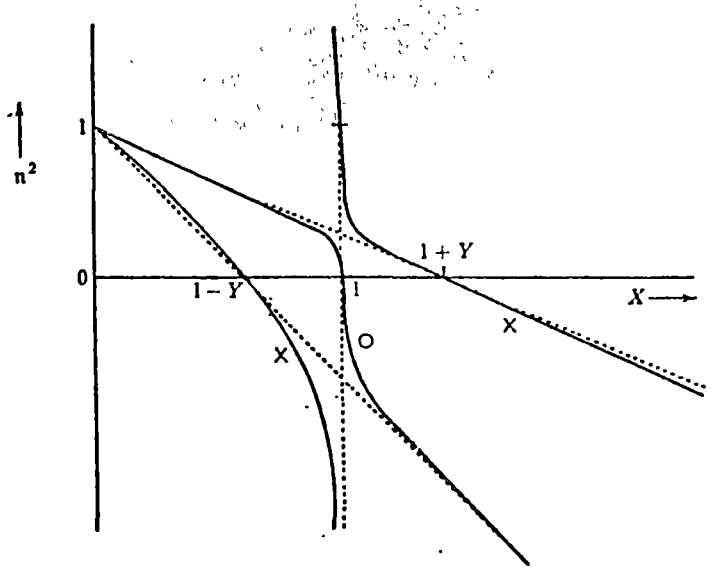

FIG.2.4 Variation of n^2 with X when the propagation is almost longitudinal and $Y < 1$.

FIG.2.5

(Fig.8.11 of Budden, 1961)

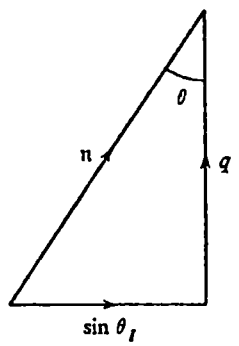

Relation between the refractive index n, the variable q, and the angle θ between the wave-normal and the vertical.

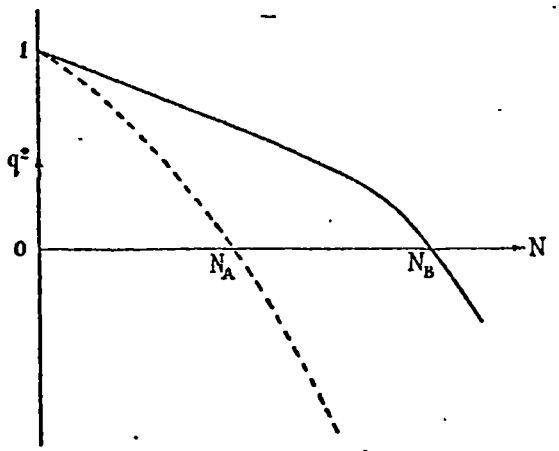

FIG.2.6 q^2 as a function of N, vertical incidence.

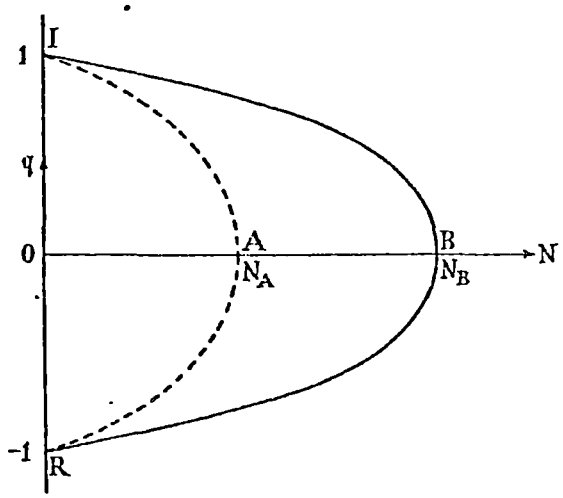

FIG.2.7 q as a function of N, vertical incidence.

(Figs.5 and 6 of Booker, 1938)

cosines S_1, S_2, C where $C=\cos\theta$, $S_1^2+S_2^2 = \sin^2\theta$ so that θ, as before, is the angle of incidence. We now approximate to the ionosphere an arbitrarily large number of arbitrarliy thin strata in each of which the medium is homogeneous, the degree of approximation being dependent upon the number and thickness of the strata. The plane wave entering the plasma is partially reflected and transmitted at the successive boundaries so that in each stratum there are several plane waves. Consider now the refractive index as a vector $\underline{p}$ in the direction of the wave normal, with length n and components p_x, p_y, p_z so that in a given stratum one of the waves has such a refractive index $\underline{p}$. Then every field component contains x,y,z only through a factor

$$\exp -ik(xp_x+yp_y+zp_z) \qquad 2.9$$

At any boundary plane between two strata the boundary conditions constrain the dependence of the fields on x and y to be the same on each side of the boundary, so that p_x and p_y are constant throughout the plasma. In free space below the plasma the factor 2.9 reduces to

$$\exp -ik(S_1 x+S_2 y+Cz) \qquad 2.10$$

Hence $p_x = S_1$, $p_y = S_2$ which holds true in the limit when the strata are infinitesimally thin.

An expression for p_z in terms of X and Z at a given level may now be derived. Put $q = p_z$, in accordance with the notation of Booker(1939). The refractive index n for one of the waves in a given stratum is given by

$$n^2 = S_1^2 + S_2^2 + q^2 = q^2 + 1 - C^2 \qquad 2.11$$

The angle Θ between the wave normal and the vector $\underline{Y}$ is given by

$$n.\cos\Theta = S_1 l_1 + S_2 m_1 + q n_1 \qquad 2.12$$

Combining 2.11 with the Appleton-Hartree formula gives us

$$U(U-X)-1/2.Y^2\sin^2\Theta+X(U-X)(q^2-C^2) = \left\{1/4.Y^4\sin^4\Theta+(U-X)^2 Y^2\cos^2\Theta\right\}^{\frac{1}{2}} \qquad 2.13$$

Eliminating n from 2.11 and 2.12 we obtain

$$\cos^2\Theta = (S_1 l_1 + S_2 m_1 + q n_1)^2/(q^2+1-C^2) \qquad 2.14$$

Squaring both sides of 2.13 and substituting for $\cos^2\Theta$ from 2.14 we have

$$(U-X)\left(U+\frac{X}{q^2-C^2}\right)^2 - Y^2\left(U+\frac{X}{q^2-C^2}\right)\frac{+XY^2(S_1 l_1 + S_2 m_1 + q n_1)^2}{q^2-C^2} = \emptyset$$

which is a quartic in q which may be written

$$\alpha q^4 + \beta q^3 + \gamma q^2 + \delta q + \epsilon = \emptyset$$

where

$$\alpha = U^2(U-X)-UY^2+n_1^2 Y^2 X,$$

$$\beta = 2n_1 XY^2(S_1 l_1 + S_2 m_1),$$

$$\gamma = -2U(U-X)(C^2U-X)+2Y^2(C^2U-X)+XY^2\left\{1-C^2 n_1^2+(S_1 l_1 + S_2 m_1)^2\right\}$$

$$\delta = -2C^2 n_1 XY^2(S_1 l_1 + S_2 m_1),$$

$$\epsilon = (U-X)(C^2U-X)^2 - C^2Y^2(C^2U-X) - CXY^2(S_1 l_1 + S_2 m_1)^2$$

The Booker quartic equation in general yields four distinct roots for q and at any level in the stratified magnetoplasma gives the four characteristic waves, two of which are up-going waves and two are down-going waves. For Z-mode theory we are concerned with oblique propagation in the magnetic meridian so that $m_1 = \emptyset$ and $l_1^2 + n_1^2 = 1$. Since the magnetic meridian plane coincides with the plane of incidence

the path of the ray does not deviate from this plane and we may set $S_2 = \emptyset$. If we further neglect collisions, the expressions for $\alpha, \beta, \gamma, \delta, \epsilon$ then reduce to the following

$$\alpha = 1-X-Y^2+Xn_1^2Y^2$$

$$\beta = 2Sl_1n_1XY^2$$

$$\gamma = -2(1-X)(C^2-X)+2Y^2(C^2-X)+XY^2(1-C^2n_1^2+S^2l_1^2)$$

$$\delta = -2SC^2l_1n_1XY^2$$

$$\epsilon = (1-X)(C^2-X)^2-C^2Y^2(C^2-X)-C^2XY^2l_1^2S^2$$

One root of the quartic is infinite when $\alpha = \emptyset$ which occurs

when $$X = \frac{1-Y^2}{1-n_1^2Y^2}$$

One solution of the quartic is zero when $\epsilon = \emptyset$ which is a cubic for X and does not in general have simple solutions, though one zero of q always occurs when X is between C^2 and 1. When $S = \emptyset$ the three different zeroes of q become $X = 1$, $X = 1+Y$, $X = 1-Y$ which are the three zeroes of n as given by the Appleton-Hartree formula. It can also be shown that the curves touch the line $X = 1$ except in the critical case when S is given by

$$S = \pm l_1\sqrt{\frac{Y}{Y \pm 1}}$$

Figs.2.6 to 2.8 illustrate the difference between vertical and oblique incidence. For vertical incidence the quartic equation reduces to a quadratic in q^2, and the two values of q^2 are shown in Fig.2.6 plotted against N for fixed values of H_o and f, one curve (say the broken one) referring to the

extraordinary component and the other to the ordinary component. However, if the quadratic in q^2 is regarded as a quartic in q there are two pairs of opposite and equal roots which, when plotted against N for fixed values of H_o and f as shown in Fig.2.7, give the symmetrical arrangement about the N-axis of the four curves IA, RA, IB, RB. IA refers to the upgoing extraordinary wave, AR to the downcoming extraordinary wave, IB to the upgoing ordinary wave and BR to the downcoming ordinary wave. N_A is the critical electron density required to produce reflection of the extraordinary wave and at this point the pair of roots corresponding to the extraordinary wave passes from real to complex conjugate values via equality. Similarly for N_B and the ordinary wave.

For oblique incidence the quartic in q may no longer be reduced to a quadratic in q^2 and the symmetry vanishes, as shown in Fig.2.8. Below the stratified magnetoplasma each field component of the incident wave contains the factor

$$\exp\left[ik\left\{ct-(\sin\theta)y-(\cos\theta)z\right\}\right]$$

where y is the horizontal coordinate in the direction of the horizontal projection of the wave normal. Thus when N = 0, $q = \cos\theta$ for the incident wave and $q = -\cos\theta$ for the reflected wave. The propagation as two magnetoionic components between the points of entering and leaving the ionosphere (or stratified magnetoplasma) is represented by the curves IDAR and IBER. Although q vanishes at D and E, these are not the reflection points of the components as it can be seen that

propagation continues to higher electron densities and reflection takes place at N_A and N_B for the extraordinary and ordinary components respectively. The critical elctron density is obtained not when q = 0 (the angle of refraction $\theta = 1/2\pi$ in Snell's law) but when the wave packet as a whole is travelling horizontally. Fig.2.9 is a general example of a wave packet in a doubly refracting medium. Fig.2.10 shows the phase rays of the magnetoionic components and corresponding group rays. As Booker states "The unusual form of the phase-rays merely expresses the effect of the earth's magnetic field in producing asymmetry between the propagation of the upgoing and downcoming waves".

Figs.2.11 to 2.13 show typical curves of q against X for $Y < 1$ for north-south propagation. The curves for the one critical angle of incidence are shown in Fig.2.12 where it is seen that the curves for the ordinary and extraordinary rays meet on the line X = 1. For incidence angles very close to the critical angle the curves revert to those shown in Fig.2.11 but with the O and upper X curves approaching very close to each other at point T so that coupling between the modes may occur (for some non-zero collision frequency).

Booker (1938,1949) showed that the group ray paths could be calculated for a slowly varying medium but until the recent advent of advanced ray tracing computer programs calculation has been very involved except for the special cases where the

FIG.2.8

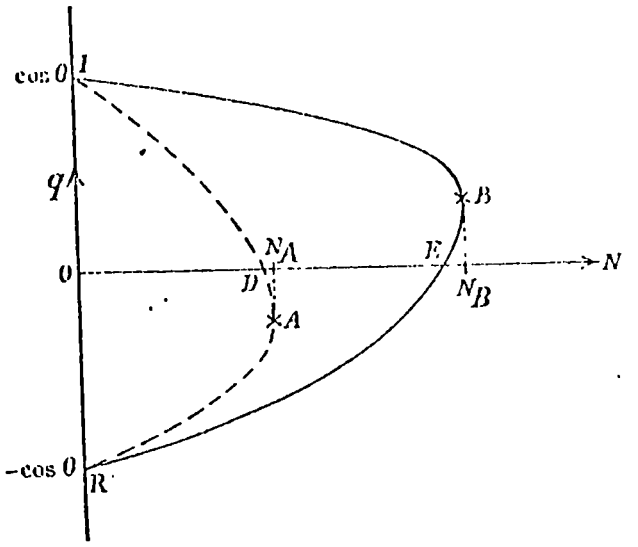

q as a function of N, oblique incidence.

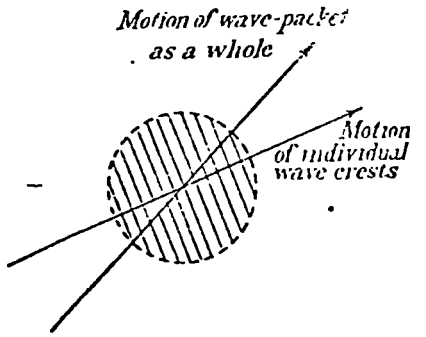

FIG.2.9 Propagation of a wave-packet in a doubly refracting medium.

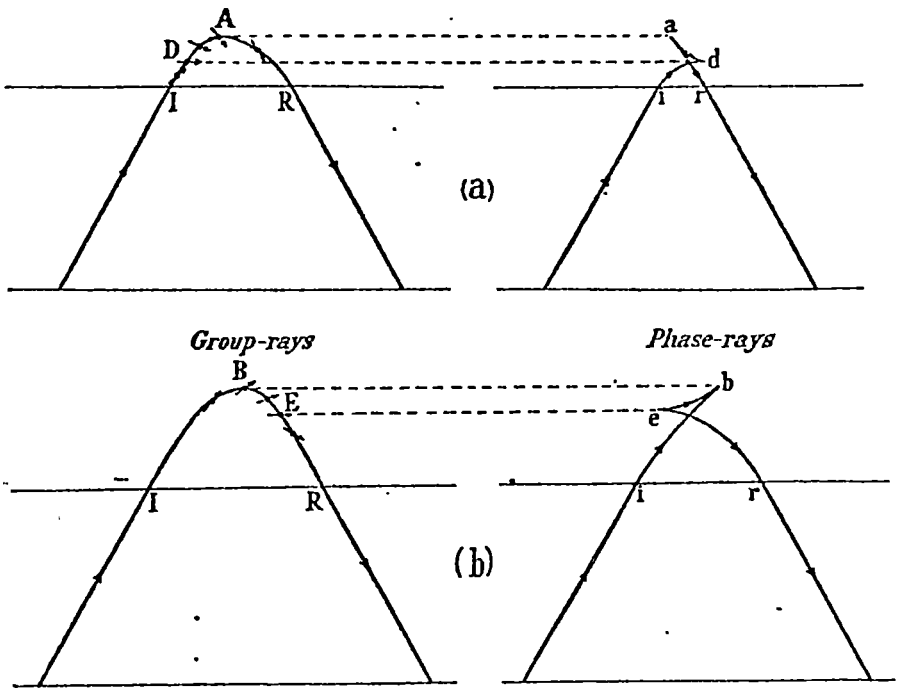

FIG.2.10 Group- and phase-rays of magneto-ionic components.

(Figs.7,9 and 11 of Booker,1938)

FIG.2.11

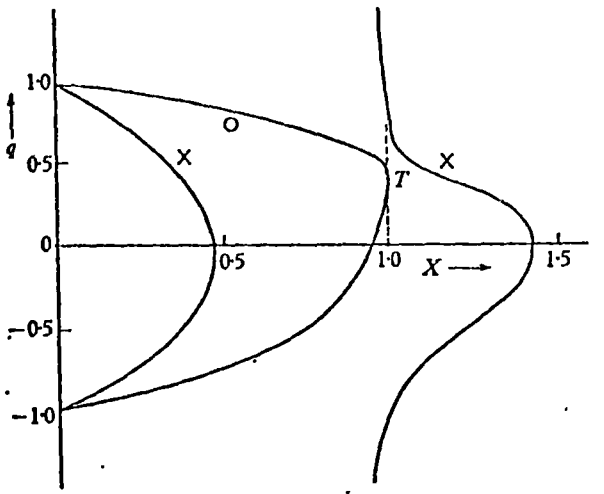

Solutions of the Booker quartic for north–south propagation when $Y = \frac{1}{2}$. Earth's field at 30° to the vertical. Angle of incidence $\theta_I = 15°$. The line $X = 1$ touches the curve at the point T.

FIG.2.12

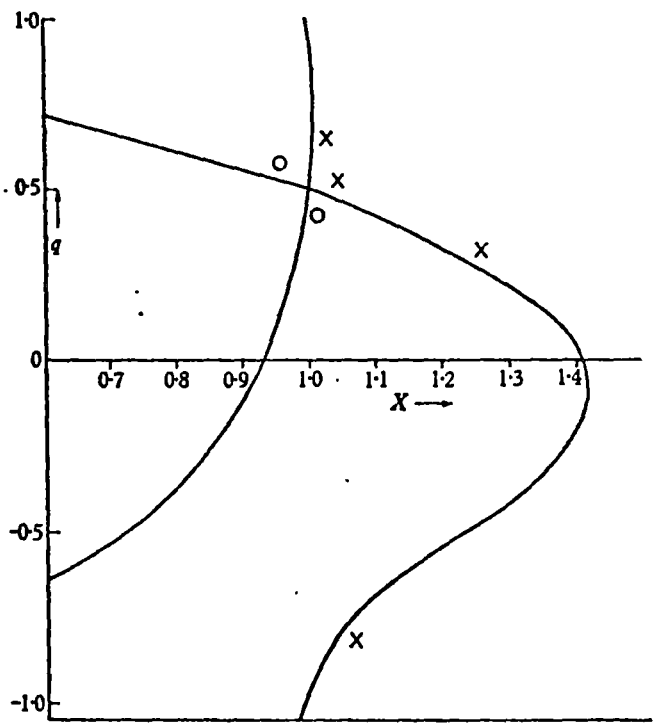

Solutions of the Booker quartic for north–south propagation when $Y = \frac{1}{2}$. Earth's field at 30° to the vertical. The angle of incidence has the critical value 16·6° (13.31) so that the curves for the ordinary and extraordinary rays meet on the line $X = 1$.

(Figs.13.5 and 13.6 of Budden,1961)

FIG.2.13

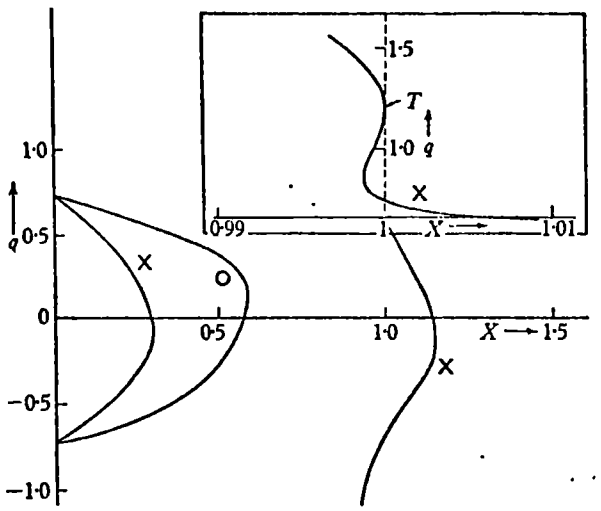

Solutions of the Booker quartic for north–south propagation when $Y = \frac{1}{2}$. Earth's field at 30° to the vertical. Angle of incidence $\theta_I = 45°$. The right branch of the curve for the extraordinary wave touches the line $X = 1$ at the point T as shown in the inset diagram with an expanded scale of X.

FIG.2.14

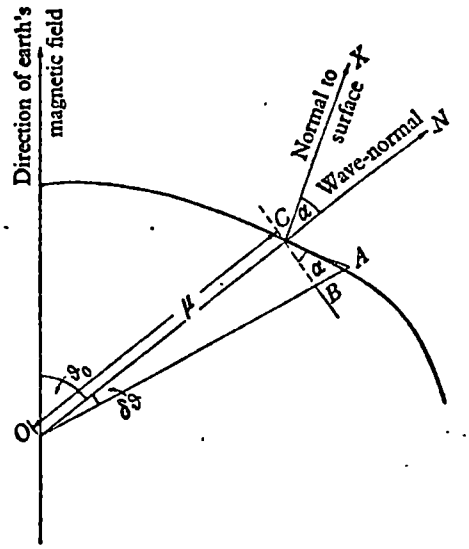

Cross-section of refractive index surface by a plane containing the direction of the earth's magnetic field. CX and CA are the normal and tangent, respectively, at the point C. CB is perpendicular to OC.

(Figs.13.7 and 13.19 of Budden,1961)

quartic reduces to a quadratic in q^2. These cases are : (A) vertical incidence, when q is the same as n; (B) propagation from magnetic east to west, or west to east; (C) propagation at the magnetic equator. In the case where electron collisions are neglected, it has often been easier to find group ray directions by employing the graphical construction of Poverlein.

2.4 Poeverlein's Graphical Construction.

When electron collisions are neglected, as is the usual case for this method, the refractive index n becomes the same as its real part μ. For X and Y held constant μ is a function only of Θ and if we plot μ versus Θ in the polar diagram form we obtain a surface of revolution about the direction of H_o, the refractive index surface or μ-surface. It can be shown that the group ray (or path of the wave packet), the wave normal and the earth's magnetic field are coplanar. Let the direction of travel of the wave packet make an angle α with the wave normal. It can be shown that

$$\tan\alpha = \frac{1}{\mu} \cdot \frac{\partial \mu}{\partial \Theta}$$

From Fig.2.14 we can see that $\frac{1}{\mu} \cdot \frac{\partial \mu}{\partial \Theta}$ is the tangent of the angle between the radius and the normal to the refractive index surface. Thus if we know the wave normal direction then using the appropriate refractive index surface we can determine the

group ray direction by constructing the normal to that surface at the point at which its radius vector is the wave normal direction.

Poeverlein's technique was to divide a stratified medium into many layers and to apply the graphical method described above to trace the ray in each layer. The method is best illustrated by a simple example. Let the stratified magnetoplasma be a horizontally stratified ionosphere so that the electron density is a function of height only. Fig.2.15 is a cross section through the ordinary mode refractive index surfaces for different X values, each contour representing the refractive index at the corresponding X level of the ionosphere. The direction of magnetic field shown is the projection of the earth's magnetic field onto the plane of incidence. The outermost curve or contour is a circle of unit radius representing the refractive index in free space below the ionosphere. For any angle of incidence the wave normal and group ray have the same direction at this contour, but at levels within the ionosphere the contours are no longer circular and the wave normal and group ray in general have different directions. Let the wave packet be incident upon the ionosphere from below with its wave normal at an angle θ_I to the vertical. Now draw a vertical line in the plane of incidence (the plane of cross section of the refractive index surfaces) at a distance $S = \sin\theta_I$ from the origin P. At the X = Ø.2 level this line cuts the refractive index surface at

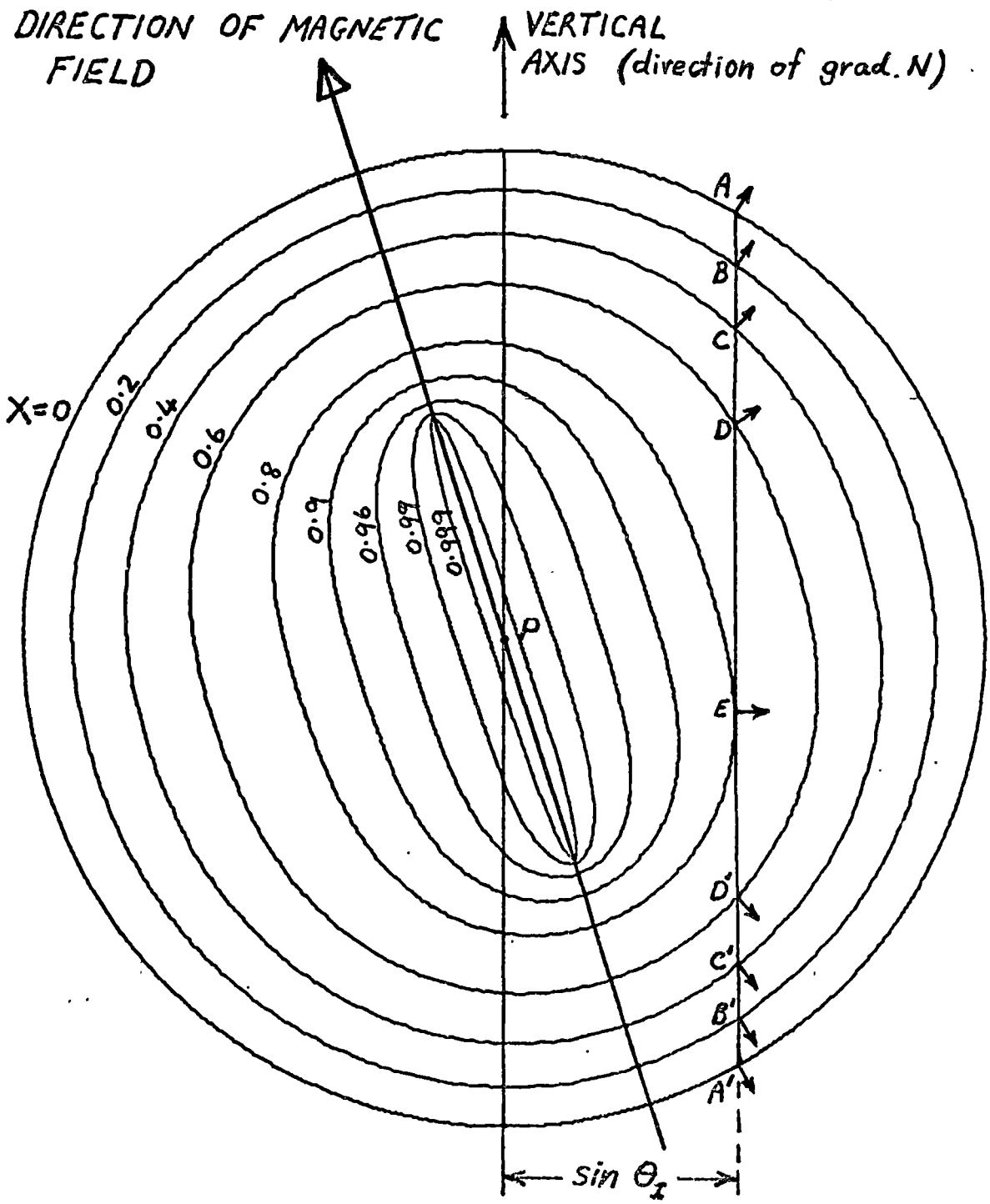

FIG.2.15 O-mode ray tracing in a horizontal stratified magnetoplasma using the Poeverlein diagram.

two points B and B′. Let PB make an angle θ with the vertical axis. Then PB is the refractive index μ for a wave whose normal is in the direction PB. From Fig.2.15 we see that $PB\sin\theta = \mu\sin\theta = S$, which is just Snell′s law. Thus PB is one possible direction for the wave normal of the ordinary wave and PB′ is another possible direction and similarly two other directions are found from the intersection of the line AA′ with the X = Ø.2 refractive index surface for the extraordinary wave. We can also see from the figure that $BQ = \mu\cos\theta = q$. The same argument applies for each contour and we therefore know the wave normal directions at each level throughout the ionosphere.

As the ray direction is perpendicular to the refractive index surface the small arrows of Fig.2.15 show the group ray directions at each level. At the X = Ø.2 level for instance there are two possible ray directions given by the arrows at B and B′, the arrow at B being inclined upwards and that at B′ inclined downwards. Though the wave normal is always in the plane of the diagram the ray direction in general will not be in this plane as the group ray direction must be coplanar with the wave normal direction and the direction of the imposed magnetic field. To determine the propagation path of the wave packet we move along the line from A (where the wave normal is that of the upgoing wave obliquely incident upon the ionosphere from below) to A′ (where the wave normal is that of the downgoing wave emerging obliquely into free space below the

ionosphere). The successive intersections A,B,C,D,E,D′,C′,B′,A′ with the refractive index surfaces give the successive directions of propagation in the appropriate layers. The more refractive index surfaces utilised (corresponding to thinner and more numerous strata) the better the approximation to the actual propagation path. Energy propagates upwards through the ionosphere until the point E is reached where the the line AA′ is tangential to the refractive index surface and here the group ray is horizontal and thus reflection occurs. Along the line AA′ beyond E the wave packet is propagated downwards through the ionosphere. It should be noted that a plot of the wave and group ray directions from this diagram will lead to exactly the same result for the ordinary wave as that shown in Fig.2.10(b) and using Poeverlein′s construction for the extraordinary ray leads to the same result as Fig.2.10(a).

CHAPTER THREE

REVIEW OF Z MODE THEORY

3.1 Introduction

Section 3.2 describes the accepted Z mode generation mechanism in terms of the original explanation. Sections 3.3, 3.5, 3.7 and 3.9 detail various proposals for the mechanism responsible for the return of the Z ray. Following directly after each of these sections is a section of critical discussion of the material just presented. Section 3.12 summarises the conclusions drawn throughout the chapter.

3.2 Z Mode Generation Mechanism

Ellis (1953a) reported that measurements of angle of arrival of Z echoes made at Hobart (dip 72^{o}) on a frequency of 4.65 MHz gave a mean direction of 7.8^{o} north of vertical in the magnetic plane. In all cases the height of reflection of the Z echoes was between 170 km and 210 km. Ellis noted that according to the Quasi-longitudinal hypothesis of Z mode (e.g.Scott,1950) a collision frequency of about 1.5×10^{5} per second would be required to explain the observed angle, this being inconsistent with previous estimates which put the collision frequency at about 10^{4} per second at 200 km.

According to Scott the Z mode at a place of dip 72° (e.g.Hobart) would be caused by quasi-longitudinal propagation of the O mode in a narrow cone around the magnetic field direction (i.e. 18° north of vertical in the magnetic meridian), the width of the cone increasing with increasing collision frequency. For a non-vertical magnetic field Scott postulated that the Z mode would be seen when the ionosphere was sufficiently rough to return the Z echo to the transmitter - in Hobart's case an ionospheric reflecting cone of half angle around 18° would be required.

In the same year Ellis (1953b) published further experimental details and the following explanation for Z mode generation. For vertical incidence the transition from transverse to longitudinal propagation may be illustrated by refractive index curves for different values of $\textcircled{M}$. The curves for vertical magnetic field and very high dip magnetic field are given by the curves of Figs.2.1 and 2.4. The transition may be described in terms of the change in the shape of the curves near the X = 1 line, as shown in Fig.3.1. Ellis (1953b) pointed out that in the Z region there is no qualitative difference between the transverse extraordinary mode and the longitudinal ordinary mode.

Consider a wave packet obliquely incident from below upon a horizontally stratified ionosphere. As shown in the previous chapter its wave normal direction will vary continuously (for

infinitesimally thick strata) as it propagates upwards through the ionosphere. For the critical angle of incidence (see Fig.3.2) the wave normal becomes parallel to the magnetic field at the ordinary reflection level and penetration of this level may occur for zero collision frequency. The penetrating wave propagates on upwards to the Z reflection level.

We shall now illustrate the wave propagation by means of Poerverlein constructions. Fig.3.3 is a polar diagram of the ordinary mode refractive index curves for the various electron densities shown (as X values). Fig.3.4 is a polar diagram for the upper extraordinary mode. The dip angle is 72° and the wave frequency such that $f = 3f_H$ (f would be about 4.3 MHz for Hobart). For an angle of incidence of θ_I we draw the vertical line a distance $\sin\theta_I$ from the diagram origin. The common value of the refractive index for $X = 1$, $\Theta = \emptyset$ is denoted by P and that for $X = 1$, $\Theta = 180$ by Q. P and Q are the coupling points. We choose our line so that it passes through P in order that the incident wave reaches this coupling point. We may then graphically determine θ_c, the necessary critical value of θ_I. Alternatively, since the angle of refraction of the wave normal θ at any level in a plane stratified magnetoplasma is given by Snell's law

$$\sin\theta_I = n.\sin\theta$$

and the magnitude of the refractive index for $\Theta = \emptyset$, $X = 1$, $Y = \emptyset$ is given by

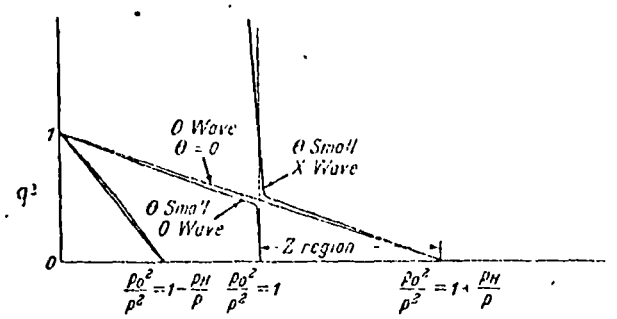

FIG.3.1

Refractive index as a function of electron density.

(Fig.2 of Ellis,1953)

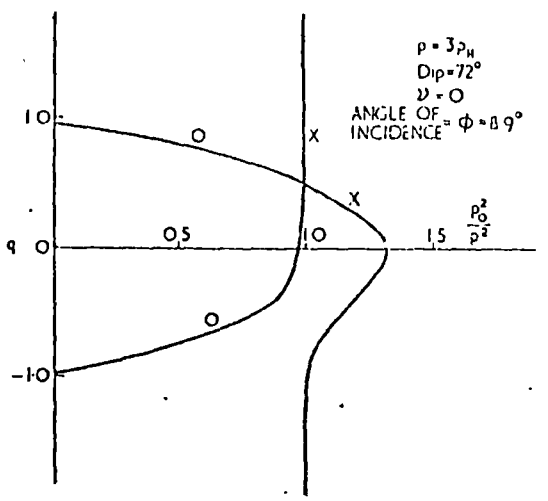

FIG.3.2

Refractive index curves at the critical angle of incidence.

(Fig.1 of Ellis,1956)

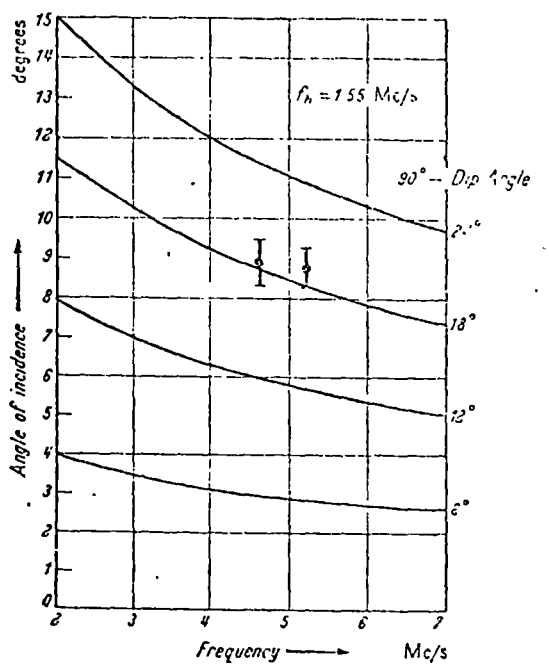

FIG.3.5

Critical angles of incidence for Z reflection.

(Fig.5 of Ellis,1953)

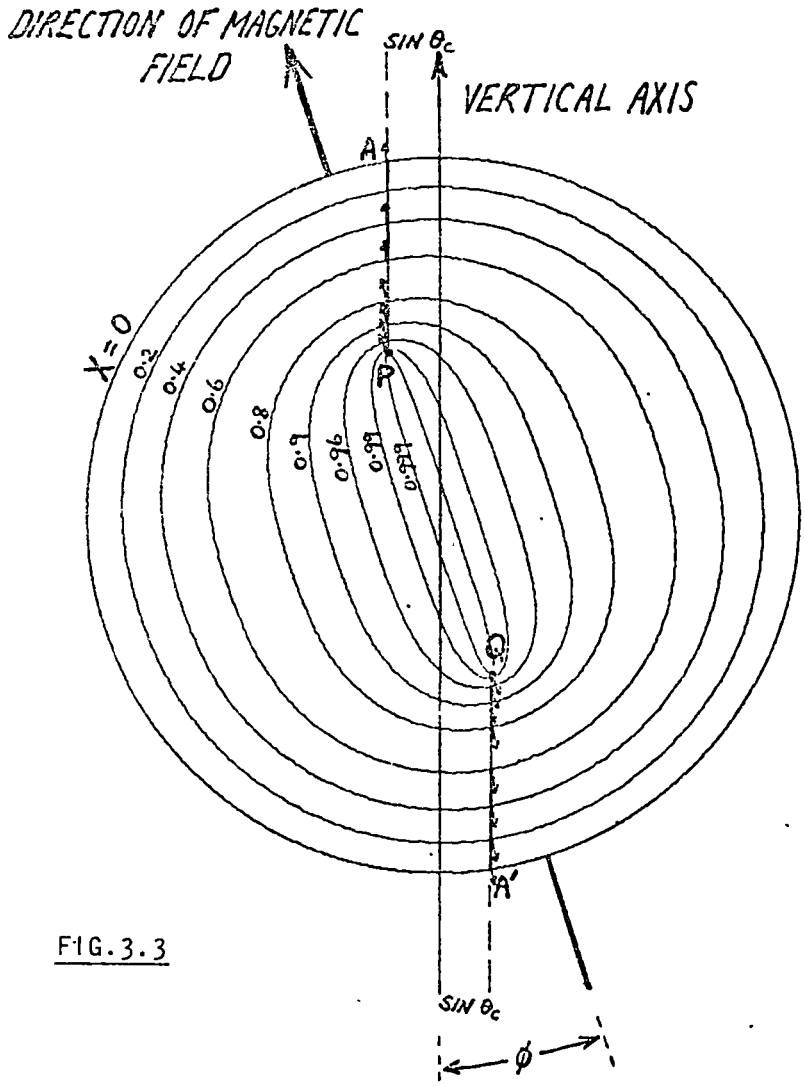

FIG.3.3

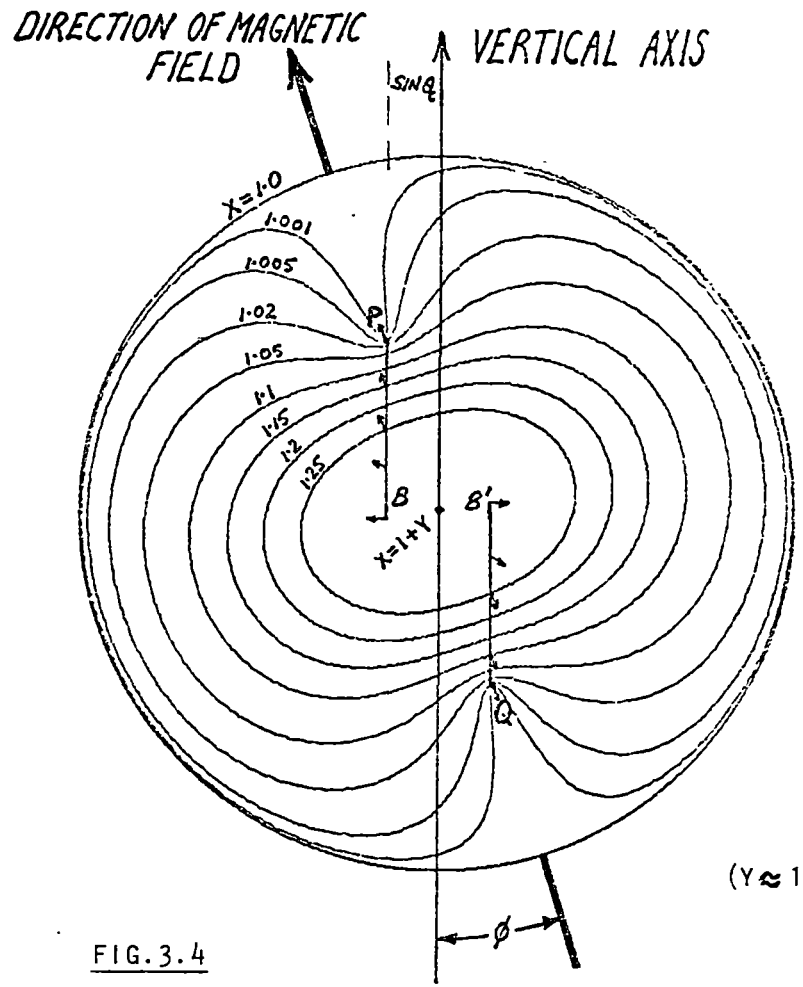

(Y ≈ 1/3)

FIG.3.4

$$\sqrt{\frac{Y}{1+Y}}\ ,$$

then $$\sin\theta_c = \sqrt{\frac{Y}{1+Y}}\sin\phi$$

where ϕ is the angle the earth's magnetic field makes with the vertical.

The ordinary wave propagates upwards as shown by traversing the line AP (Fig.3.3) from A to P. At the coupling point P conversion to extraordinary mode takes place and we transfer to point P on the extraordinary diagram (Fig.3.4). The wave is now a Z mode wave and continues upwards as represented by traversing the line from P to B. B represents the Z reflection point and as we require the wave to couple again at the X = 1 level and return to the transmitter it is necessary that it be reflected backwards along its incident path. We therefore jump from point B to point B', this jump representing reversal of both the wave normal and group ray directions. Traversing the line from B' to Q represents the reflected Z mode wave travelling back down its path to the coupling point Q at the X = 1 level. Since the upward and downward propagation paths are identically located in physical space then P and Q are representative of the same physical point in the ionosphere. The extraordinary wave at Q couples back to an ordinary wave which propagates downwards to the transmitter as represented by the Q to A' line of Fig.3.3. Ellis (1956) noted that Poeverlein (1949) and Millington (1954)

had also pointed out the possibility of mode conversion at the X = 1 level giving rise to the upper extraordinary mode at oblique incidence.

Ellis calculated the critical angle of incidence θ_c as a function of frequency for different values of magnetic dip. Fig.3.5 shows his results together with his observed directions of arrival for Z echoes at Hobart. Fig.3.6 is a copy of one of the records from Ellis's direction finder and it can be clearly seen how closely the Z echo is confined to the magnetic meridian plane.

So far collisions have been neglected. The effect of a non zero collision frequency is to increase from zero the propagation angle at which the transition from transverse to longitudinal propagation occurs such that the X = 1 layer may be penetrated by partial coupling of rays whose wave normals make small angles with the magnetic field in the coupling region. From an analysis of the distribution of Z echo angle of arrival measurements, Ellis estimated the coupling cone to be approximately circular and to have an angular half width of a little under half a degree at 4.65 MHz when the edges of the cone are defined as the half power points. This further confirmed the oblique incidence coupling theory of the Z mode as the theory predicts that fixed relative to a single radiating point on the ground there will be an effective "hole" at the level X = 1 through which both the upward and downward Z

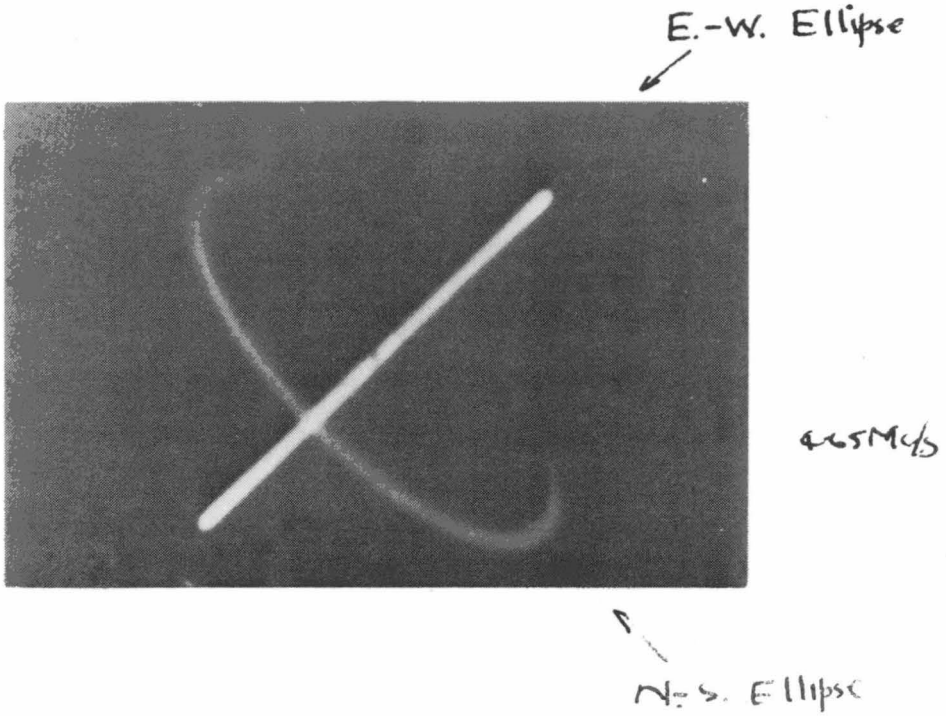

Z Echo N.S. and E.W. Ellipses.

FIG.3.6

(Fig.48 of Ellis,1954)

FIG.3.7

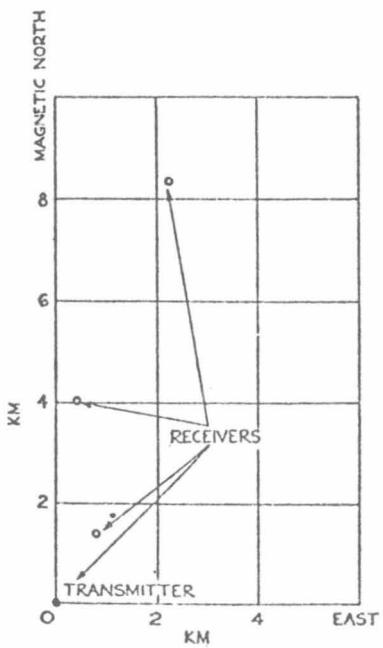

The relative positions of the transmitting and receiving stations.

(Fig.4 of Ellis,1956)

rays must pass, downward rays not passing through this hole being unable to reach the ground. Z echo amplitude will thus fall quickly away from the transmitter and beyond a relatively short radius Z echoes will not be detectable. Ellis (1956) provided experimental proof of this when he estimated the NS angular width of the Z hole by measuring the relative power of simultaneous Z echoes at receivers spaced varying distances from the transmitter. Fig.3.7 shows the location of the receivers relative to the transmitter and Fig.3.8 shows the the results achieved. The NS angular half width deduced from these measurements is in good agreement with that deduced from the angle of arrival measurements.

The oblique incidence coupling theory of the Z mode as expounded by Ellis is widely accepted as the correct explanation of Z mode generation and the coupling region is often referred to as the "Ellis Window".

3.3 Return Of The Z Ray - Backscatter

Following a suggestion by Scott (1950), Ellis (1953b,1956) proposed that the oblique incidence Z ray was returned to the transmitter by backscatter from a rough ionospheric layer at the reflection level. Fig.3.9 illustrates the return of the Z ray. Ellis (1953b) examined the available evidence for roughness in the ionospheric layer. At that time only one

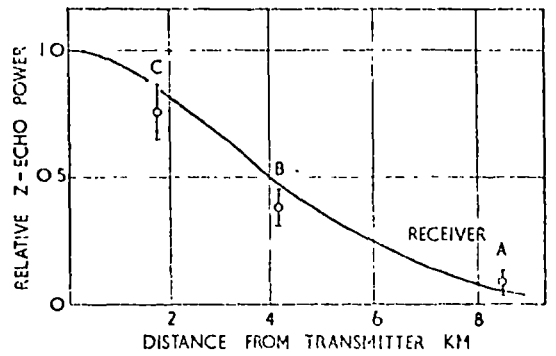

FIG.3.8

The variation of Z echo power in the vicinity of the transmitter.

(Fig.5 of Ellis,1956)

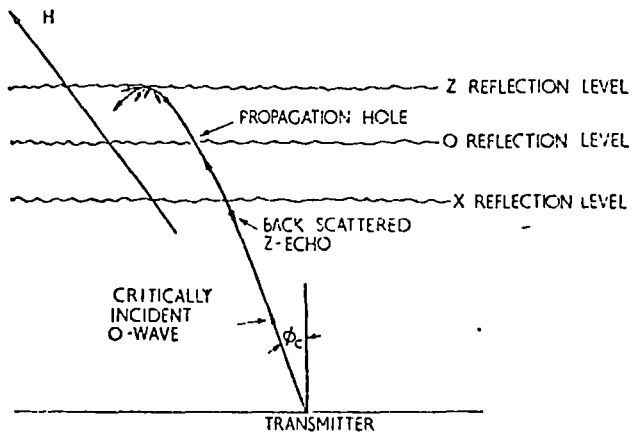

FIG.3.9

Illustrating the mechanism of occurrence of F-region Z echoes.

(Fig.2 of Ellis,1956)

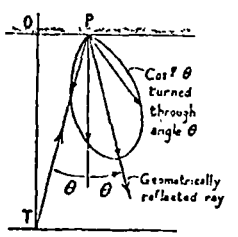

FIG.3.10

The polar diagram of an element of the screen when illuminated from a transmitter at T.

(Fig.3(b) of Briggs and Phillips,1950)

series of observations had been reported, those made by Briggs and Phillips (1950). Briggs and Phillips carried out a series of vertical incidence experiments in order to determine the extent of the angular spreading of the downcoming wave from measurements of the correlation of the fading of the reflectd wave. They concluded that their F region results could be explained by the existence at the reflecting level of a horizontal layer of reflecting irregularities of lengths of the order of 50 to 500 metres. They assumed that the angular spreading of a downcoming wave reflected by a small element of the layer could be described by the function $\cos^n\psi$ where ψ is the angle of scattering measured from the direction of specular reflection. In the absence of contradictory information this was a very reasonable assumption to make, especially as they mainly considered n large, for which case the function approaches a Gaussian distribution of standard deviation $1/\sqrt{n}$. In order to have a simple measure of the "spread" of the function $\cos^n\psi$ Briggs and Phillips defined ψ_0 as the angles at which the function is equal to 1/4. As they used the function to represent the angular spread of power, this is the angle at which the amplitude has fallen to one half. Briggs and Phillips stated that it was not possible to rigorously predict the form of the oblique scattering function from a knowledge of the normal scattering function but made the reasonable assumption that the main effect of oblique illumination of a scattering element is to turn the normal scattering polar diagram through an angle ψ so that its maximum lies in the

direction of the geometrically reflected ray as shown in Fig.3.10. The response is then given by writing 2ψ instead of ψ in the function $\cos^n\psi$. They showed that

$$\cos^n 2\psi \approx \cos^{4n}\psi \quad (n \text{ large}, -1/4\pi < \psi < +1/4\pi)$$

Briggs and Phillips made F region night time observations on 2.4 MHz from January 1949 to January 1950 and found the most frequently observed value of ψ_o to be 5° and the maximum ψ_o value to be under 25°. Further F region day and night observations on 4.8 MHz (Jan.-March 1950) gave a peak value for ψ_o of about 2.5° and a maximum value for ψ_o of about 8° (Fig.3.11). Since Ellis had observed daytime F region Z echoes on frequencies between 4.5 and 5.5 MHz, ψ_o would have had to reach about 18° and he concluded that the Hobart F layer must at times be considerably rougher than the F layer observed in Southern England by Briggs and Phillips.

Ellis recorded the 5.8 MHz ordinary echo amplitude at two loops spaced 2/3 wavelength apart along a north south line with the transmitter centrally located between them. If we denote the amplitudes at the receivers by A1 and A2 respectively and the receiver separation by f in wavelengths then the difference correlation

$$\Delta(f) = \overline{|\,A1-A2\,|}$$

Briggs and Phillips showed that $\Delta(f)/\bar{A}$ is generally proportional to ψ_o for moderately small angles (say, less than 10°) provided f is less than one wavelength. For Ellis's

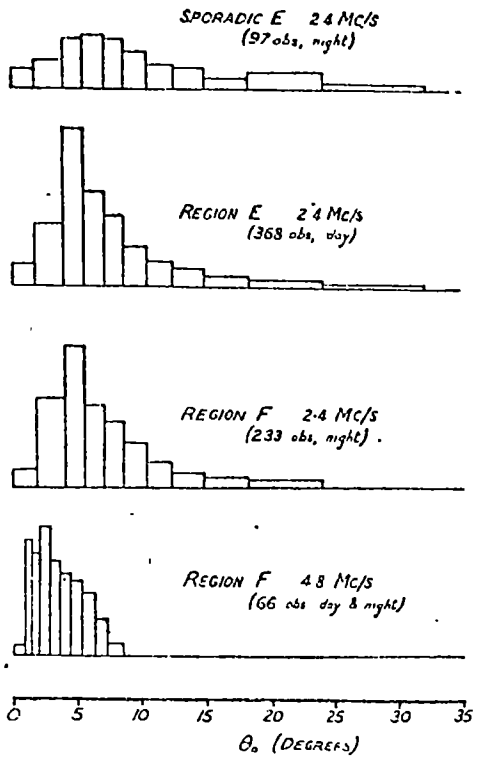

FIG.3.11

Histograms showing the frequency of occurrence of different values of the parameter θ_0 which specifies the degree of angular spreading of the downcoming wave. Separate histograms are shown for regions E_s, E, and F (2·4 Mc/s.), and region F (4·8 Mc/s.).

(Fig.8 of Briggs and Phillips,1950)

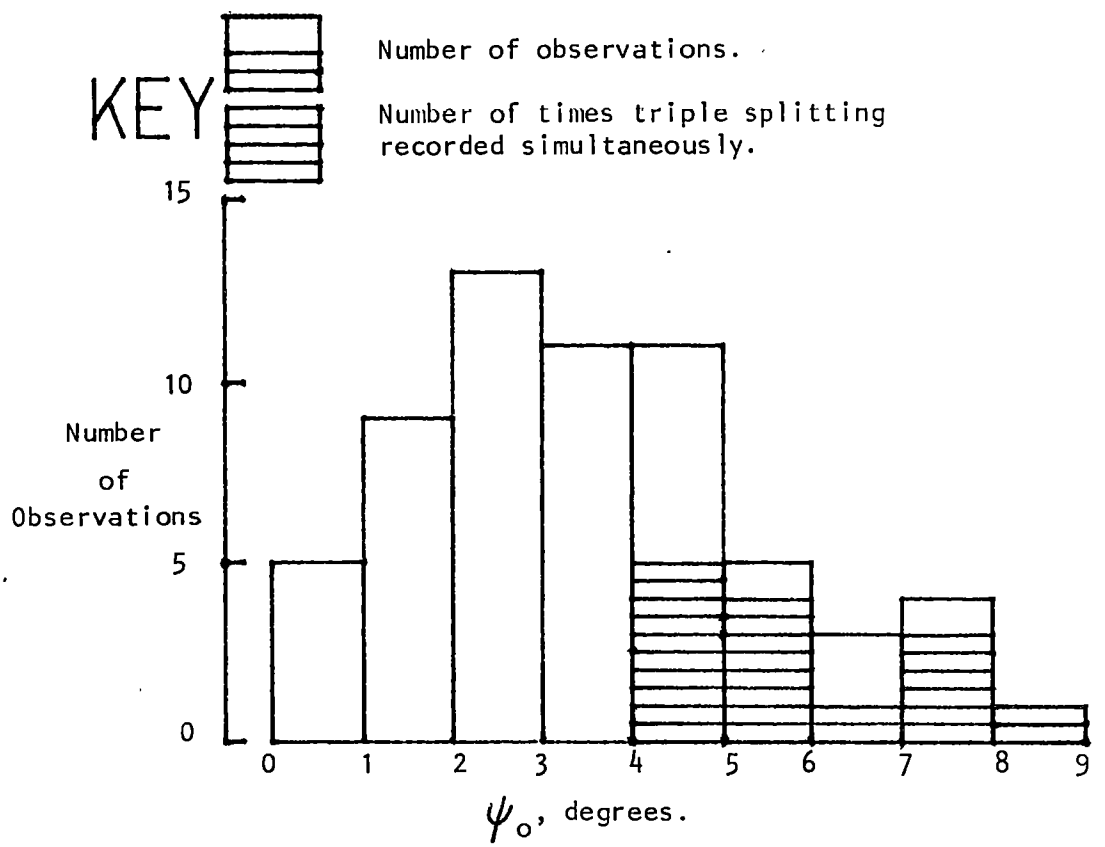

FIG.3.12 Histogram constructed from the data of Table 4 of Ellis (1954).

experiment where $f = 2/3$ and ψ_0 was measured in degrees

$$\frac{\Delta(f)}{\bar{A}} = \frac{\psi_0}{40}$$

Between the hours of 1300 and 1500 L.M.T. during the months of July and August 1953, Ellis (1954) made measurements of $\Delta(f)/\bar{A}$ and thus obtained values for ψ_0. The results are shown in the histogram of Fig.3.12 and superposed on it is a histogram of the simultaneous occurrence of Z echoes on the h'f ionograms.

It can be seen that there is good qualitative agreement between Z echo occurrence and increased values of the ionospheric roughness parameter ψ_0. Ellis concluded that because of the very approximate nature of the roughness measuring technique and because the theory did not take possibly important secondary factors into account that an attempt at a more detailed correlation of the occurrence of Z echoes with ionospheric roughness was not warranted. Ellis had observed an increase in Z echo amplitude near the critical frequency and he suggested that enhanced scattering occurred at this level and produced observable triple splitting at smaller values of ψ_0 than would otherwise be expected.

3.4 Critical Discussion

The term "backscatter", when applied to contemporary ionospheric sounding, usually means the return of radiowave

energy back along its incident path either by the process of partial reflection or that of incoherent scatter. Partial reflection occurs because the electrons have a distribution that is irregular on a scale much greater than the distance between them and much less than a radiowavelength; incoherent or Thompson scatter occurs when energy is returned from individual electrons, each scattering independently (Ratcliffe,1972). Sounding techniques utilising these backscatter processes require transmitters of very high power and antennae of great sensitivity as the returned echoes are very weak compared with the totally reflected waves detected by traditional ionospheric sounding. Many workers, especially before the advent of backscatter sounders, have employed the term backscattering merely to denote that some radiowave energy has been returned along an oblique incidence path by some small irregularities near the reflection level. A particular physical process has not always been specified and may not be either of the partial reflection or incoherent scatter processes but rather partial specular reflection in the required direction. In this context I would suggest that the term "small irregularities" means large enough to cause some specular reflection at the irregularity yet small enough that the ionosphere as a whole may still be considered as essentially plane horizontally stratified. We may picture this case as a flat ionosphere imbedded (at least in the vicinity of the normal reflecting level of the sounding wave) with small irregularities acting as tiny individual specular reflectors,

the direction of the reflected energy depending upon both the direction of the incident energy and the orientation and shape of the specular surface of the irregularity.

In the early and mid-1950's the available evidence all pointed to backscattering from small irregularities at the reflection level as being the most likely candidate for return of the Z echo. Apart from the work of Briggs and Phillips (1950), and the experiment of Ellis (1954) scattering by small ionospheric irregularities was deemed resposible for the results of many other experiments concerned with fading and scintillations. Additionally Booker (1955), quoting previous work, had pointed out that not only might the scattered power increase as the square of the mean ionization density (and the greatest ionization density encountered is in the reflecting stratum) but also that there existed the possibility of plasma resonance of irregularities in or near the reflecting stratum. He suggested scattering by irregularities in and near the classical reflecting stratum to be nearly as important a mechanism for returning energy as classical internal reflection itself.

A greatly increased backscattering effect at the reflection level would provide the required physical process for the backscattering return mechanism of the Z ray. However Pitteway (1958,1959) examined the scattered wave which accompanies reflection from a stratified ionosphere in which

there are weak irregularities and considered the possibility of enhanced scattering near the reflection level. He concluded that any special resonance effect of this kind would be largely destroyed by the collsional damping of the ionospheric electrons. In 1958 Bowles carried out experiments at 41 MHz verifying the existence of incoherent or semi-incoherent scatter by free electrons in the ionosphere. As had been expected, enormous sensitivity was required and Bowles used a half megawatt (peak) transmitter feeding a 116 x 140 m antenna of beam width 3.75°. His results showed a rise in noise level peaking broadly at about 350 km. range but no noise peak anywhere near the strength required to explain Z echoes in terms of backscatter. Similar results are obtained by large backscatter sounders which have since been constructed. The requirement of great sensitivity in order to detect partial reflection has also been confirmed by these sounders. It becomes obvious then that in order to explain Z ray return by a partial reflection or incoherent backscatter type mechanism a reflection stratum resonance or similar enhancement phenomenon must be invoked in order to amplify the Z echo to observed levels. However in view of Pitteway's general findings it appears highly likely that the suppression of such a phenomenon under the Z mode conditions would be sufficient to prevent Z echo signal levels reaching the strengths observed despite the fact that the Z echo is usually observed as a relatively weak signal.

We shall now examine the possibility of backscattering from "small irregularities" of the type discussed in the first paragraph. Of particular interest to this question are two papers by Renau (1959,1960) in which he examined a theory of spread-F based first on a scattering screen model and then on aspect sensitive backscattered echoes. Renau (1959) based his scattering screen model on a scattering mechanism of the type discussed by Briggs and Phillips (1950), referred to in the previous section. This same scattering screen is thus of a type which would be responsible for backscattered Z echoes. The screen permits off vertical echoes to return to the sounder and Renau made calculations of the virtual heights associated with these oblique rays in order to establish the type of ionogram that would result from such a model. He hoped that by varying the height of the scattering screen he would obtain some idea of the height principally responsible for spread-F occurrences. Fig.3.13 shows the expected form of the ionograms for various screen heights and included is the situation in which the scattering screen is at the level of reflection, being the situation required for backscatter of Z echoes. Renau compared his theoretical ionograms with actual observations and found that the scattering screen theory could satisfy a certain class of spread-F ionograms but not other types. Fig.3.14 shows the spread-F phenomenon on a Godhavn ionogram and Fig.3.15 shows it replotted on a linear scale together with the corresponding model, the observed spread being indicated by the horizontally shaded area. This spread

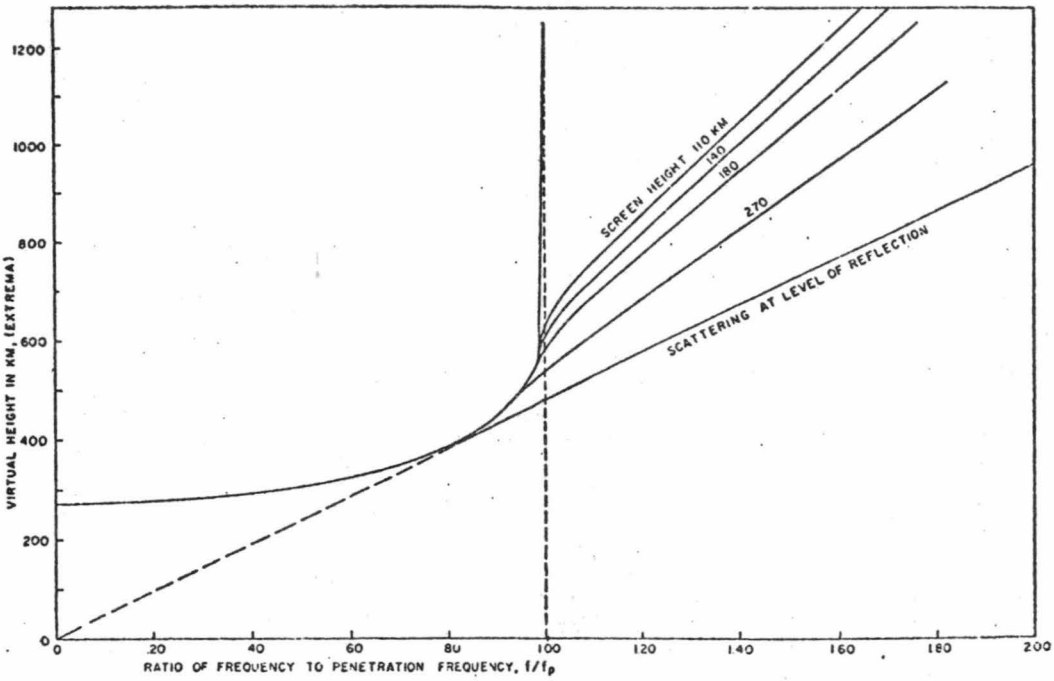

FIG.3.13 -Theoretical spread-F ionogram

(Fig.4 of Renau,1959)

FIG.3.15

Record from Godhavn Ionospheric Station, March 9, 1955, replotted on linear -frequency scale.

(From Fig.6 of Renau,1959)

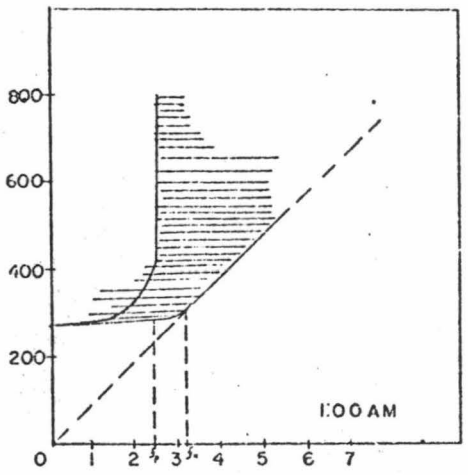

FIG.3.14

Record from Godhavn Ionospheric Station, March 9, 1955.

(From Fig.5 of Renau,1959)

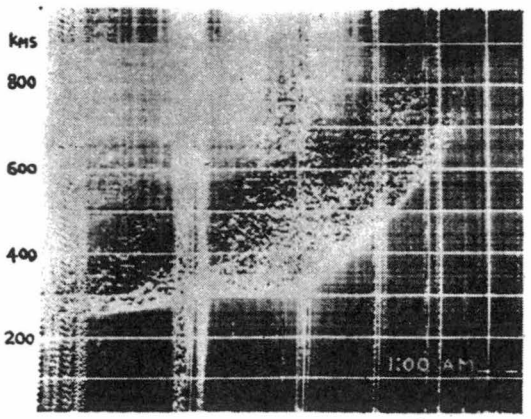

ionogram agrees reasonably well with the theoretical predictions of the scattering screen model with the screen at the level of reflection and is hence the type of ionogram we would expect to see in conjunction with Z echo observations if backscattering is the Z ray return mechanism. Fig.3.16 shows a spread-F ionogram which cannot be explained by the scattering screen model as is demonstrated by Fig.3.17 which shows the ionogram replotted on a linear scale together with the calculated area of spread-F. It should be noted that the features of this ionogram include a good example of the Z echo. Renau concluded that in general, when the inner and outer frequency edges of a spread ionogram are so separated that the frequency difference of the two edges is much larger than the gyro frequency (for Arctic ionograms) or half the gyro frequency (for middle latitude ionograms) and both of the edges resemble normal ionogram traces in shape then the scattering model fails to explain the observations. However examination of Fig.3.13 would suggest that if both inner and outer edges of the spreading resemble approximately the same normal ionogram trace and are not appreciably displaced in virtual height relative to each other (that is, we have the common form of frequency spreading of which Fig.3.16 is an example) then this is a sufficient criterion for the ionogram to be inexplicable in terms of the scattering screen model, independent of the extent of the frequency spreading.

The second paper by Renau (1960) considered the form of

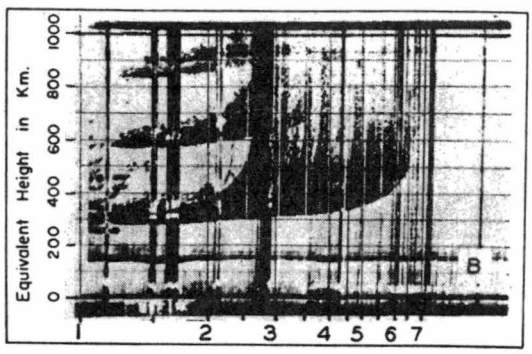

Arctic spread-F ionogram published by *Reber* [1956]

FIG.3.16

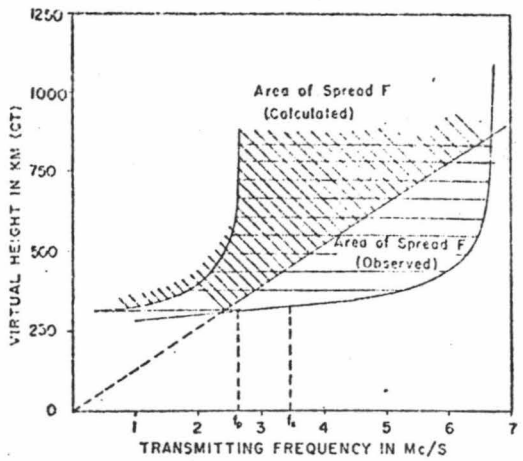

FIG.3.17 —Arctic spread-F ionogram of Figure replotted on linear-frequency scale

(Figs.7 and 8 of Renau,1959)

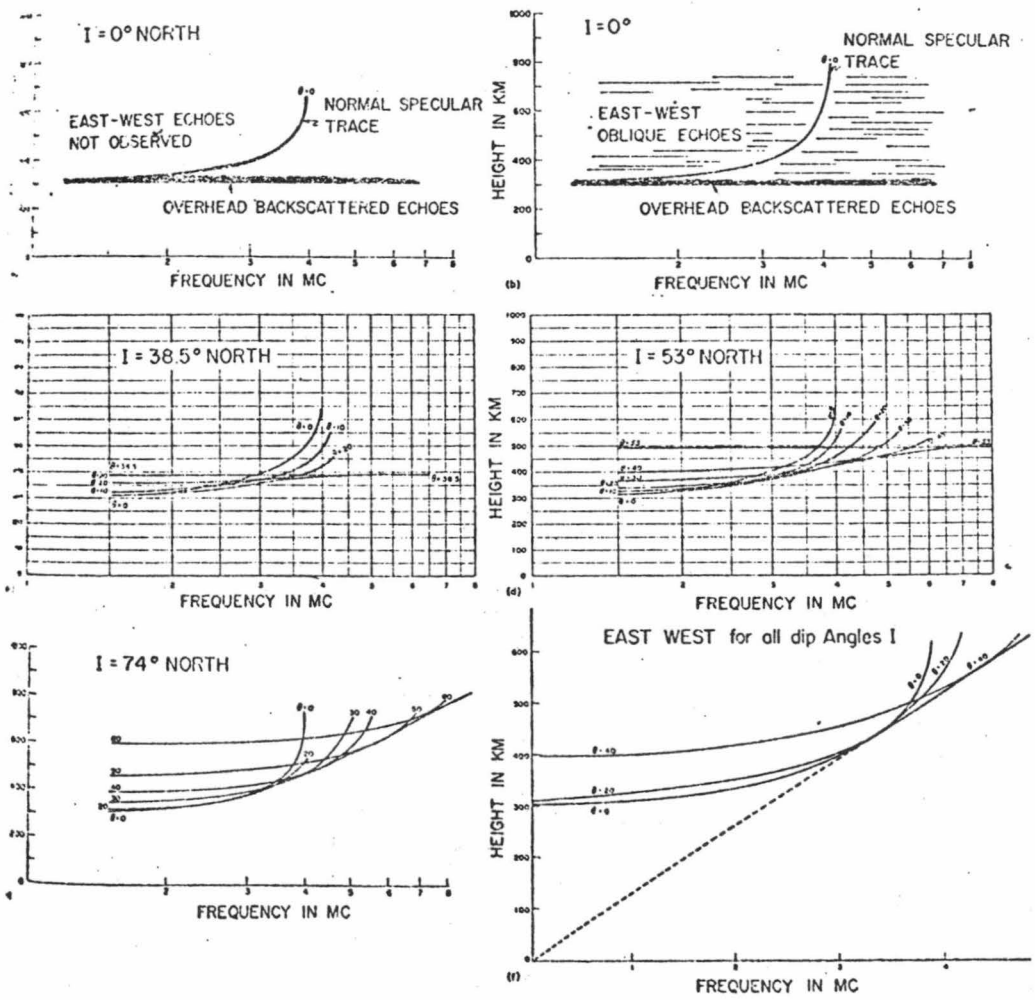

FIG.3.18 Predicted ionograms for ionospheric stations at various magnetic latitudes.

(Fig.6 of Renau,1960)

the ionogram traces if spread-F is generated by aspect sensitive backscattered echoes and the predicted results for various dip angles are shown in Fig.3.18. It can be seen that as the sounder stations approach closer and closer to magnetic north, corresponding predicted ionograms resemble more and more the ionograms predicted by Renau's scattering screen model with the scattering screen located at the reflection level. Fig.3.19, a comparison of an observed ionogram with the predicted model, demonstrates that there is a large class of high to middle latitude spread-F which cannot be explained by the aspect sensitive echo model - the same class in fact which could not be explained by the scattering screen model. Renau could find no mid-latitude ionogram observations which resembled the predicted ionograms of Fig.3.18. At the magnetic equator, however, he was able to show that the model was capable of explaining certain forms of spread-F.

In concluding this section we can safely rule out partial reflection or incoherent scatter as backscattering processes by which the Z echo is observed. Neither theoretical nor experimental evidence lend any support to a view that these processes might produce echoes of the required strength. Furthermore, the Z echo typically appears as a clean, well defined trace (even under strong spreading conditions) and this would be very difficult to explain without there being a very strong resonance confined to the reflection level. Neither theory nor experiment support the existence of such a

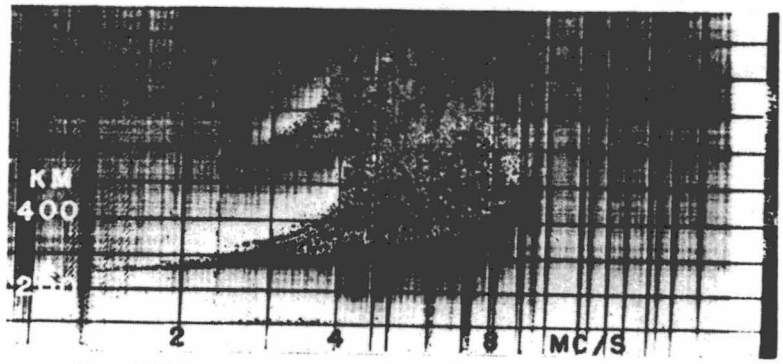

Spread F ionogram photographed at Godhavn (magnetic dip 81°).

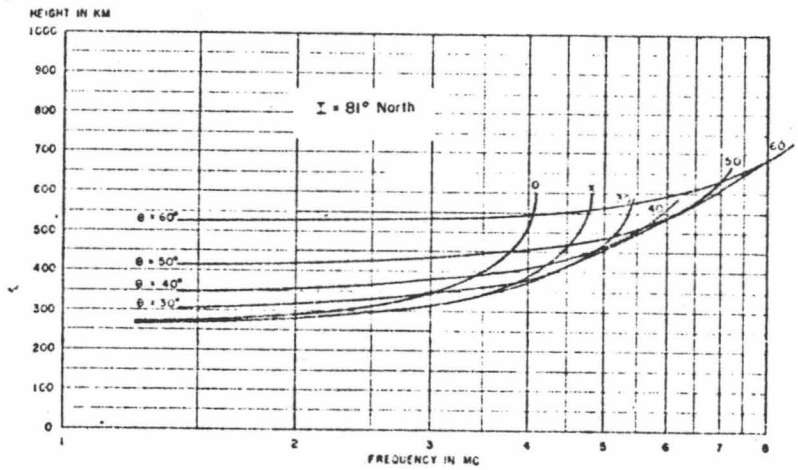

Theoretically predicted ionograms for Godhavn.

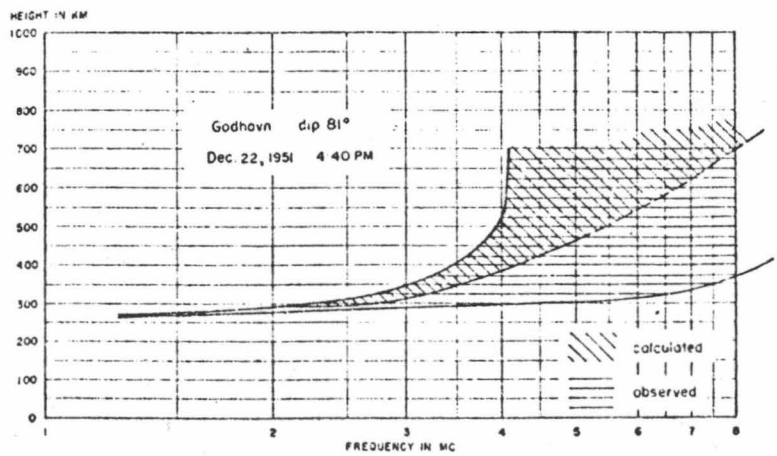

Comparison of calculated and observed ionograms.

FIG.3.19 (Figs.7,8 and 9 of Renau,1960)

resonance.

We are then left with the idea that Z echoes may be caused by backscattering from the type of specularly reflecting irregularities mentioned in the first paragraphs. This conclusion is not entirely unexpected as Ellis (1954) used the Briggs and Phillips (1950) two hundred metre estimate as an indication of the expected average size of his proposed F region irregularities. Two hundred metres is several wavelengths at the operating frequencies used by Ellis and thus the irregularities are too large for the process of partial reflection to operate satisfactorily. It can reasonably be assumed that Renau's models also involve irregularities of this type as he specifically references Briggs and Phillips when introducing his scattering screen (Renau,1959).

3.5 Return Of The Z Ray - Bowman

Bowman studied the occurrence of F2 region Z traces on ionograms and came up with several important results. He found that Z echoes are predominantly a daytime phenomenon at most latitudes and that the diurnal variations show a systematic shift, with magnetic inclination, of the time of maximum occurrence (Fig.3.20). Maximum occurrence is in the daytime morning sector and the time of the maximum increases with increasing dip angle. Brisbane exhibits a somewhat different

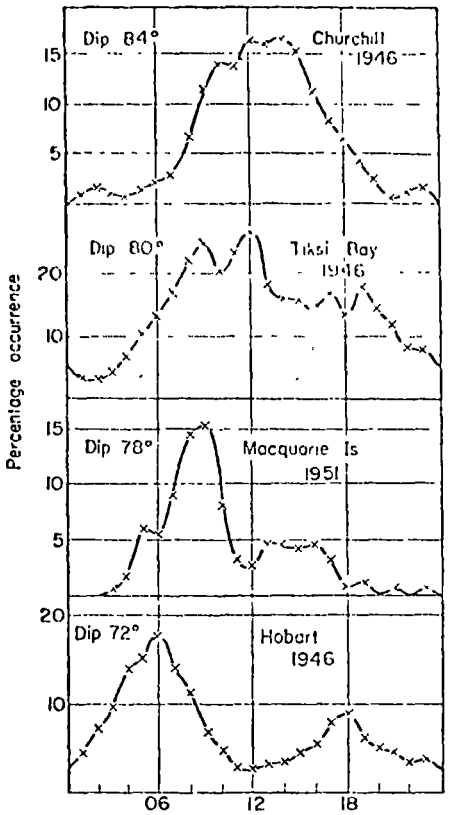

FIG.3.20

Diurnal variations of percentage occurrence of z-rays at Churchill, Tiksi Bay and Hobart in 1946, and Macquarie Island in 1951.

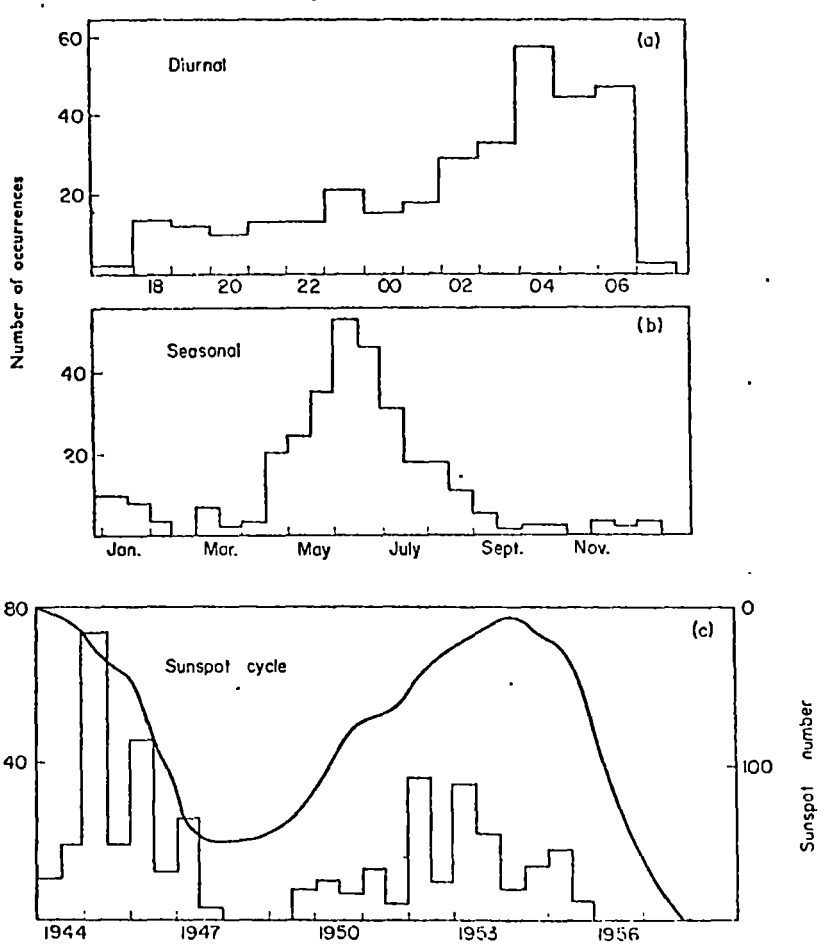

FIG.3.21

Occurrence of z-rays at Brisbane 1944–1956 (inclusive). Ionograms available every 15 min 1944–July 1947 ; every 10 min July 1947–1953. (a) Diurnal variation. (b) Seasonal variation. (c) Sunspot-cycle variation.

(Figs.1 and 6 of Bowman,1960)

diurnal variation as Brisbane Z echoes occur mostly at night although the maximum nevertheless occurs near dawn (Fig.3.21). Seasonal variation revealed a winter maximum and a summer minimum (Figs.3.22,3.21) and an inverse sunspot cycle relationship was found to exist (Figs.3.23,3.21). A maximum Z echo occurrence was found for magnetic dip angles of between 70^{o} and 80^{o} with a fairly quick fall off for lower and higher dip angles (Fig.3.24). Bowman reported the presence of spread-F in virtually every Z echo ionogram for Brisbane and 91 per cent of Hobart Z echo ionograms. He plotted contours of equal ionization density for selected ionogram series by calculating true heights and assuming all F2 layer reflections to be vertical. On the same diagrams he also plotted the Z ray trace lengths indicated by the ionograms and drew lines along the positions of corresponding troughs or corresponding crests and extended these lines to ground level as shown in Figs.3.26 and 3.27. Bowman stated that "an apparent association between the upward slopes of ionization contours and the occurrence of Z rays is revealed." Fig.3.28 is a third diagram made by Bowman, this time for a single occurrence of a Z echo at Hobart. Fig.3.29 shows ionization contours for a Z echo occurrence at Brisbane.

Bowman found that the irregularities of his ionization contours were the same sort of irregularities as those he (Bowman,1960a) has suggested as being responsible for spread-F. He noted that for Brisbane the diurnal,seasonal and sunspot

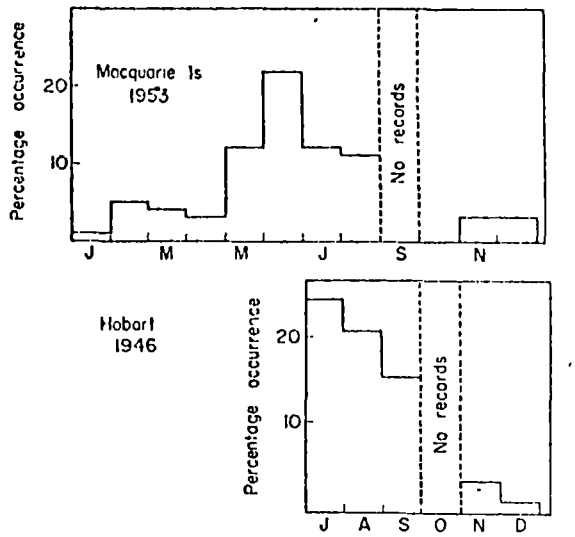

FIG.3.22

Seasonal variations of percentage occurrence of z-rays at Macquarie Island (1953) and Hobart (1946).

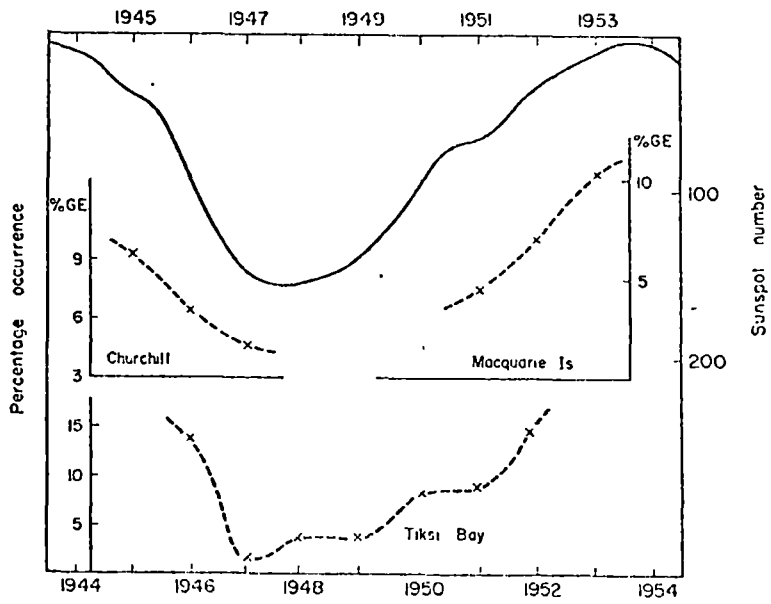

FIG.3.23

Sunspot-cycle variations of percentage occurrence of z-rays at Churchill, Tiksi Bay and Macquarie Island.

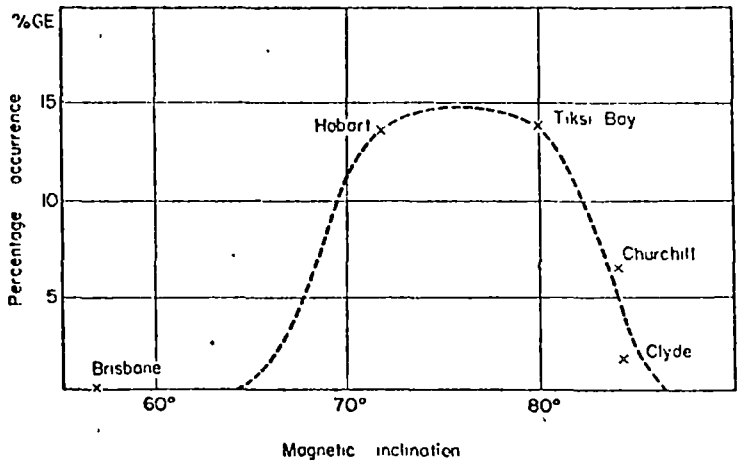

FIG.3.24

Variation with magnetic inclination of the percentage occurrence of z-rays during 1946.

(Figs.2,3 and 4 of Bowman,1960)

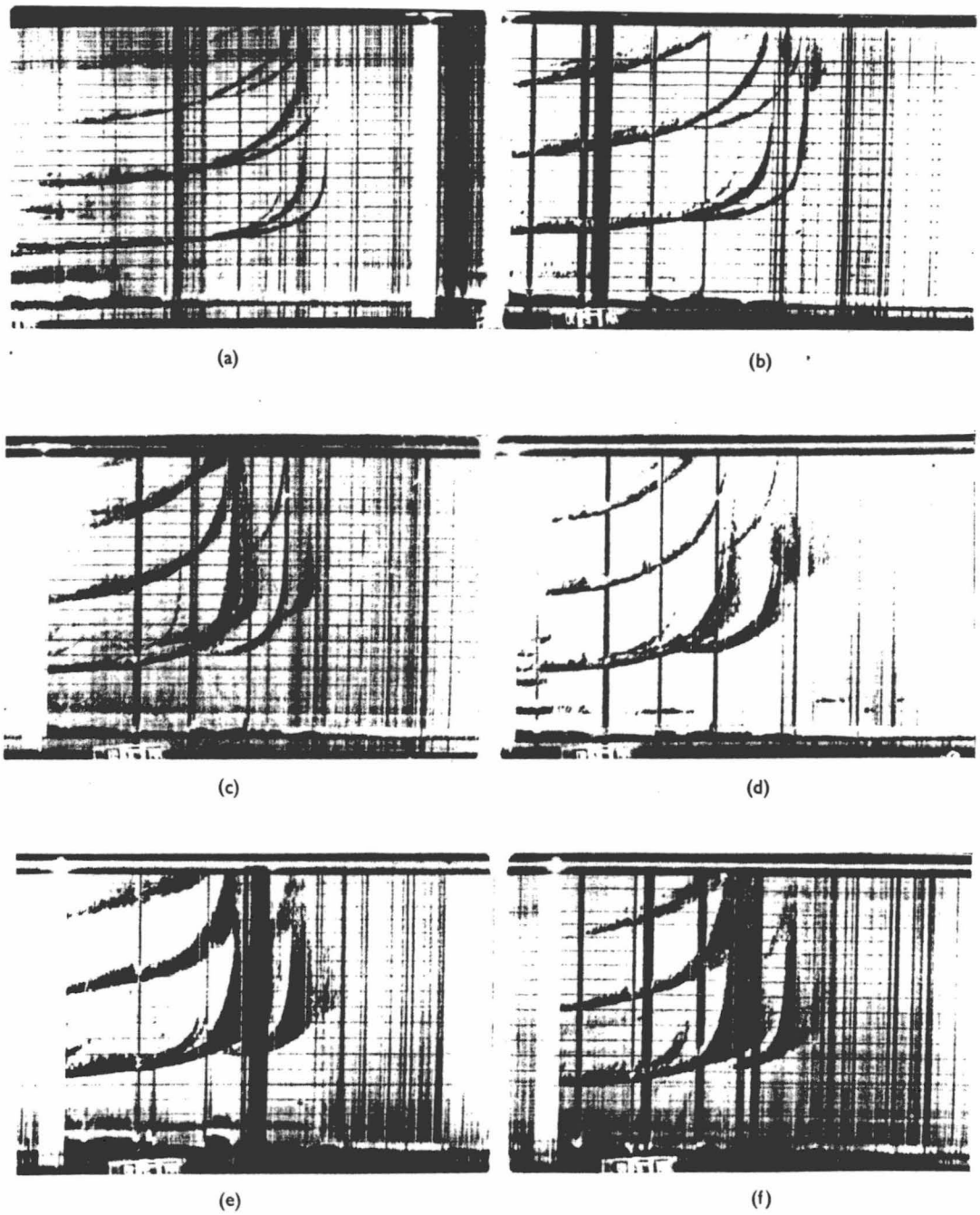

(a) (b)

(c) (d)

(e) (f)

Various aspects of z-ray trace occurrence at Hobart.

FIG.3.25A (Fig.5 of Bowman, 1960)

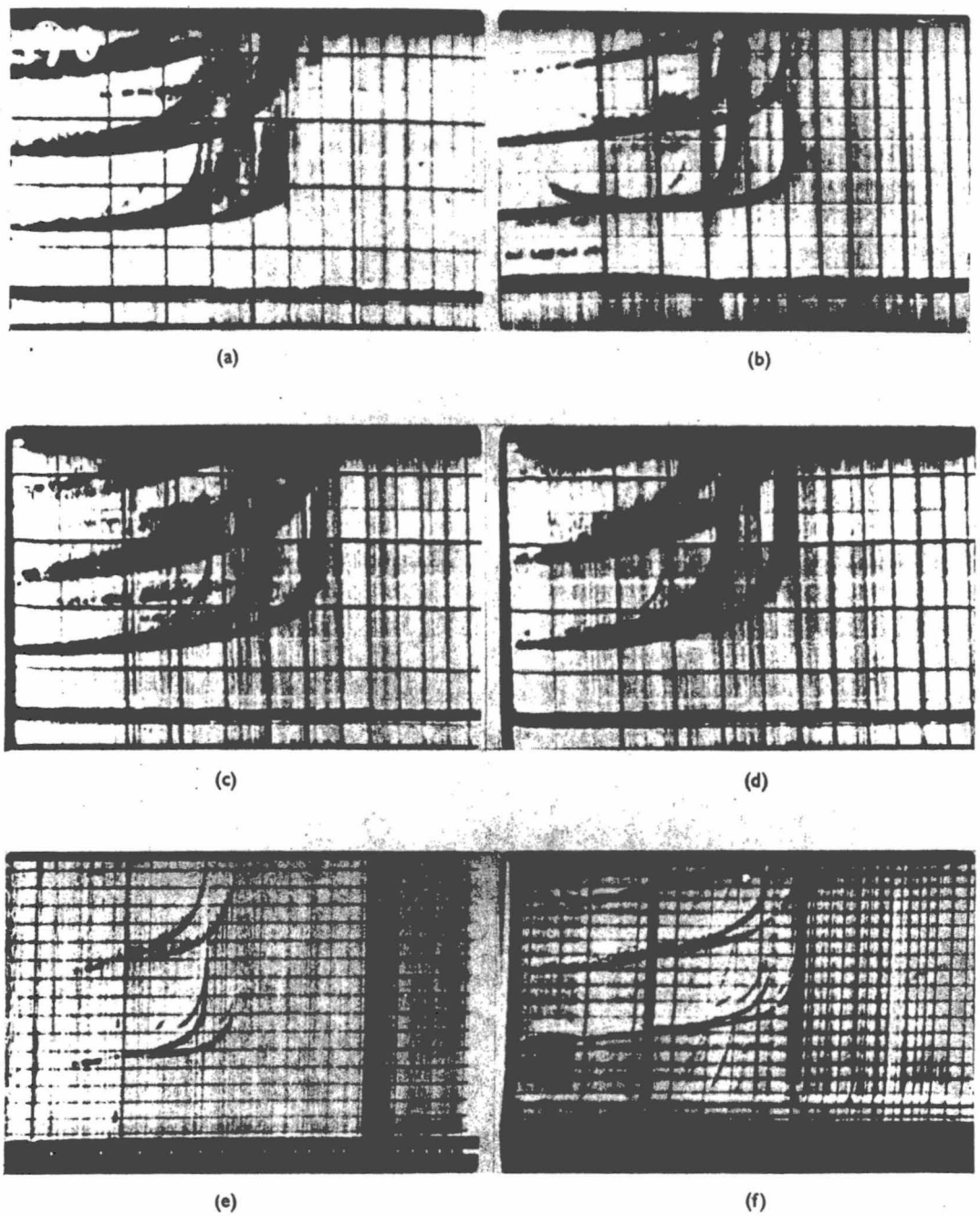

Various aspects of z-ray trace occurrence at Brisbane.

FIG. 3.25B (Fig. 7 of Bowman, 1960)

FIG.3.26

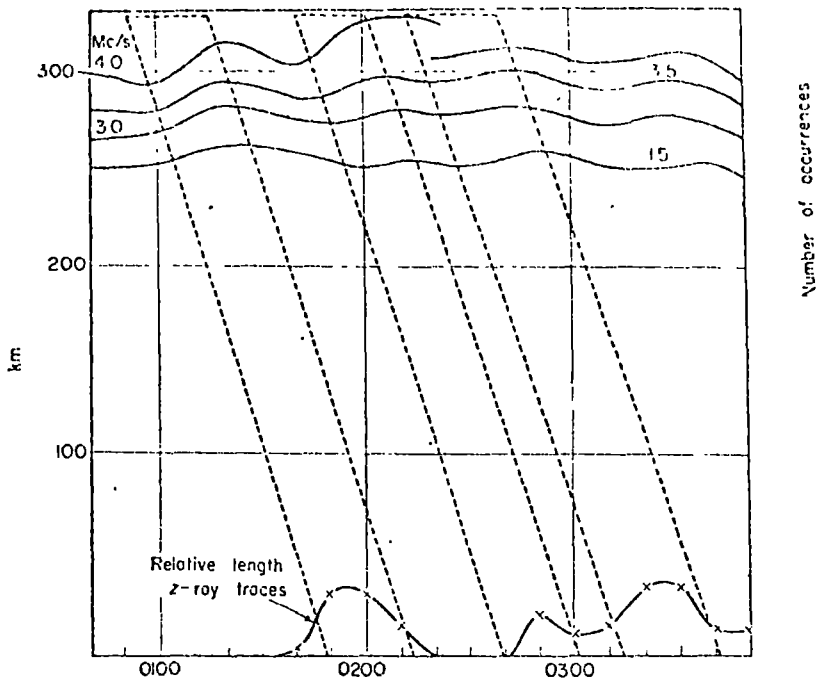

F2-layer ionization contours and z-ray trace lengths around 02.00 on 4 July 1946 at Hobart.

FIG.3.27

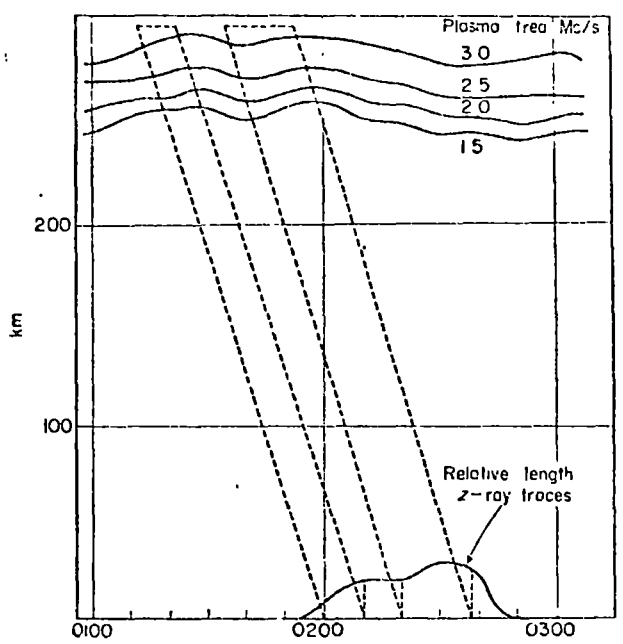

F2-layer ionization contours and z-ray trace lengths around 02.00 on 11 August 1946 at Hobart.

(Figs.8(a) and 8(b) of Bowman,1960)

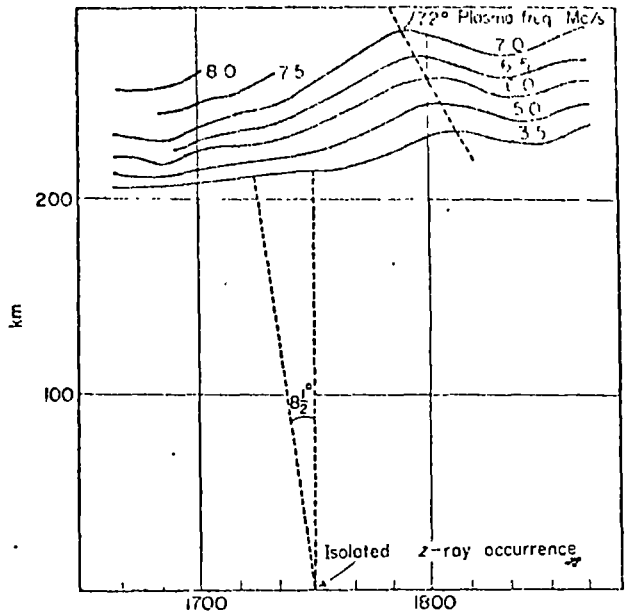

FIG.3.28 F2-layer ionization contours at Hobart around 17.30 on 25 July 1946, the time of an isolated occurrence of a z-ray trace.

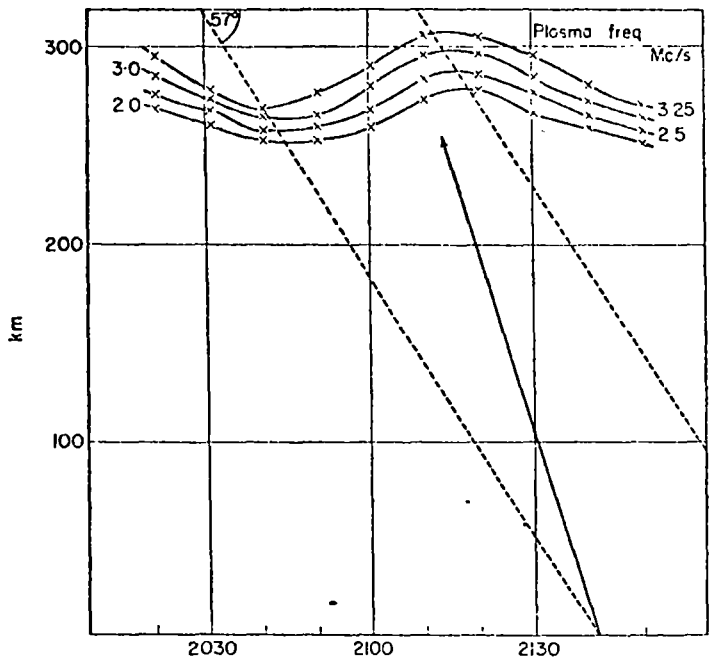

FIG.3.29 . F2-layer ionization contours apparently associated with resolved range-spreading and z-ray occurrence at 21.42 on 28 August 1953, at Brisbane.

(Figs.8(c) and 9 of Bowman,1960)

cycle variations for Z echoes were very similar to those for spread-F; for Hobart the seasonal variations were the same; and for Macquarie Island the winter maximum and summer minimum of Z echoes was the same as that found at high latitudes for spread-F. Since very high latitude spread-F had been reported to vary directly with sunspot activity, Bowman concluded that the sunspot cycle variations for spread-F and Z echoes would be dissimilar at stations such as Churchill and Tiksi Bay.

Bowman (1960a) had previously suggested that kinking of the ionization contours of the F2 layer were responsible for spread-F at middle latitudes and as he had found such a strong association between spread-F and Z echoes he made the further suggestion that the return of the Z ray might result from the same kinking. He postulated that the spread-F irregularities could have extended fronts aligned perpendicularly to the magnetic meridian such that the Z wave could possibly be reflected back along its path, in the plane of the magnetic meridian, because of the sloping ionization contours of the irregularity. The ionization contours may remain approximately horizontal up to the normal O ray reflection level as the only requirement is that the ionization contours above this level should be so shaped that a ray which is longitudinal at the O reflection level and passes through the coupling cone will be normal to the ionization contours when it reaches the Z mode reflection level.

Using the Poeverlein diagrams Figs.3 & 4 of Ellis (1953b) Bowman traced ray paths in the two types of model ionization distributions, one corresponding to a Figs.3.26 and 3.27 type distribution ("spread-F irregularity") and the other corresponding to Fig.3.28 ("sunset period"), and found ionization distributions which satisfied the requirements that the ray path allowed longitudinal propagation at the X = 1 level and normal incidence to the layers at the Z reflection level. The angle of incidence for the "sunset period" model was 8.5^{o} and that for the "spread-F irregularity", 14^{o} (Figs.3.30,3.31).

3.6 Critical Discussion

Bowman's (1960) paper makes firstly some useful contributions to knowledge of the morphology of the Z echo and secondly proposes an alternative mechanism for the return of the Z ray. On a cautionary note it should be remembered that much of Bowman's information on the morphology of the Z mode has been gathered from other papers and publications and there has been no standardisation or cross comparison of the scaling or ionosondes of the stations involved. The Z mode can be a very difficult parameter to scale and high latitude ionograms can be very hard to interpret. Variations in sounding equipment may affect the relative occurrence on the ionograms of weak phenomena such as the Z mode. In the past the Z mode

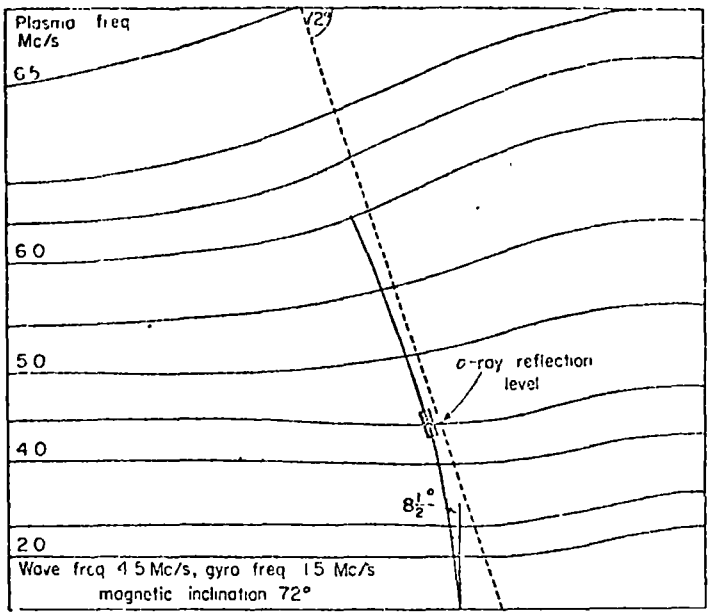

FIG.3.30 Ray-path drawn in a model of ionization distribution similar to that shown in Fig. 8 (c), illustrating proposed reflection path for z-ray.

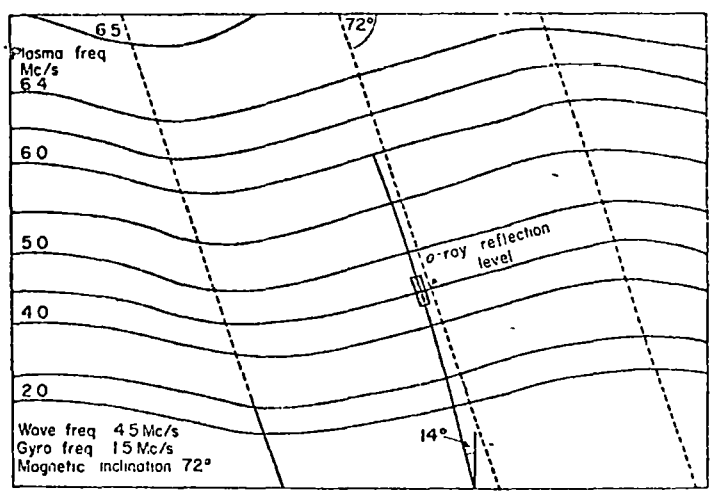

FIG.3.31 Ray-path drawn in a model of ionization distribution similar to that found for "Spread-F" irregularities, illustrating proposed reflection path for z-ray.

(Figs.10 and 11 of Bowman,1960)

has not always been correctly identified. Rivault (1950), for instance, reports seeing the Z mode mainly on the second order reflections but on examination of the ionograms illustrating his paper it appears the Z mode is being confused with satellite traces and is not in fact present.

Bowman's Z ray return mechanism is a sound alternative to the backscatter mechanism. Probably its most important feature is that return of the Z ray along its path at the upper X mode reflection level takes place by the usual total reflection process thereby avoiding the confusion over whether or not backscattering will provide an echo of the observed strength. Bowman takes note of Ellis's experimental evidence, suggesting that most of the tilting would occur above the O ray reflection level and noting that one of the two calculated angles of arrival is larger than those observed by Ellis. Bowman links Z mode occurence with that of spread-F and suggests that his ionization contours would be responsible for both phenomena. Strong backscattering, however, would also be expected to produce spread-F. The tilt mechanism is a very worthwhile idea as there seems to be no doubt that the Z ray would be returned if the appropriate ionospheric configuration occurred.

The main problem with the tilt theory is that it is an extremely restrictive model in that it must not only return the oblique Z ray back along its path but it must also provide for upgoing and downgoing Z rays to have their wave normals making

no more than $1/2^{o}$ angle with the magnetic field at the O mode reflection level. An important consequence of these conditions is that the Z ray is for all practical purposes confined to the magnetic meridian at least up to the coupling point. Bowman's paper does not address the question of whether or not the special combination of tilts required might occur sufficiently often to account for the observed frequency of Z mode. Tilts unquestionably occur in the ionosphere (e.g. Munro,1953) and relatively frequently but tilt observations indicate that the larger tilts (such as the $18+^{o}$ required at the Z reflection level) occur only rarely and the requirement that such tilts be in the magnetic meridian may mean that the required conditions occur much less frequently than the Z echo except at very high latitudes where the tilt requirements are smaller and the Z echo occurs less frequently according to Bowman (Fig.3.24). As insufficient is known about the statistical occurrence af the various ionization contour perturbations the answer to this problem must be an experimental one. Bowman (1960) claimed to have observations supporting his alternative. However there are some serious objections to the method of analysis and these are detailed as follows :

A) A multi-point (Schmerling 5 pt. and 10 pt. method) method of estimating true heights has been used. These methods are valuable for estimating the true height of a particular event but great care must be exercised when making true height versus time plots as these methods do not

usually provide the required accuracy. For example, subtle changes in the underlying layers, especially if accompanied by partial cusp development, may produce apparent variations in the true heights of higher levels which do not necessarily bear any resemblance to the real variations. Reliable real height versus time plots of the type attempted by Bowman require high repetition frequency of ionograms (e.g. one per minute), first class ionograms showing very little perturbation and appropriate high accuracy real height reduction techniques. Unfortunately under quite perturbed conditions such as those postulated for the occurrence of Z mode the required accuracy is normally unattainable. Errors in the multi-point height method will tend to correspondingly raise or depress values at other levels so that the shape correspondence of various ionization contours is no valid check on the accuracy of the result.

If Figs.3.26 to 3.28 are taken from ionograms at 10 minute intervals (as would appear to be the case though I was unable to obtain the original records) then we have only four readings per quasi-periodic cycle of the ionization contours and it is doubtful that peaks and troughs could be seen to be aligned at a certain angle, given so little information. If appropriate error bars were put on the height points it might be hard to justify the positioning of the peaks and troughs. In any case examination of the

contours as drawn reveal that the peaks and troughs do not fit very well along the dashed magnetic field line direction.

These, however, are relatively minor quibbles compared with the following objections.

B) Assuming that the real height analysis is correct, no justification has been given for the unstated assumption that what is being viewed is travelling wave motion in the ionosphere and not simply bulk vertical motion of the whole or part of the F2 region.

C) Assuming that the real height analysis is correct and assuming that the results represent travelling horizontal and not bulk vertical motions in the ionosphere then no justification has been given for the again unstated assumption that the travelling motion is not only along the magnetic meridian but furthermore is in the correct direction along that meridian. In addition, for successful Z mode propagation there may be no east-west (magnetic) tilts across the magnetic meridian below the X = 1 level in order that the Z ray wave normal be parallel with the magnetic field at this level. It could be argued that a particular lateral vertical distribution of ionization could allow significant east-west tilts yet still fulfill this condition but in view of the already restrictive nature of

the tilt model in the magnetic meridian it would be such an extremely unlikely possibility that it can be ignored. In short, the tilt model will probably have difficulty satisfying reasonable electron density distributions without introducing unreasonable ones. Large east-west tilts above the X = 1 level are more likely but nevertheless impose further restrictions in that they must allow the Z ray to retrace its path to the coupling region.

D) Assuming all the preceding objections to be satisfied there will be O mode and X mode reflections from approximately the same region of the ionosphere as that producing the Z mode. Bowman has stated the assumption that all F2 layer reflections are vertical and this is clearly not a good assumption under the circumstances (there may or may not be additional reflections from overhead depending upon whether or not the overhead contours are horizontal). For instance the 3 MHz O mode echo at 0155 hrs ,4/7/46HO (Fig.3.26) would be coming from around the 0105 hrs region and thus the "true heights" of such times/points are well out. In other words, the results are found to invalidate this assumption.

Assume all the preceding objections to be satisfied - the following further objections apply :

E) The Z mode length graphs as drawn in Figs.3.26 and

3.27 are not what would be expected from the ionization contours drawn on the same figures. Furthermore if, as seems to be the case, the ionograms are at 10 minute intervals then this is too low a sampling rate to attempt this sort of correlation between Z echo occurrence and shape of ionization contours. The variation in the strength of the Z echo and also its appearance and disappearance commonly take place on a much shorter time scale than this sampling interval.

F) Since Bowman has drawn his vertical and horizontal distances to scale (with lines of actual dip angle 72^{o} on the Hobart figures and 57^{o} on the Brisbane figure) then we see that his ripples have wavelengths of about 60 km. to 90 km. in Figs.3.26 and 3.27 and about 230 km. in Fig.3.29. It can be calculated that the following speeds are required to move the ripples from overhead when they are observed to their appropriate drawn position at the time of observation of the corresponding Z echo :

60 km.	31 m/s
90 km.	31 m/s
230 km.	48 m/s

In other words it must be assumed that these ionospheres move at 31 m/s north along the magnetic meridian at Hobart and 48 m/s along the magnetic meridian at Brisbane. This is a curious result and nothing has been stated in the paper which could justify it. If these ripples were travelling

ionospheric disturbances (TID's) then their speeds are lower than would be expected for such wavelengths and it is probably unknown to find TID's travelling together in such a non-dispersive manner.

G) Bowman's ray tracing was based on the Poeverlein diagrams published by Ellis (1953b). Such ray tracing would be crude to say the least. Poeverlein diagrams are very useful for checking out the possibility of mechanisms such as the one discussed here but would not enable specific examples to be traced accurately unless very many contours were used corresponding to thin stratifications. Even with a highly detailed Poeverlein diagram it is much more difficult to maintain accuracy in the sort of ionospheres used by Bowman than with the usual horizontally stratified ionosphere where the line offset $\sin\theta_r$ can be employed.

To summarise, the only thing which can reasonably be deduced from the experimental data is that the ionosphere was probably undergoing quasi-periodic true height variations at some heights during the observations of the Z echo. Whether or not these perturbations might be associated with the Z echo is not at all clear. It is not shown whether or not the perturbations occurred before and/or continued after the Z mode observations. Furthermore the ionosphere is a fluid perpetually in motion to a greater or lesser degree. It has

not in any way been demonstrated that the observed perturbations are peculiar to the existence of the Z echo.

In conclusion, although Bowman's alternative Z ray return mechanism is a clever idea warranting further investigation, the experimental evidence presented in support of this idea is quite unacceptable.

3.7 Return Of The Z Ray - Papagiannis

Papagiannis (1965) stated that the backscattering postulated by Ellis was not generally accepted and constituted the only disputable part of an otherwise sound theory. Papagiannis proposed the alternative explanation of a favourable horizontal gradient which can reduce, or eliminate, the need for backscattering. He defined a favourable horizontal gradient as one which tilts the planes of equal electron density near the reflection layer in such a way as to make them normal, or near normal, to the earth's magnetic field. Papagiannis claimed that ionograms showing Z echoes generally yielded increased values of the local cyclotron frequency and he stated that this was a clear indication of a N-S gradient. Assuming a Chapman β model electron density profile for the daytime F layer he postulated that N-S gradients caused by the latitudinal change in the sun's zenith angle can explain Z mode echoes under given physical

conditions. He obtained an expression for the change in the sun's zenith angle for change in latitude between coupling and reflection points of the Z mode and thus was able to show that the change in the electron density profile caused the ionoization contours to be tilted at an angle α from the horizontal where

$$\cot\alpha = \left(\frac{R\cot\omega}{H\tan\chi}\right)^{\frac{1}{2}}\left[\frac{\ln(1+Y\sin^2\omega)}{2}\right]^{\frac{1}{4}} \qquad 3.1$$

where R is the Earth's radius, H is the scale height, ω is the dip angle, Y is f_H/f as usual and χ is the sun's zenith angle. Figs.3.32 and 3.33 show the relevant diagrams.

Papagiannis considered the measurements of Ellis (1953b,1956) made in Hobart and substituted $\omega = 72^\circ$, $Y = 1/3$ and $H = 50$ km (for a reflection altitude of 210 km). From Hobart's latitude, the season and time of day (which Papagiannis stated to be 42.9°S, Fall and early afternoon respectively) he assumed the zenith angle of the sun to be about 60°. Substituting this in Eqn.3.1 along with the other values gave

$$\cot\alpha = 2.95$$

$$\alpha = 18.7^\circ$$

This is the result required in order for the plane at which the Z mode is reflected to be practically normal to the magnetic field ($\alpha+\omega \approx 90^\circ$) such that the reflected Z wave will retrace the incident path without need of backscattering.

Fig.3.32

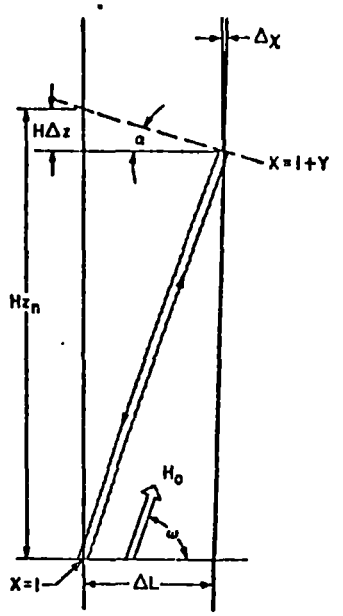

The approximate path of the Z-mode echoes between the region of coupling ($X = 1$) and the layer of reflection ($X = 1 + Y$).

Fig.3.33

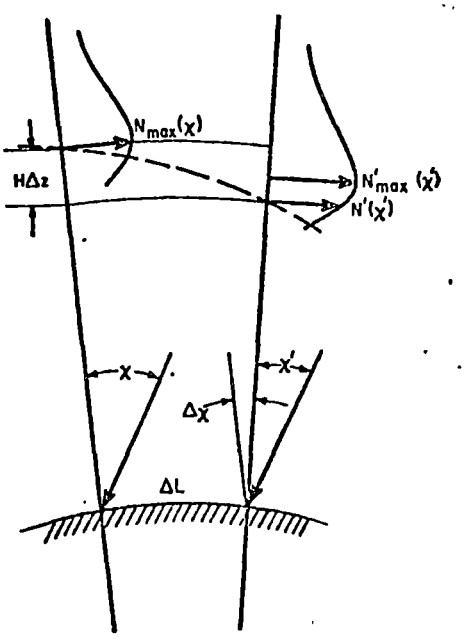

The dependence of the ionospheric electron density profile on the sun's zenith angle χ.

(Figs.1 and 2 of Papagiannis,1965)

Papagiannis allowed that the near perfect numerical agreement obtained is undoubtedly beyond the general accuracy of the computation presented but considered that the result nonetheless is a convincing argument in favour of the proposed theory. He stated that Equation 3.1 shows that at a given location the angle α is a function of the angle χ (i.e. a function of the sun's zenith angle) and that this is in agreement with Ellis's measurements which suggest that Z mode echoes are observed during consecutive days at nearly the same local time. He noted that Eqn.3.1 also shows that as we advance towards the equator the angle α decreases whereas $(90-\omega)$ increases, making the appearance of Z mode echoes progressively more difficult, which is also borne out by observations.

Papagiannis obtained a simple relation between α and ω by assuming that the sun's zenith angle χ is approximately equal to the geomagnetic latitude so that for a dipole magnetic field the Eqn.3.1 reduces to

$$\tan\omega \approx 10 \tan\alpha \qquad 3.2$$

Since Eqn.3.2 clearly shows the previously mentioned latitude effect he concluded that Eqn.3.1 is in basic agreement with the available observational results. Papagiannis stated that although one could try to derive a more precise expression for the angle α, the horizontal gradients of electron density are not always caused by the sun's varying zenith angle and thus this refinement would not be very meaningful. He considered

that it would be more profitable to try to verify the process by ray tracing the Z mode using several electron density profiles with chosen horizontal gradients at various magnetic latitudes to yield the range and type of gradients required by his proposed theory.

Papagiannis suggested that his theory could be tested experimentally by a system of ionospheric sounders located along the magnetic meridian and measuring the N-S horizontal gradient of electron density whenever Z echoes are observed. He noted that the deflection of the ordinary rays towards the pole and of the extraordinary rays towards the equator can be used very profitably in interlacing the system of ionospheric sounders.

3.8 Critical Discussion

The idea proposed by Papagiannis explains the Z mode in terms of solar radiation generated tilts in the ionosphere and the resulting ionospheric model thus becomes a special case of the Z ray return mechanism suggested by Bowman (1960). Certainly, if the ionosphere at Hobart behaves as Papagiannis has numerically predicted then it will be an ideal ionosphere for return of the Z mode, the magnetic field being perpendicular to the stratifications. But there are some objections and qualifications to Papagiannis's proposal,

detailed as follows :

A) Perhaps somewhat surprisingly in view of all the qualifications to the assumptions of the Chapman Layer Theory, the E and F1 layers behave approximately as predicted. This is graphically demonstrated by Figs.3.34 and 3.35. We are primarily concerned with Z mode occurrence in the F2 region. Papagiannis has used a Chapman β model electron density profile and while this is the better model to use in the F2 region its predicted results are often at variance with observations. To quote from Papagiannis (1972,p35) "......the F2-region is much more complex and a simple theory, like the Chapman layer theory, cannot provide a very adequate description." A Chapman β model could not be expected to predict the profile of the ionosphere to anywhere near the accuracy required to determine whether or not the Z mode would be returned. Nevertheless it was perhaps the best model to choose under the circumstances. Whether or not the results are reasonable in terms of known observations shall be examined later and for the moment the model will be accepted.

B) In his derivation of Eqn.3.1 Papagiannis begins by assuming that the Z ray is an oblique incidence ray. While this is strictly true (except of course for a flat ionosphere at the magnetic dip poles) it is incorrect to apply the conditions of oblique incidence to the Z ray when

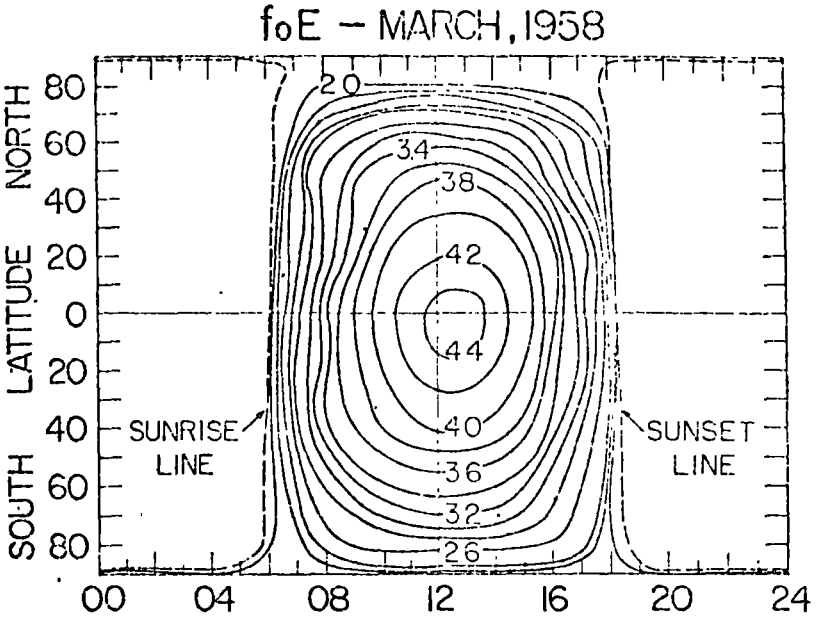

(After R. W. Knecht, unpublished.)

FIG.3.34 Map of f_oE.

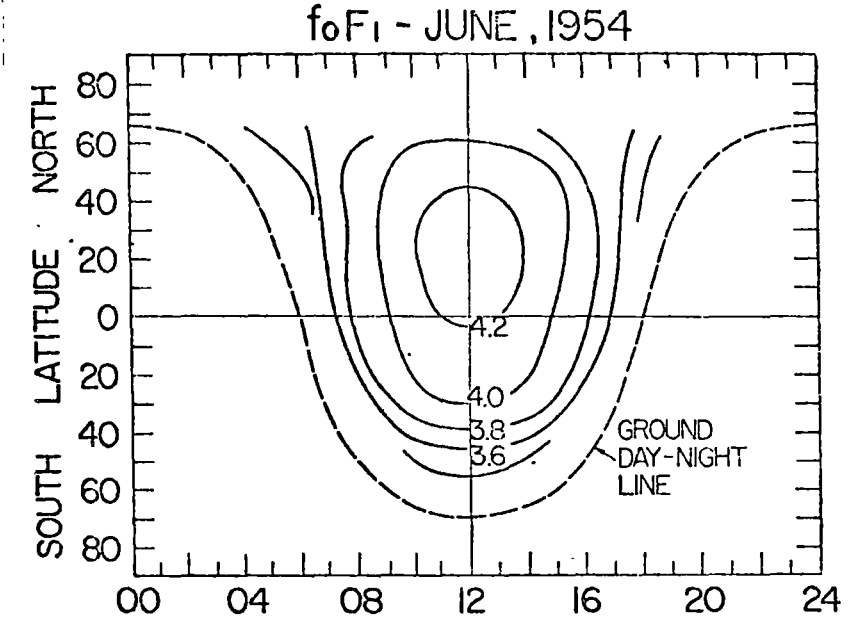

(After R. W. Knecht, unpublished.)

FIG.3.35 Map of f_oF1.

(From Figs.3.21 and 3.23 of Davies,1965)

invoking the tilt model used by Papagiannis. For this model the Z ray is a normally incident ray and should be treated as such. Thus terms such as $\cos^2\theta_z$ and $\sin^2\theta_z$ should be omitted in the derivation, leading to the deletion of the $\sin^2\omega$ term from Eqn.3.1. When this is done and the numerical example recalculated the "near-perfect numerical agreement" comes even closer to perfection.

C) Papagiannis correctly states that Equation 3.1 "....shows that as we advance towards the equator, the angle α decreases whereas the angle $(90-\omega)$ increases. This makes the appearance of the Z-mode echoes progressively more difficult, which is also borne out by observations." He omits to point out that as we approach high latitudes the angle α increases whereas the angle $(90-\omega)$ decreases making the appearance of Z-mode echoes progressively more difficult, which is not borne out by observations as the Z echo is mainly a mid to high latitude phenomenon. For instance, consider Macquarie Island which has a high incidence of Z echoes and a dip angle of 78°. Substituting this dip angle into Papagiannis's simple relation between α and ω (Eqn.3.2) we obtain an value of around 25°, just twice the required angle for Z ray return.

D) Papagiannis claimed that "Ionograms which yield values of the cyclotron frequency higher than those actually present are a clear indication of a NS gradient....." and

"Ionograms in which the Z mode appears (Meek,1948; Newstead,1948) yield in general, increased values of the local cyclotron frequency." Meek and Newstead show only one ionogram each. Meek makes no comment on the cyclotron frequency. Newstead commented that he regularly found the Z mode critical frequency to be higher than he expected. If the gyro frequency is to be taken as the difference between the X mode and Z mode critical frequencies, as is commonly done, then it would appear from Newstead's expectations that his ionograms yield decreased values of the gyro frequency. Papagiannis suggests calculating the gyro frequency from the O and X mode critical frequencies but furnishes no evidence or arguments to support his contention that Z mode ionograms generally indicate N-S gradients.

Ellis (1957) has looked into this question with the requisite thoroughness but as his calculations and theory are based on his backscattering mechanism of return of the Z ray his results may not be directly used as evidence for or against the Papagiannis tilt model without reanalysis of the observational data. We shall look at Ellis's (1957) results more closely in Section 3.10.

E) The tilted layer ionosphere model of Papagiannis takes into account the zenith angle of the sun but appears to ignore the azimuth angle. However, since the Z ray must (at least up to the coupling level) travel within the

magnetic meridian plane in all but the most exceptional and unlikely circumstances, the azimuth angle of the the sun is of crucial importance to the success or otherwise of this model. Papagiannis has considered the N-S gradients caused by the latitudinal change in the sun's zenith angle without taking into account the inseparably concomitant and comparable magnitude E-W gradients caused by the longitudinal change in the sun's zenith angle. Curiously enough when discussing evidence for horizontal electron density gradients, Papagiannis states "Steep EW gradients are almost always observed near sunrise and sunset at low and mid-latitudes (HUGUENIN and PAPAGIANNIS,1965)." and near sunrise is where Bowman (1960) found the peak occurrence of the Z echo at Hobart with a second smaller peak towards sunset.

The tilt model proposed by Papagiannis will work only when the sun's rays lie in the magnetic meridian plane. Give that the declination at Hobart is about 13°E and the longitude 147.5°E (time zone based on 150°E) one would expect to see Z mode occurring most frequently on the 1100, 1115 and 1130 hrs. LMT ionograms if this theory is correct; not in the afternoon as indicated by Papagiannis when applying his theory to Hobart. If we alter the time of day to late morning we can assume the zenith angle of the sun to be about 50° and substitution into Eqn.3.1 gives us an answer of about 15.5° rather than the required 18°±0.5°.

The time of day (early afternoon) chosen by Papagiannis when substituting the parameters appropriate to Ellis's observations into his equation is not the time of day when Ellis reported recording Z echoes. Ellis (1953b) states "In all cases the observations were made between 1500 and 1800 hours L.M.T. .....". Ellis (1956) tabulates his results and by weighting the observation times by the appropriate number of observations we find that the average time of observation is 1646 hours LMT, all observations occurring between 1500 and 1800 hours. An equinox zenith angle (although some results are from winter months which would increase the zenith angle) more appropriate to this time of day would be about 80° and sustituting this into Eqn.3.1 we find that α now has a value of 31° which is far too large an answer. An equinox zenith angle of 60° as used by Papagiannis corresponds to about 1400 hours which is an hour earlier than the earliest of Ellis's published observations.

It can be seen from the points raised that not only has Papagiannis's tilt model been applied at a time other than when the sun's rays lie in the magnetic meridian but also that the "near perfect numerical agreement" vanishes when we substitute a solar zenith angle more appropriate to the actual conditions of Ellis's observations. Nevertheless, despite the demonstrated shortcomings, it is an interesting idea and it is worth examining whether it might not have some relevance if

correctly applied. Ionospheric stations Hobart, Macquarie Island and Brisbane are the locations which will be considered for application of the solar zenith angle tilt model. Transforming Eqn.3.1 we obtain the following expression for χ

$$\chi = \arctan\left[\frac{R}{H.\tan^3\omega} \cdot \left(\frac{\ln(1+Y)}{2}\right)^{1/2}\right] \qquad 3.3$$

from which we can calculate the solar zenith angle required to produce the $\propto$ appropriate to the dip angle of the location in question. Tabulating the required results for various Y values at the three stations we have

STATION/(ω)	Y = ...	1/6	1/3	1/2	2/3
MACQUARIE I./(78°)	χ = ...	19°	25°	29°	32°
HOBART/(72°)	χ = ...	51°	59°	63°	66°
BRISBANE/(57°)	χ = ...	85°	86°	87°	87°

We see that Z mode echoes at Brisbane would be expected shortly after dawn and shortly before sunrise. As the declination at Brisbane is about 10°E the sun's rays lie nowhere near the magnetic meridian at these times and we would not expect this mechanism to be responsible for any Z echoes at Brisbane. An examination of world maps of magnetic dip and declination show that this mechanism could not produce Z echoes at any time of the day at any time of the year over quite a large area of the earth including all locations of less than 30° geographic latitude. This automatically excludes the mechanism operating at all at many places where the Z mode is a well known, if relatively infrequent, occurrence such as

Brisbane (Bowman,1960) and India (Toshniwal,1935; Banerji,1952; Satyanarayana et al.,1959). Consider now high latitude stations where the Z mode is a well known and relatively frequent occurrence, such as Macquarie Island. Macquarie Island's declination is 27°E and its minimum solar zenith angle of 31° occurs at noon, summer solstice. The tabulated results indicate that this mechanism could be responsible for Macquarie Island Z echoes only at frequencies no higher than 2 MHz at mid to late morning at summer solstice. Fig.3.36 is an excellent example of Z echo at F2 frequencies at Macquarie Island. Figs.3.20 and 3.22 show the 1951 diurnal and 1953 seasonal variation of Macquarie Island Z echo. This mechanism is clearly unable to account for Macquarie Island Z echo occurrence. The Z echo also occurs relatively frequently at Hobart whose latitude falls between that of Brisbane and Macquarie Island. Papagiannis's solar zenith angle tilt mechanism can probably provide Z echo at Hobart for about half the year but only at one particular frequency on any given day and only at about 1115 hours LMT. The approximate annual variation of the allowed frequency is plotted in Fig.3.37. Reference to Figs.3.20,3.22 and published Hobart ionograms (e.g. Newstead,1948; Bowman,1960) will respectively show a morphology of the Hobart Z echoes and actual examples which cannot be explained by this tilt mechanism.

Clearly then, even if this mechanism were to function adequately in the F2 region (which is unlikely) it is of such

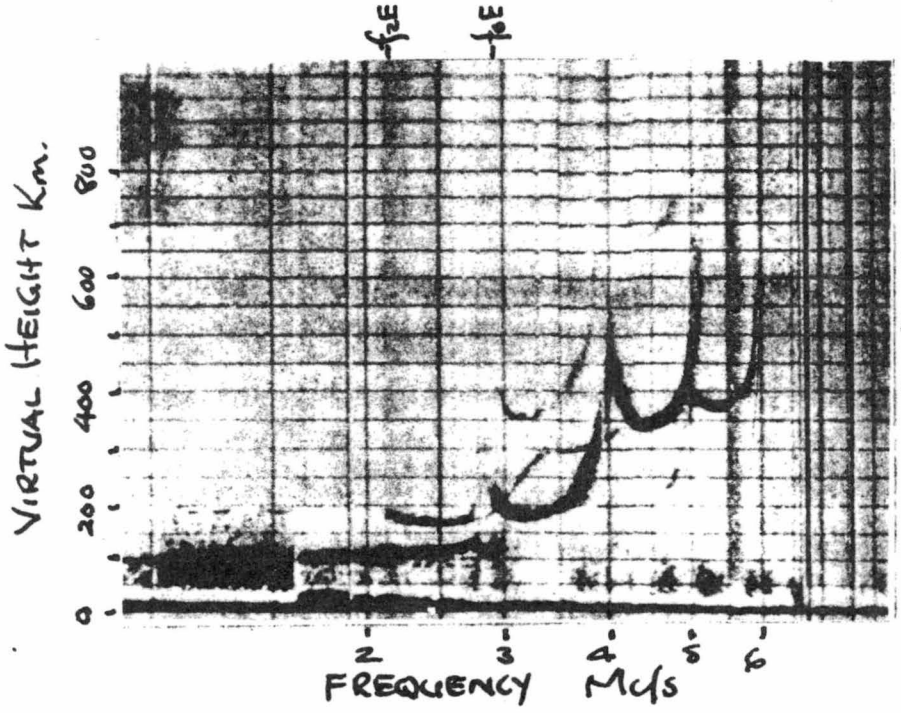

P'f Record of 1020 hours; 22-12-50, Macquarie Is., showing split Z trace at f_0E.

Geographic Coordinates
54·5°S 160°E

Magnetic Coordinates
61°S 243°E

FIG. 3.36 (Fig.24 of 'Ellis, 1954)

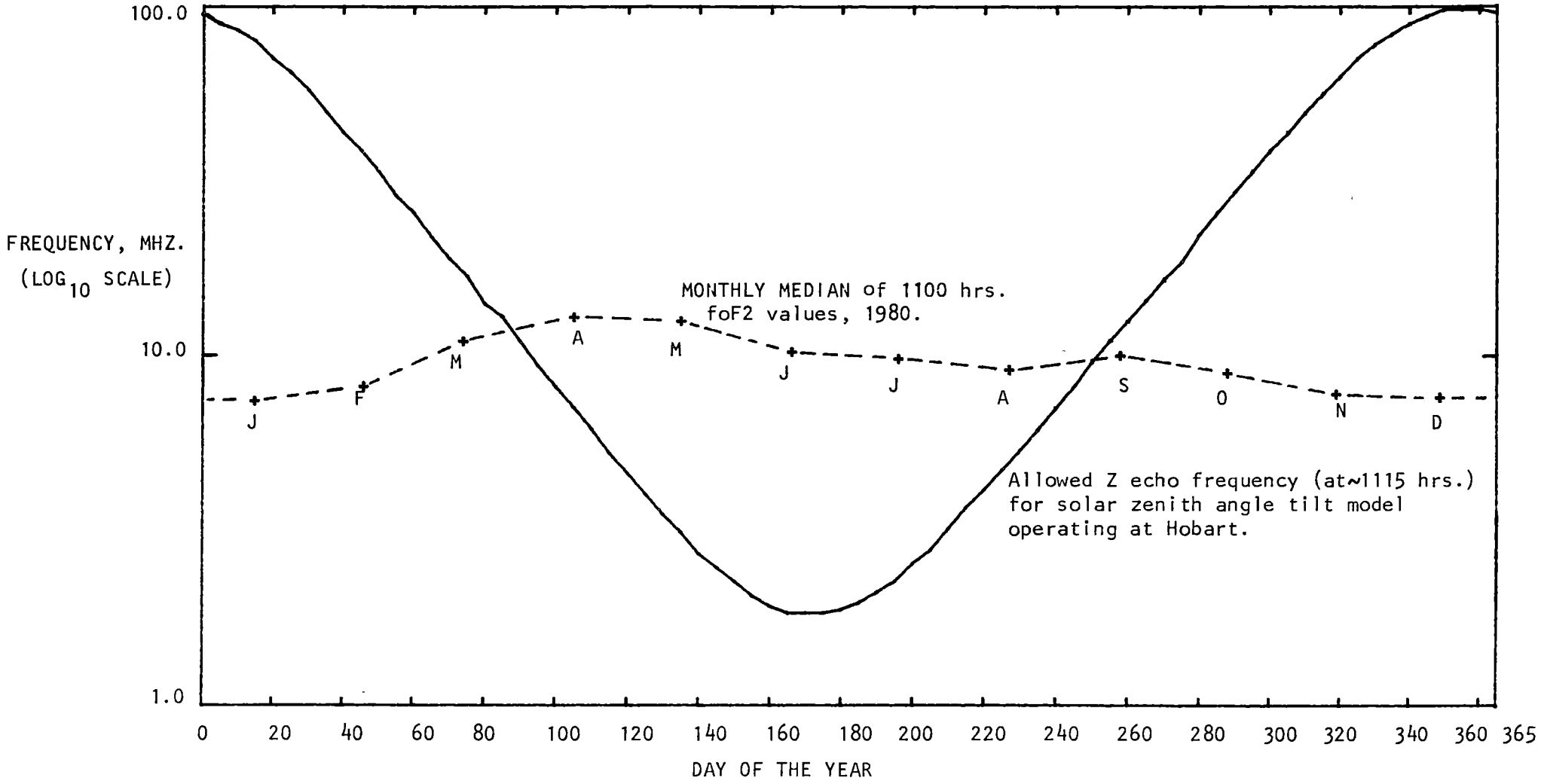

FIG.3.37 Annual variation of allowed frequency for Z echoes if solar zenith angle tilt model is operating at Hobart (latitude 43°S, dip angle 72°).

limited application that it would be a highly optimistic estimate which would allow it to account for even one percent of global Z echo occurrences. Since the electron density profile model used by Papagiannis is known to be a generally inadequate model for the F2 layer, it was thought worthwhile to examine world FoF2 maps with a view to establishing whether favourable N-S tilts of the type proposed might be expected to occur over Hobart, bearing in mind that the magnetic east-west tilt would be required to be very small. Two of the maps examined are shown in Figs.3.38 and 3.39. Upon superficial examination a couple of regions on the maps appeared to be suitable candidates but a few calculations based on the separation and values of adjacent contour lines demonstrated that there would need to be completely unrealistic variations in height with latitude of the various plasma frequency levels in order to provide the needed tilts.

Papagiannis's proposal for experimental testing of his theory by a system of sounders located along the magnetic meridian would have some problems in that in the presence of the Z echo returned by his tilt mechanism the sounders would no longer be sounding overhead nor would his sounders remain interlaced by deflection of O and X modes. The situation would be practically the same as sounding a plane horizontally stratified ionosphere at the dip pole with the main difference being that the ground plane would not be parallel to the ionosphere. This difference does not alter in any way the

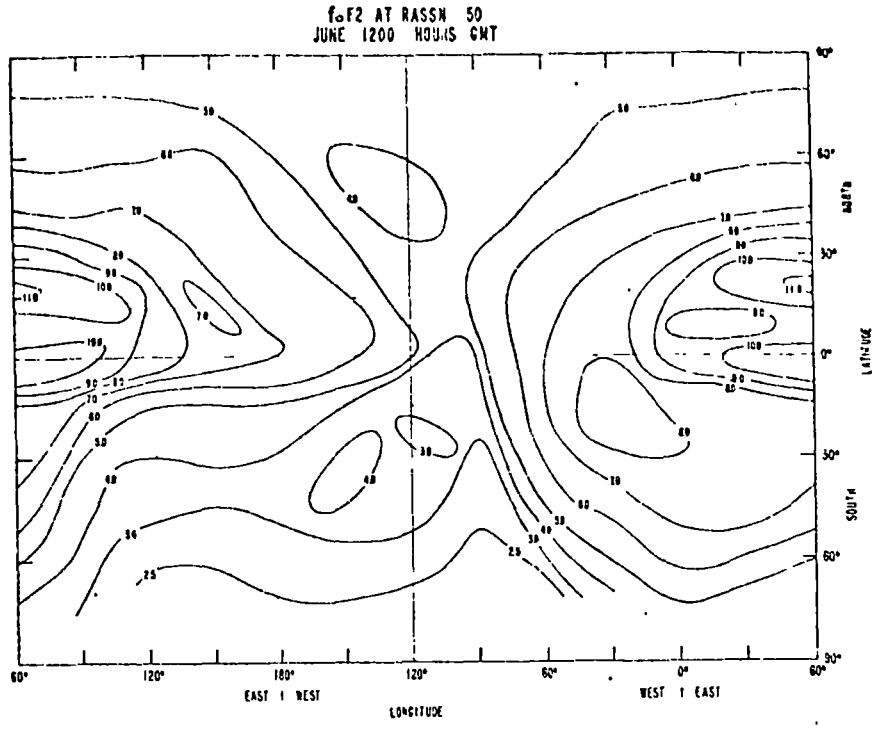

FIG.3.38 *World map of f_0F_2, June.*

(After D. H. Zacharisen, 1959, World maps of F2 critical frequencies and maximum usable frequency factors, NBS Tech. Note 2 (Apr. 1959), and NBS Tech. Note 2/2 (Oct. 1960).

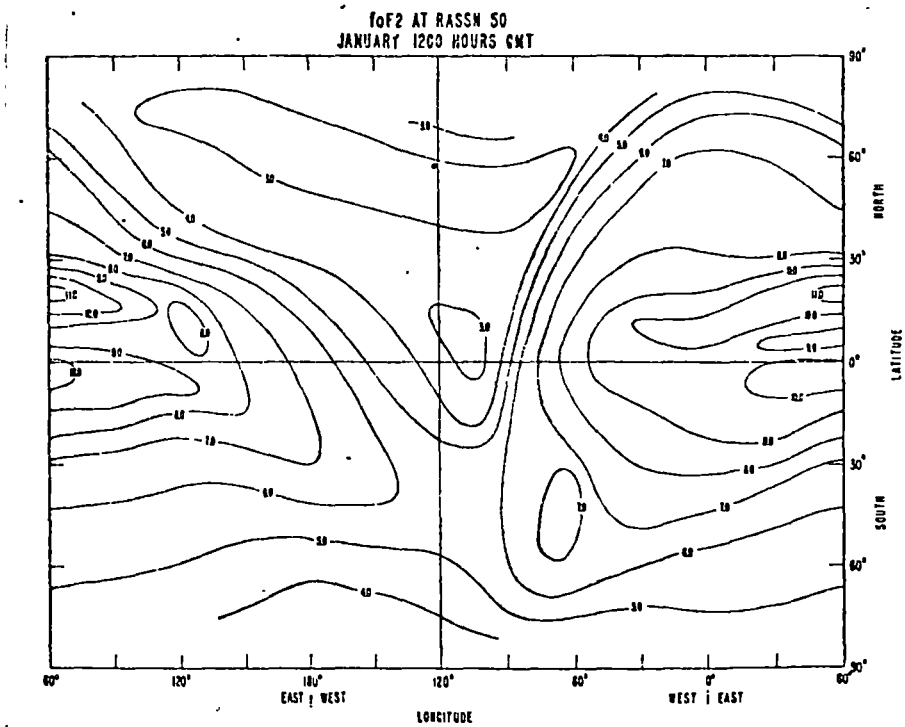

FIG.3.39 *World map of f_0F_2, January.*

(After D. H. Zacharisen, 1959, World maps of F2 critical frequencies and maximum usable frequency factors, NBS Tech. Note 2 (Apr. 1959), and NBS Tech. Note 2/2 (Oct. 1960).)

(Figs.3.24a and b of Davies,1965)

results which would be obtained by a receiver/transmitter ionosonde. A much simpler and less ambiguous test would be to measure the angle of arrival of the Z echo. This is precisely what Ellis did and as previously stated he found the angle of arrival of the Z echo to be consistently about 9°N of zenith and in the magnetic meridian. Ellis observed no angles of arrival at or near 18°N of zenith, the angle predicted by Papagiannis's solar zenith angle tilt model.

If a detailed global study of the occurrence of the Z echo were undertaken it would be interesting to calculate the times, days and frequencies for which Papagiannis's model would be expected to work in the E and F1 regions at the various locations and to see if any increased occurrence of Z echo occurred under these conditions. The varied range of declination and dip values found at a given geographic latitude would facilitate the isolation of this effect.

3.9 Return Of The Z Ray - Papagiannis And Miller

Papagiannis and Miller (1969) discussed Ellis's postulate of strong backscattering at the reflection level. They stated "PITTEWAY(1959) objects to this scheme on the grounds that backscattering would not be sufficiently large at a level where the index of refraction is much smaller than unity" and considered another difficulty with the backscattering to be

"....the fact that Z-mode echoes are received over a fairly wide range (1 MHz) of transmitted frequencies. This implies that conditions of strong backscattering also exist at lower heights heights, while Z-mode echoes of higher frequencies appear to propagate undisturbed in these regions." They then proposed the alternative explanation of a favourable tilting of the ionospheric layers, stating that "BOWMAN(1960), on a basis of experimental observations, and PAPAGIANNIS(1965), on the basis of a theoretical analysis have shown independently that this could be the mechanism which allows the return of the Z-mode echoes. Supporting evidence of this mechanism also comes from the fact that ionograms containing Z-mode echoes generally show a tilting of the ionospheric layers toward the equator (MEEK,1948; NEWSTEAD,1948; ELLIS,1957)." They considered that Ellis's (1957) analysis (for horizontal gradients) of Z echo ionograms and implied that the presence of measurable gradients supported the tilt theory.

Papagiannis and Miller then ray traced the Z-mode in a variety of tilted layer configurations of the ionosphere in order to obtain actual supporting evidence for the tilt mechanism. As coupling regions are not amenable to ray tracing techniques they incorporated the qualitqtive effects of the coupling cone by skipping the coupling zone in the ray tracing and simply continuing the rays from the two boundaries of the zone, using the chosen coupling angle ψ_c as the starting angle ψ. They developed a method for choosing the boundaries of the

zone and defining the boundary properties, and their ray tracing results showed that the thickness of the coupling zone is not a very critical parameter, thereby justifying their approximations and enabling them to adopt the following simplified version of their equation for the semithickness of the coupling zone

$$u_o = 1/2.Y.\sin\psi_o \qquad 3.3$$

where u_o is the semithickness of the coupling zone in terms of X and ψ_o is the coupling angle which the wave normal makes with the magnetic field at the two boundaries of the coupling region.

Papagiannis and Miller ray traced in the magnetic meridian over a spherical earth and employed a parabolic electron density profile. They made the maximum electron density (N_m) and the height (r_m) at which it occurs be functions of the horizontal coordinate so that they could obtain different types of tilted layers. By holding N_m and r_m constant they generated the typical horizontally stratified ionosphere, varying r_m only resulted in parallel tilted layers, and varing N_m only produced a wedge like layer formation. By varying N_m and r_m simultaneously they generated a combination of the wedge and tilt cases. Their equations describing the electron density variations are as follows :

$$N(r,\theta) = N_m(\theta)\left\{1-\left(\frac{r_m(\theta)-r}{2H}\right)^2\right\} \qquad 3.4$$

$$r_m(\theta) = r_m(\theta_o)\left\{1-a(\theta-\theta_o)\right\} \qquad 3.5$$

$$N_m(\theta) = N_m(\theta_o)\left\{\frac{1+b.r_m(\theta_o)(\theta-\theta_o)}{z_m(\emptyset)}\right\} \qquad 3.6$$

The values they substituted in the above formulae were $z_m(\emptyset)=r_m(\theta_o)-R_o=250km$; $R_o=6375km$; $N_m(\theta_o)=3x10^5 el/cc$; $\theta_o=33^o$; $H=50km$. For the Earth's magnetic field they used the standard dipole approximation.

They ray traced from X = 1 with the wave normal parallel to the magnetic field or from $X = 1+u_o$ with the wave normal at an angle ψ_o to the magnetic field. They also traced the Z mode downwards from X = 1 or $X = 1-u_o$ in order to establish the location of the transmitter at the ground level. They adjusted the ray tracing starting point along the X = 1 line in order to make rays of all frequencies have a common transmitting point at ground level.

Using a variety of values for the parameters a and b (which define the tilting of the layers), Papagiannis and Miller ray traced for possible Z mode returns. It is worth quoting their results and conclusions as reported in their paper.

"When a=b=0, no ray can return to the ground. When b=0 but $a\neq0$, i.e. in the case of paralell tilted layers, there is generally no ray of any frequency that can return to the ground; however, in the particular case when the layers are tilted at right angles to the magnetic field, i.e. when $a=\cot\omega$,

where ω is the dip angle of the magnetic field, the rays of practically all the frequencies return to the ground (Fig.3.40). This is almost identical to vertical propagation with a vertical magnetic field in a horizontally stratified ionosphere.

"On the other hand, when $a=0$, but $b\neq0$, i.e. in the case of a wedge-like layer formation, if b is within reasonable limits, there is a single ray, corresponding to a particular frequency, that returns to the ground, but rays of adjacent frequencies do not return (Fig.3.41). Actually one can obtain the return of a very narrow spectrum of rays, instead of a single ray, if the effect of the coupling cone at X = 1 is allowed for. In the more realistic case of $a\neq0$ and $b\neq0$, i.e. with layers that are tilted both with respect to the horizontal and to each other, we find that rays from a small range of frequencies ($\sim$0.1 MHz) can return (Fig.3.42). When the effect of the coupling cone at X = 1 is taken into consideration, the range of frequencies over which rays may return to the ground is substantially increased (Fig.3.43). In conclusion, when b tends to zero and a to $\cot\omega$ the spectral range of the Z mode echoes becomes very wide, whereas, when a tends to zero and b to some reasonable value it becomes very narrow; one can, therefore, expect to find some intermediate values of a and b which will allow the return of Z-mode echoes over a given spectral range.

"This is very nicely demonstrated in the ionograms of

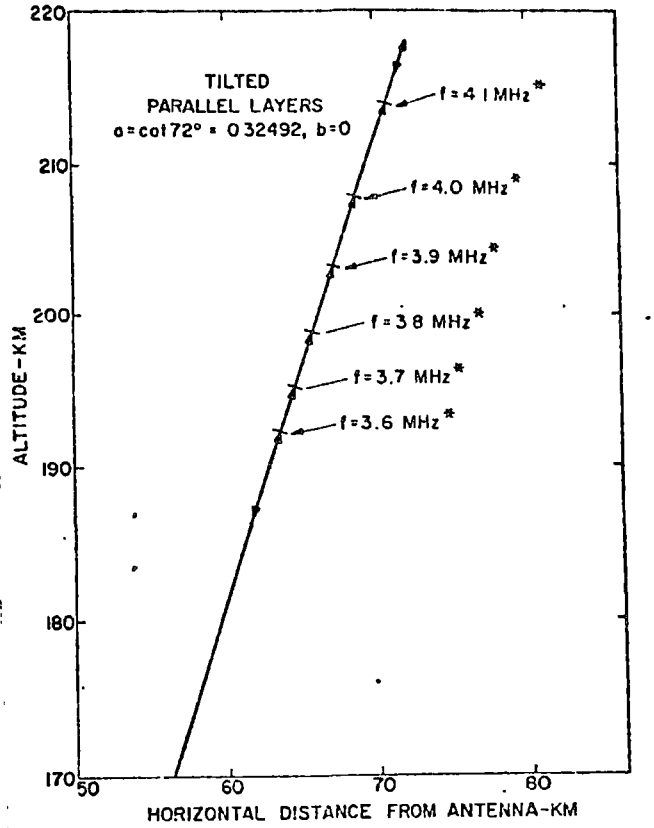

FIG.3.40

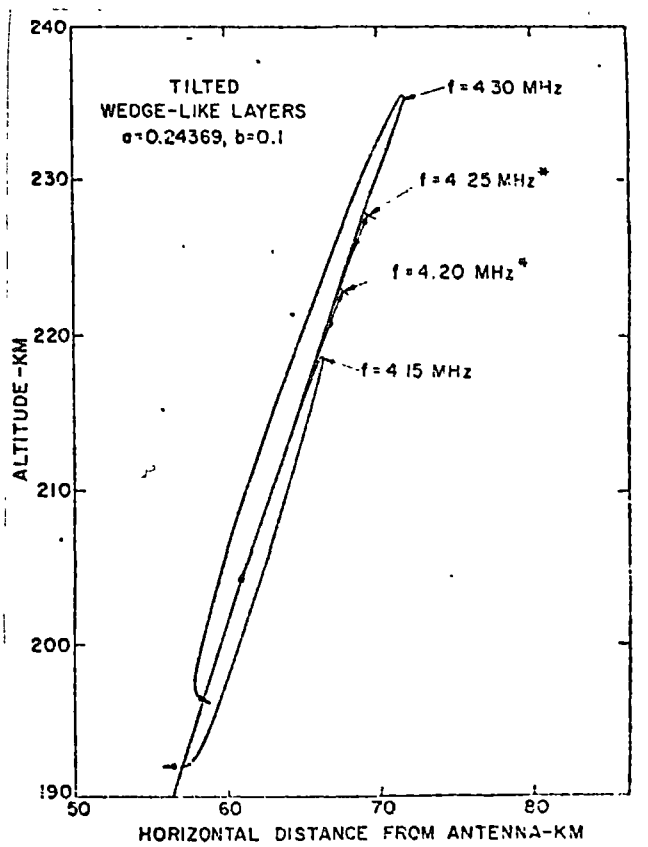

FIG.3.42

(Figs.2 and 4 of Papagiannis and Miller,1969)

FIG.3.43

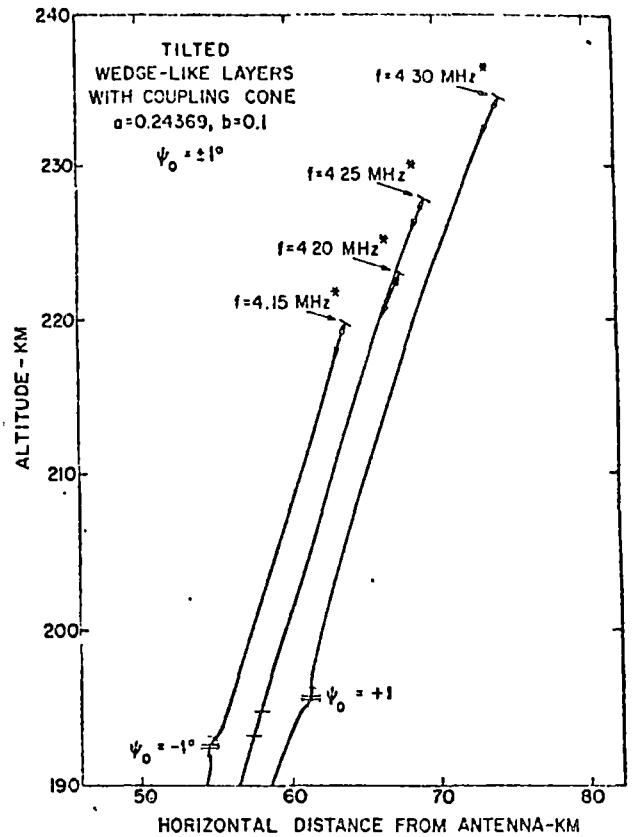

FIG.3.41

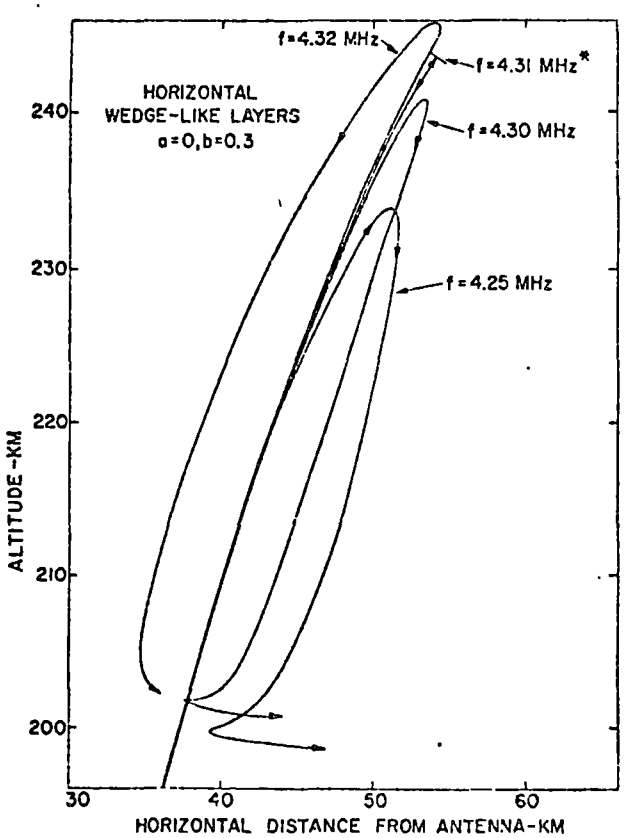

(Figs.5 and 3 of Papagiannis and Miller,1969)

Fig.3.44 which were obtained from the Wallops Island ionospheric station. In these ionograms the ordinary and extraordinary rays show the characteristic structure of spread-F, whereas the Z-mode has the appearance of a single clear echo. This in itself provides further support for the tilted layer theory because if backscattering were the predominant mechanism, one would expect to find a spread-F effect in the Z-mode also. During spread-F conditions it is believed that the F-layer assumes either a blobby (RATCLIFFE and WEEKES,1960) or a wavy (BOWMAN,1960a) structure. As a result, the ordinary and extraordinary modes are reflected at many points, producing the spread-F effect. However, the ionograms of Fig.3.44 show that there is only one possible path for the Z-mode echoes which do not show a spread-F effect. It is also known that the appearance of Z-mode echoes, especially over a wide spectral range, is an infrequent phenomenon, and our ray-tracing analysis has shown that a special combination of the tilting parameters a and b is required for the Z-mode echoes to return to the ground. The appropriate combinations of a and b are rather rare but in the case of spread-F where we have a varied structure of the ionosphere it is far more likely to find the appropriate tilting that provides the necessary single path for the return of the Z-mode echoes. This last conclusion is in agreement with the ionograms of Fig.3.44 and yield strong support to the tilted layer theory."

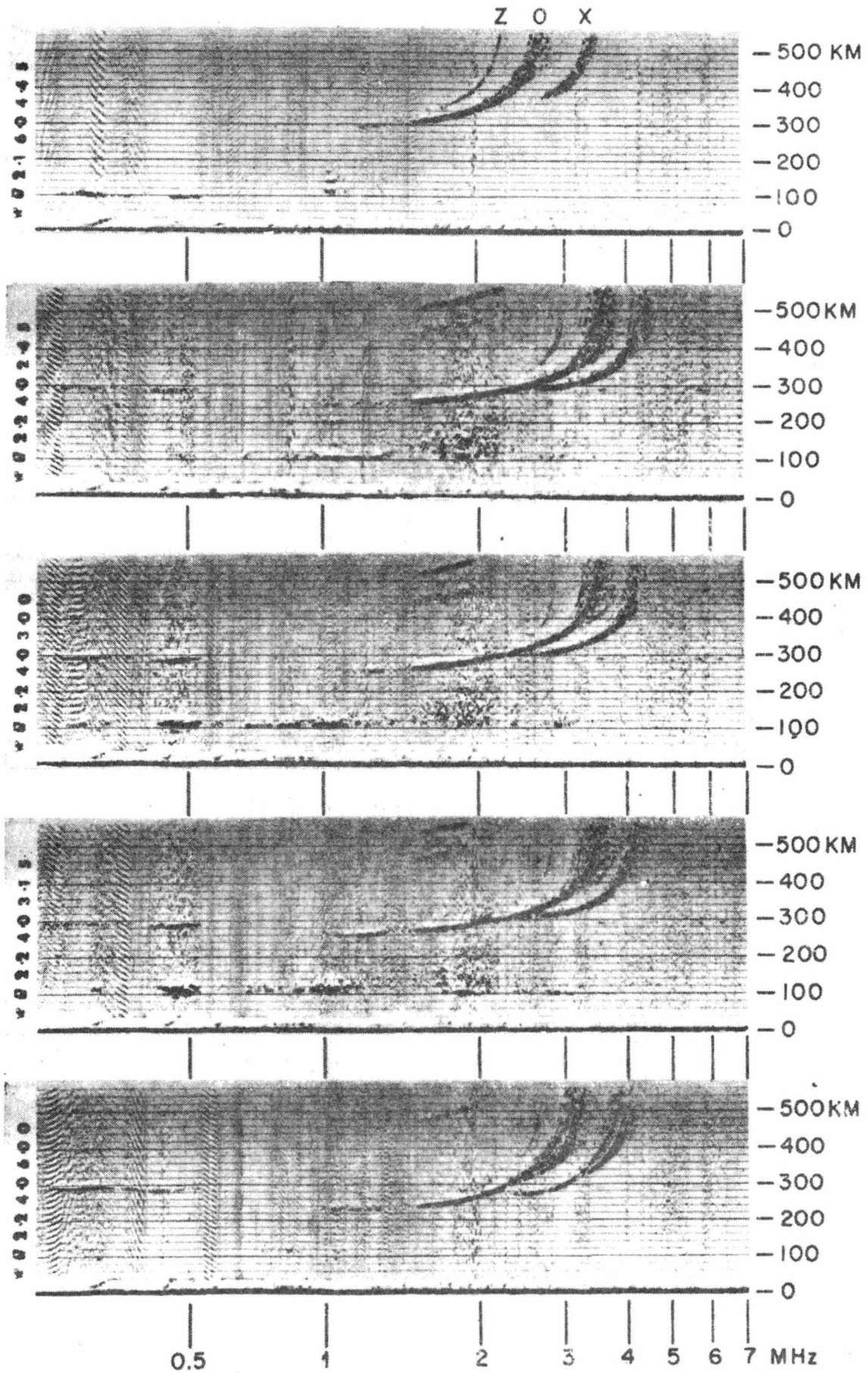

FIG. 3.44 Wallops Island ionograms showing Z echo.
(Fig.6 of Papagiannis and Miller, 1969)

3.10 Critical Discussion

Papagiannis and Miller, through their ray tracing and definition of appropriate electron density profiles, have provided us with a satisfactory, well explored model for the tilt mechanism of return of the Z ray. They have recognized the need to confine the Z mode within the magnetic meridian plane and have established the conditions under which a reasonable range of Z mode frequencies would be returned. This is the model by which the tilt mechanism should be judged. The ray tracing method uses well accepted techniques (i.e. numerical integration of Haselgrove differential ray equations) and their clever, innovative method of skipping the coupling region appears from their reported results to be eminently satisfactory for their particular application. Where comparison is appropriate, the behaviour of their Z rays appears to be in general agreement with the ray tracing of Lockwood (1962). While there are no apparent difficulties with their model and results, some objections could be raised when considering their general discusion of the problem and the conclusions drawn from their results. These are as follows :

A) The experimental results of Bowman (1960) and theoretical results of Papaagiannis (1965) do not demonstrate that the tilt mechanism is a likely contender to produce Z echoes, as has been shown by the discussion in Sections 3.6 and 3.8. Although it has been shown to be a

possible Z ray return mechanism it has not been established that it is likely.

B) Pitteway (1959) did not specifically reference Ellis's Z mode return mechanism and his work is not exhaustive of backscattering possibilities, as discussed in Section 3.4. Papagiannis and Miller's comment perhaps follows the lead given by Ratcliffe (1959) in his discussion of the Z mode. Ratcliffe states (p.129) "If, however, there are irregularities in the electron distribution near the level where X = 1+Y, where μ (real part of refractive index) is small, there will be strong† backwards scattering and an appreciable part of the energy will return along the incident path." to which he adds the footnote " †More recent work (Pitteway,1958) seems to indicate, however that backscattering would *not* be accentuated at a level where μ was small."

Establishing that a proposed scattering resonance (Booker,1955) would be suppressed because of the expected collision frequency is quite another matter to establishing that no backscattering mechanism can give rise to the Z echo. Ellis did not propose a scattering resonance and, as discussed, if Briggs and Phillips (1950) scintillation irregularities could produce spread-F as postulated by Renau then there is no reason why sufficient Z mode energy might not be reflected back along the incident path.

C) The claim that ionograms containing Z mode echoes generally show a tilting of the ionospheric layers was made previously by Papagiannis (1965) and has been discussed in Section 3.8. Again no direct evidence or analysis of ionograms is given in support of this contention. Papagiannis and Miller claim that Ellis's (1957) results support their tilt proposal and further claim that the 5 examples out of 23 which do not support it "...are propbably the result of small (less than 1 per cent) reading errors of the critical frequencies from the ionograms." They show how a small change in the critical frequencies can alter a large negative horizontal gradient to a positive gradient. They do not state why the 18 cases of positive gradient should not turn out to be large negative horizontal gradients as a result of small reading errors of the critical frequencies. As already pointed out in Section 3.8, Ellis (1957) analysed the ionograms on the assumption that the Z echo was occurring in an essentially flat ionosphereand his equations must be radically altered if they are to be applied to the tilt/wedge model of Papagiannis and Miller. Until Papagiannis and Miller reanalyse these or similar ionograms taking tilts into account they cannot conclude whether or not such ionograms support the tilt theory. As a matter of interest, it is worth examining the magnitude of the tilts which might be represented by the horizontal electron density gradients deduced by Ellis. As a first

approximation it shall be assumed that the peak height of the layer is constant and that the electron density varies parabolically as assumed by Papagiannis and Miller. The expression for electron density is then

$$N(x,h) = N_m(x)\left\{1-\left\{\frac{h_m-h}{pH}\right\}^2\right\} \qquad 3.7$$

$$N_m(x) = N_m(x_o) + m^*(x-x_o) \qquad 3.8$$

where x is the horizontal coordinate in km., positive towards the equator; h is the height in km. above the Earth's surface; H is the scale height (=50km. as assumed by Papagiannis and Miller); h_m is the peak height as calculated by Ellis; $N_m(x_o)$ is the overhead peak electron density as calculated from the Z mode critical frequency of Ellis; m^* is the horizontal electron density gradient in el/cc[km]$^{-1}$ as calculated from the gradient m in c/s[km]$^{-1}$ deduced by Ellis (m^* is positive for peak electron density increasing towards the equator); p equals 2 or 3 for parabolic ionospheres of semithickness 100 and 150 km. respectively; x_o is the horizontal coordinate of the Z mode reflection point. We determine m^* from

$$m^* = \frac{2mf_o}{80.5}$$

where f_o is the O mode critical frequency, in MHz.

To determine the tilt of a layer of given electron density N_X at a given x coordinate we put $N(x,h) = N_X$ = const. X (plasma frequency) is calculated from.

the corresponding N_X and the critical frequency of the Z mode. We now transform the Equation 3.7 to

$$h = h_m - pH\sqrt{1 - \frac{N_X}{N_m(x)}} \qquad 3.9$$

from which the tilt at the x coordinate corresponding to the Z mode reflection point is given by

$$\text{tilt}(x_o, X) = \arctan\left(\frac{pHm^* N_X}{2\sqrt{1 - \frac{N_X}{N_m(x_o)}}\, N_m^2(x_o)}\right) \qquad 3.10$$

The tilts for parabolic ionospheres of semithickness 100 km. and 150 km. were calculated for the levels X = 1, X = 1+0.5Y, x = 1+0.9Y, X = 1+0.95Y, X = 1+0.99Y, X = 1+0.995Y and X = 1+0.999Y (f=fz) for each of Ellis's results. The calculations are tabulated in Tables 3.1 to 3.7. The contours of equal electron density are vertical at the very peak but the tilts become relatively small only a few kilometres below the peak. It would appear from the tables that the tilts are too small (except so close to the peak over such a short distance that the effect is more akin to backscattering over an extremely narrow frequency range e.g <0.005 MHz) to cause Z mode reflection back along the incident path. This is verified by ray tracing in Section 3.11.

The Ellis (1957) results claimed by Papagiannis and Miller to support the tilt return theory actually demonstrate that the necessary favourable gradients are

TABLE 3.1

TILT AT LEVEL WHERE X = 1 + 0.999Y -INPUT DATA FH,FZ,m FROM ELLIS (1957)

FH	FZ	NMAX	m	DELTAN	NX999	DX999 (2H)	DX999 (3H)	TILT (2H)	TILT (3H)
1.530	2.45	121130	305	22.7	121083	1.961	2.941	25.5	35.6
1.550	2.75	146894	-190	-16.1	146841	1.899	2.848	-16.1	-23.4
1.560	2.63	136890	-140	-11.4	136839	1.930	2.894	-12.2	-17.9
1.550	2.40	117763	-285	-21.6	117717	1.981	2.971	-24.8	-34.8
1.540	3.02	171070	350	31.2	171013	1.838	2.757	26.4	36.7
1.510	2.48	122921	480	35.8	122875	1.945	2.918	36.8	48.3
1.530	2.22	103416	620	42.1	103373	2.020	3.030	45.2	56.5
1.530	2.16	99011	250	16.8	98970	2.036	3.054	22.6	32.0
1.560	2.78	149878	67	5.7	149824	1.896	2.844	5.7	8.6
1.520	1.97	85407	320	19.9	85370	2.087	3.130	29.2	39.9
1.525	2.27	107014	690	51.4	106971	2.005	3.007	50.1	60.9
1.530	2.33	111724	360	26.9	111679	1.991	2.986	31.2	42.2
1.520	1.85	77447	275	16.4	77412	2.124	3.186	26.5	36.8
1.520	1.86	78096	590	34.7	78061	2.121	3.181	46.3	57.5
1.550	1.80	74906	730	41.0	74872	2.151	3.227	51.8	62.3
1.510	2.43	118934	122	9.2	118888	1.958	2.937	11.2	16.5
1.540	2.26	106683	-540	-40.0	106639	2.013	3.020	-43.0	-54.4
1.545	2.35	113704	600	42.8	113659	1.992	2.987	43.4	54.8
1.540	2.30	109714	120	8.8	109670	2.003	3.004	11.3	16.7
1.545	2.26	106823	-410	-30.3	106780	2.015	3.023	-35.1	-46.5
1.535	2.32	111100	180	13.1	111056	1.995	2.993	16.5	23.9
1.505	2.32	110236	60	4.3	110192	1.984	2.975	5.6	8.4
1.535	2.44	120464	320	23.9	120437	1.965	2.948	26.8	37.1

KEY: FH -GYRO FREQUENCY,MHZ; FZ -Z CRITICAL FREQUENCY,MHZ; NMAX -PEAK ELECTRON DENSITY,el/cc; DELTAN -NS HORIZONTAL CHANGE IN PEAK ELECTRON DENSITY PER KM, el/cc[km] ; NX999 -ELECTRON DENSITY AT X = 1+0.999Y, el/cc; DX999 -DEPTH OF NX999 LAYER BELOW FZ POINT, KM; 2H,3H - PARABOLIC ELECTRON DENSITY PROFILE OF SEMI-THICKNESS 2H OR 3H FROM THE BASE (X = 0) TO THE PEAK; FZ POINT -POINT OF REFLECTION OF CRITICAL FREQUENCY Z RAY (AT THE IONOSPHERE PEAK); H -SCALE HEIGHT (=50km); m -NS HORIZONTAL GRADIENT OF PEAK ELECTRON DENSITY, c/s per km.; TILT -TILT OF THE NX999 LAYER, DEG.

TABLE 3.2

TILT AT LEVEL WHERE X = 1 -INPUT DATA FH,FZ,m FROM ELLIS(1957)

FH	FZ	NMAX	m	DELTAN	NX10	DX10 (2H)	DX10 (3H)	TILT (2H)	TILT (3H)
1.530	2.45	121130	305	22.7	74565	62.002	93.003	0.5	0.8
1.550	2.75	146894	-190	-16.1	93944	60.039	90.058	-0.3	-0.5
1.560	2.63	136890	-140	-11.4	85924	61.018	91.526	-0.2	-0.4
1.550	2.40	117763	-285	-21.6	71552	62.642	93.963	-0.5	-0.8
1.540	3.02	171070	350	31.2	113296	58.114	87.170	0.6	0.9
1.510	2.48	122921	480	35.8	76402	61.518	92.277	0.8	1.3
1.530	2.22	103416	620	42.1	61222	63.875	95.812	1.1	1.6
1.530	2.16	99011	250	16.8	57957	64.392	96.588	0.4	0.7
1.560	2.78	149878	67	5.7	96004	59.954	89.931	0.1	0.2
1.520	1.97	85407	320	19.9	48209	65.995	98.992	0.6	0.9
1.525	2.27	107014	690	51.4	64011	63.391	95.087	1.3	1.9
1.530	2.33	111724	360	26.9	67439	62.958	94.437	0.7	1.0
1.520	1.85	77447	275	16.4	42515	67.159	100.739	0.5	0.7
1.520	1.86	78096	590	34.7	42976	67.060	100.590	1.0	1.6
1.550	1.80	74906	730	41.0	40248	68.021	102.032	1.2	1.9
1.510	2.43	118934	122	9.2	73352	61.907	92.861	0.2	0.3
1.540	2.26	106683	-540	-40.0	63448	63.660	95.490	-1.0	-1.5
1.545	2.35	113704	600	42.8	68602	62.981	94.472	1.0	1.5
1.540	2.30	109714	120	8.8	65714	63.328	94.992	0.2	0.3
1.545	2.26	106823	-410	-30.3	63448	63.722	95.582	-0.8	-1.1
1.535	2.32	111100	180	13.1	66862	63.102	94.653	0.3	0.5
1.565	2.32	110236	60	4.3	66862	62.727	94.090	0.1	0.2
1.535	2.44	120484	320	23.9	73957	62.142	93.213	0.6	0.8

KEY: FH,FZ,NMAX,m,DELTAN,FZ POINT,2H,3H AS FOR TABLE 3.1; NX10 -ELECTRON DENSITY AT X = 1, el/cc; DX10 -DEPTH OF NX10 LAYER BELOW FZ POINT, KM; TILT -TILT OF NX10 LAYER, DEG.

TABLE 3.3

TILT AT LEVEL WHERE X = 1 + 0.5Y -INPUT DATA FH,FZ,m FROM ELLIS(1957)

FH	FZ	NMAX	m	DELTAN	NX15	DX15 (2H)	DX15 (3H)	TILT (2H)	TILT (3H)
1.530	2.45	121130	305	22.7	97847	43.842	65.763	1.0	1.5
1.550	2.75	146894	-190	-16.1	120419	42.454	63.681	-0.6	-0.9
1.560	2.63	136890	-140	-11.4	111407	43.146	64.719	-0.5	-0.7
1.550	2.40	117763	-285	-21.6	94658	44.295	66.442	-1.0	-1.4
1.540	3.02	171070	350	31.2	142183	41.093	61.639	1.1	1.6
1.510	2.48	122921	480	35.8	99662	43.500	65.250	1.6	2.3
1.530	2.22	103416	620	42.1	82319	45.166	67.750	2.1	3.1
1.530	2.16	99011	250	16.8	78484	45.532	68.298	0.8	1.3
1.560	2.78	149878	67	5.7	122941	42.394	63.591	0.2	0.3
1.520	1.97	85407	320	19.9	66808	46.665	69.998	1.1	1.7
1.525	2.27	107014	690	51.4	85512	44.824	67.237	2.5	3.7
1.530	2.33	111724	360	26.9	89581	44.518	66.777	1.2	1.9
1.520	1.85	77447	275	16.4	59981	47.489	71.233	1.0	1.5
1.520	1.86	78096	590	34.7	60536	47.419	71.128	2.1	3.1
1.550	1.80	74906	730	41.0	57577	48.098	72.147	2.5	3.8
1.510	2.43	118934	122	9.2	96143	43.775	65.662	0.4	0.6
1.540	2.26	106683	-540	-40.0	85065	45.015	67.522	-1.9	-2.9
1.545	2.35	113704	600	42.8	91153	44.534	66.802	1.9	2.9
1.540	2.30	109714	120	8.8	87714	44.780	67.169	0.4	0.6
1.545	2.26	106823	-410	-30.3	85136	45.058	67.587	-1.4	-2.2
1.535	2.32	111100	180	13.1	88981	44.620	66.930	0.6	0.9
1.505	2.32	110236	60	4.3	88549	44.354	66.532	0.2	0.3
1.535	2.44	120484	320	23.9	97221	43.941	65.912	1.0	1.6

KEY: FH,FZ,NMAX,m,DELTAN,FZ POINT,2H,3H AS FOR TABLE 3.1; NX15 -ELECTRON DENSITY AT X = 1+0.5Y, el/cc; DX15 -DEPTH OF NX15 LAYER BELOW FZ POINT, KM; TILT -TILT OF NX15 LAYER, DEG.

TABLE 3.4
TILT AT LEVEL WHERE X = 1 + 0.9Y -INPUT DATA FH,FZ,m FROM ELLIS(1957)

FH	FZ	NMAX	m	DELTAN	NX19	DX19 (2H)	DX19 (3H)	TILT (2H)	TILT (3H)
1.530	2.45	121030	305	22.7	116473	19.607	29.410	2.6	3.9
1.550	2.75	146894	-190	-16.1	141599	18.986	28.479	-1.6	-2.4
1.560	2.63	136890	-140	-11.4	131794	19.295	28.943	-1.2	-1.8
1.550	2.40	117763	-285	-21.6	113142	19.809	29.714	-2.5	-3.8
1.540	3.02	171070	350	31.2	165293	18.377	27.566	2.7	4.1
1.510	2.48	122921	480	35.8	118269	19.454	29.181	4.1	6.2
1.530	2.22	103416	620	42.1	99196	20.199	30.299	5.5	8.3
1.530	2.16	99011	250	16.8	94905	20.363	30.544	2.3	3.4
1.560	2.78	149878	67	5.7	144490	18.959	28.439	0.6	0.8
1.520	1.97	85407	320	19.9	81687	20.869	31.304	3.1	4.6
1.525	2.27	107014	690	51.4	102713	20.046	30.069	6.6	9.8
1.530	2.33	111724	360	26.9	107295	19.909	29.864	3.3	5.0
1.520	1.85	77447	275	16.4	73954	21.238	31.857	2.7	4.1
1.520	1.86	78096	590	34.7	74584	21.206	31.809	5.7	8.5
1.550	1.80	74906	730	41.0	71440	21.510	32.265	6.9	10.3
1.510	2.43	118934	122	9.2	114376	19.577	29.365	1.1	1.6
1.540	2.26	106683	-540	-40.0	102359	20.131	30.197	-5.1	-7.6
1.545	2.35	113704	600	42.8	109194	19.916	29.875	5.2	7.8
1.540	2.30	109714	120	8.8	105314	20.026	30.039	1.1	1.7
1.545	2.26	106823	-410	-30.3	102486	20.151	30.226	-3.9	-5.8
1.535	2.32	111100	180	13.1	106676	19.955	29.932	1.6	2.4
1.505	2.32	110236	60	4.3	105898	19.836	29.754	0.5	0.8
1.535	2.44	120484	320	23.9	115831	19.651	29.477	2.8	4.2

KEY: FH,FZ,NMAX,m,DELTAN,FZ POINT,2H,3H AS FOR TABLE 3.1; NX19 -ELECTRON DENSITY AT X = 1+0.9Y, el/cc; DX19 -DEPTH OF NX19 LAYER BELOW FZ POINT, KM; TILT -TILT OF NX19 LAYER, DEG.

TABLE 3.5

TILT AT LEVEL WHERE X = 1 + Ø.95Y -INPUT DATA FH,FZ,m FROM ELLIS(1957)

FH	FZ	NMAX	m	DELTAN	NX95	DX95 (2H)	DX95 (3H)	TILT (2H)	TILT (3H)
1.530	2.45	121130	305	22.7	118802	13.864	20.796	3.8	5.7
1.550	2.75	146894	-190	-16.1	144246	13.425	20.138	-2.3	-3.4
1.560	2.63	136890	-140	-11.4	134342	13.644	20.466	-1.7	-2.6
1.550	2.40	117763	-285	-21.6	115453	14.007	21.011	-3.7	-5.5
1.540	3.02	171070	350	31.2	168182	12.995	19.492	3.9	5.9
1.510	2.48	122921	480	35.8	120595	13.756	20.634	5.9	8.9
1.530	2.22	103416	620	42.1	101306	14.283	21.424	7.9	11.8
1.530	2.16	99011	250	16.8	96958	14.399	21.598	3.3	4.9
1.560	2.78	149878	67	5.7	147184	13.406	20.109	0.8	1.2
1.520	1.97	85407	320	19.9	83547	14.757	22.135	4.4	6.6
1.525	2.27	107014	690	51.4	104864	14.175	21.262	9.4	14.0
1.530	2.33	111724	360	26.9	109510	14.078	21.117	4.8	7.2
1.520	1.85	77447	275	16.4	75700	15.017	22.526	3.9	5.9
1.520	1.86	78096	590	34.7	76340	14.995	22.493	8.2	12.3
1.550	1.80	74906	730	41.0	73173	15.210	22.815	10.0	14.8
1.510	2.43	118934	122	9.2	116655	13.843	20.764	1.6	2.4
1.540	2.26	106683	-540	-40.0	104521	14.235	21.352	-7.4	-11.0
1.545	2.35	113704	600	42.8	111449	14.083	21.125	7.5	11.1
1.540	2.30	109714	120	8.8	107514	14.161	21.241	1.6	2.4
1.545	2.26	106823	-410	-30.3	104654	14.249	21.373	-5.6	-8.3
1.535	2.32	111100	180	13.1	108888	14.110	21.165	2.3	3.5
1.505	2.32	110236	60	4.3	108067	14.026	21.039	0.8	1.2
1.535	2.44	120484	320	23.9	118158	13.895	20.843	4.0	6.0

KEY: FH,FZ,NMAX,m,DELTAN,FZ POINT,2H,3H AS FOR TABLE 3.1; NX95 -ELECTRON DENSITY AT X = 1+Ø.95Y, el/cc; DX95 -DEPTH OF NX95 LAYER BELOW FZ POINT, KM; TILT -TILT OF NX95 LAYER, DEG.

TABLE 3.6
TILT AT LEVEL WHERE X = 1 + 0.99Y -INPUT DATA FH,FZ,m FROM ELLIS(1957)

FH	FZ	NMAX	m	DELTAN	NX99	-----DX99------ (2H)	(3H)	----TILT---- (2H)	(3H)
1.530	2.45	121130	305	22.7	120664	6.200	9.300	8.6	12.7
1.550	2.75	146894	-190	-16.1	146364	6.004	9.006	-5.2	-7.8
1.560	2.63	136890	-140	-11.4	136381	6.102	9.153	-3.9	-5.8
1.550	2.40	117763	-285	-21.6	117301	6.264	9.396	-8.3	-12.3
1.540	3.02	171070	350	31.2	170493	5.811	8.717	8.9	13.2
1.510	2.48	122921	480	35.8	122456	6.152	9.228	13.3	19.5
1.530	2.22	103416	620	42.1	102994	6.387	9.581	17.6	25.5
1.530	2.16	99011	250	16.8	98600	6.439	9.659	7.5	11.1
1.560	2.78	149878	67	5.7	149339	5.995	8.993	1.8	2.7
1.520	1.97	85407	320	19.9	85035	6.599	9.899	10.0	14.8
1.525	2.27	107014	690	51.4	106584	6.339	9.509	20.7	29.5
1.530	2.33	111724	360	26.9	111281	6.296	9.444	10.8	15.9
1.520	1.85	77447	275	16.4	77097	6.715	10.074	8.9	13.2
1.520	1.86	78096	590	34.7	77745	6.706	10.059	18.3	26.3
1.550	1.80	74906	730	41.0	74560	6.802	10.203	21.8	31.0
1.510	2.43	118934	122	9.2	118478	6.191	9.286	3.6	5.3
1.540	2.26	106683	-540	-40.0	106250	6.366	9.549	-16.3	-23.8
1.545	2.35	113704	600	42.8	113253	6.298	9.447	16.6	24.1
1.540	2.30	109714	120	8.8	109274	6.333	9.499	3.6	5.4
1.545	2.26	106823	-410	-30.3	106389	6.372	9.558	-12.5	-18.4
1.535	2.32	111100	180	13.1	110658	6.310	9.465	5.3	7.9
1.505	2.32	110236	60	4.3	109802	6.273	9.409	1.8	2.7
1.535	2.44	120484	320	23.9	120019	6.214	9.321	9.0	13.4

KEY: FH,FZ,NMAX,m,DELTAN,FZ POINT,2H,3H AS FOR TABLE 3.1; NX99 -ELECTRON DENSITY AT X = 1+0.99Y, el/cc; DX99 -DEPTH OF NX99 LAYER BELOW FZ POINT, KM; TILT -TILT OF NX99 LAYER, DEG.

TABLE 3.7

TILT AT LEVEL WHERE X = 1 + 0.995Y -INPUT DATA FH,FZ,m FROM ELLIS(1957)

FH	FZ	NMAX	m	DELTAN	NX995	-----DX995----- (2H)	(3H)	-----TILT---- (2H)	(3H)
1.530	2.45	121130	305	22.7	120897	4.384	6.576	12.0	17.7
1.550	2.75	146894	-190	-16.1	146629	4.245	6.368	-7.3	-10.9
1.560	2.63	136890	-140	-11.4	136635	4.315	6.472	-5.5	-8.2
1.550	2.40	117763	-285	-21.6	117532	4.429	6.644	-11.7	-17.2
1.540	3.02	171070	350	31.2	170781	4.109	6.164	12.5	18.4
1.510	2.48	122921	480	35.8	122689	4.350	6.525	18.5	26.6
1.530	2.22	103416	620	42.1	103205	4.517	6.775	24.2	34.0
1.530	2.16	99011	250	16.8	98805	4.553	6.830	10.5	15.6
1.560	2.78	149878	67	5.7	149608	4.239	6.359	2.6	3.8
1.520	1.97	85407	320	19.9	85221	4.667	7.000	14.0	20.5
1.525	2.27	107014	690	51.4	106799	4.482	6.724	28.1	38.7
1.530	2.33	111724	360	26.9	111502	4.452	6.678	15.1	22.0
1.520	1.85	77447	275	16.4	77272	4.749	7.123	12.5	18.5
1.520	1.86	78096	590	34.7	77921	4.742	7.113	25.1	35.0
1.550	1.80	74906	730	41.0	74733	4.810	7.215	29.6	40.4
1.510	2.43	118934	122	9.2	118706	4.377	6.566	5.0	7.5
1.540	2.26	106683	-540	-40.0	106467	4.501	6.752	-22.6	-31.9
1.545	2.35	113704	600	42.8	113479	4.453	6.680	22.9	32.3
1.540	2.30	109714	120	8.8	109494	4.478	6.717	5.1	7.6
1.545	2.26	106823	-410	-30.3	106606	4.506	6.759	-17.4	-25.2
1.535	2.32	111100	180	13.1	110879	4.462	6.693	7.5	11.2
1.505	2.32	110236	60	4.3	110019	4.435	6.653	2.5	3.8
1.535	2.44	120484	320	23.9	120251	4.394	6.591	12.7	18.7

KEY: FH,FZ,NMAX,m,DELTAN,FZ POINT,2H,3H AS FOR TABLE 3.1; NX995 -ELECTRON DENSITY AT X = 1+0.995Y, el/cc; DX995 -DEPTH OF NX995 LAYER BELOW FZ POINT, KM; TILT -TILT OF NX995 LAYER, DEG.

absent during Z echo occurrence.

D) The best Z mode return tilt model proposed by Papagiannis and Miller has a = Ø.24369, b = Ø.1. This corresponds to a minimum tilt (at the bottom of the ionosphere) of 13.7° and we would thus expect the angle of incidence of the Z ray to be greater than this (Papagiannis and Miller do not state what this angle is but our expectation is verified by ray tracing in Section 3.11). However, this does not agree with Ellis's observations which put the Z echo angle of incidence at 8°to 9° for a dip angle of 72°.

E) Papagiannis and Miller published the ionograms shown in Fig.3.44 in support of their proposal. The top ionogram shows the Z mode occuring over a much wider frequency range than provided by their "realistic" models. All the ionograms show spread-F. Lack of spreading on the Z trace does not imply lack of backscatter because as Papagiannis and Miller correctly point out "....there is only one possible path for the Z mode echoes...". Papagiannis and Miller incorrectly state what the condition of the ionosphere is believed to be in the presence of spread-F. There have been almost as many spread-F theories and variants of these theories as there have been research groups studying this phenomenon. Furthermore, spread-F has appeared to be different at different locations and at least

shows some form of latitude dependence. Papagiannis and Miller have picked a vague form of spread-F which suits the tilt theory but have provided no evidence to demonstrate that it is operating for these ionograms. Topside sounding and intense equatorial studies have brought a degree of clarification to the spread-F problem and field aligned structures are currently thought to be responsible for much more spread-F than "blobby" or "wavy" structure. In any case Ratcliffe and Weekes (1960) did not say that the F layer assumes a blobby structure during spread-F conditions but they did say "There is evidence that the spread of the echo is caused by scattering in depth rather than by scattering from irregularities at distances considerably removed from the vertical reflection point". The presence of spreading on the iongrams together with lack of spreading on the Z trace does not yield support for the tilted layer theory - it merely does not preclude it as it does not preclude the existence of many other irregularities.

3.11 Ray Tracing

Using the Jones (1975) ray tracing program, ordinary and extraordinary type rays were traced in the Papagiannis/Miller tilt/wedge ionosphere for a = 0.24369 and b = 0.1, with other parameters as set by Papagiannis and Miller. Papagiannis and Miller stated that for the Earth's magnetic field they used the

standard dipole approximation but did not state what field strength they assumed on the ground at the equator. However, from Fig.3.43 it should be possible to determine the gyro frequency by calculating the electron densities at the coupling regions and reflection points. This was done for the frequencies 4.15, 4.225 and 4.30 MHz for θ_o placed at the diagram origin but the results were inconsistent with the requirements of these regions. It was found that when θ_o was shifted 39.75 km. equatorward of the diagram origin then self consistency was achieved for a gyro frequency of 0.867 MHz. on the ground at the equator. It is not known why θ_o is not coincident with the diagram origin but it may be an indication that it is not easy to construct a tilt model having a satisfactory frequency spread of returned Z echoes for reasonable values of a and b. The O and X mode frequencies corresponding to reflection from the same ionospheric layer as the Z mode 4.225 MHz ray were then found to be 4.865 and 5.602 MHz respectively. Fig.3.45 shows magnetic meridian ray tracing, in this ionosphere, of the 4.865 MHz O mode for various zenith angles at 2^o intervals and Fig.3.46 is a similar diagram for the X mode at 5.602 MHz. The O mode was also traced in a similar fashion for 4.225 MHz to find the lower half of the 4.225 MHz Z mode ray of Fig.3.43 and these traces are shown in Fig.3.47. The 4.225 MHz O mode ray must have a wave normal angle parallel to the magnetic field direction in the coupling region in addition to returning to the transmitter and this condition was satisfied. To the nearest half degree

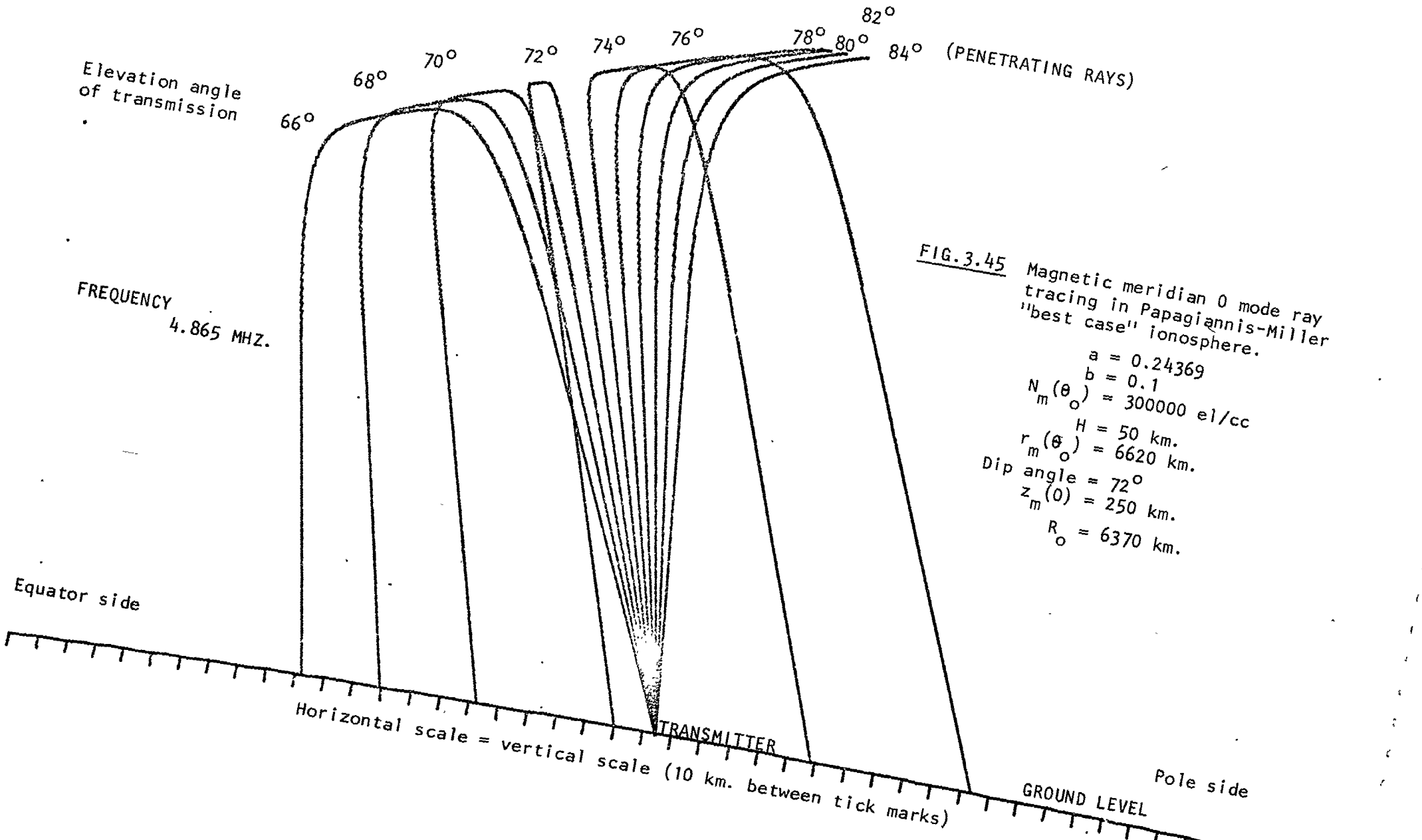

FIG.3.45 Magnetic meridian O mode ray tracing in Papagiannis-Miller "best case" ionosphere.

$a = 0.24369$
$b = 0.1$
$N_m(\theta_o) = 300000$ el/cc
$H = 50$ km.
$r_m(\theta_o) = 6620$ km.
Dip angle $= 72^o$
$z_m(0) = 250$ km.
$R_o = 6370$ km.

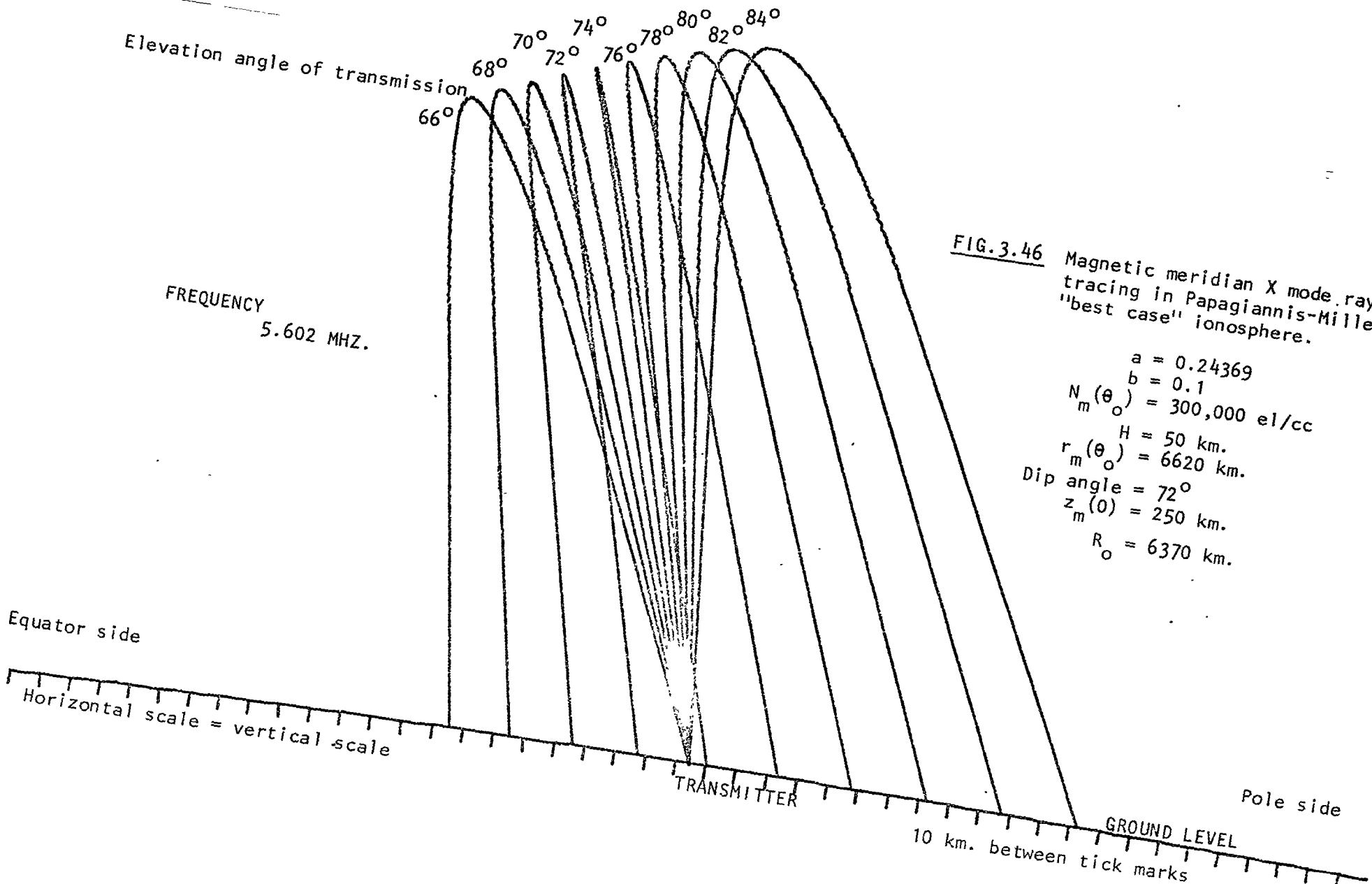

FIG.3.46 Magnetic meridian X mode ray tracing in Papagiannis-Miller "best case" ionosphere.

$a = 0.24369$
$b = 0.1$
$N_m(\theta_o) = 300{,}000$ el/cc
$H = 50$ km.
$r_m(\theta_o) = 6620$ km.
Dip angle $= 72^\circ$
$z_m(0) = 250$ km.
$R_o = 6370$ km.

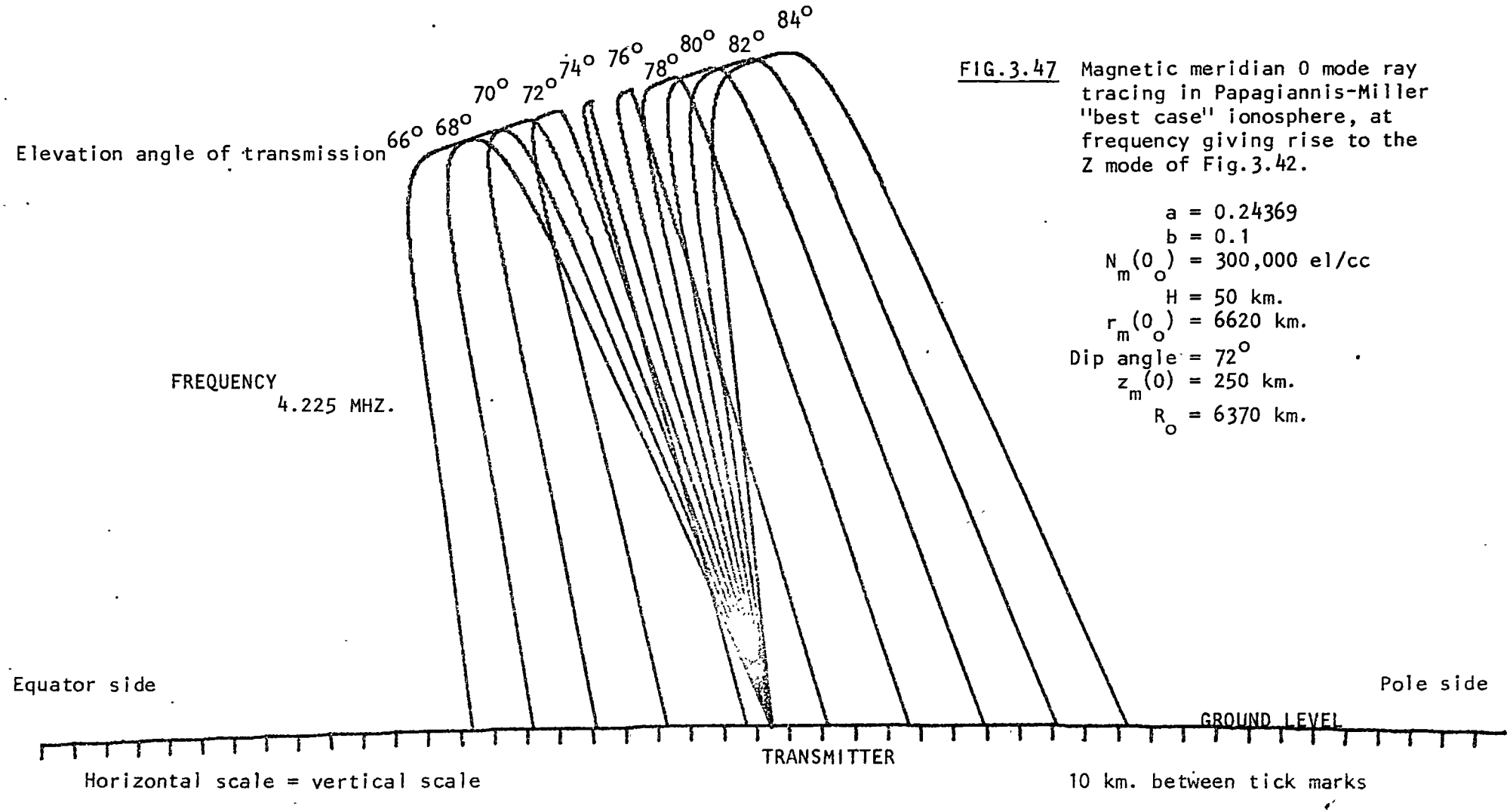

FIG.3.47 Magnetic meridian O mode ray tracing in Papagiannis-Miller "best case" ionosphere, at frequency giving rise to the Z mode of Fig.3.42.

$a = 0.24369$
$b = 0.1$
$N_m(0_o) = 300{,}000$ el/cc
$H = 50$ km.
$r_m(0_o) = 6620$ km.
Dip angle $= 72^o$
$z_m(0) = 250$ km.
$R_o = 6370$ km.

the O, X and Z modes were found to be returned to the transmitter at equatorward zenith angles of 17.5°, 16.5° and 15.5° respectively. This confirmed that a reasonable tilt/wedge model for Hobart would return Z echoes at equatorward zenith angles in the range >9° to about 18° with a strong bias toward the 18° end of the spectrum and further that simultaneous O and X echoes returned from the same ionospheric layer would have approximately the same zenith angles as the Z echo. The ray tracing shows that the O and X echoes can be expected at very slightly (1° or 2°) greater zenith angles. Ray tracing was tried in two other "reasonable" Papagiannis/Miller models and produced essentially similar results.

In order to construct Papagiannis/Miller tilt/wedge ionosphere's for Ellis's (1957) results we put a = 0 and

$$b = \frac{m^{*}.z_m(0)}{N_m(\theta_c)}$$

where $N_m(\theta_c)$ = 300000 el/cc and $z_m(0)$ = 250 or 300 km. so that

$b = 8.3 \times 10^{-4}.m^{*}$ for $z_m(0)$ = 250 km.

$b = 0.001.m^{*}$ for $z_m(0)$ = 300 km.

The two cases examined were both of tilts in a direction favouring return of the Z ray. The first case (m^{*}=22.7, b=0.019) was a typical such result in the presence of the Z echo and the second case (m^{*}=51.4), being the most favourable case for the tilt mechanism, was examined for ionospheres of parabolic semithickness 100 (b=0.043) and 150 (b=0.051) km. in order to enhance the chances of return of the

Z ray. Ray tracing of the Z mode starting upwards from the appropriate coupling region for a variety of closely spaced frequencies near the critical frequency (tnis corresponding to the only regions where the tilts might be of sufficient magnitude to return the Z rays) showed that the tilt mechanism of return of the Z ray could not be operating in any of the cases of observed Z echoes reported by Ellis (1957). Figs.3.48 to 3.50 show the plots of the Z rays and for comparison purposes Fig.3.51 is a plot of the Z rays in a similar but flat ionosphere.

3.12 Summary And Proposals For Experimental Tests

The oblique incidence coupling mechanism of generation of the Z mode as expounded by Ellis is the accepted Z mode explanation. Ellis proposed that the return of the Z ray was accomplished by a backscattering mechanism and this was not inconsistent with the results of his experiments although from Renau's work it appears that there are many ionograms which show the Z echo yet do not allow the presence of the appropriate type of scattering screen.

Bowman suggested favourable ionospheric tilting as an alternative Z ray mechanism and this has been formulated as a working model by Papagiannis and Miller. The expected results of this model are inconsistent with existing angle of arrival

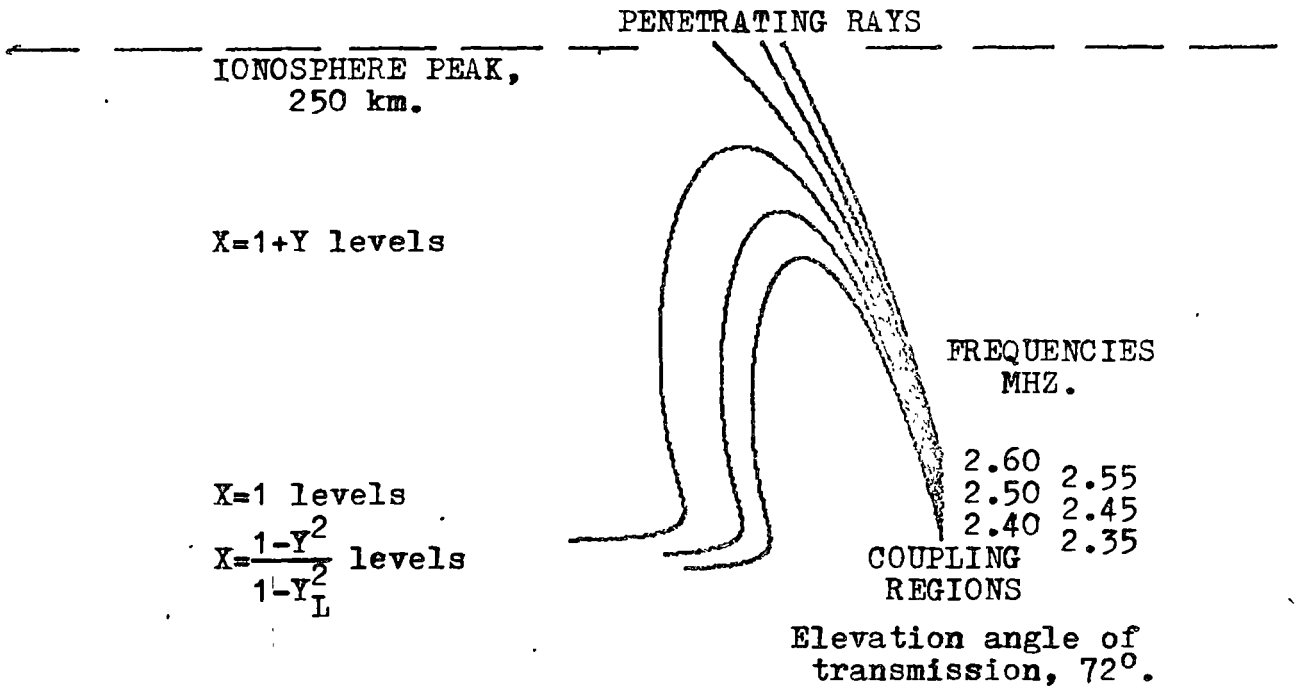

FIG.3.48 Ray tracing of Z rays in Papagiannis-Miller model ionosphere using parameters deduced from Ellis (1957) experimental results.

$a = 0$
$b = 0.019$
$N_m(\theta_o) = 121130$ el/cc
Dip angle = 72°

(Horizontal scale = vertcal scale,
10 km. between tick marks)

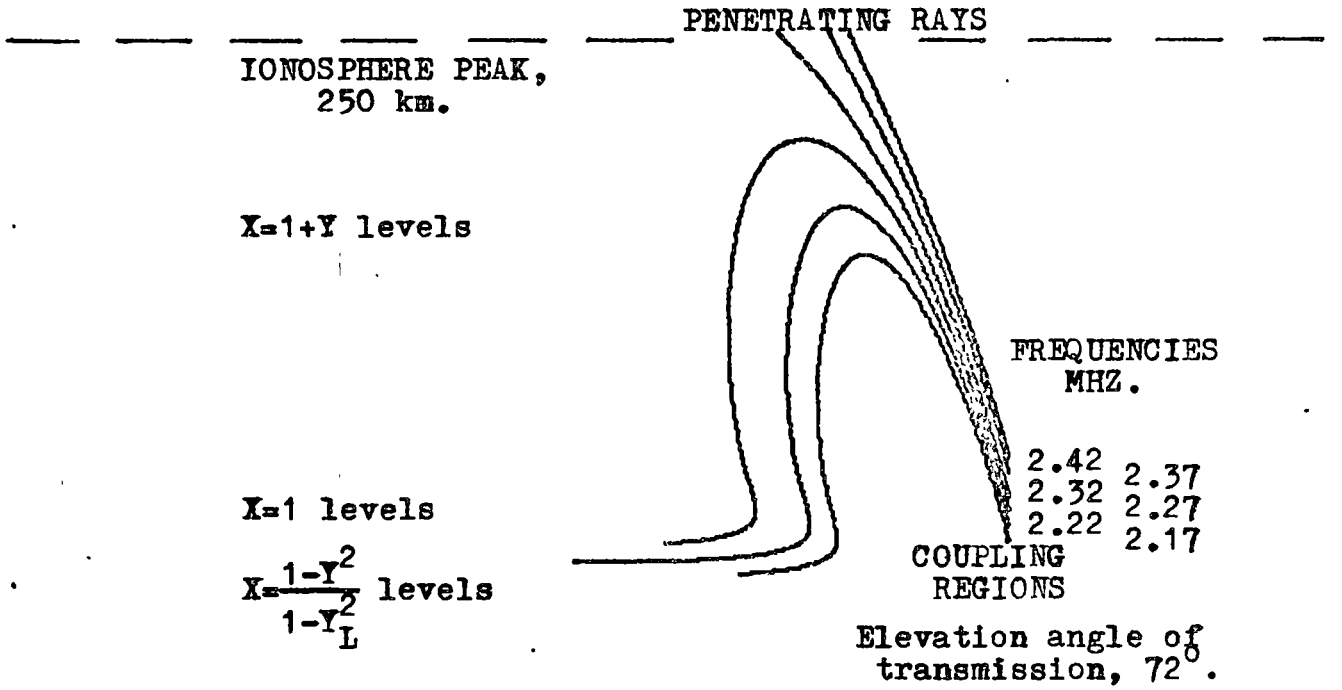

FIG.3.49 Ray tracing of Z rays in Papagiannis-Miller model ionosphere using parameters deduced from Ellis (1957) experimental results.

a = 0
b = 0.043
$N_m(\theta_o)$ = 107014 el/cc
Dip angle = 72°

(Horizontal scale = vertical scale, 10 km. between tick marks)

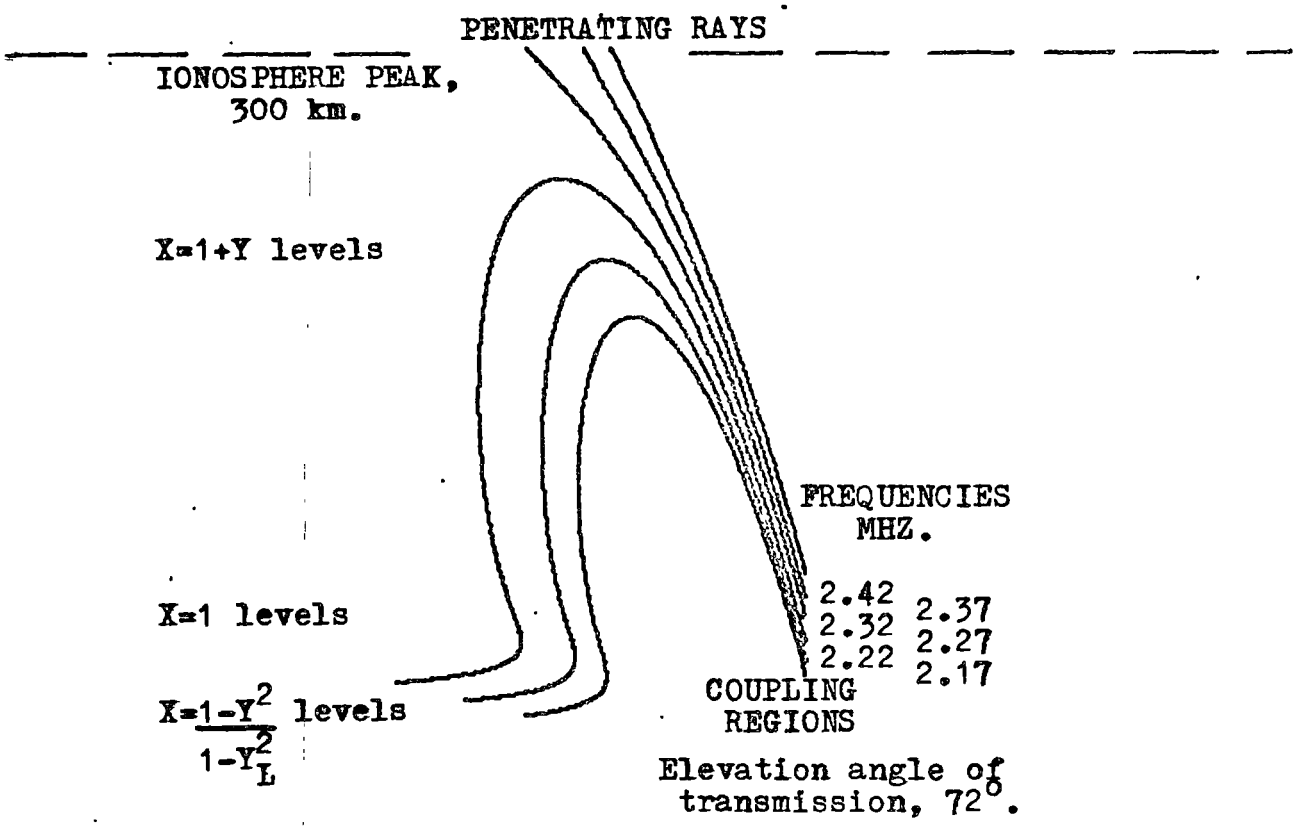

FIG.3.50 Ray tracing of Z rays in Papagiannis-Miller model ionosphere using parameters deduced from Ellis (1957) experimental results.

$a = 0$
$b = 0.051$
$N_m(\theta_o) = 107014$ el/cc
Dip angle = 72°

(Horizontal scale = vertical scale, 10 km. between tick marks)

GROUND LEVEL

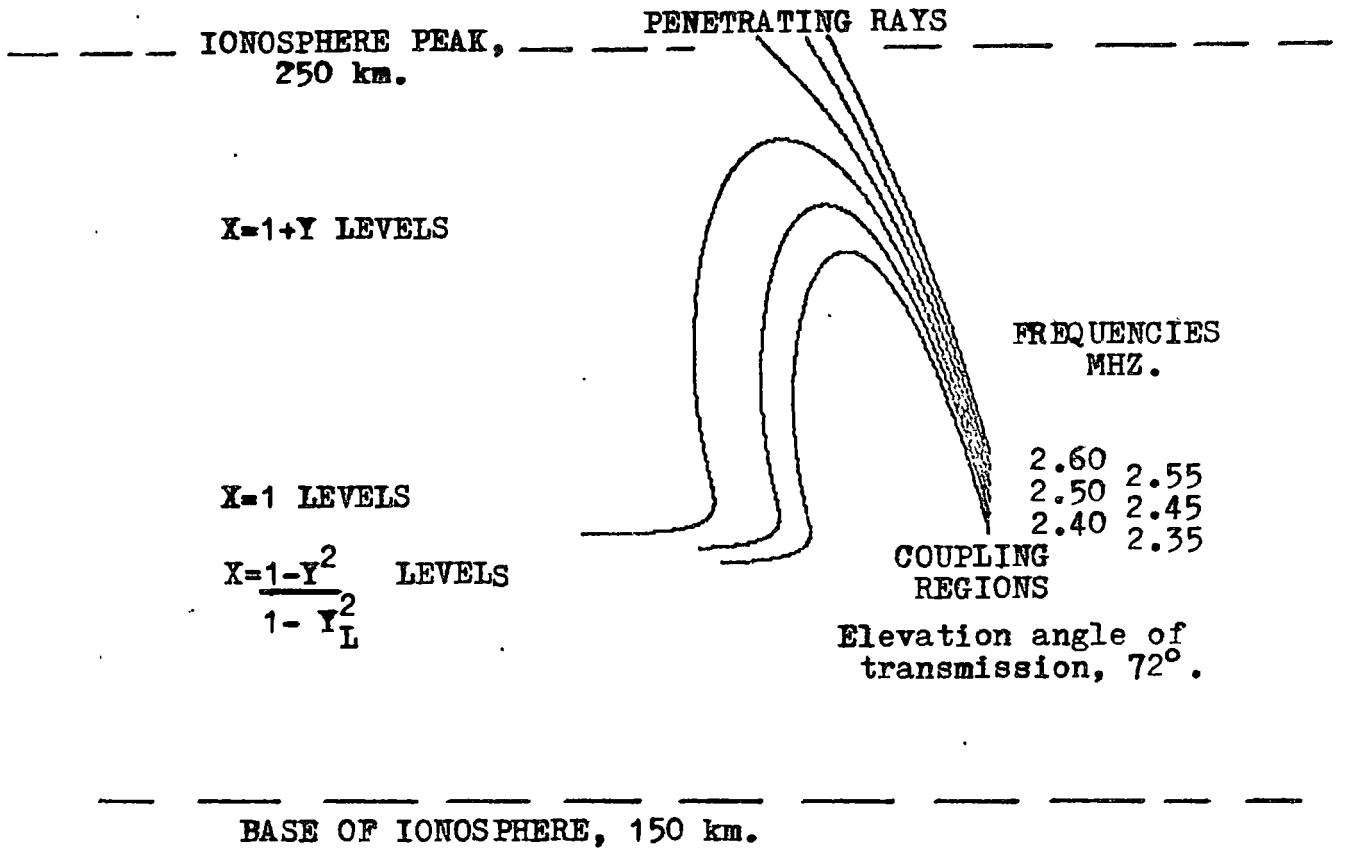

FIG.3.51 Ray tracing of Z rays in a flat ionosphere.
(a=0,b=0)

$N_m(\theta_o)$ = 121130 el/cc

Dip angle = 72°

(Horizontal scale = vertical scale, 10 km. between tick marks)

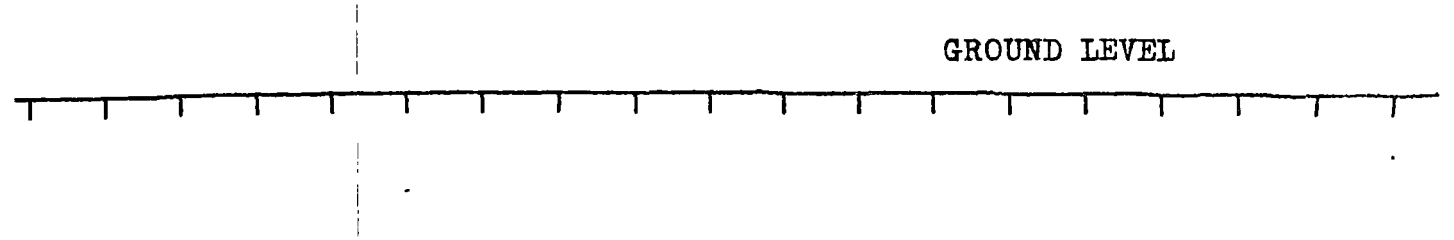

measurements. There is no satisfactory experimental evidence in favour of this model.

Papagiannis suggested return of the Z ray by a special solar zenith angle controlled case of the tilt model. There is no satisfactory experimental evidence in favour of this model and existing angle of arrival measurements are all strongly against it.

Satisfactory physical processes have not been advanced by the proponents of either the solar zenith angle return mechanism or the backscatter mechanism. The tilt/wedge return mechanism operates by means of well accepted physical processes but its proponents have not explained how the very special arrangement of the ionospheric layers is to be generated.

The examination of Papagiannis and Miller's formulation of the tilt/wedge model shows that the Z echo would have angles of arrival centred around 14° to 17°N for Hobart with the X and O modes from the same ionospheric layer having similar angles of arrival, the X echo angle of arrival being about a degree further north and the O echo angle of arrival being about two degrees further north. Simultaneous measurements of the zenithal angles of arrival coincident with angles of transmission of the Z, O and X rays would thus provide two unambiguous experimental tests of the operation of the tilt/wedge return mechanism in the presence of the Z echo.

Such experiments would also conclusively test the solar zenith angle return mechanism.

Widening of the returned O and X echo angular spectrum in the presence of the Z echo would be expected if backscattering were the operating return mechanism but it is not considered to be a definitely conclusive test. On the other hand the complete form of a wide beam h′f ionogram in the presence of the Z echo can be used to determine the presence or absence of a scattering screen at the reflection level.

CHAPTER FOUR

OBSERVATIONAL TECHNIQUE

4.1 Introduction

The aim of the observations was to make narrow beam soundings at 1° intervals along the N-S meridian at fixed and swept frequency in order to determine the distribution of angles of arrival of the Z echo and the angular location of the simultaneously occurring X and O echoes. It was also desirable to make some observations of the Z echo at high repetition rate in order to obtain information about its temporal behaviour. From the results it was hoped to be able to decide whether or not the tilt mechanism was operating.

While narrow beam sounding provides some information pertinent to the backscattering mechanism it is felt for reasons previously outlined that wide beam swept frequency sounding provides a better test of whether or not the mechanism is operating. Wide beam soundings were provided by a separate instrument.

Hobart is a place of relatively high Z echo occurrence. Bowman used Hobart records to support his tilt hypothesis, Papagiannis used Hobart as the location for his calculations based on his solar zenith angle model and Papagiannis and

Miller used Hobart values for the key parameters when developing their most likely tilt configuration. Ellis carried out his experimental investigation into the Z echo at Hobart and postulated a backscattering mechanism from his results. The logical location to carry out further investigations was therefore Hobart. Hobart's geographic coordinates are 42.8°S, 147.3°E and its geomagnetic coordinates are 51.7°S and 224.3°E. The declination is 13°E, the dip angle 72° and the total field at the ground is Ø.63 oersted.

Zenith angles equatorward of zenith are assigned a positive sign and those poleward of zenith a negative sign. As Hobart is in the southern hemisphere, a positive zenith angle at Hobart will mean to the north of zenith and a negative zenith angle to the south of zenith.

4.2 The Instruments

The SOUTH LEA IONOSONDE near Hobart is a Type 4A feeding a wide beam delta antenna and is operated by the Ionospheric Prediction Service. Peak power is 5 KW, sweep range 1-22 MHz in 12 seconds and the maximum repetition rate for h'f ionograms is every 2Ø seconds. Under normal operating practices an ionogram is made every 15 minutes.

The LLANHERNE HF RADIO TELESCOPE situated near Hobart and

about 18 km. NE of South Lea was used as the antenna of a narrow beam ionospheric sounding system. The antenna was a square array 609 m x 609 m consisting of 64 east-west rows each of 32 broadband dipoles. The operating range was 2-18 Mhz, with corresponding resolutions of 12.4° to 1.4° respectively as a radiotelescope and 8.8° to 1.0° respectively as an ionospheric sounder. The beam could be swept through the meridian in 1° steps from 55° south of zenith to 55° north of zenith at rates of up to 5° per second. The angular sweep limits were indvidually adjustable and there was provision for external control of the beam. Fig.4.1 shows the 5 Mhz profile of the beam for receiving only at zenith, for sounding at zenith and for sounding at 5° north of zenith. Fig.4.2 is an aerial view of the array. The actual steering of the array was done in terms of integral "beam number" and not in integral values of declination, the relationship between the beam number (B) and the zenith angle of the beam (z degrees) being

$$z = \arcsin (B \times 0.01745)$$

However the zenith angles of interest to this investigation were not large enough to make the difference between z and B significant so the zenith angle may be taken as equivalent to the beam number. Zenith angles north of zenith were defined as positive and those south as negative. The general features of the array were described in greater detail by Ellis (1972).

At the time of the investigation the array was not in use, was in inoperable condition and deteriorating at a fast rate.

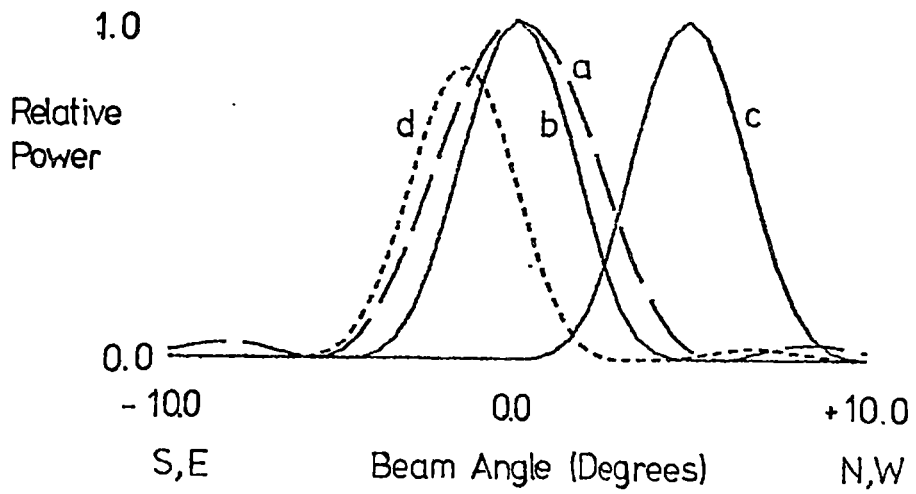

FIG.4.1 Llanherne HF Array beam patterns at 5 MHz.

(a) E-W profile and N-S profile at zenith, array operating as radio-telescope.

(b) E-W profile and N-S profile at zenith, array operating as ionospheric sounder.

(c) N-S profile at 5^{o} N of zenith, array operating as ionospheric sounder.

(d) Modified E-W profile after re-phasing, array operating as ionospheric sounder.

FIG.4.2 Aerial view of the Llanherne HF Radio Telescope. Most of the poles are 18m. apart.
(Reproduced, with permission, from a photograph by Vern Reid.)

Over a period of six months I carried out a massive repair program which brought the array into satisfactory operating condition. I estimated that it would not be possible to hold the array in this condition for more than six months. Within this period the operating system was developed and some observations made. Consequently it has not been possible to make further observations following analysis of the data obtained. Although further observations were desirable the existing data has nevertheless proved sufficient for the original purposes.

Each array row of 32 dipoles was connected by a "Christmas Tree" type feed. In order to phase the array slightly off zenith in the E-W direction each dipole row was separated into an east half and a west half (each of 16 dipoles) and the signal from one half was delayed relative to the other half to achieve the desired effect. This also had a slight east-west widening effect on the beam and the resultant modified east-west profile is shown in Fig.4.1. The transmitted beam could then be expected to become parallel to the magnetic field at the O reflection level when the beam was pointing about 9^{o} north of zenith.

The ionosonde used in conjunction with the array was an IPS Type IIIE modified to produce logarithmic sweep h'f ionograms from 1.3 to 7.3 Mhz at a rate of four per minute without loss of resolution or information (fxf2 generally being

below 7.5 Mhz at this time). The ionosonde was further modified to provide two continuously variable receiver gains. Switching between the two gains could be done either manually or else automatically at the end of each h'f ionogram. A control was also added to allow automatic beam position increment of one or three degrees at the end of each ionogram. The 10 KW power was reduced to a few watts (about 8 watts, initially) but as it was found that more power could be fed into the array than had been anticipated the power was increased to about 200 watts and most of the relevant observations were made at this power.

In addition to the usual IIIE continuous photographic record of intensity scan (for production of h'f or h't type records) a video camera and recorder were set up to record the A scans displayed on a monitor unit. A second channel on the monitor unit was set up to offset the position of a marker in proportion to beam position. The video system recorded at 50 frames per second, the ionosonde pulsed at 50 cycles per second and the persistence of the CRO monitor unit was such that the reflection train from each individual pulse could be separately identified. The video tapes lasted about 40 minutes each but the film capacity of the IIIE camera was equivalent to at least 8 hours continuous running. The automatic 3 degree increment was found to be somewhat unreliable and as video tape could not be spared for long 3 degree runs, beam position recording was carried out in these cases by attaching a camera to the monitor

and displaying only a beam position dot. Such beam position recording was limited to at most 3 hours duration by the low film capacity of this camera.

4.3 Observing Programme

As the Z echo is a sporadic phenomenon it was not possible to institute a programme of unattended recording. The Llanherne array was visited as often as possible and initially trial film recording was carried out followed by trial film and video recording. These early records were made in September and October of 1977 (Video records from mid-October). Few Z echoes were seen on the films and none on the video tapes which were wiped for re-recording. By early November it had become possible to identify the presence of Z echoes by observing the echoes on the various monitor units and so Llanherne was visted more often but recording was commenced only if Z echoes were identified as present. As South Lea is much closer to the Physics Department than is Llanherne, the South Lea monitor was also frequently checked but it was found that the half hour travel time from South Lea to Llanherne was often sufficient for the disappearance of the Z echo before recording could take place.

The main Z echo results were obtained during November 1977. The film recording and video recording were normally

carried out simultaneously though in many cases film recording continued well after the video tapes were finished. Records of h'f type were produced every 15 seconds and at the end of each frame the beam position incremented by 1° and the gain changed to the alternate setting. The beam scan limits were normally set at 10° S and 21° N ,the bias towards north angles being because all theories predicted the Z echo to occur in the approximate range 9°N to 18°N. The two gains were set by experience, one high to allow the Z echo to be detected and the other low to avoid the saturated O and X echoes normally obtained at high gain levels. Beam change limits of 4° N and 14° N, 20° S and 20° N, 25° S and 25° N were used on occasions. Some fixed frequency records were also made with the beam scanning at 5° per second with manual gain changes. The scan limits for this type of recording were 10°S and 21°N, 20°S and 20°N, 21°S and 21°N, 25°S and 25°N. The Z echoes were observed at various times of the day and night.

4.4 Analysis

Films displaying Z echoes were scaled to provide angle of arrival information and the O and X h'f traces were examined for variation with angle which might indicate the presence of a scattering screen. Wide beam ionograms from South Lea for the same observing period were also examined for evidence of scattering screens. The video records were analysed to provide

echo strength information at various angles and frequencies. On the low gain records the noise was generally insignificant compared with the O and X echoes but on the high gain records the noise was sufficiently strong compared with the Z echoes for it to be worthwhile making an estimate of the noise contribution. This was done by measuring the noise peaks which occurred at about 50 km. greater virtual height than the Z echo. This provides a reasonable estimate assuming that the noise occurs independently of the transmitted pulses.

During fast scans the beam stayed at a particular angle for about 10 pulses. Examination of the video records showed that the first one or two records of a particular beam position displayed interference from the automatic process of re-phasing the array to reposition the beam. These records were discarded from the analysis. The remaining 8 or 9 records were scaled for either Z echo strength or else O and X echo strength as appropriate. The values were squared to obtain relative power and then averaged to provide a single power value for the particular mode at each beam position. In the case of the Z mode the estimated effect of the noise was removed from the result. In order to maintain uniformity the measurements were expressed as a fraction of the voltage of the virtual height markers. Comparison of the Z echo strength with that of the X and O modes was possible through knowledge of the gains used when recording. Analysing the video tapes for amplitude information was found to be extremely time consuming. The time

taken to analyse the data was generally well over three hundred times as long as the time taken to record it. Since the same information was usually recorded on film there existed the possibility of obtaining reasonably accurate amplitude information by determining the density variations of the film. The problems encountered with this sort of information retrieval are the non-linear nature of the photographic processes and the limited density range of the film. Investigation of the process and some calibration tests using the original equipment assisted in assessing the viability of the method but the most conclusive test of its validity was provided by comparing amplitude results made by the film reader with those measured from the video records (Fig.4.3).

A film density reader was constructed and consisted mainly of a phototransistor mounted on the x-travelling bar of an x-y plotter. An image of the film was projected downwards onto the bed of the plotter and a ramp generator fed into the x terminals moved the bar mounted detector smoothly across the region of interest. Since the recording pen was also mounted to the bar (and travelled backwards and forwards along it as the output from the detector varied) the x component of the plot was automatically scaled no matter how irregular the x motion might be. The direction of traverse was invariably in the direction of the film's time axis. On the h'f records the virtual height of the Z echo was determined and traversing the X and O mode echoes at this virtual height for each angle

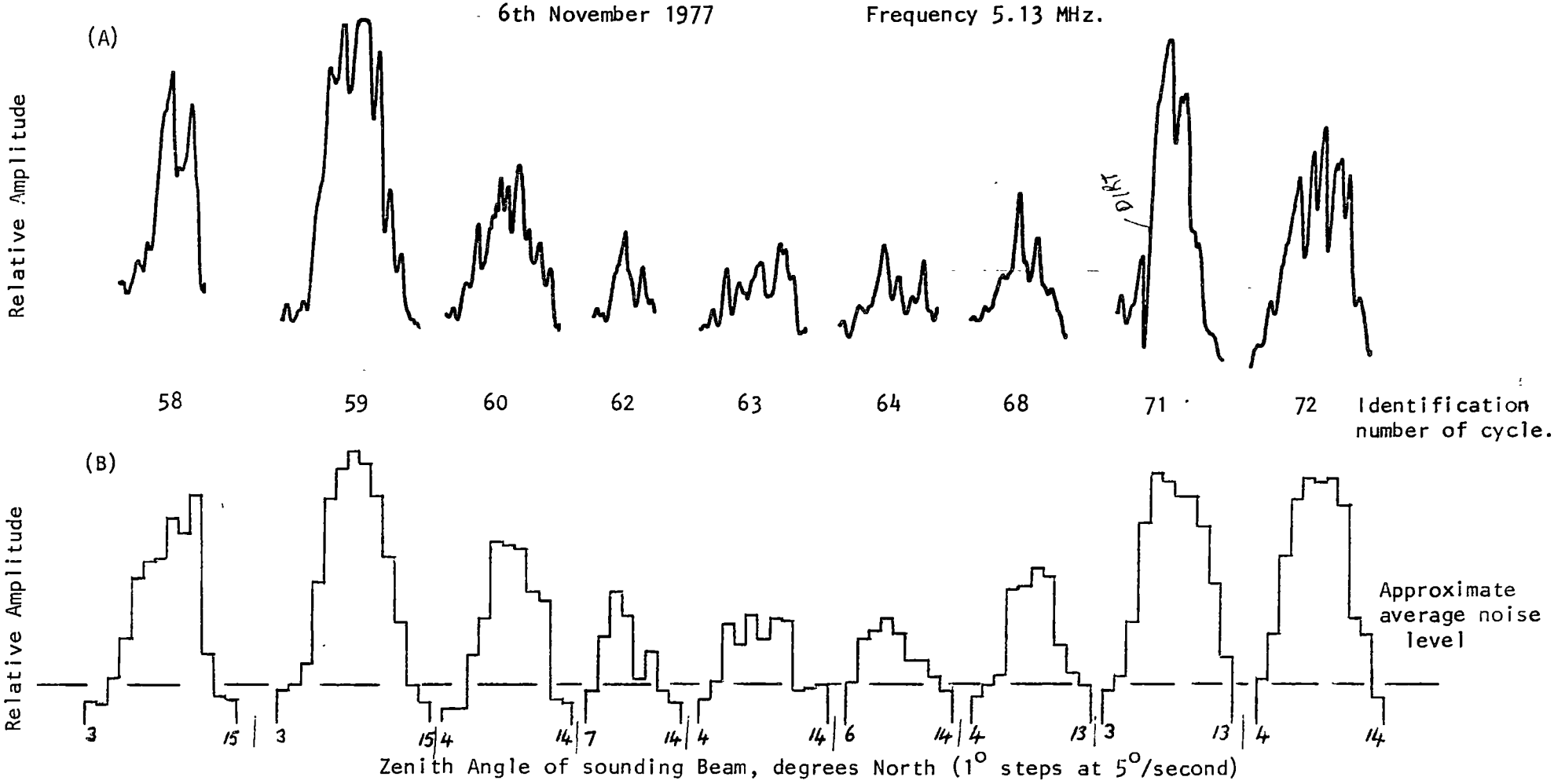

FIG.4.3 Comparison of Z echo profiles (of amplitude with zenith angle) obtained from film reading and measurements from video A(amplitude) scans.
(A) Film reader profiles.
(B) Profiles from video A scans (the amplitude at each beam position is the average of the 8 or 9 usable measurements. One A scan every 20 msec.)

provided the variation in echo strength with angle for these modes. Choosing the same virtual height for the modes is effectively choosing the same height region in the ionosphere (for this region of interest) and in the case of the modes also having the same angle of arrival we are looking at echoes from the same part of the ionosphere (see sections 3.11 and 3.12).

CHAPTER FIVE

RESULTS

5.1 Angle Of Arrival - Z echoes

The angle of arrival measurements are in excellent agreement with those obtained by Ellis (1953a,b;1954;1956). The swept frequency records totalled 499 angular scans or cycles on a total of 25 days between September and December 1977. Z echoes were found on 53 cycles and in all cases the zenith angle of arrival was in the vicinity of $+8/9^{o}$. As the Z echo can vary quite markedly in strength over the minute and a half taken to record 6 h'f sweeps (say, $+6^{o}$ to $+11^{o}$ in 1^{o} steps) an individual cycle can not be taken as unambiguously defining the angular centre of the Z echo at that time. For instance the Z echo may have its angular centre between $+8^{o}$ and $+9^{o}$ yet would appear strongest at $+6^{o}$ or $+7^{o}$ if it were fading quickly at the time of observation, or strongest at $+10^{o}$ or $+11^{o}$ if it were quickly strengthening. The total occurence of Z echo with zenith angle is therefore plotted as the histogram of Fig.5.1(A) and Fig.5.1(B) is a histogram of the median zenith angles of the Z echo occurrences.

To determine the angular centre of arrival more rigorously some fixed frequency high speed scans were carried out, the time spent scanning 6 degrees of sky being less than a second

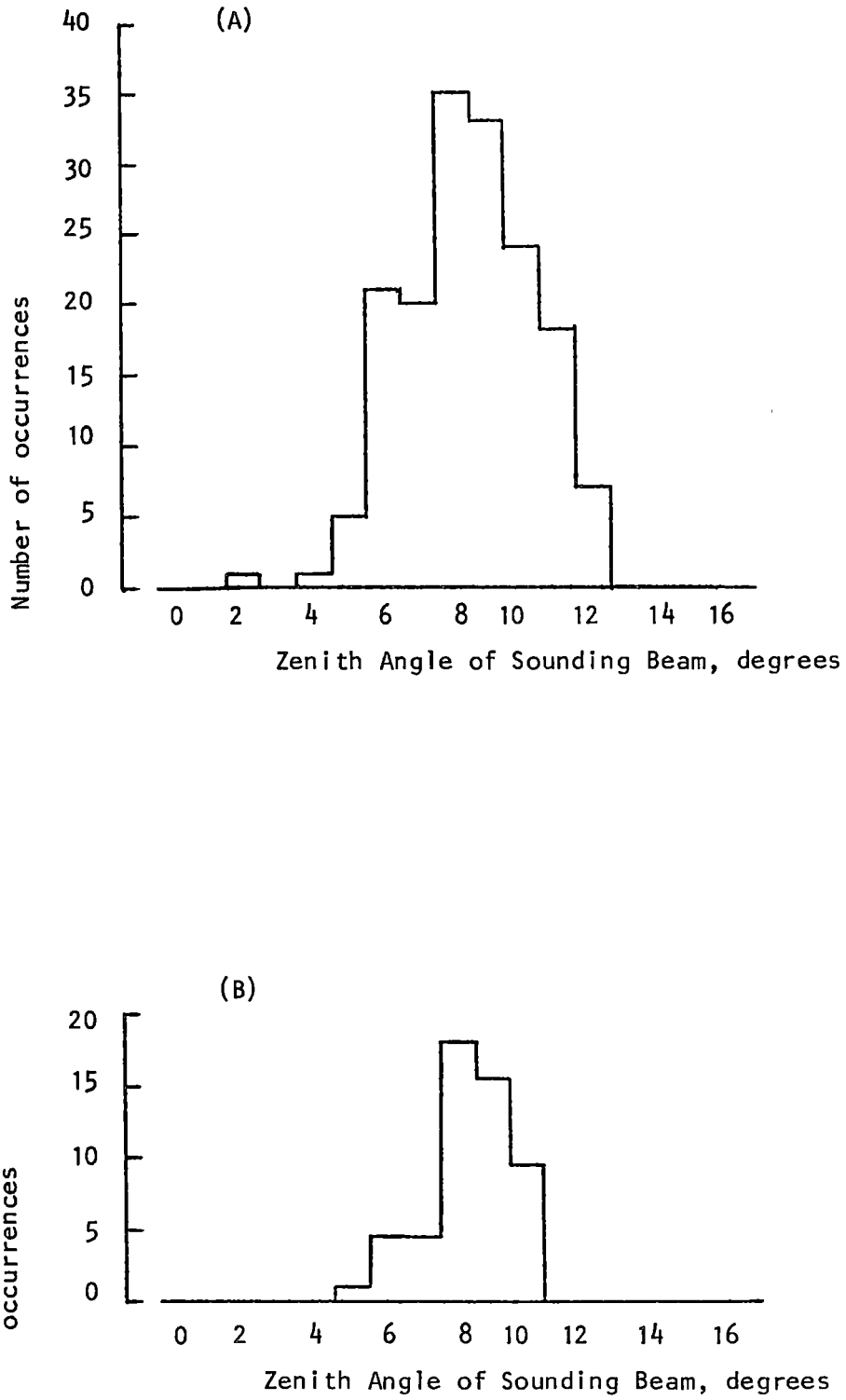

FIG.5.1 (A) Histogram of zenith angles (of Llanherne sounding beam) at which the Z echo was recorded.

(B) Histogram of median zenith angles of the angular spectra of the Z echoes recorded at Llanherne.

and a half. Examples of the records obtained are shown in Figs.5.2 to 5.4, 5.31 to 5.33 and 4.3. It can clearly be seen from the examples that the Z echo returns cluster around $+8/9^{o}$ and this is also true of those examples not shown here.

On no records were Z echoes found centred around angles intermediate between $+11^{o}$ and $+18^{o}$. No Z echo returns were seen in the vicinity of $+18^{o}$.

5.2 Angle Of Arrival - O And X Echoes

Figs.5.5 to 5.11 are typical examples of the angular variation of the O and X echo strengths at the Z mode virtual height in the presence of Z echoes. It can be seen that the angular centre of the O and X echoes is sometimes negative, sometimes positive but in only one case was it found to be around $+9^{o}$; that is, in the same direction as the Z echo (Fig.5.12). The returned O and X beams were variable in width during the presence of the Z echo but showed much the same sort of variation during its absence. The angle of arrival of the centre of the O and X beams appeared to be similarly unaffected by the presence or absence of the Z echo. A relatively common feature of the O and X echo distributions on cycles detecting Z echoes, and often on cycles not detecting Z echoes but adjacent to those displaying the Z trace, was a strengthening of the O and X echoes in the general angular region of the Z echo,

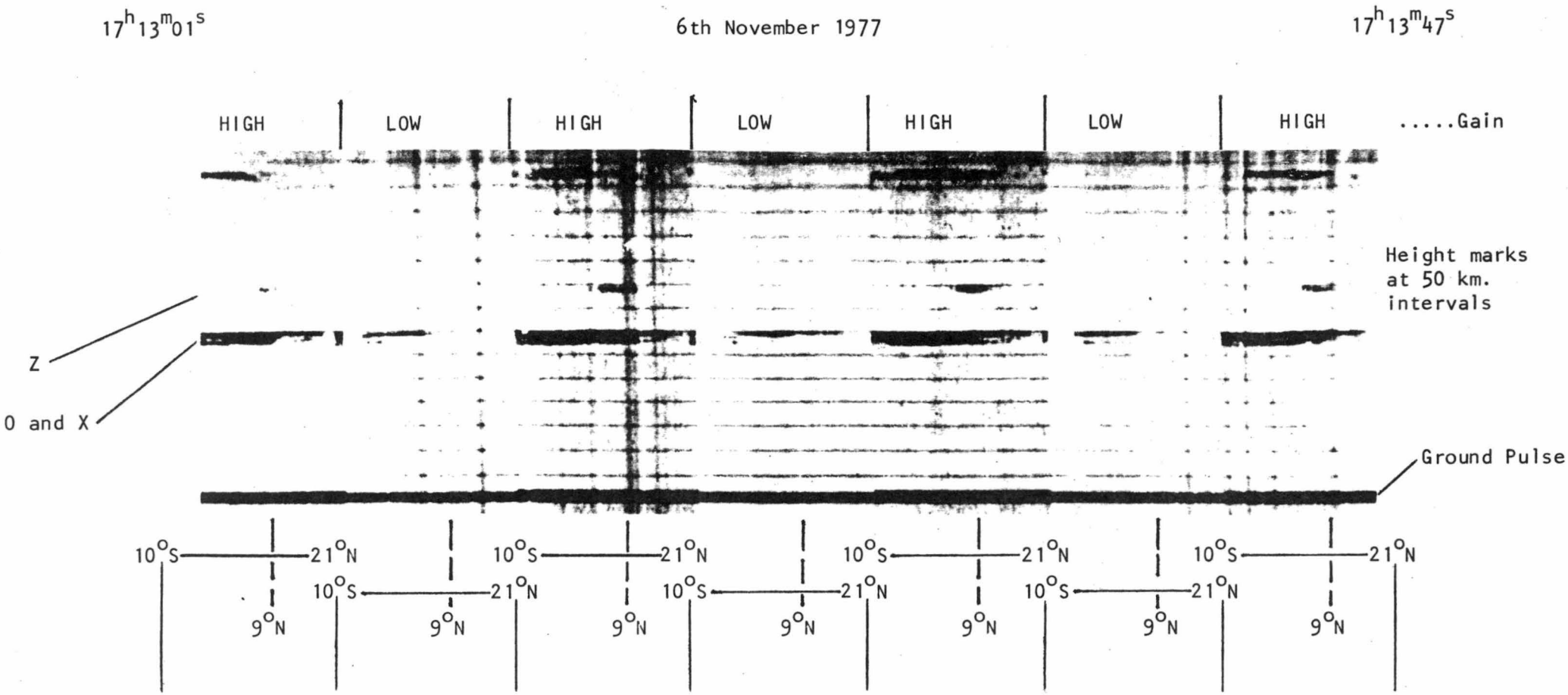

FIG.5.2A Llanherne h't record showing variation of O, X and Z echo strengths with zenith angle. Angular scan 10°S to 21°N in 1° steps at 5°/sec. (6.6 seconds per scan) High and low gain records (gains ratio HIGH:LOW = 22dB). Frequency 5.13 MHz.

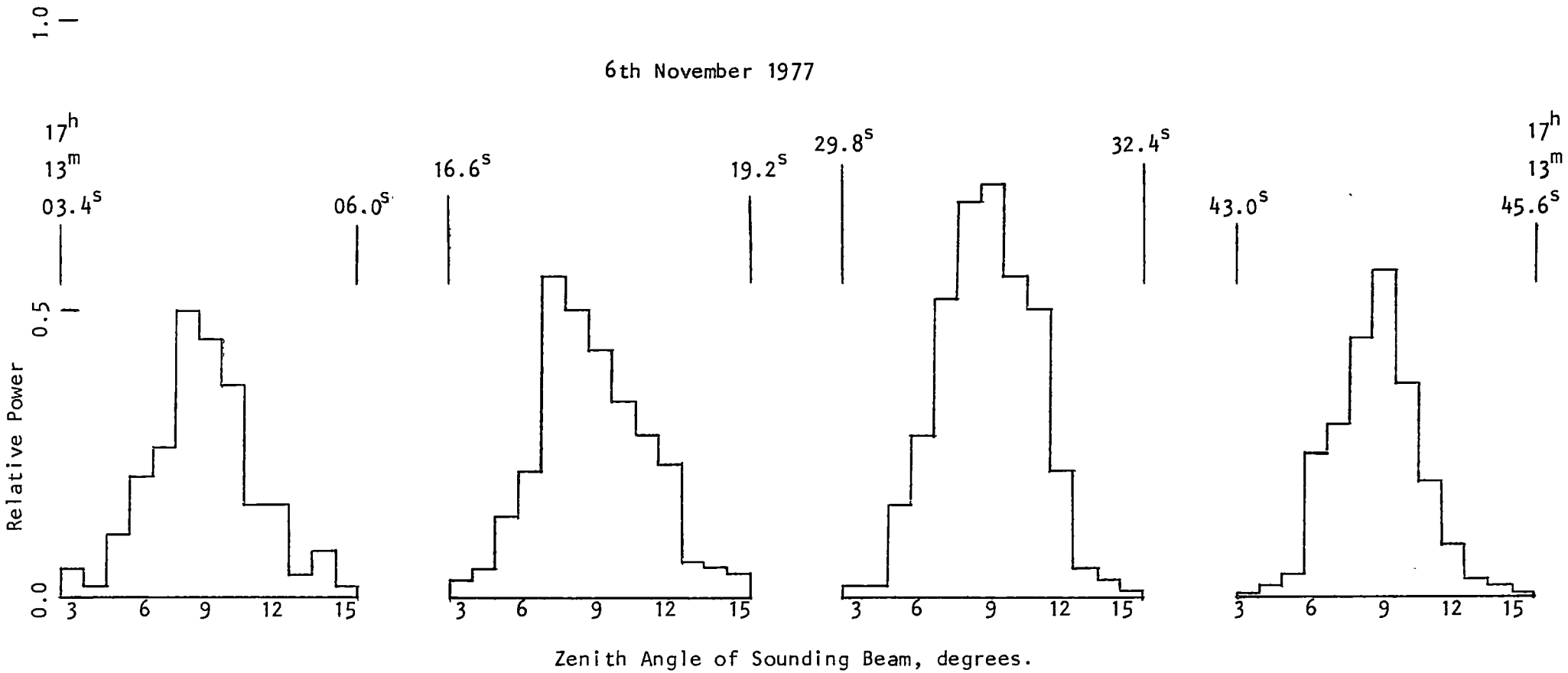

FIG.5.2B Profiles of Z echo power with zenith angle. The profiles correspond to the Z echoes shown in Fig.5.2A. Measurements made from video records of A(amplitude) scans. One A scan every 20 msec. 8 or 9 usable measurements per sounding beam position. Frequency 5.13 MHz.

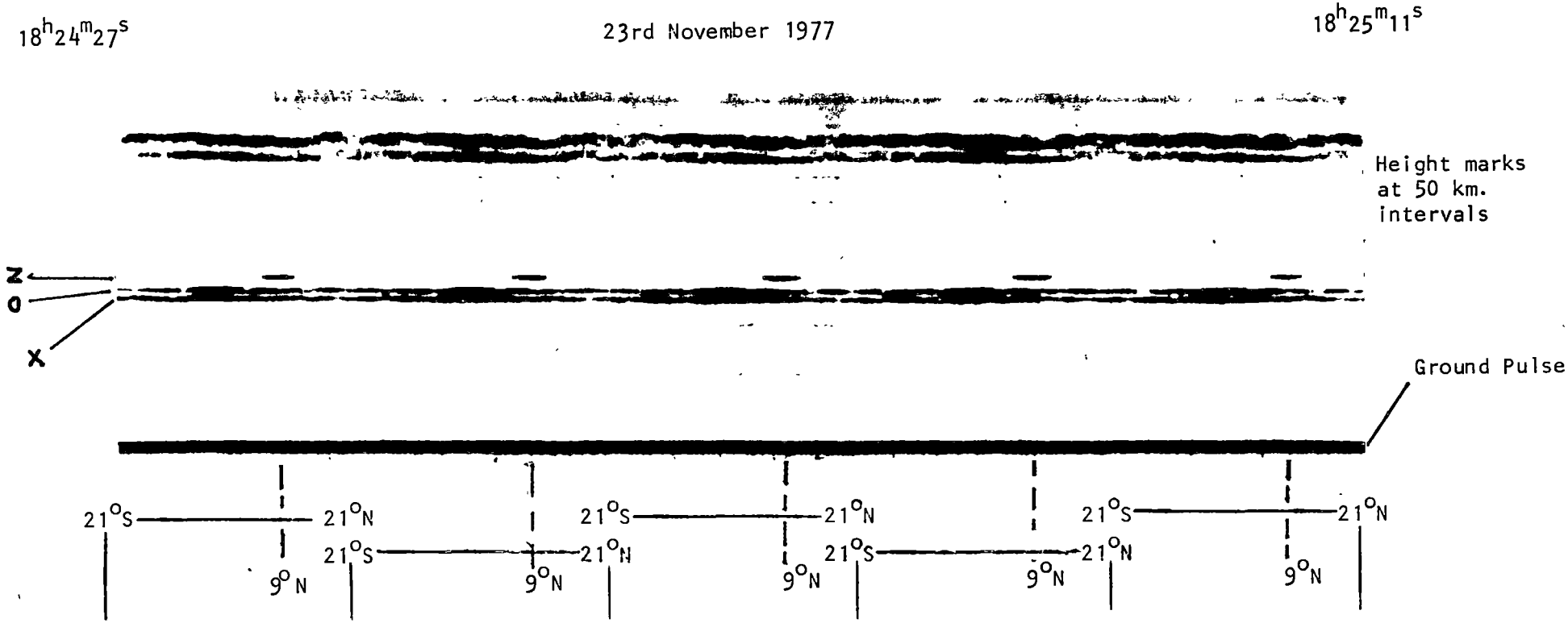

FIG.5.3 Llanherne h't record showing variation of O, X and Z echo strengths with zenith angle. Angular scan 21°S to 21°N in 1° steps at 5°/sec. (8.8 seconds per scan) High gain records. Frequency 5.9 MHz.

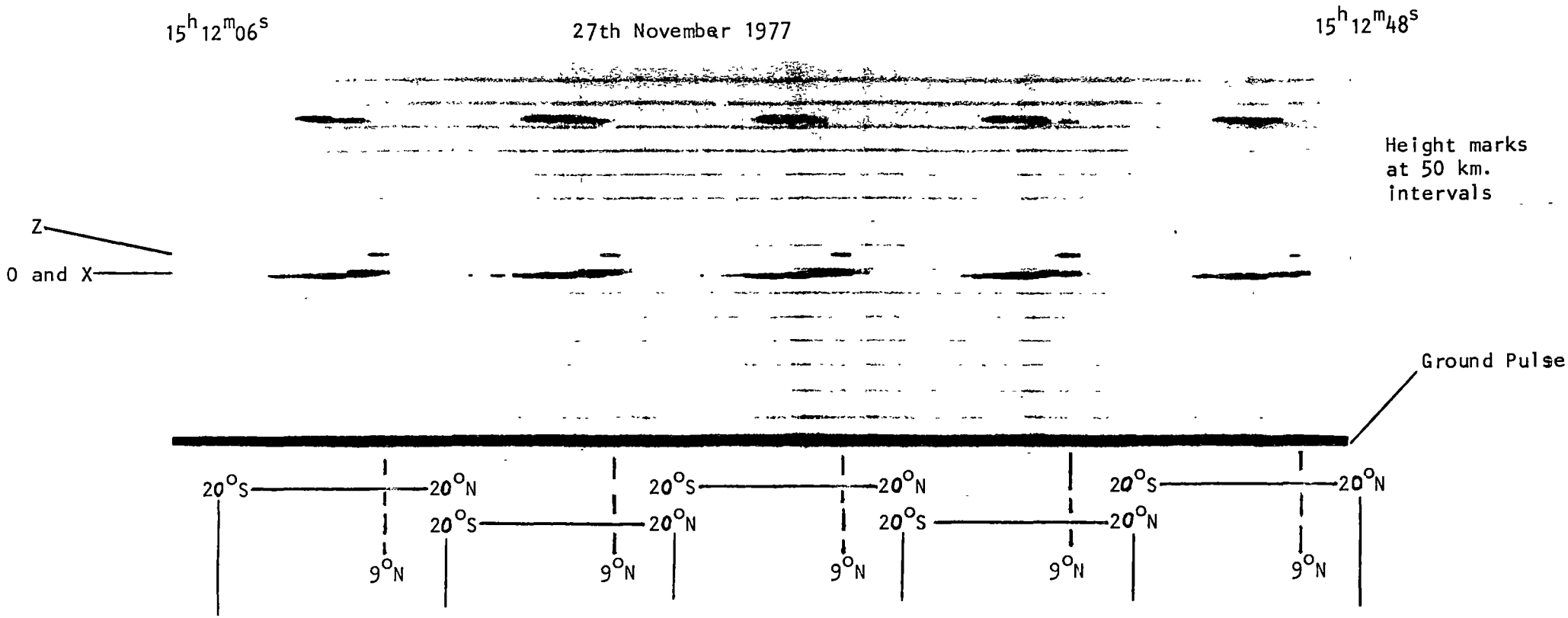

FIG.5.4 Llanherne h't record showing variation of O, X and Z echo strengths with zenith angle. Angular scan 20°S to 20°N in 1° steps at 5°/sec. (8.4 seconds per scan) Low gain records. Frequency 6.7 MHz.

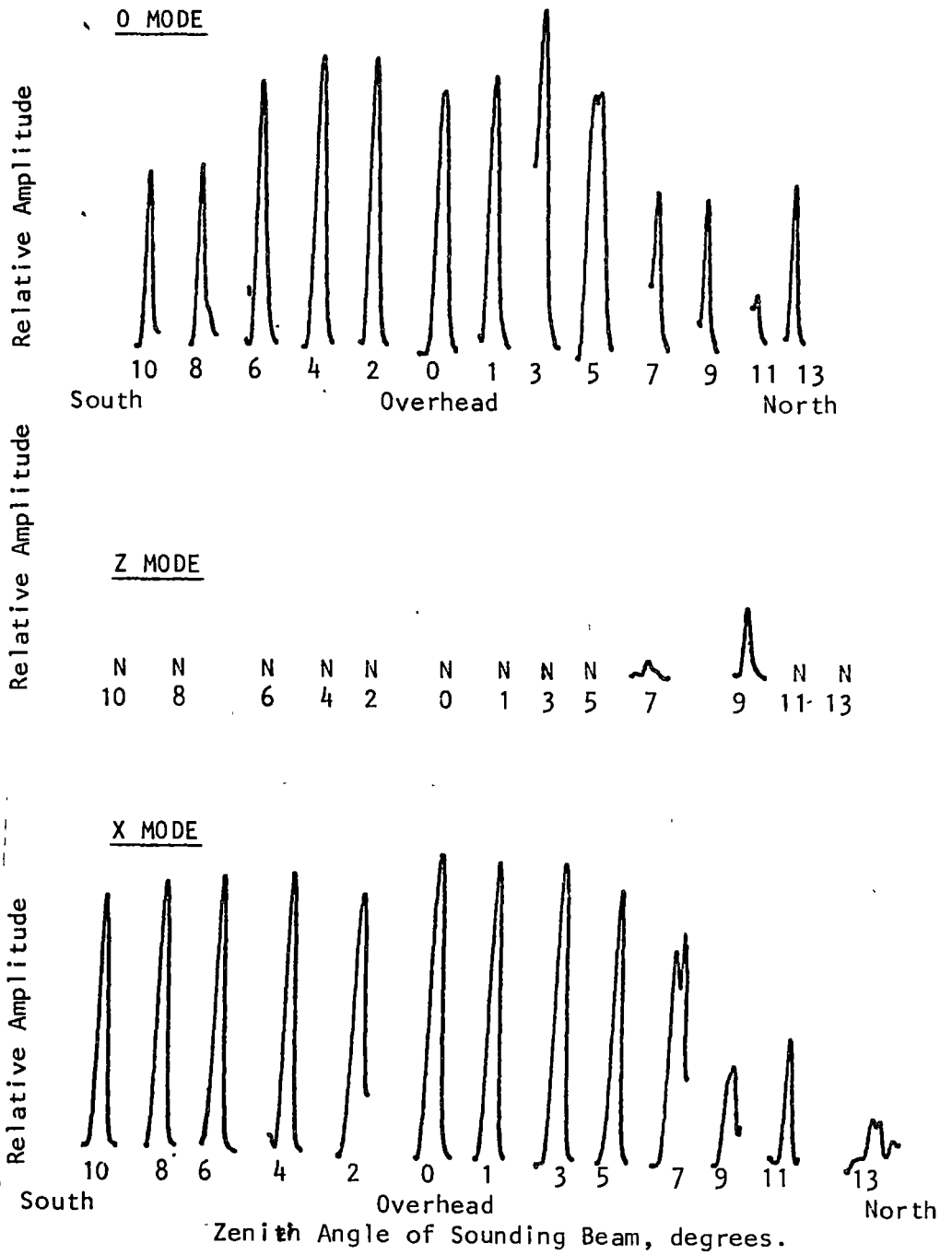

FIG.5.5 Variation with zenith angle of the 380 km. virtual height O,X and Z echo strengths. Profile of trace shown. High gain records only used. Angular scan 10^{o}S to 14^{o}N for this cycle.
N: Noise only, no trace.

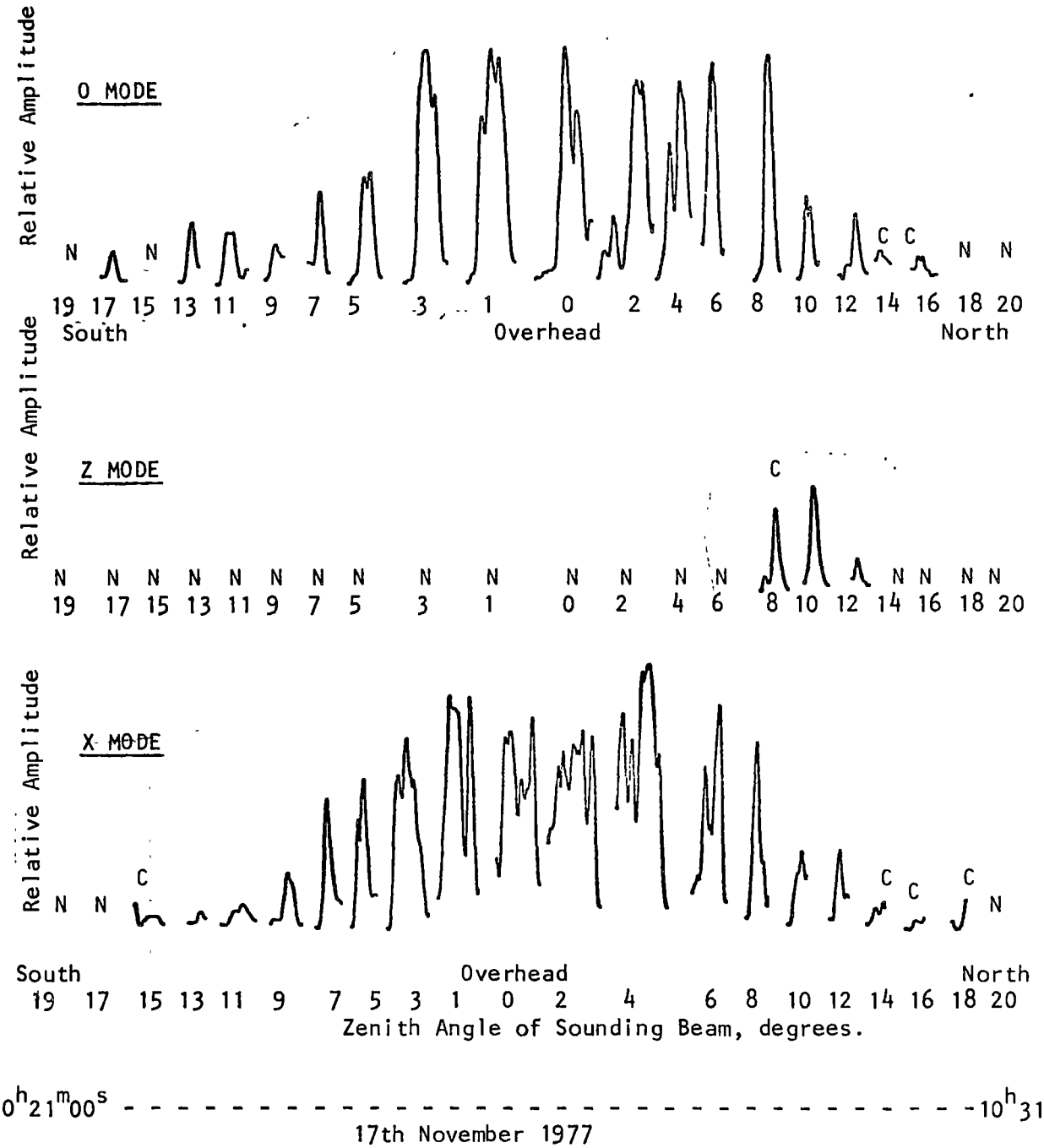

FIG.5.6 Variation with zenith angle of the 450 km.virtual height O, X and Z echo strengths. Profile of trace shown. High gain records only used. Angular scan 20°S to 20°N for this cycle.
N: Noise only, no trace.
C: Trace profile confused by noise.

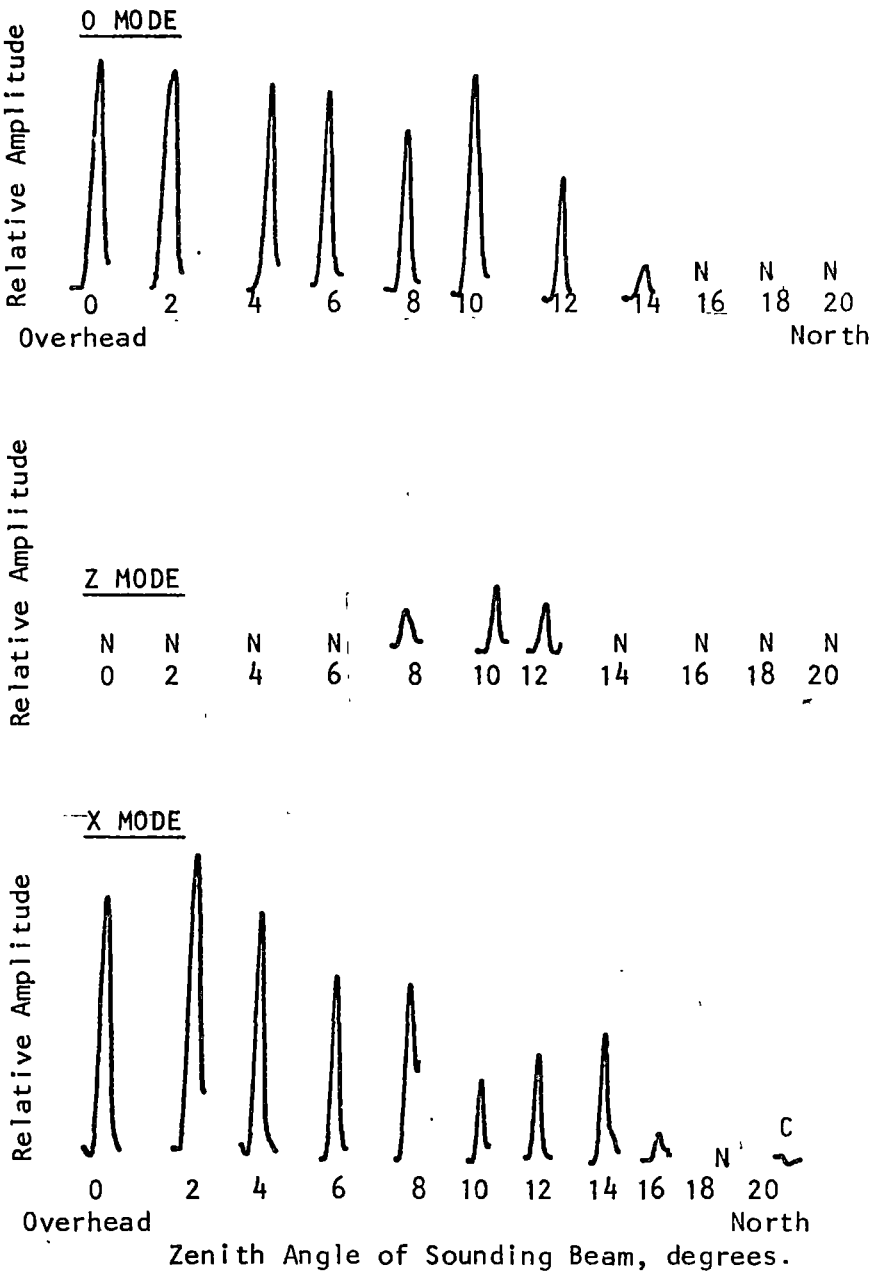

$23^h42^m00^s$ - - - - 25th November 1977 - - - - - - $23^h47^m15^s$

FIG.5.7 Variation with zenith angle of the 450 km. virtual height O, X and Z echo strengths. Profile of trace shown. High gain records only used. Angular scan 0^o(zenith) to 21^oN for this cycle.
N: Noise only, no trace.
C: Trace profile confused by noise.

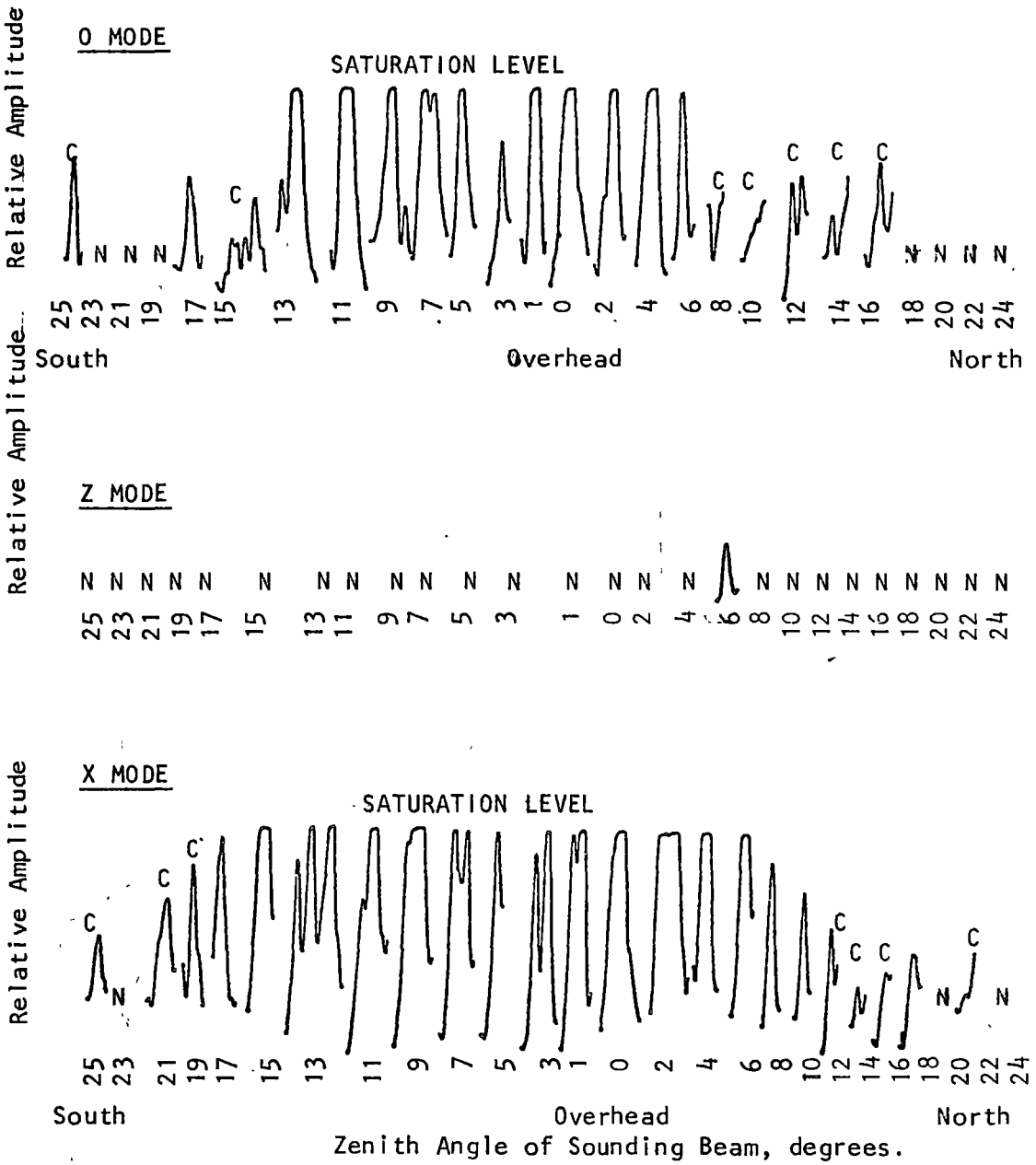

$21^h41^m30^s$ - $21^h54^m15^s$

23rd November 1977

FIG.5.8 Variation with zenith angle of the 415 km. virtual height O, X and Z echo strengths. Profile of trace shown. High gain records only used. Angular scan 25^oS to 25^oN for this cycle.
N: Noise only, no trace.
C: Trace profile confused by noise.

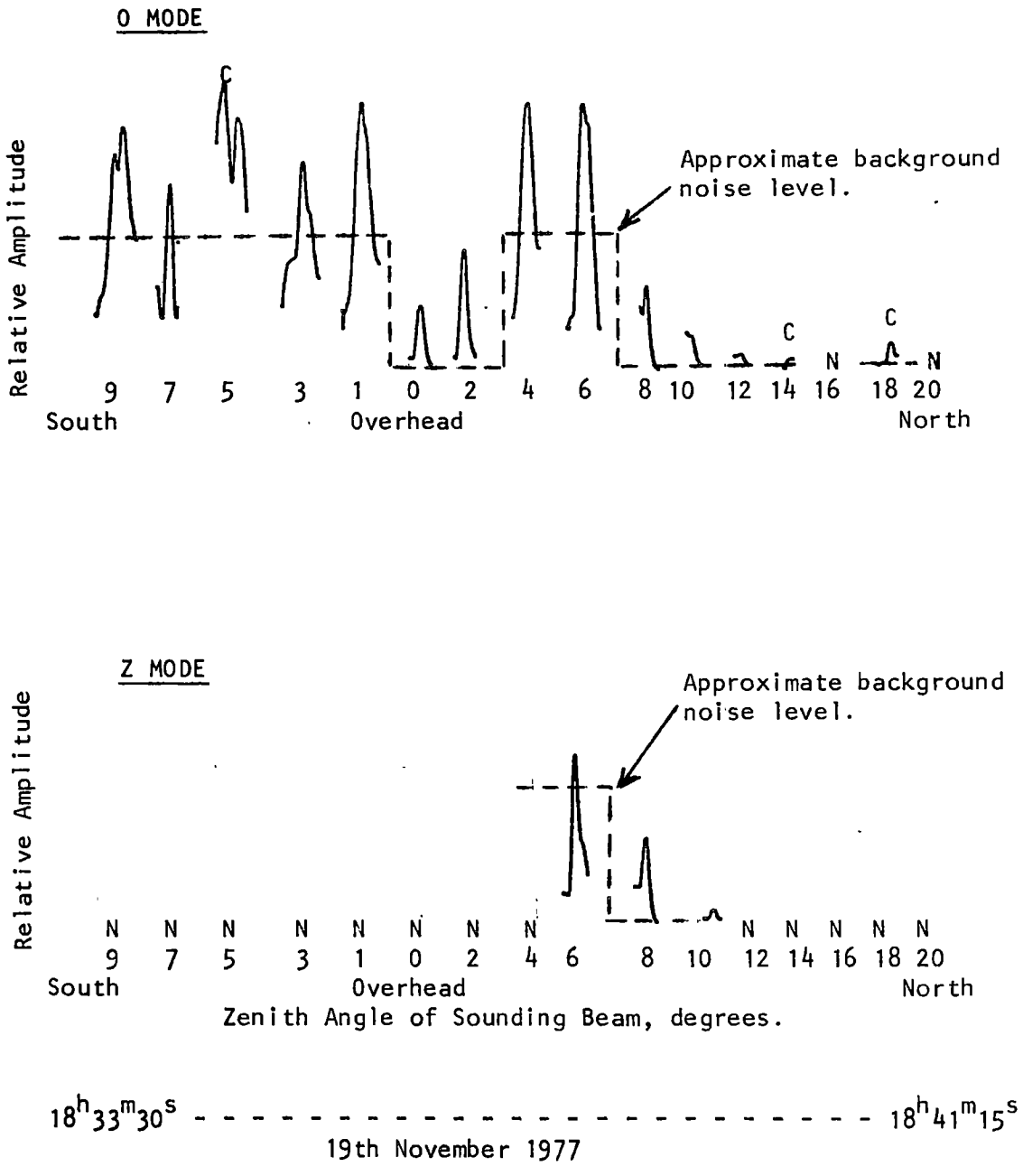

FIG.5.9 Variation with zenith angle of the 380 km. virtual height O and Z echo strengths. Profile of trace shown. High gain records only used. Angular scan 10^oS to 21^oN for this cycle.
N: Noise only, no trace.
C: Trace profile confused by noise.

(X mode measurements not possible)

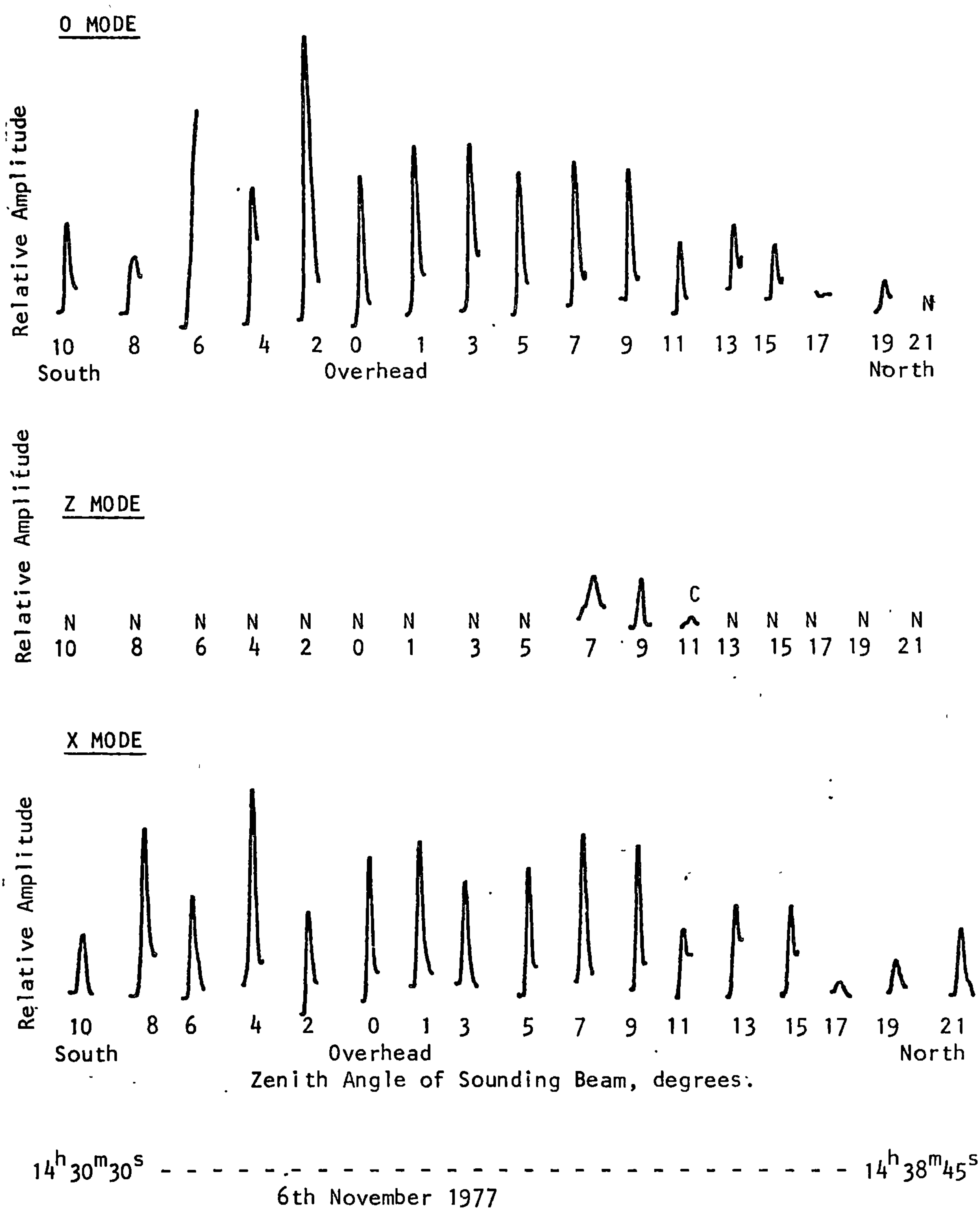

FIG.5.10 Variation with zenith angle of the 475 km. virtual height O, X and Z echo strengths. Profile of trace shown. High gain records only used. Angular scan 10°S to 21°N for this cycle.
N: Noise only, no trace
C: Trace profile confused by noise.

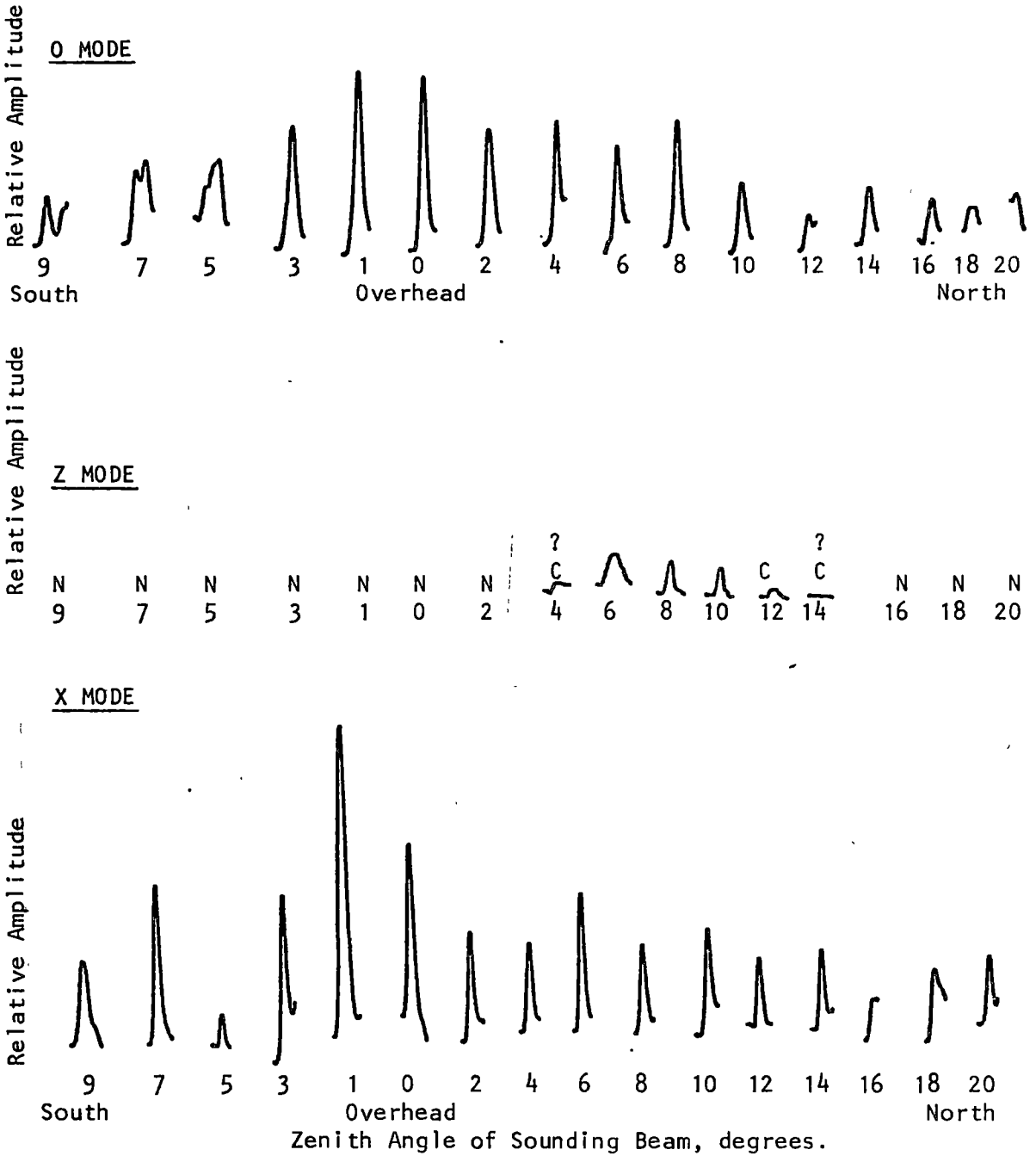

FIG.5.11 Variation with zenith angle of the 475 km. virtual height O, X and Z echo strengths. Profile of trace shown. High gain records only used. Angular scan 10^{o}S to 21^{o}N for this cycle.
N: Noise only, no trace.
C: Trace profile confused by noise.
?: Possible but not positive Z trace.

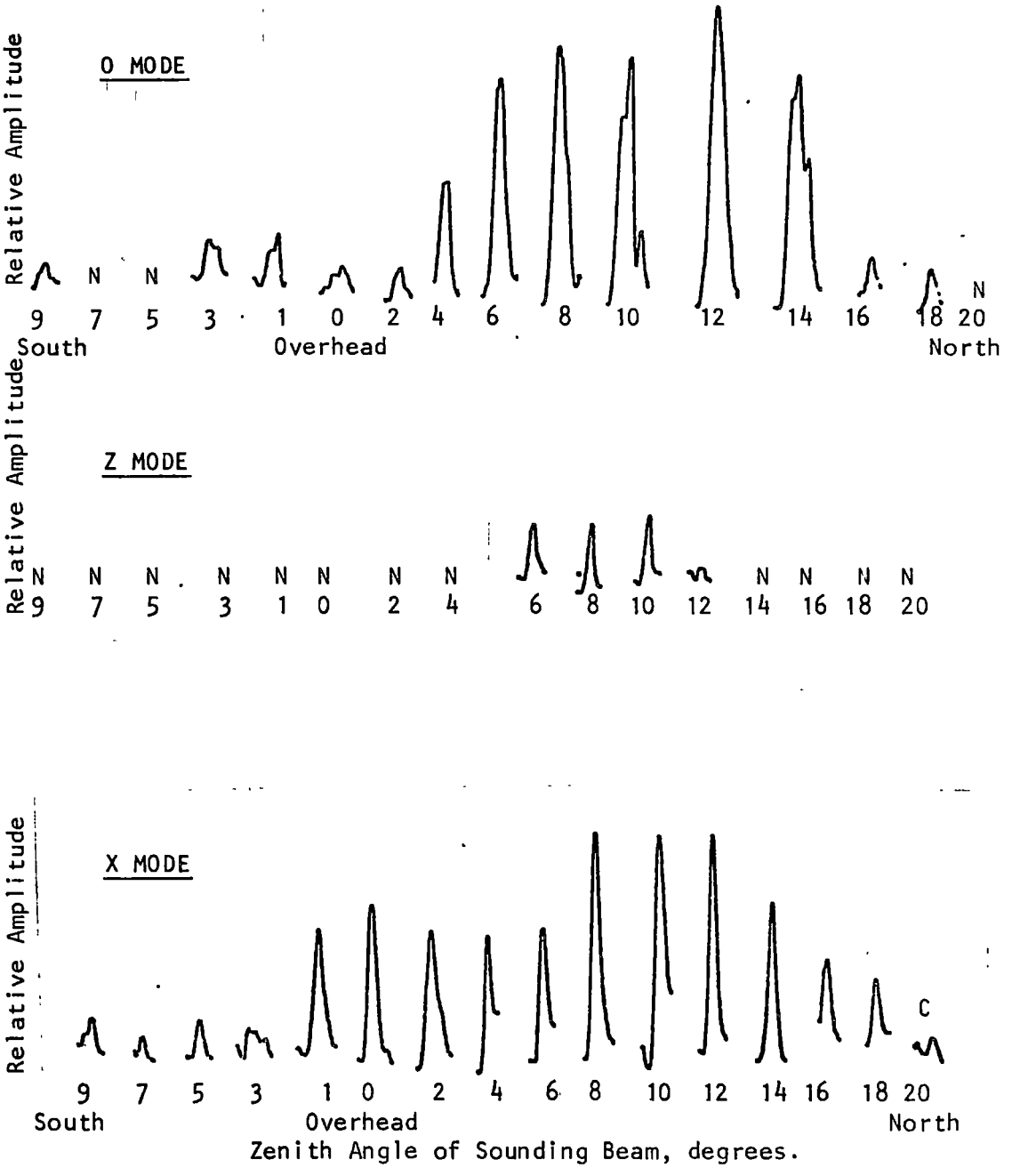

FIG.5.12 Variation with zenith angle of the 340 km. virtual height O, X and Z echo strengths. Profile of trace shown. High gain records only used. Angular scan 10^{o}S to 21^{o}N for this cycle.
N: Noise only, no trace.
C: Trace profile confused by noise.

producing a second (generally smaller) broad peak which merged into the main peak on the negative (southern) side and usually dropped fairly quickly on the northern side. This effect is illustrated by Figs.5.6, 5.7, 5.10 and 5.11. However, this feature is by no means unique to Z echo presence as examples could readily be found during Z echo absence (it should be noted that this effect is real and is not due to side-lobes detecting the main reflection). In fact, for any O and X angular distribution found during the presence of the Z echo a similar example could be found during its absence. The converse is not true. The Z echo was not found to be present on any records without the O and/or X echoes being present at the same zenith angles.

The average variation of O and X echo strengths with zenith angle during an extended period of Z echo presence is shown by Figs.5.13 and 5.14. For comparison, average variations of the O and X echo strengths with zenith angle during periods of absence of the Z echo are shown by Figs.5.15 to 5.18. Figs.5.19 and 5.20 are examples of O and X echo distributions for individual cycles in the absence of the Z echo. The virtual height chosen when making a comparison record was the virtual height which might be expected to fall on the centre of the Z trace, had Z echoes been present.

FIG.5.13

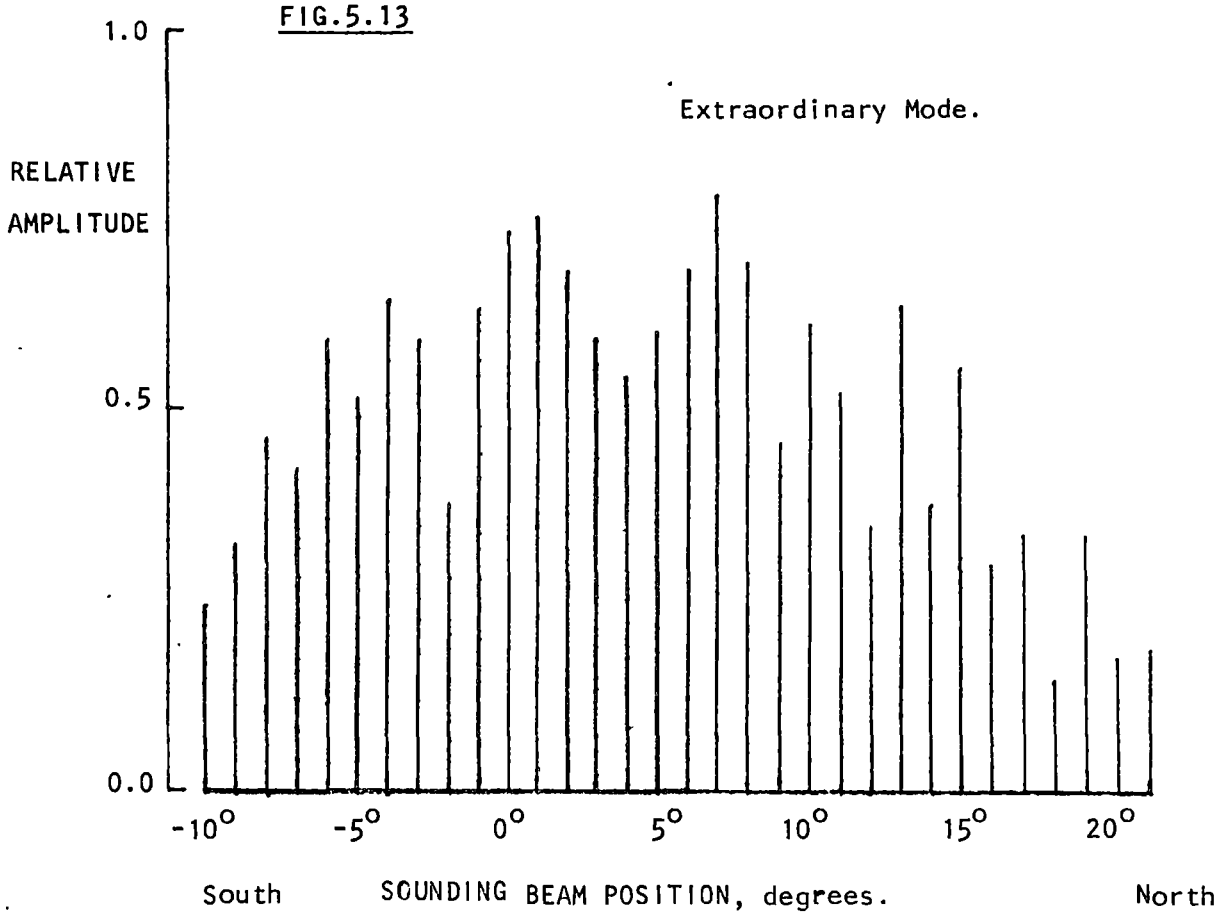

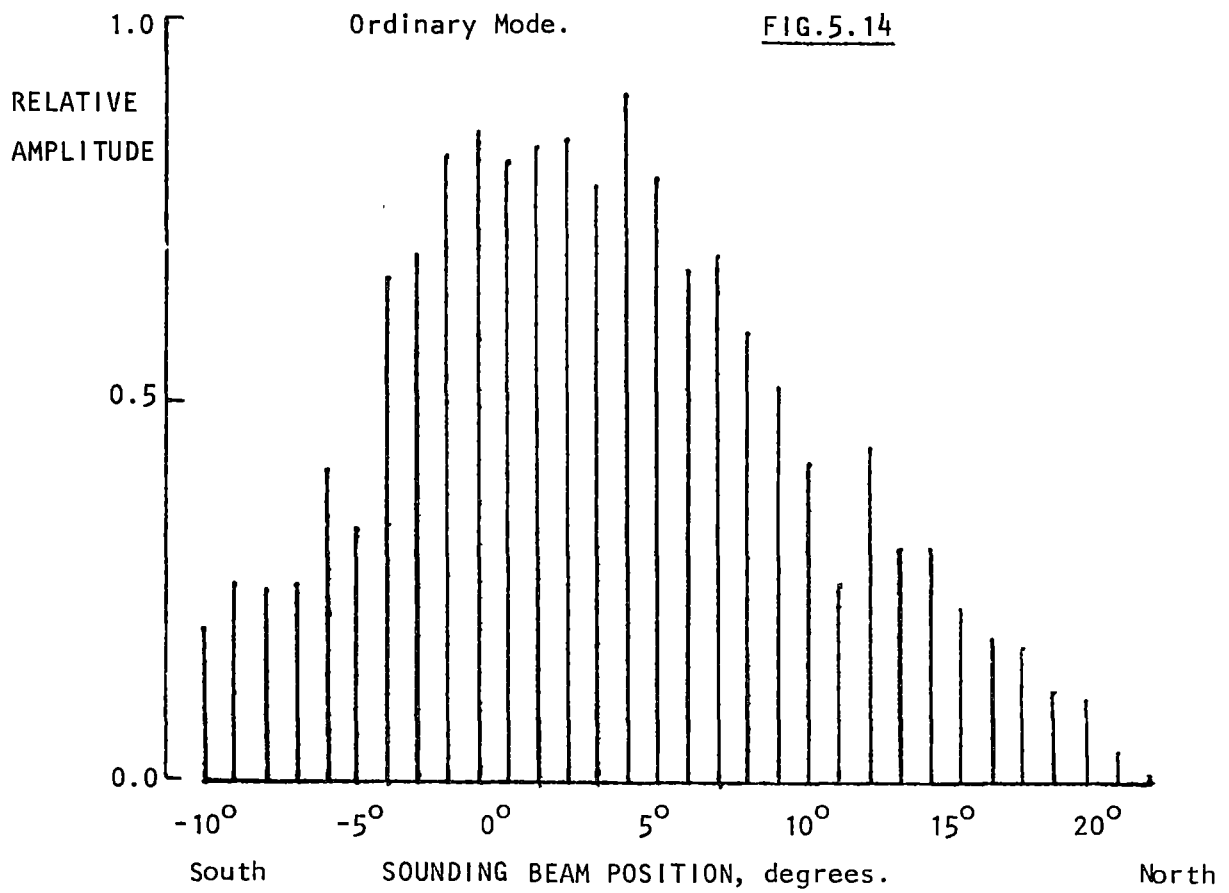

FIG.5.14

FIGS.5.13 and 5.14 Average variation of O and X echo amplitudes at virtual height 475 km. during 15 h'f cycles (beam zenith angle 10°S to 21°N in 1° steps; 15 seconds per h'f ionogram at each beam position; alternate high and low gain ionograms). High gain ionograms only used. Amplitude at each beam position is average of 7 or 8 measurements (15 measurements at zenith). Z echo present throughout this period (1425 to 1626 hrs., 6th November, 1977).

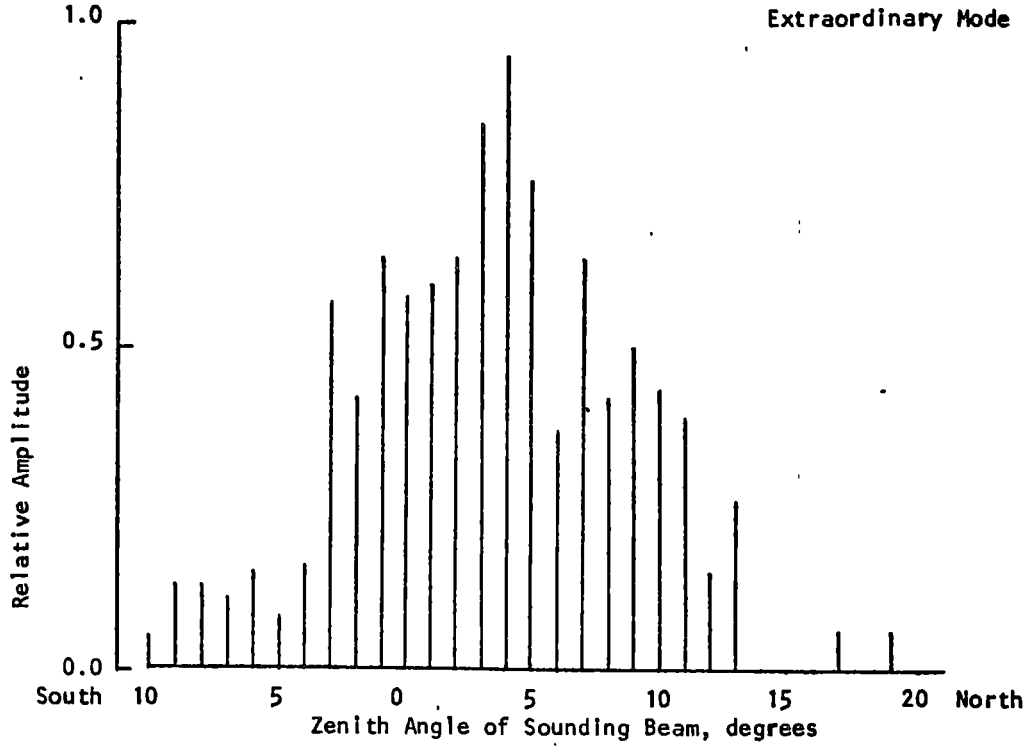

FIG.5.15 Average variation of X echo amplitude at virtual height 525 km. during 6 h'f cycles (beam zenith angle 10°S to 21°N in 1°steps; 15 seconds per h'f ionogram at each beam position; alternate high and low gain ionograms). High gain ionograms only used. Amplitude at each beam position is average of 3 measurements (6 measurements at zenith). Z echo is absent throughout this period (1252 to 1341 hrs., 30 October 1977).

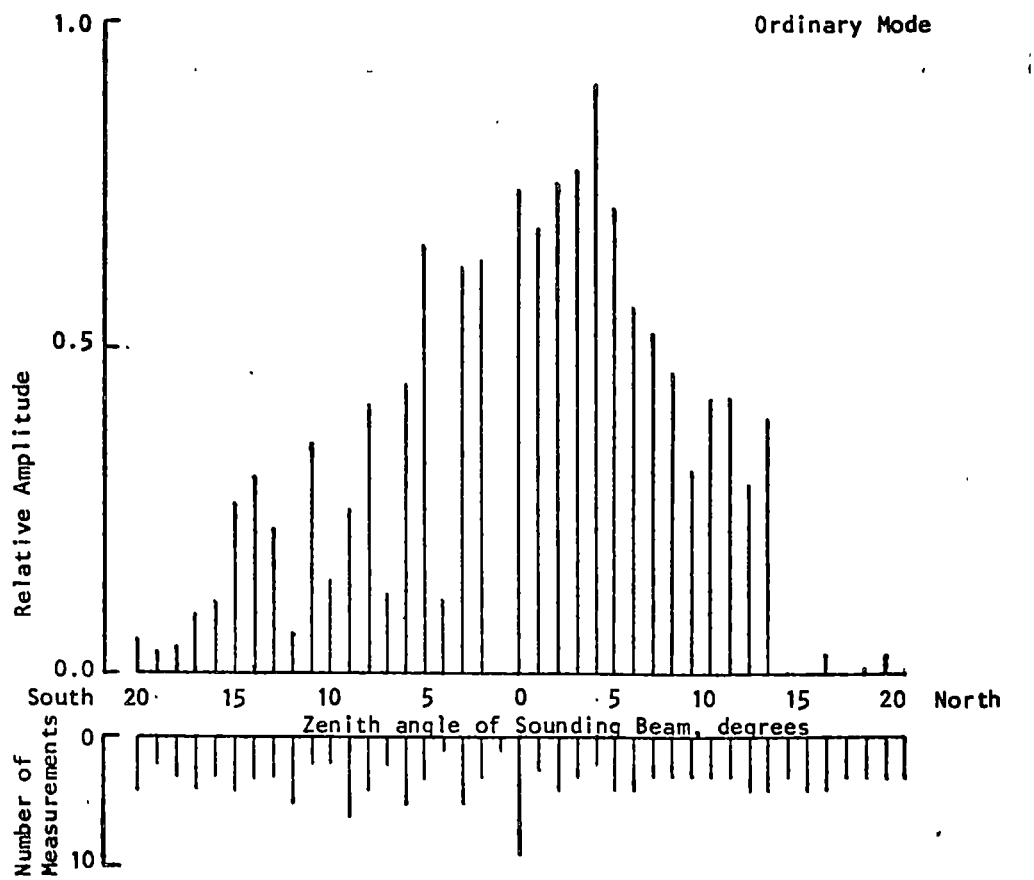

FIG.5.16 Average variation of O echo amplitude at virtual height 375 km. during 9 h'f cycles (beam zenith angle 20°S to 20°N in 3°*steps; 15 seconds per h'f ionogram at each beam position; all ionograms high gain). Amplitude at each beam position is average of number of measurements shown. Z echo is absent throughout this period (1047 to 1122 hrs., 1st December 1977) but present 4 hours later.

*Nominal beam position increment - 1° and 2° steps also occurred.

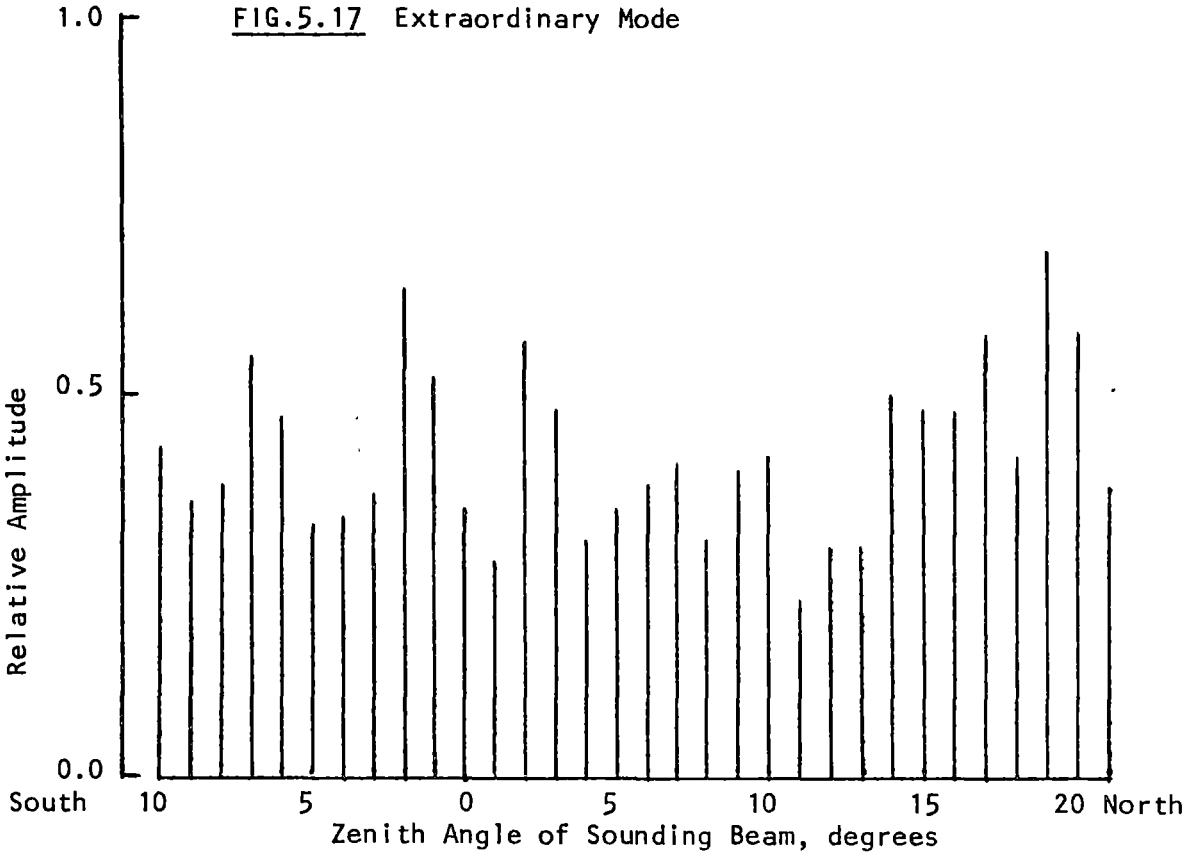

FIG.5.17 Extraordinary Mode

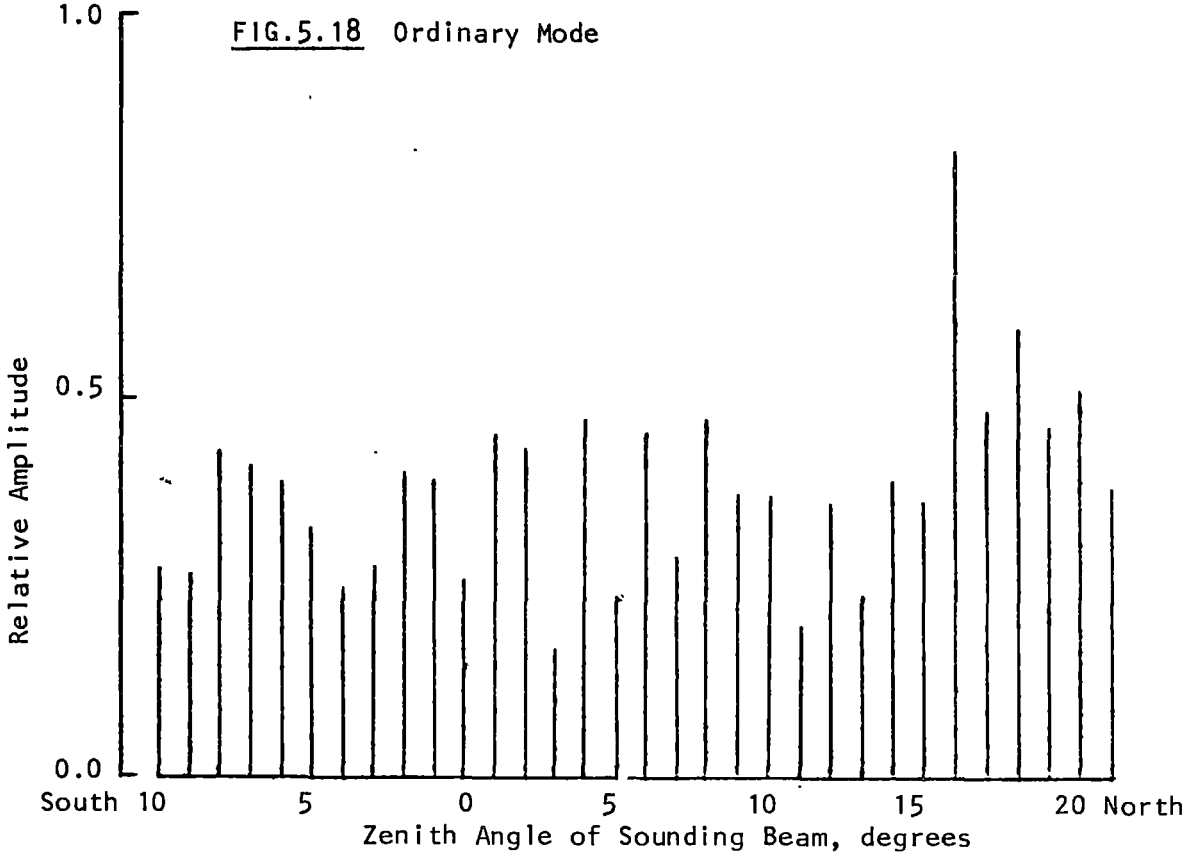

FIG.5.18 Ordinary Mode

FIGS.5.17 and 5.18 Average variation of O and X echo amplitudes at virtual height 425 km. during 11 h'f cycles (beam zenith angle 10^{o}S to 21^{o}N in 1^{o} steps; 15 seconds per h'f ionogram at each beam position; alternate high and low gain ionograms). High gain ionograms only used. Amplitude at each position is average of 5 or 6 measurements (11 measurements at zenith). Z echo absent throughout this period (2017 to 2140 hrs., 26th October 1977).

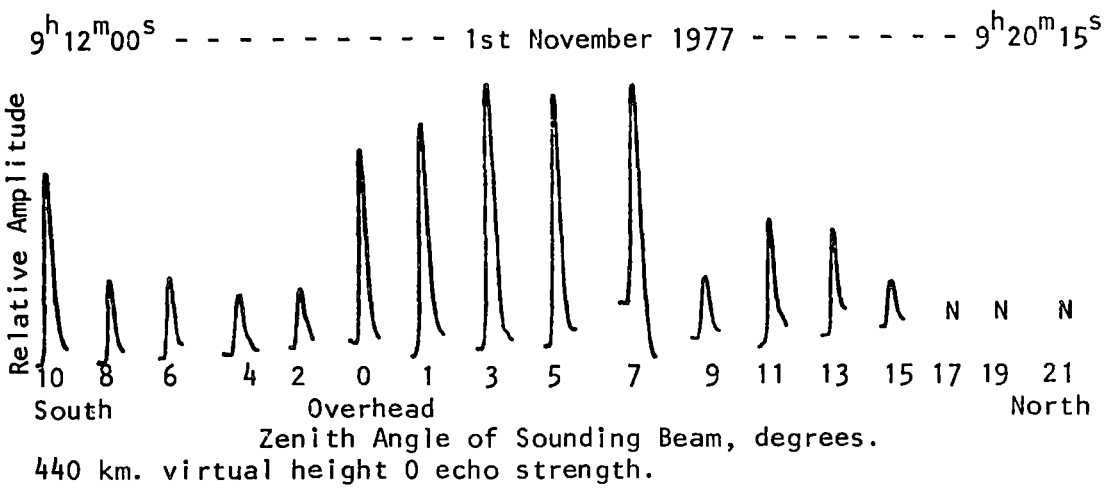

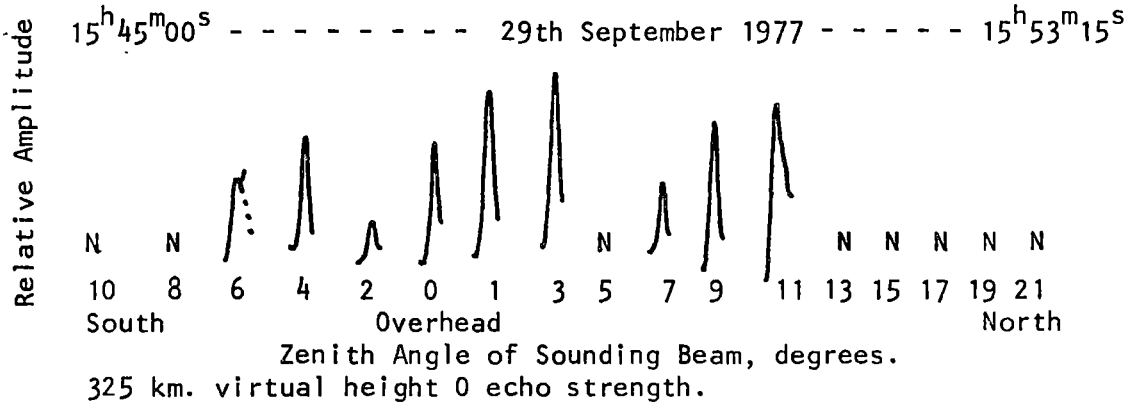

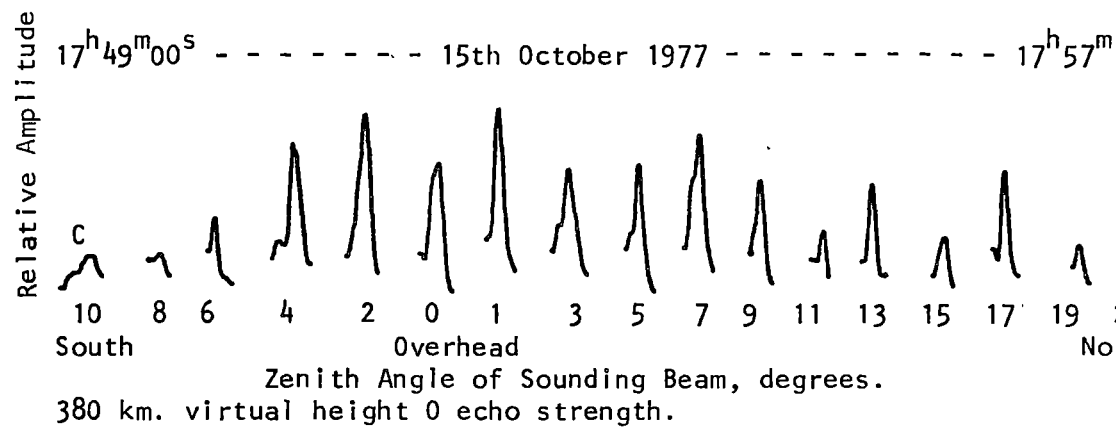

FIG.5.19 Examples of the variation with zenith angle of the 0 mode echo strength (at Z echo virtual heights) in the absence of the Z echo. Profile of trace shown. High gain records only used. Angular scan 10°S to 21°N for these cycles.
N: Noise only, no trace.
C: Trace profile confused by noise.

(See Fig.5.20 for corresponding extraordinary mode records)

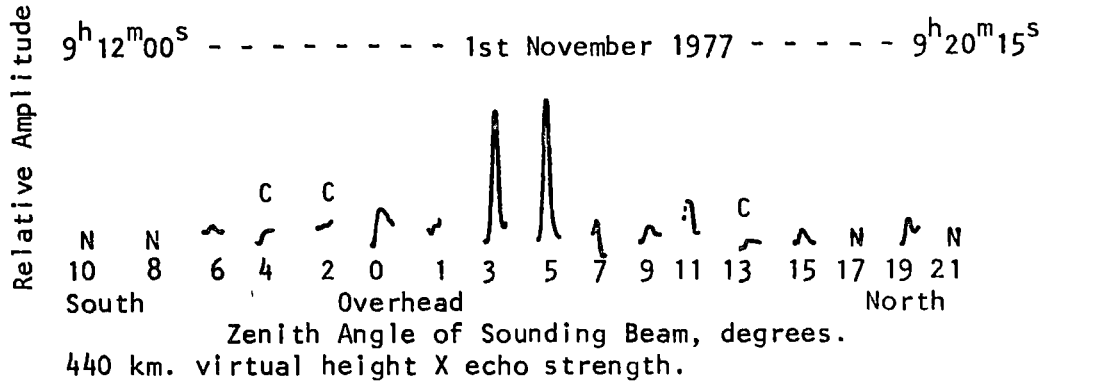

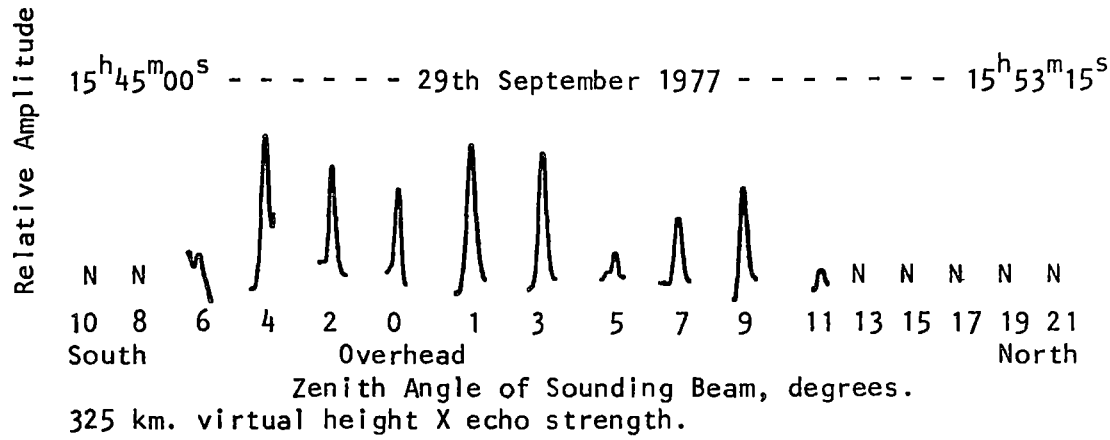

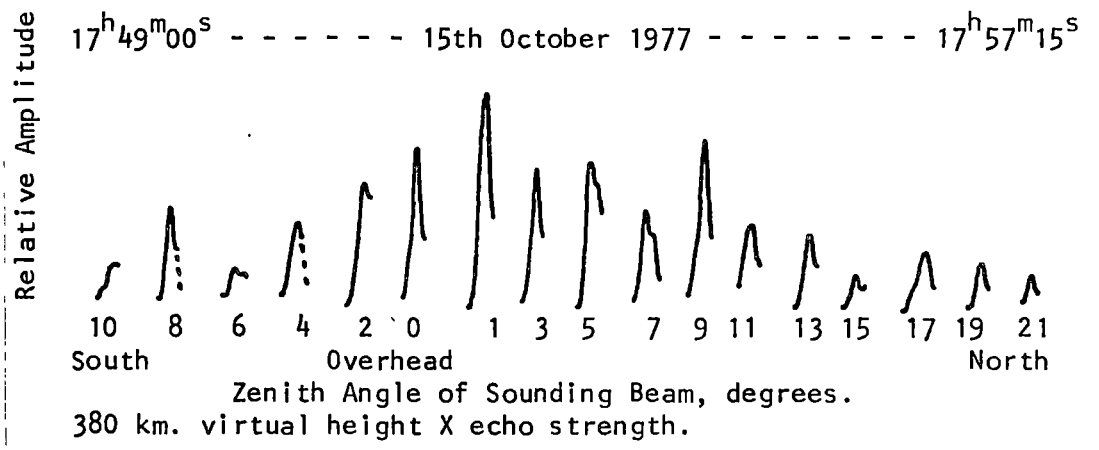

FIG.5.20 Examples of the variation with zenith angle of the X mode echo strength (at Z echo virtual heights) in the absence of the Z echo. Profile of trace shown. High gain records only used. Angular scan 10^oS to 21^oN for these cycles.
N: Noise only, no trace.
C: Trace profile confused by noise.

(See Fig.5.19 for corresponding ordinary mode records)

5.3 Scattering Patterns On h'f Ionograms

Over a year's worth of Hobart on the hour records were checked for Z echo occurrence during 1980 and 1981 (by Mr. G.T.Goldstone). Inspection of the ionograms showing the Z trace revealed that in no case was the ionogram of a type which could be explained by Renau's(1959,1960) scattering models. Ionograms showing Z mode and appearing in the literature were also examined as were records randomly selected from one or two years of Casey, Mawson, Macquarie Island, Mundaring and Brisbane records plus random samples selected from the last twenty years' Hobart records. Again no examples showing both Z echo and Renau type scattering could be found. The seasonal and diurnal variation of occurrence of the 1981 Hobart on-the-hour Z echoes are shown in Figs.5.21 to 5.23. Figs.5.24 to 5.26 show a representative sample of the on-the-hour Hobart Z traces for 1981.

5.4 Fast Runs

Fast runs at both Llanherne and South Lea showed that the Z echo can persist for over 15 minutes at a time with gaps of no more than 30 seconds (Figs.5.27 to 5.30). In the case of Llanherne a low gain record is presumed not to show absence of the Z echo while it has high gain records displaying Z echo on either side of it. It can be seen that there is no

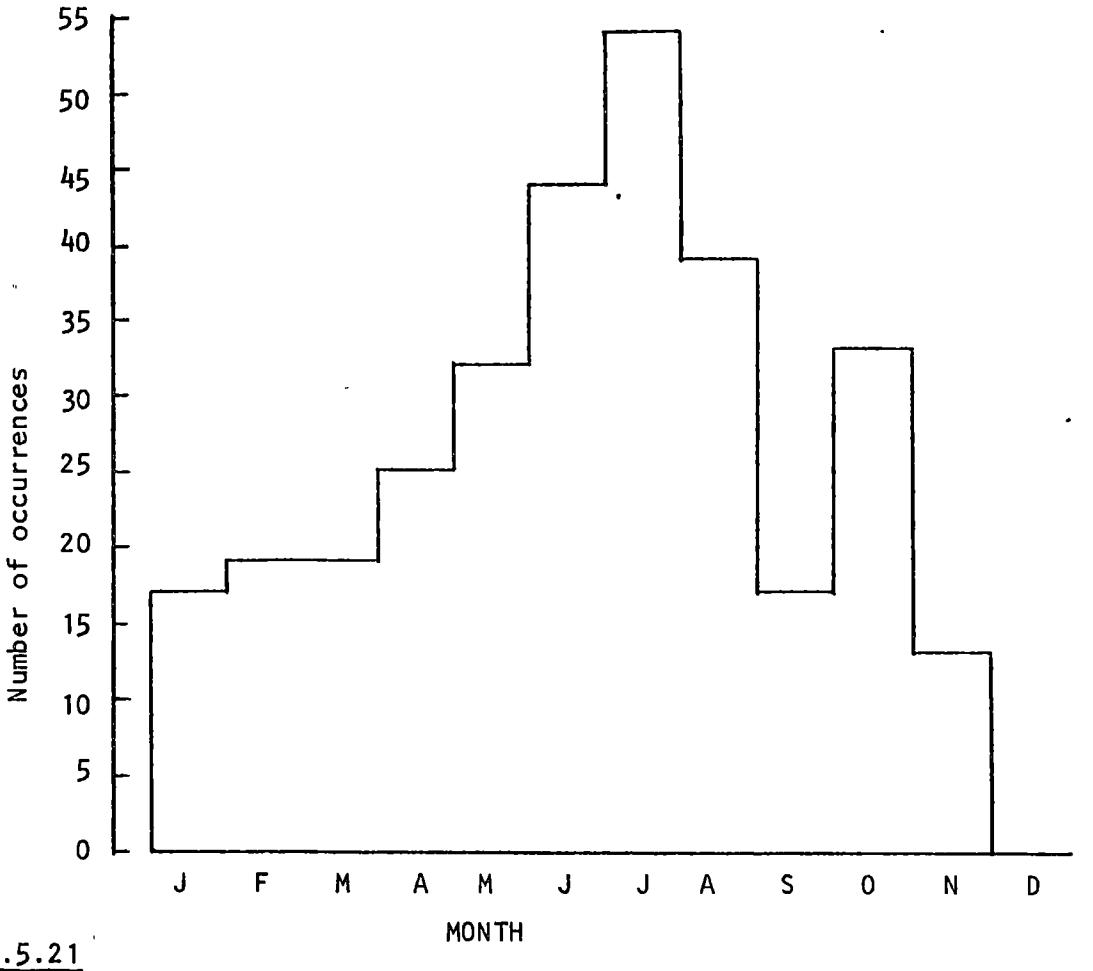

FIG.5.21

Seasonal variation of occurrence of the 1981 Hobart on-the-hour Z echoes.

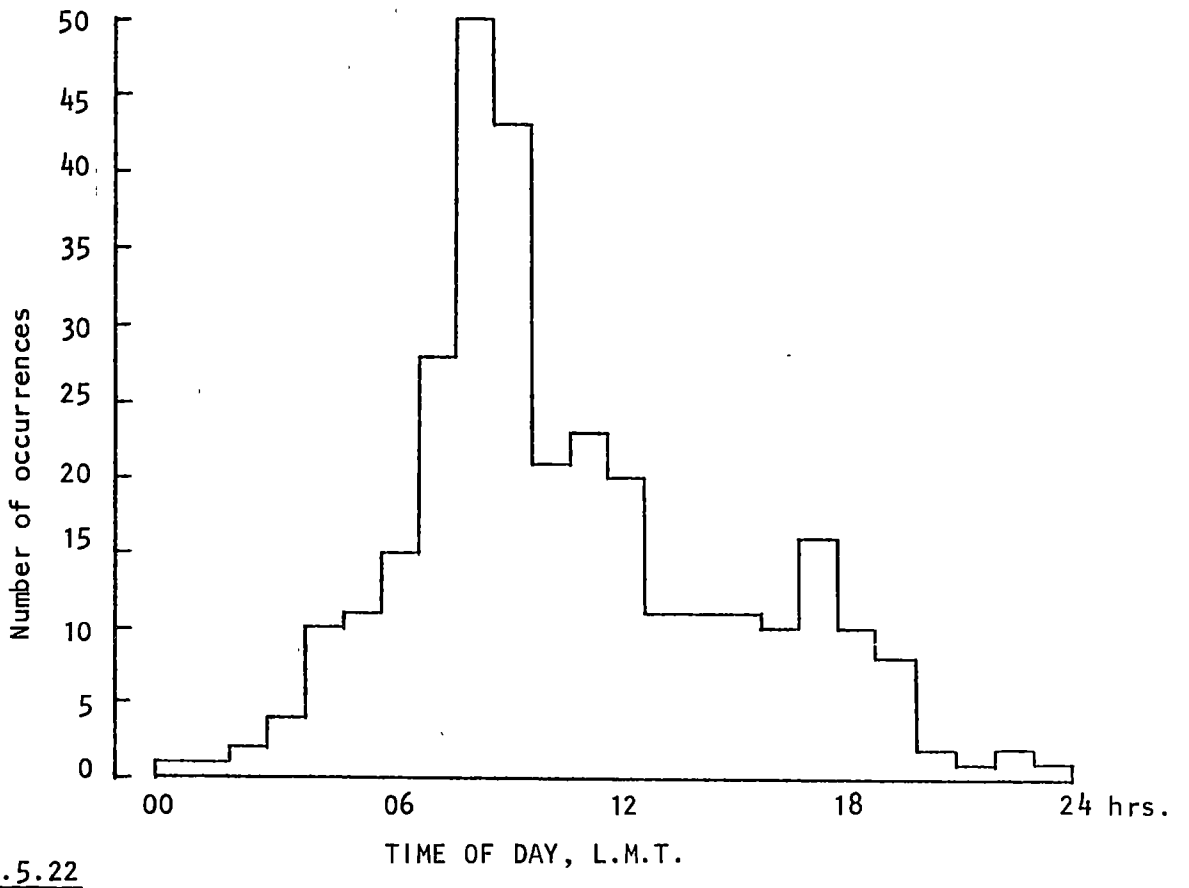

FIG.5.22

Diurnal variation of occurrence of the 1981 Hobart on-the hour Z echoes. (All days)

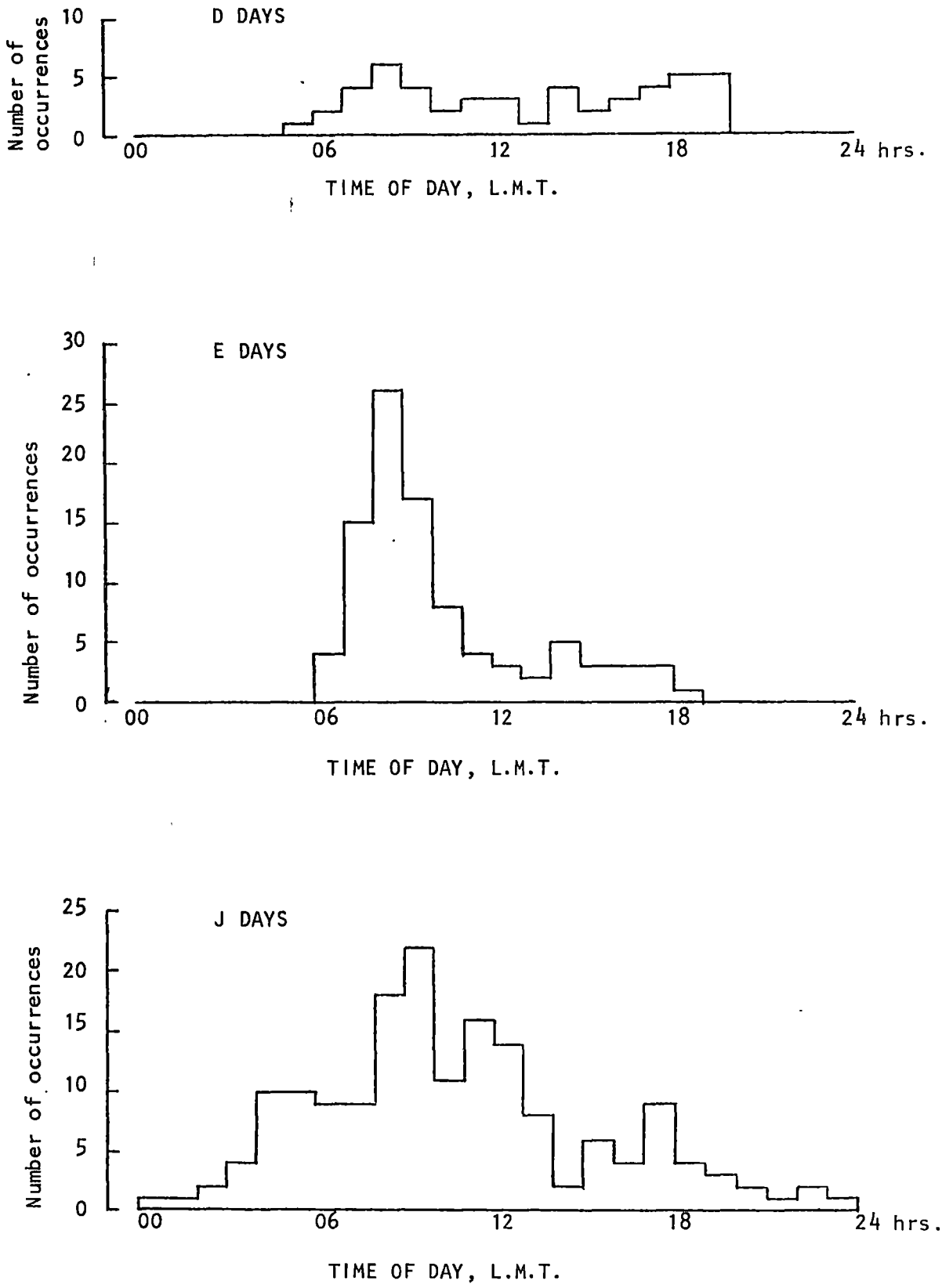

FIG.5.23

Diurnal variation of occurrence of on-the-hour Z echoes for D, E and J days at Hobart, 1981.

DAY 323
0500 hrs.

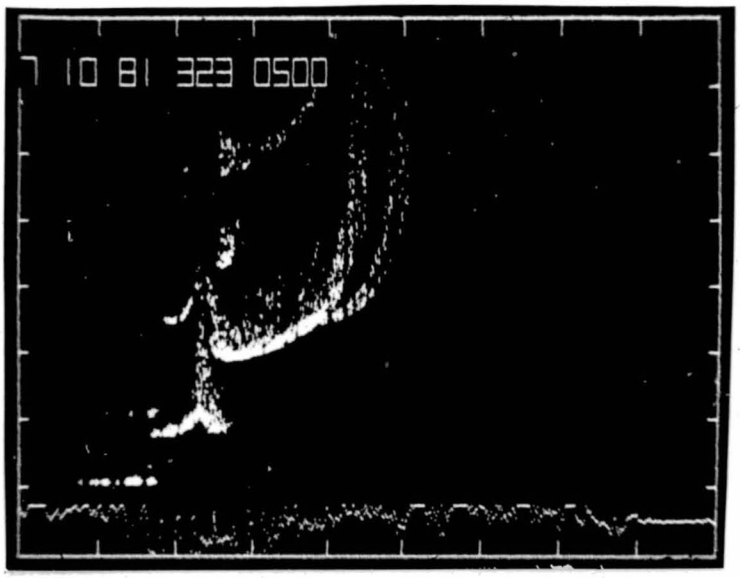

DAY 048
1300 hrs.

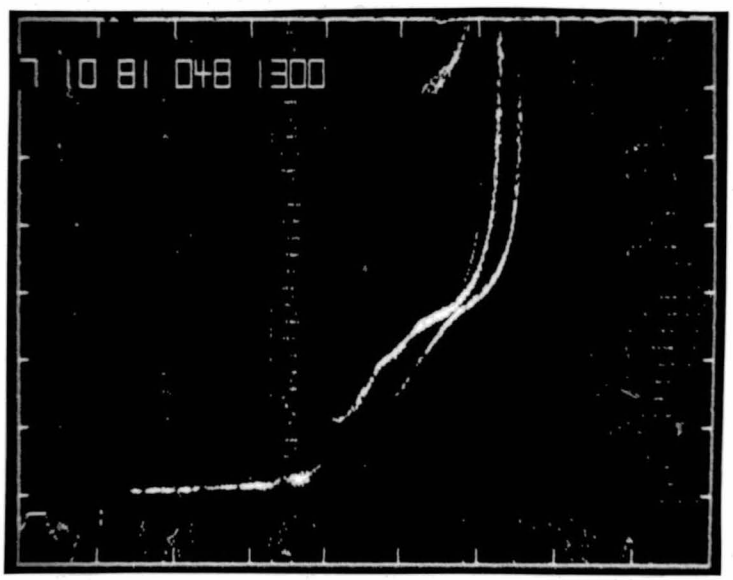

DAY 033
1900 hrs.

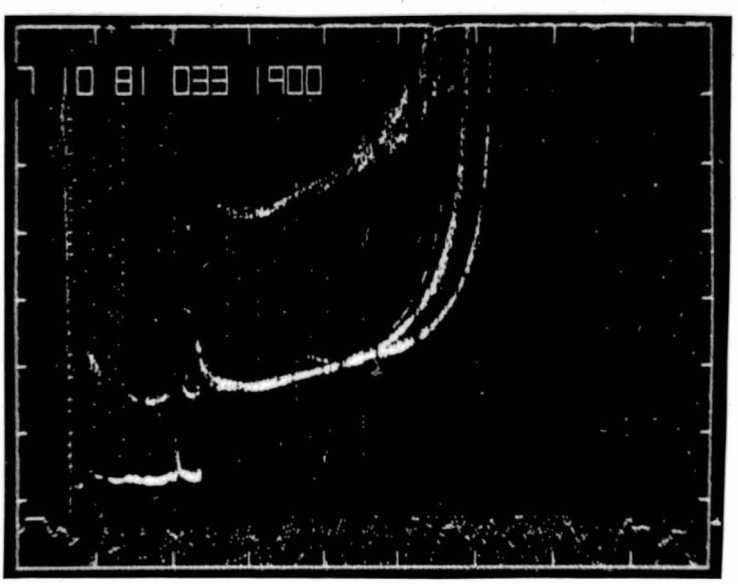

FIG.5.24 Representative sample of Hobart 1981 on-the-hour South Lea ionograms showing Z echo, D days.

DAY 104
0700 hrs.

DAY 064
1000 hrs.

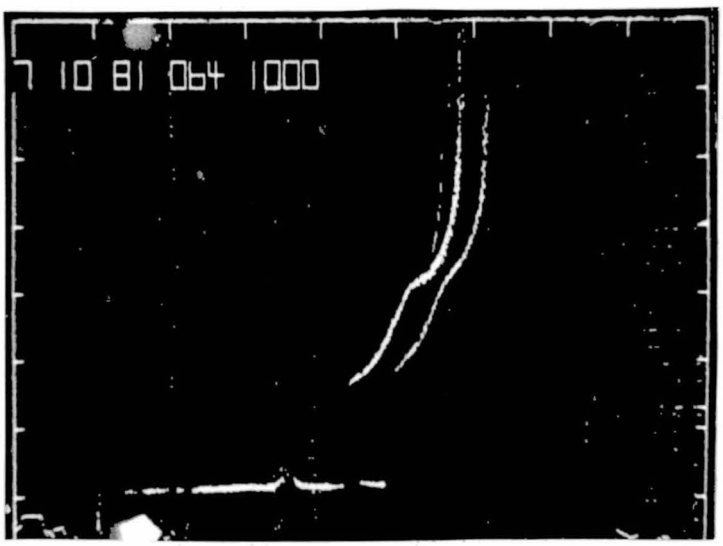

DAY 299
1400 hrs.

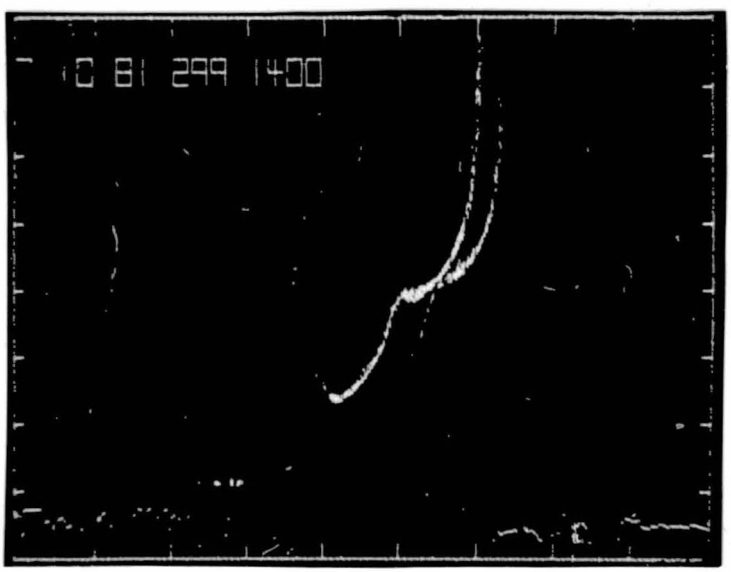

FIG.5.25 Representative sample of Hobart 1981 on-the-hour South Lea ionograms showing Z echo, E days.

DAY 219
0300 hrs.

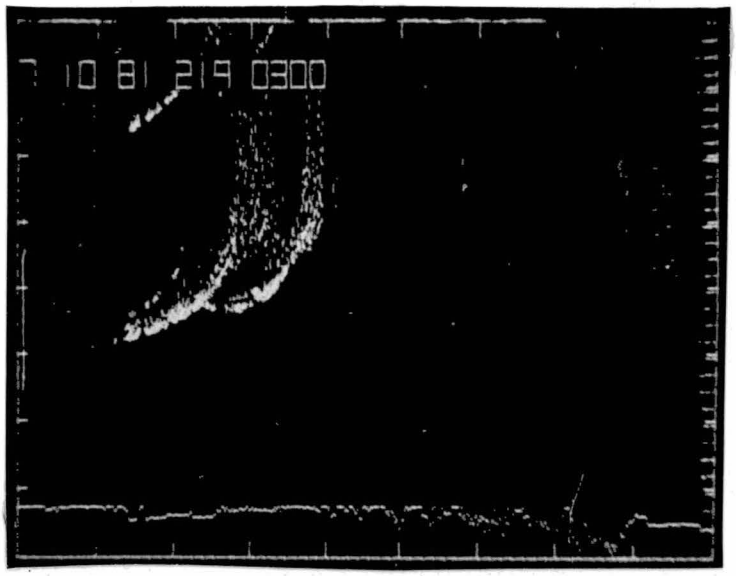

DAY 148
0600 hrs.

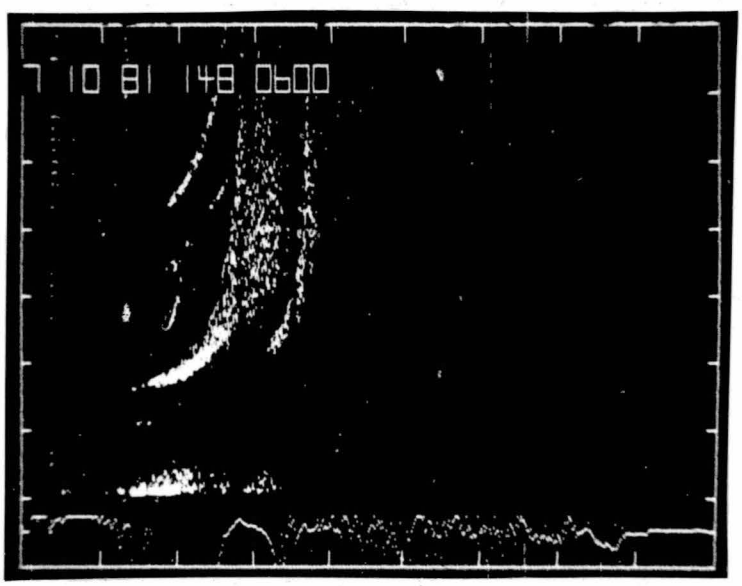

DAY 161
0900 hrs.

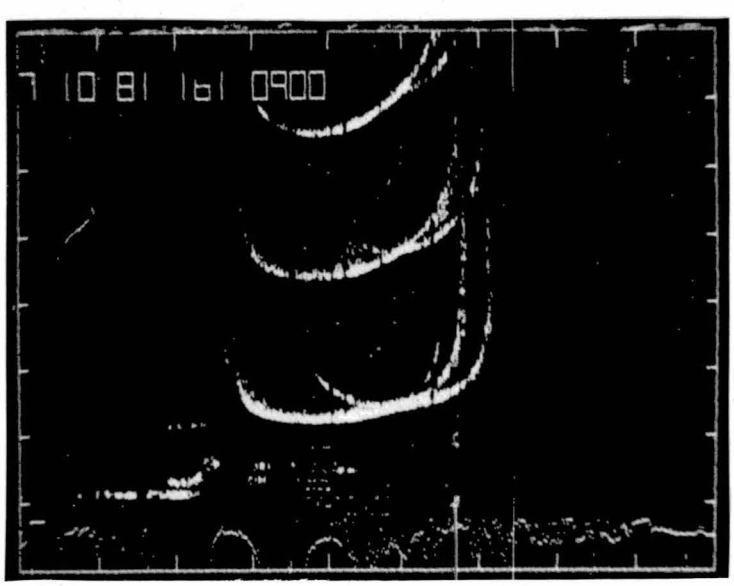

FIG.5.26A Representative sample of Hobart 1981 on-the-hour South Lea ionograms showing Z echo, J days.

DAY 236
1200 hrs.

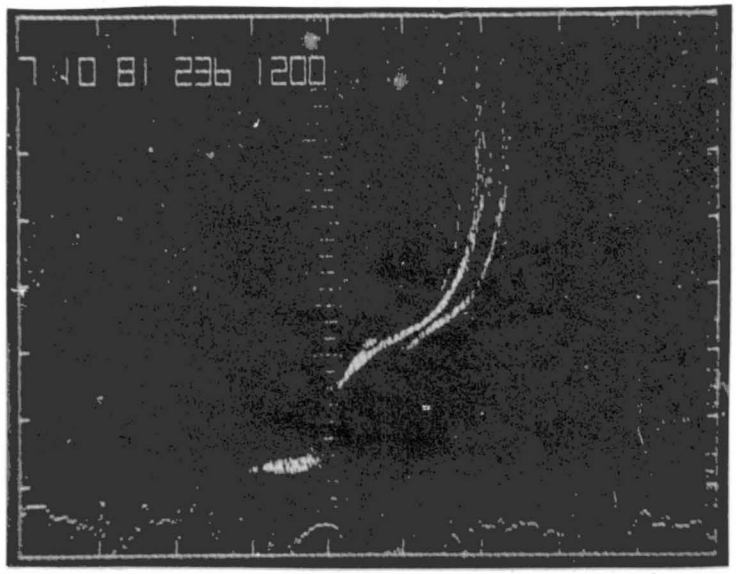

DAY 185
1500 hrs.

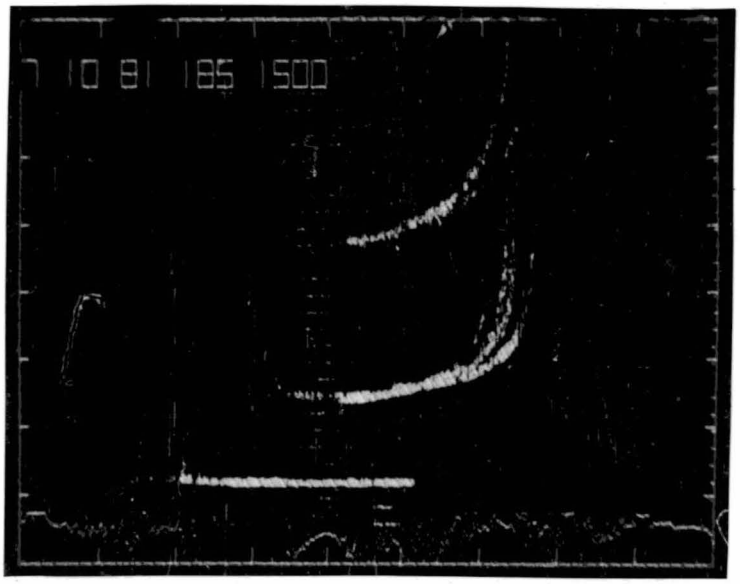

DAY 199
2100 hrs.

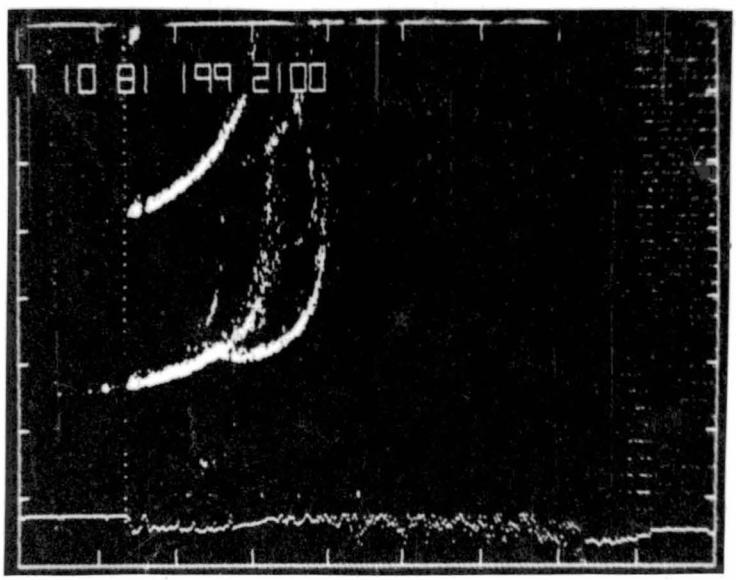

FIG.5.26B Representative sample of Hobart 1981 on-the-hour South Lea ionograms showing Z echo, J days.

START $18^h 18^m 00^s$ $18^h 26^m 48^s$ END

ZZZZZ?ZZZZZZZZZZZZZZƵZZZZZZƵZZZZZZZZZZZZZZZZZZZZZZƵZƵZ---ZZZ

HHHHHHHHHLLLHHHHHHHHLHHHHHHLHLHLHLHLHHHHHHHHHHHHHHLHLHLHLHHH H: High Gain; L: Low Gain.

FIG.5.27 Llanherne Fixed Frequency (5.9 MHz.) Fast Run, 23rd. November 1977.
The width of one letter represents the time taken for one angular scan (8.8 seconds).
Angular scan 21°S to 21°N (zenith angle) in 1° steps at 5°/sec.
The presence or absence of the Z echo is indicated as follows -

- Z - Z echo present.
- ? - Z echo possibly but not positively present.
- \- - Z echo absent.
- Ƶ - Z echo absent on low gain record but presumed present as present on flanking high gain records.

START $15^h 01^m 44^s$ END $15^h 15^m 45^s$

ZZZZZZZZZZZZZZZZZ?ZZZZZZZ?ZZZZZZZZƵZZZZZZZZZZZZZZZZZZZZZZZZZZZZZZZZZZZZZZZZZZZZZZZZZZZZZZZZ-

HHHHHHHHHLLLLLLLLLLLLLLLLLHHHHHHHHLHLHLLLLLLLLLLLLLHLHHHLLLLLLLLLLLLLLLLLLLLLLLLLHLLLLLLLLLL H: High Gain; L: Low Gain.

FIG.5.28 Llanherne Fixed Frequency (6.7 MHz.) Fast Run, 27th. November 1977.
The width of one letter represents the time taken for one angular scan (8.4 seconds).
Angular scan 20°S to 20°N (zenith angle) in 1° steps at 5°/sec.
The presence or absence of the Z echo is indicated as for Fig.5.27.

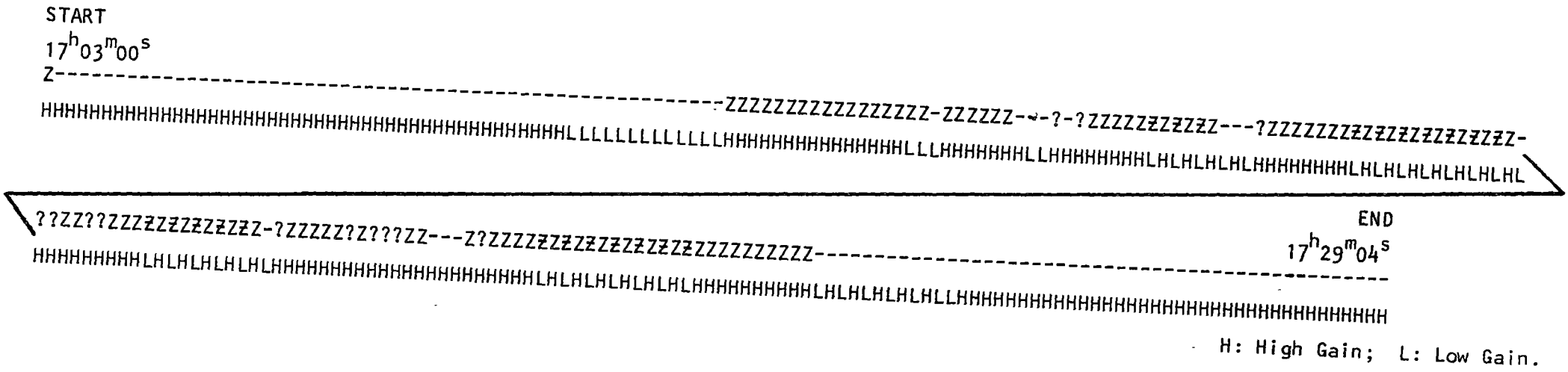

FIG.5.29 Llanherne Fixed Frequency (5.13 MHz) Fast Run, 6th November, 1977.
The width of one letter represents the time taken for one angular scan (6.6 seconds).
Angular scan 10°S to 21°N (zenith angle) in 1° steps at 5°/sec.
The presence ar absence of the Z echo is indicated as follows -

Z - Z echo present.
? - Z echo possibly but not positively present.
\- - Z echo absent.
z - Z echo absent on low gain record but presumed present as present on flanking high gain records.

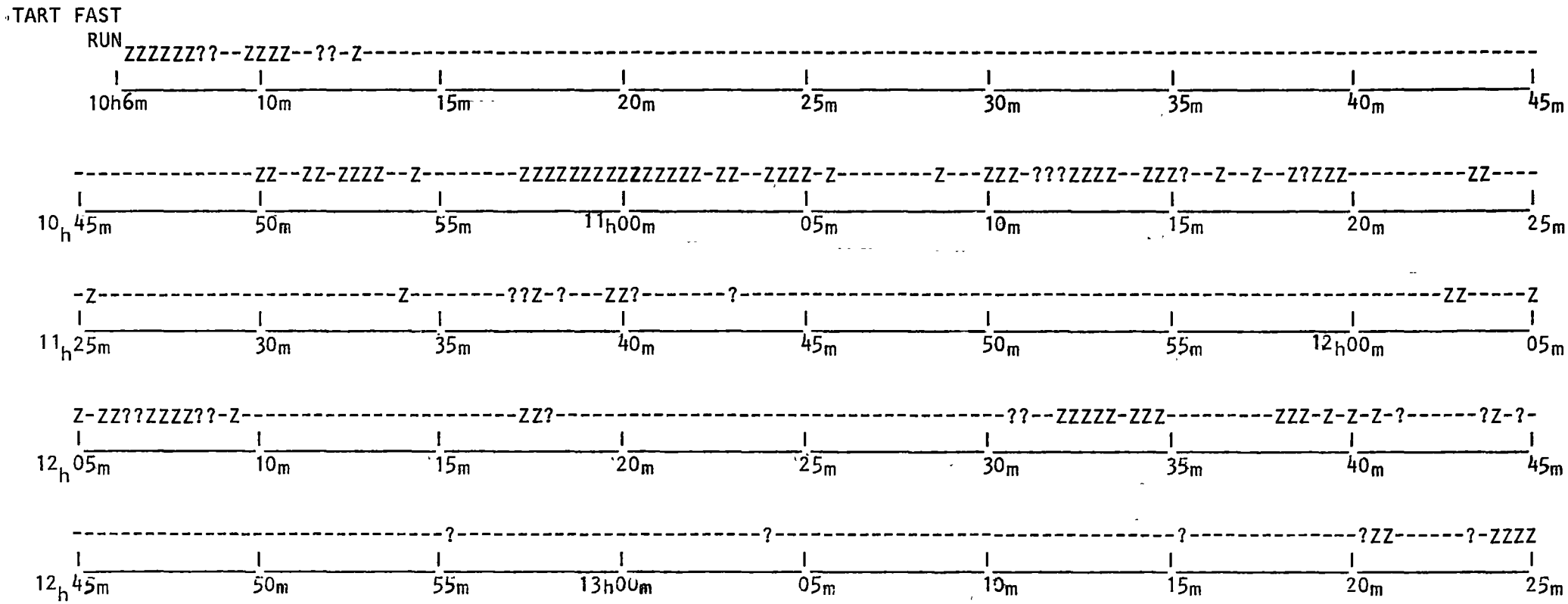

FIG.5.30 South Lea 4A Swept Frequency (usual h'f ionogram) Fast Run, 22nd October, 1977.
The width of one letter represents the time taken to produce one ionogram (20 seconds).
The presence or absence of the Z echo is indicated as follows -

Z - Z echo present.
? - Z echo possibly but not positively present.
- - Z echo absent.

.....continued next page

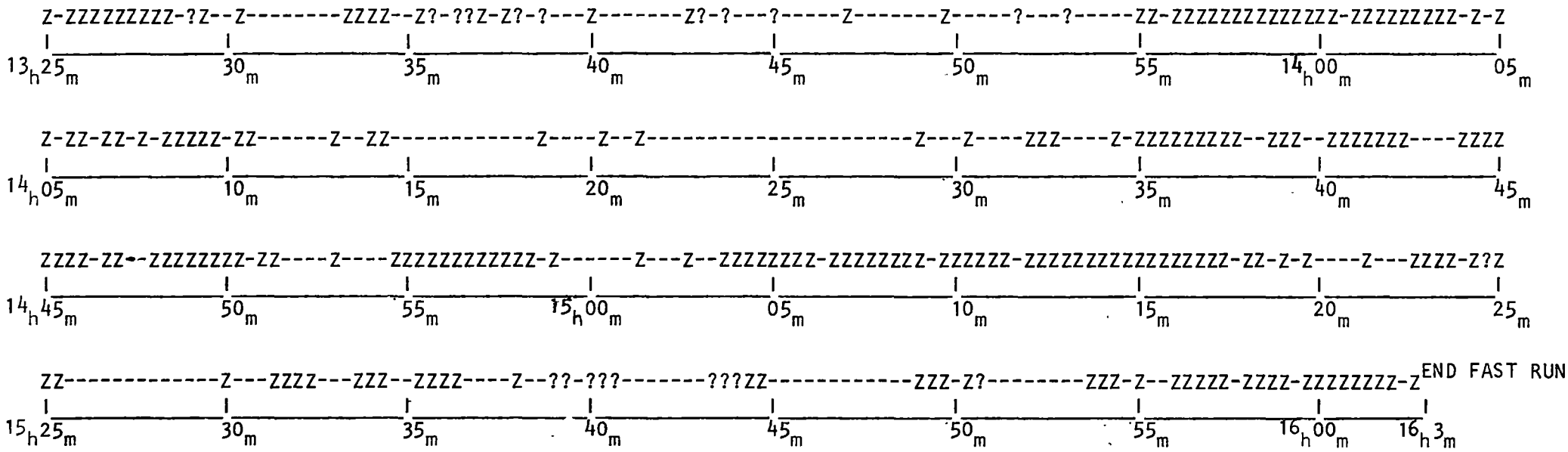

FIG.5.30 (continued.)

.....continued from previous page

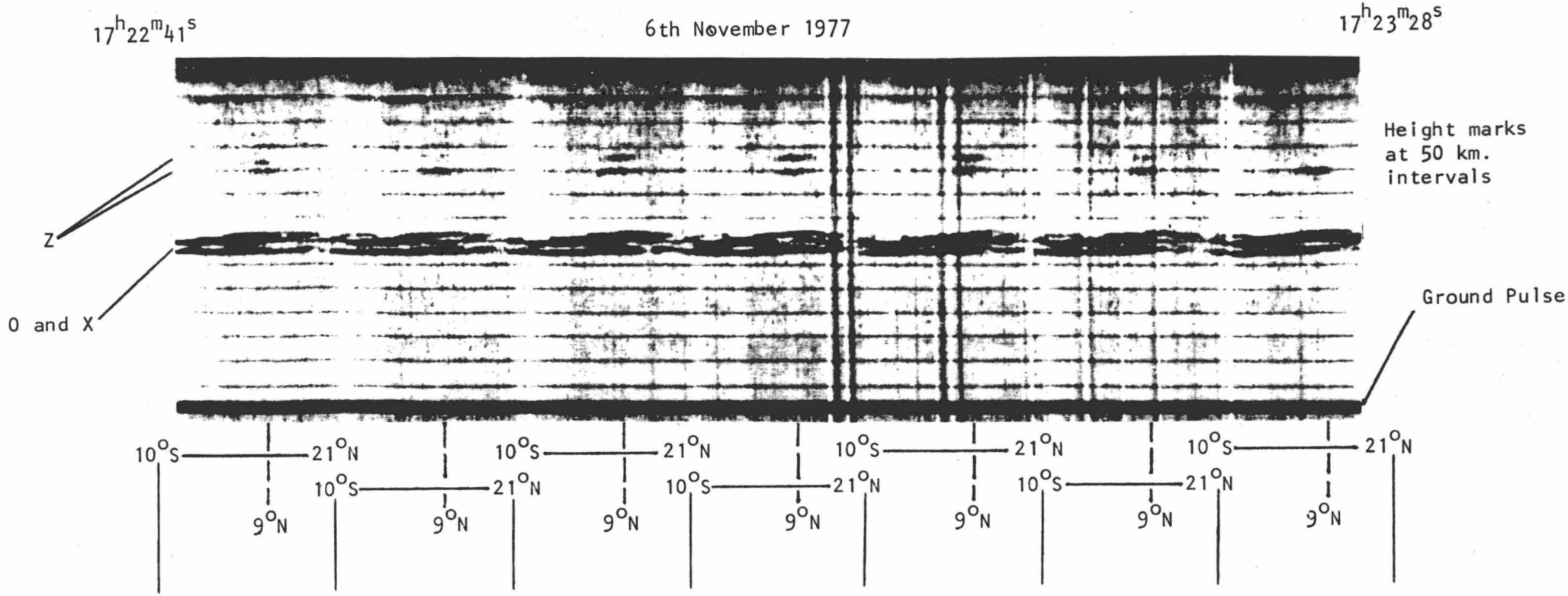

FIG.5.31 Llanherne h't record showing variation of O, X and Z echo strengths with zenith angle. Angular scan 10°S to 21°N in 1° steps at 5°/sec. (6.6 seconds per scan) "Z Splitting" is evident. High gain records. Frequency 5.13 MHz.

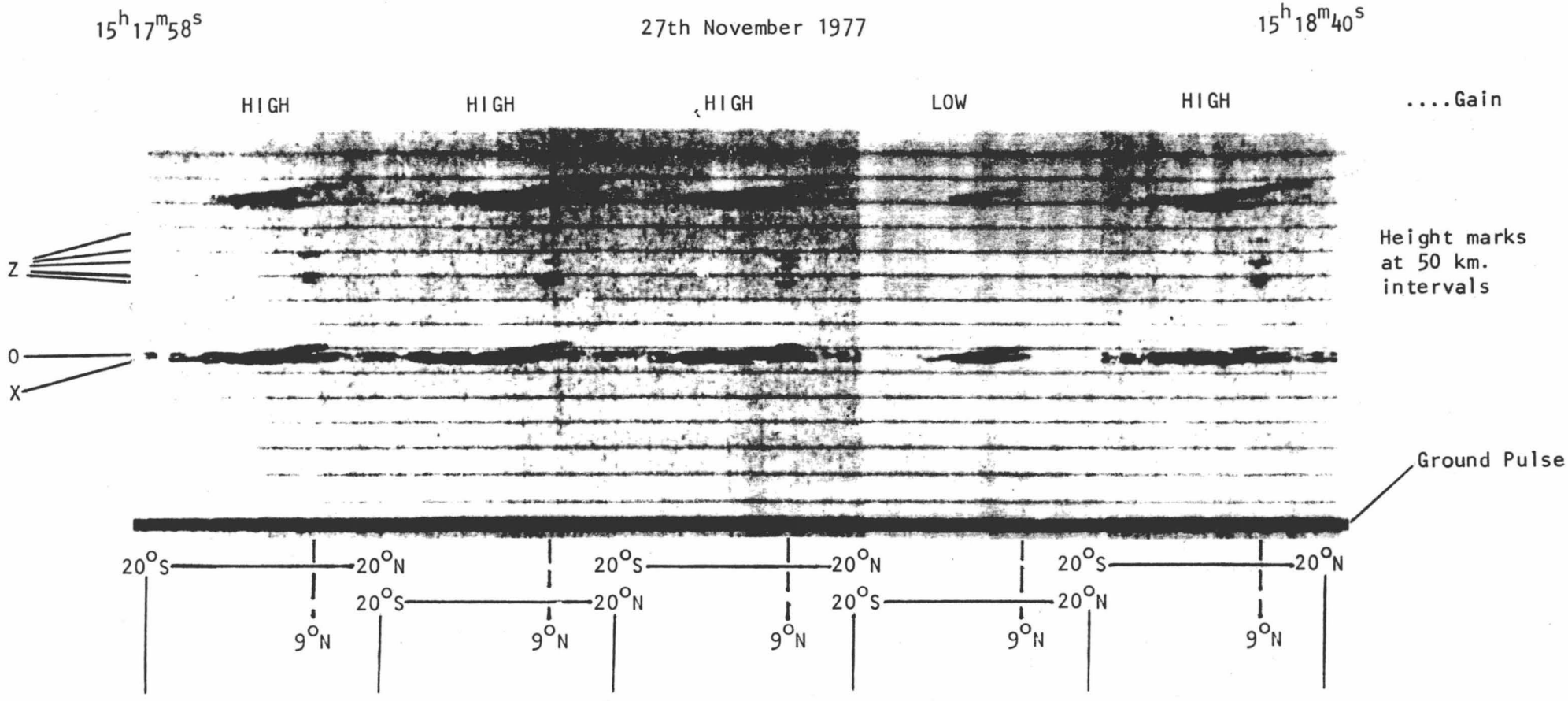

FIG.5.32 Llanherne h't record showing variation of O, X and Z echo strengths with zenith angle. Angular scan 20°S to 20°N in 1° steps at 5°/sec. (8.4 seconds per scan) "Z Splitting" is evident. High and low gain records (gains ratio HIGH:LOW = 17dB). Frequency 6.8 MHz.

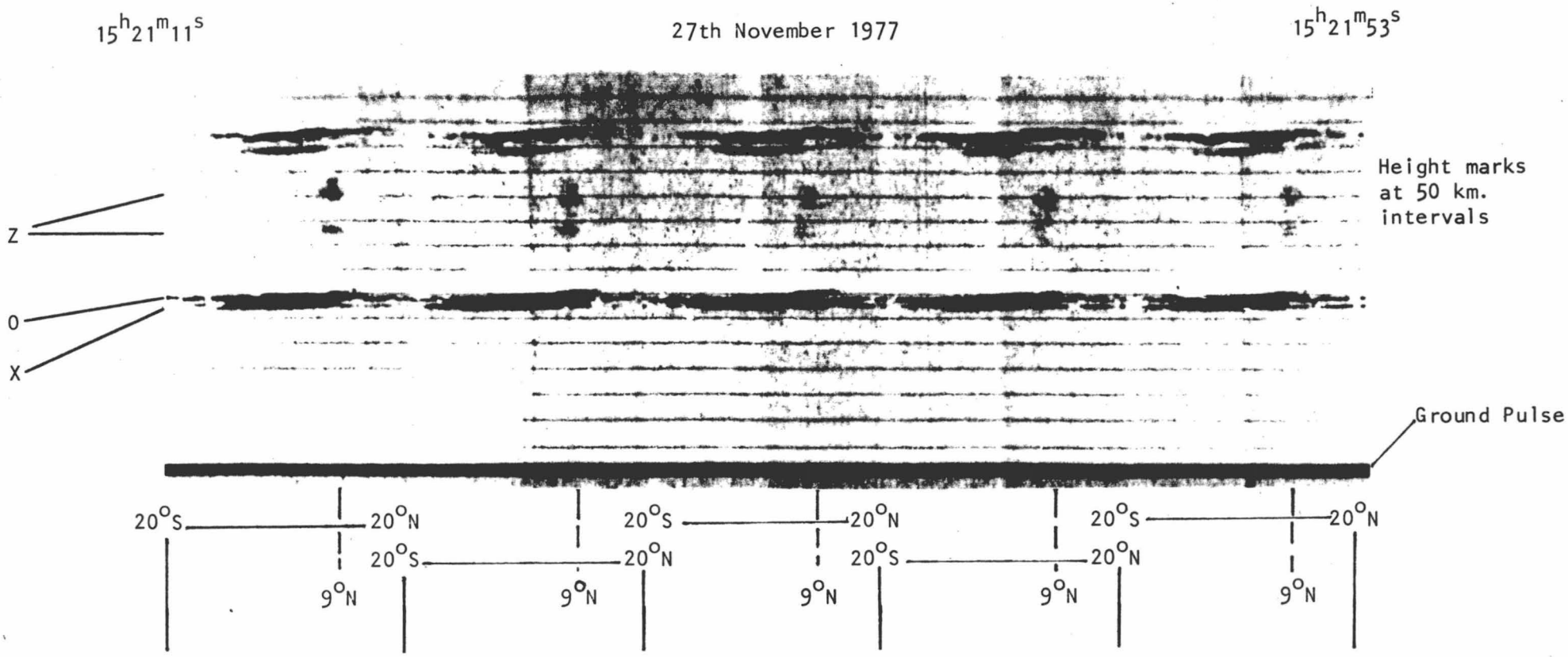

FIG.5.33 Llanherne h't record showing variation of O, X and Z echo strengths with zenith angle. Angular scan 20°S to 20°N in 1° steps at 5°/sec. (8.4 seconds per scan) "Split Z" and "Diffuse Z" echoes are evident. High gain records. Frequency 6.8 MHz.

quasi-periodicity such as that found in TID's. The Z echo is also seen to change its strength markedly within periods much less than a minute.

5.5 Z Splitting

On two days the Z echo was observed on Llanherne swept zenith angle n't records to split into two or more echoes and the phenonemon would be that described by Bowman (1960) as "z-ray trace duplication" and found by him on 2 percent of the Hobart records which he examined (five months of 1946). Figs.5.31 to 5.33 show examples of Z splitting and Fig.3.25A(e) shows an example found by Bowman. Some of the Z echoes of Fig.5.33 are seen to have a diffuse appearance and these may well correspond to Bowman's "diffuse z-ray", illustrated by Fig.3.25A(f).

CHAPTER SIX

DISCUSSION

6.1 Introduction

Very little discussion of the results is required. Consideration of the discussion sections of Chapter Three and the aims and results of the experiments quickly leads us to the conclusion that none of the theories so far advanced offers an adequate Z ray return explanation for the vast majority of Z echo occurences.

6.2 Solar Zenith Angle Tilt Theory

No Z echo angles of arrival of $+18^{o}$ were observed at any time of day even when strong O and X echoes occurred at Z echo virtual heights at zenith angles around $+18^{o}$ (implying that the ionosphere as a whole was not tilted by 18^{o}). This theory fails to explain the $+8/9^{o}$ angle of arrival of the Z echo and even smaller angles of arrival (of the centre of the angular distribution) of the O and X echoes. It is safe to discard this theory except for possible special cases as outlined in section 3.8.

6.3 Backscatter Theory

There were found no h'f ionograms displaying the required scattering patterns. Furthermore, the O and X angular profiles were not noticeably increased on average during the presence of the Z echo (apart from the secondary peak mentioned in the previous chapter and this is not easily attributable to backscattering - this feature in any case persisted during periods of absence of the Z echo). This theory also awaits a satisfactorily detailed theoretical explanation which has not as yet been forthcoming. It would be safe to discard this theory as a general Z echo explanation though it is of course still possible that it could be required to explain odd, isolated cases.

6.4 Tilt Theory

The tilt theory predicts that the centre of the Z mode angular return spectrum will have values in the general range $+9^{o}$ to $+18^{o}$ with an expected very strong bias toward values between $+14^{o}$ and $+17^{o}$ (and only the slightest practical possibilty of values less than $+9^{o}$). That this theory would fail the Z echo angle of arrival test so dramatically is to be expected from Ellis's (1953a,b;1956) results which are here confirmed. Nevertheless, it would be possible to construct a tilt model which would return the Z echo at $+9^{o}$ although it is

most improbable that this model could occur in every case (furthermore Papagiannis and Miller's 1969 results indicate that the (frequency) spectral range from such a model would be unrealistically narrow as b would need to be relatively large and a so small as to be insignificant). Given that this model has been operating in each of our observed cases then the O and X beam centres should also be at $+9^{o}$. This was observed in one instance only (Fig.5.12). This instance might be a sole example of a tilt mechanism operating although the relatively large (frequency) spectral range (Ø.4 ± Ø.Ø5 MHz.) of the Z echo on the simultaneously (1545 hrs.) recorded South Lea h'f ionogram suggests not (see Fig.3.41).

Although unlikely, it is conceivably possible that when Llanherne h'f sounding was in progress there existed a dynamic ionosphere such that flat ionospheric layers were nearly overhead when the sounding beam was near zenith and that favourable tilt/wedge layers occurred in the correct part of the sky for Z ray return by the time (say, 2 minutes later) the sounding beam reached $+8/9^{o}$. Travelling ionospheric disturbances (TID's) travelling along the magnetic meridian might provide such a situation. However, if this were to be the case, the expected Z echo frequency spectrum would be far narrower (as angles of arrival are around $+8/9^{o}$) than that observed. Secondly the Z echo could only appear for say 5% (at a very generous estimate) of the quasi-period of the TID. This makes the commonly observed appearance of the Z echo on

successive cycles unlikely; but again it is remotely possible. What is not possible with such a mechanism, however, is the persistent presence of the Z echo for relatively long periods with only relatively short breaks (this typical Z echo behaviour may be seen in the fast run results of Figs.5.27 to 5.30).

The tilt theory fairly clearly fails to explain Z mode occurrence on a global basis. It may perhaps be expected to have some application on a routine basis at very high dip angles but it has not explained the Z echoes at a station of relatively high Z echo incidence and it might be expected to have even less application at stations such as Allahabad where Z echoes are regularly if infrequently seen and the dip angle is only 36^{o}.

6.5 Conclusions

Since the current Z echo return mechanisms are unable to explain the observed results we must search for a more satisfactory proposition. Consideration of both experiment and theory suggests that it would be desirable to have a mechanism with a satisfactory physical process (as with the tilt theory) but which leaves the ionosphere unperturbed on an overall scale (as with the backscatter theory and in line with experimental results). A further desired feature of such a mechanism would

be a measure of natural selectivity as far as the Z mode is concerned so that contrived ionospheric distributions (as with the tilt theory) are not required and the mere presence of the phenomenon is sufficient to return the Z echo. As is illustrated by the experimental results, the Z ray return mechanism must also be able to operate irrespective of (and not because of) tilts in the ionosphere. An attempt to develop such a mechanism is presented in the following chapter.

CHAPTER SEVEN

THE Z DUCT RETURN MECHANISM

7.1 Introduction

Section 7.2 introduces an alternative Z ray return mechanism. Section 7.3 describes some computer modelling of the mechanism. Further sections examine available evidence and an explanation for Z splitting is given.

7.2 The Z Duct Model

Consider a horizontally stratified ionosphere upon which is superimposed a column of depletion of electron density or duct. Allow this column to be field aligned and to extend from the peak of the F2 layer downwards at least as far as the X = 1 level. The column may extend an arbitrary distance upwards from the peak electron density layer as this will not concern us. Let the column have a maximum depletion (along its axis) of less than, say, one percent of the ambient electron density, let the depletion cross section of the column be sinusoidal and let the width of the column be 10 to 100 wavelengths. Consider an O mode wave emitted at such an angle by a ground transmitter that on reaching the X = 1 level it has its wave normal parallel to the magnetic field. Around this ray there will be

a small cone of rays which make a slight angle (say, less than half a degree) with the magnetic field line. This is the cone of rays which (for this particular frequency) will generate the upper extraordinary or Z mode and no otner cone generated by this transmitter will have this property. Allow the X = 1 point for this ray cone to fall on the axis of the column of depletion. The longitudinal ray emerging upwards from the coupling zone will propagate along the axis of the column without deviation as its wave normal will be perpendicular to the on axis ionization contours (unless the duct is very weak). It will be guided upwards along the magnetic field line until the ionization density becomes such that X = 1+Y where it will be normally reflected and the reflected ray will be guided back down the column to the coupling point where its energy will be converted back to O mode and it returns to the transmitter - a Z echo. Other rays in the cone which make small angles with the magnetic field line will travel out towards the sides of the column but in doing so they will be travelling into laterally as well as vertically increasing electron densities and thus may be turned back towards the centre of the column. These rays may be contained within the column, guided up along the magnetic field line to the X = 1+Y reflection point where they will be guided back down the column to the coupling region. If the rays make too great an angle with the magnetic field direction then they will penetrate the walls of the column and escape. However Z rays emerging upwards from the coupling region necessarily make very small angles with the

magnetic field direction and thus the column may be quite weak (in depletion) yet trap most of the Z mode energy by virtue of its field alignment. Such a column therefore behaves as a duct for Z echoes. The column is also capable of ducting O and X mode rays which enter the duct with their wave normals parallel or nearly parallel to the axis. A trapped O mode can be expected to have most of its energy converted to the Z mode. The O mode and X mode energy trapped by the duct represents only a very small fraction of the O and X energy transmitted but the Z mode energy trapped may represent almost all the Z energy transmitted. We thereby have a Z return mechanism which returns the Z energy back along its path by normal total reflection and which furthermore displays great selectivity towards the Z mode. Since the ducts may be quite weak the ionosphere remains essentially unchanged as required and overhead X and O echoes are returned from the host ionosphere vertically as usual if it is flat or obliquely from the appropriate off zenith angle if it is inclined. As with the Backscatter Model, the heavy restrictions on electron density configuration required by the Tilt Model do not apply. At the same time we have the advantage of the well known physical reflection process of the Tilt Model. High in the F2 layer where the sides of the duct become steeper (in the sense that the ionization contours make smaller angles with the magnetic field direction) it would be expected that the presence of the ducts would assist the return of some oblique O and X rays travelling externally to the ducts. This might explain the

secondary peak noted in section 5.2 and the results of Ellis's experiment discussed in section 3.4 (Fig.3.12).

The duct model has been described very simply and appears to show great promise as a possible Z ray return mechanism but we must now examine it in more detail to check that it can in fact behave as outlined.

7.3 Computer Ray Tracing

Computer ray tracing of the Z mode in a flat ionosphere with superimposed ducts was carried out using the Jones (Jones and Stephenson,1975) ray tracing routines as the core of the program. Jones did not design the program for this sort of work but made it sufficiently versatile to be adaptable for many needs. Tracing the Z ray near the coupling region by itself calls for some care but the additional complication of high and spatially quickly varying lateral ionisation gradients (when ducts are introduced) means that not only is the program operating about an extreme edge of its ability but further that the assumptions of geometrical ray tracing may sometimes be violated to a greater or lesser degree. The ionosphere was modelled as parabolic of half thickness 150 km. and maximum electron density 300000 electrons/cc. The dip angle was taken as 72^0 (Hobart) and a standard earth-centred dipole field was employed. Lateral sinusoidal electron density variations were

superimposed on the ionosphere and a height dependent phase term introduced so that ducts were formed parallel to the magnetic field direction. Collisions were neglected. The Z ray was started from a "transmitter" just above the coupling region, the wave and group normals being (unrealistically, except at the coupling point itself) set in the magnetic field direction and up to half a degree either side. The maximum step length of the ray tracing was generally set to Ø.5 km. In view of all the assumptions and approximations the model must be regarded as possibly crude and the results interpreted accordingly. It had been hoped firstly to establish that trapping could take place and secondly to establish trapping criteria.

In order to establish that successful trapping had taken place in the model, two requirements were set. The first was that used by Papagiannis and Miller (1969) to test the til/wedge theory: namely that the ray return to the same physical point in space. The second requirement was that the ray be able to couple to an O mode on its return to the coupling region. Printed output from the program provided unambiguous information on the first requirement and some ray path plotting was done but very little value is gained from these plots without greatly exaggerating the scale transverse to the duct axes. Printed output information on the second requirement was not easily interpreted and so the ray's progress was plotted on a Poeverlein diagram, this providing

more information and a much clearer picture of the ray's behaviour than a plot of its physical path. Successful ray trapping was achieved in a variety of duct models, with widths ranging from 1.5 to 7km. and electron density deviations from ambient ($\Delta N/N$) of 5% to 0.1% though not all combinations were tried and not all those combinations which were tried were successful. Rays outside the coupling cone were not investigated as they would automatically fail the second requirement since they could not start at the upward coupling region of the Poeverlein diagram. Despite the rays which did fail to return and despite the approximate nature of the model it was concluded that the validity of Z ducts as a return mechanism was reasonably well established (in as far as models can establish validity), especially considering that error buildup was likely to make the program turn the ray away from the coupling region rather than towards it. Fig.7.1 is a diagram explaining the Poeverlein plots, Figs.7.2 to 7.8 show trapping situations and Fig.7.9 shows a non trapping situation. Figs.7.10 and 7.11 are plots of the physical ray paths in the ionosphere.

Unfortunately trapping criteria could not be established from the modelling results. Certainly there were results which could have been analysed but it was felt that such an analysis could be at best meaningless and at worst misleading. For many duct models, trapping conditions could be altered to non-trapping situations by relatively minute variations in such

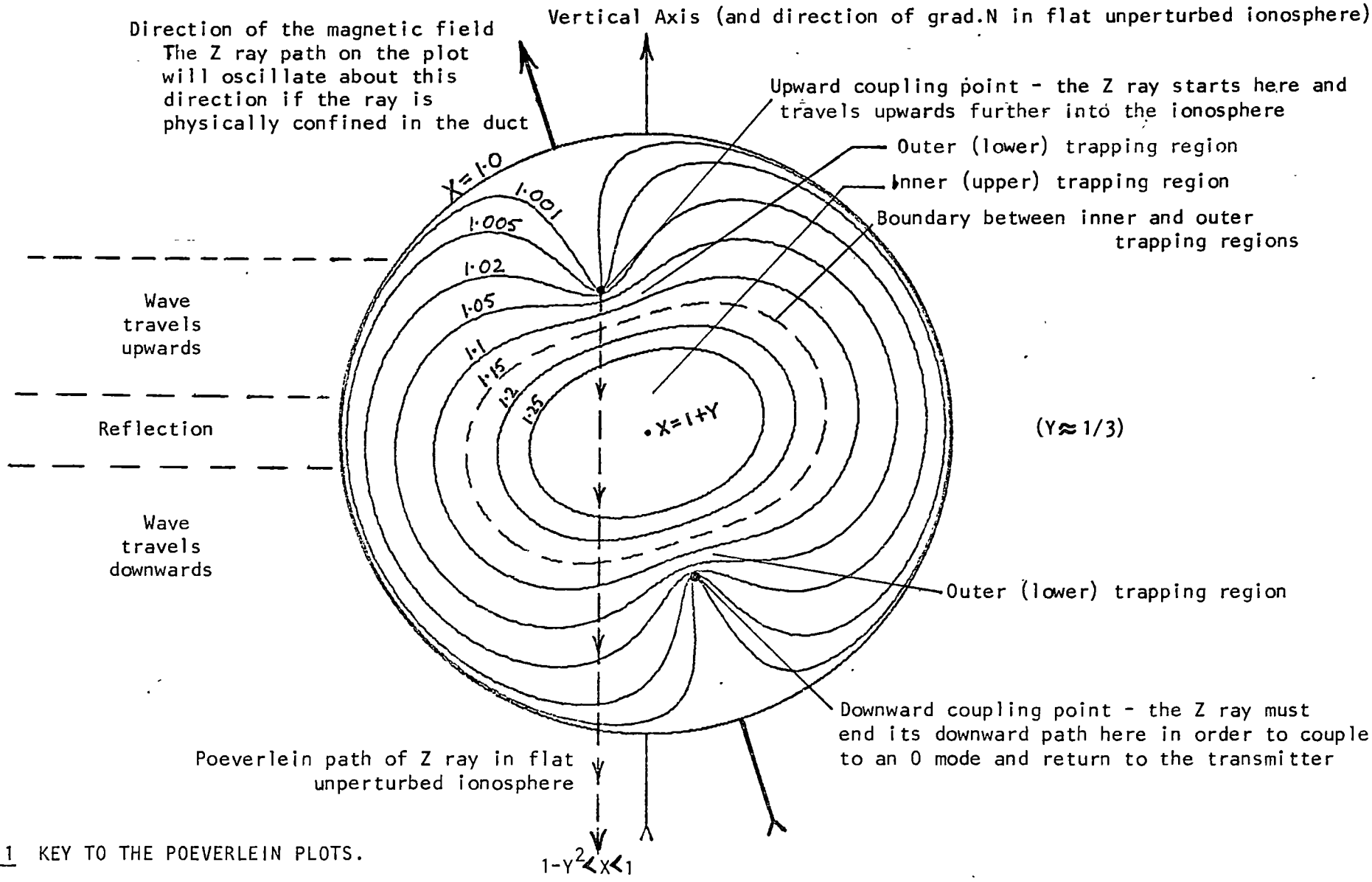

FIG.7.1 KEY TO THE POEVERLEIN PLOTS.

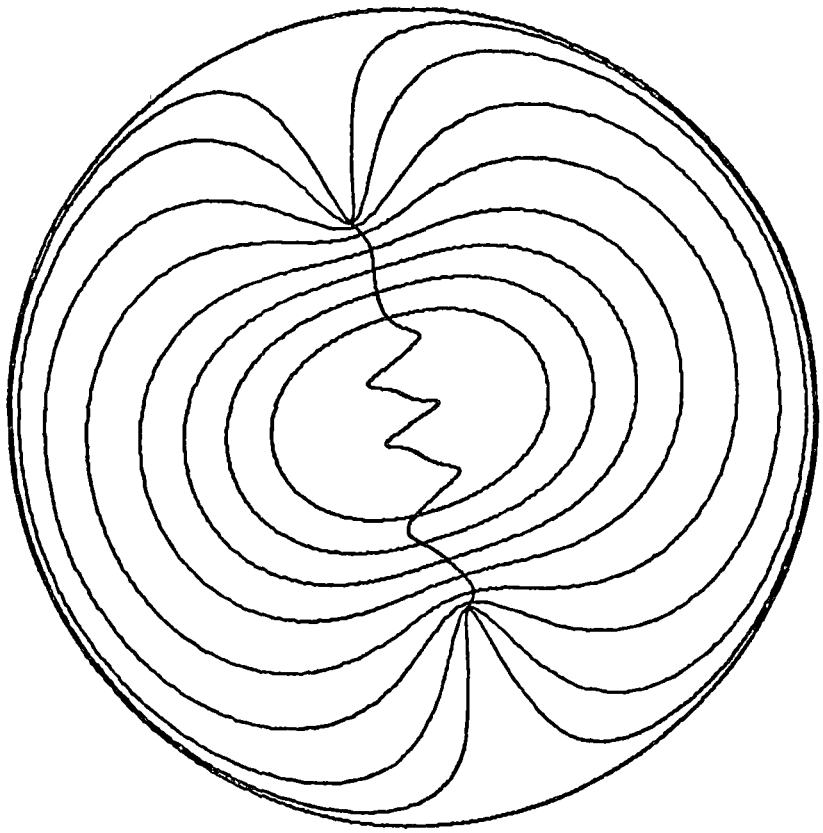

FIG.7.3 Trapped, returned Z ray. Frequency 4.225 MHz. Duct Width 2 km. $\Delta N/N = \pm 0.002$. Elevation angle of "transmission" 72^{o}.

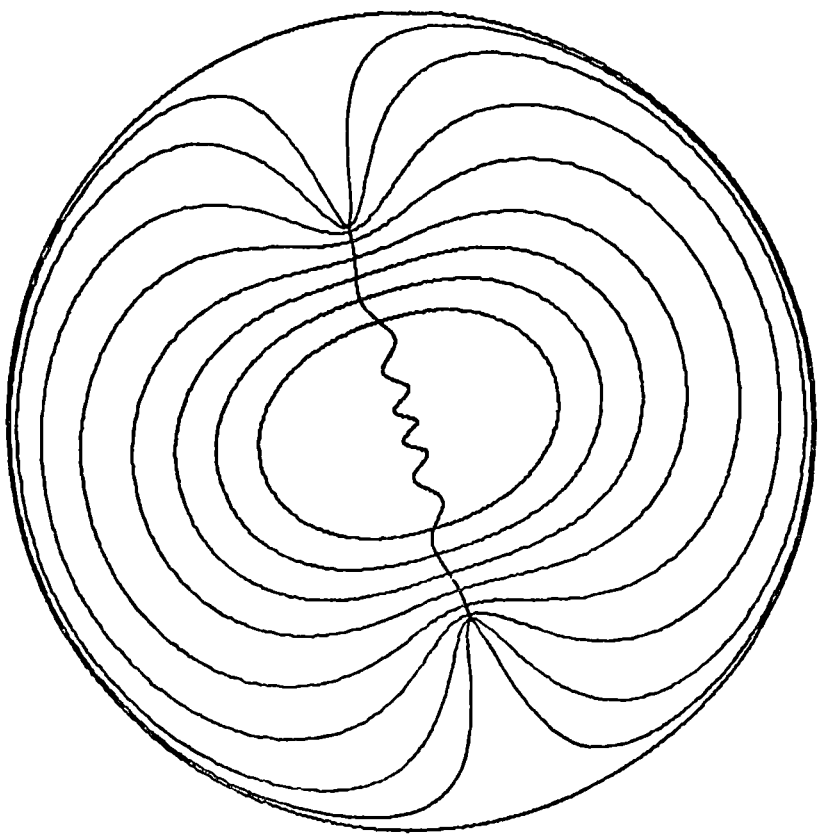

FIG.7.2 Trapped, returned Z ray. Frequency 4.225 MHz. Duct Width 1.5 km. $\Delta N/N = \pm 0.001$. Elevation angle of "transmission" 72^{o}.

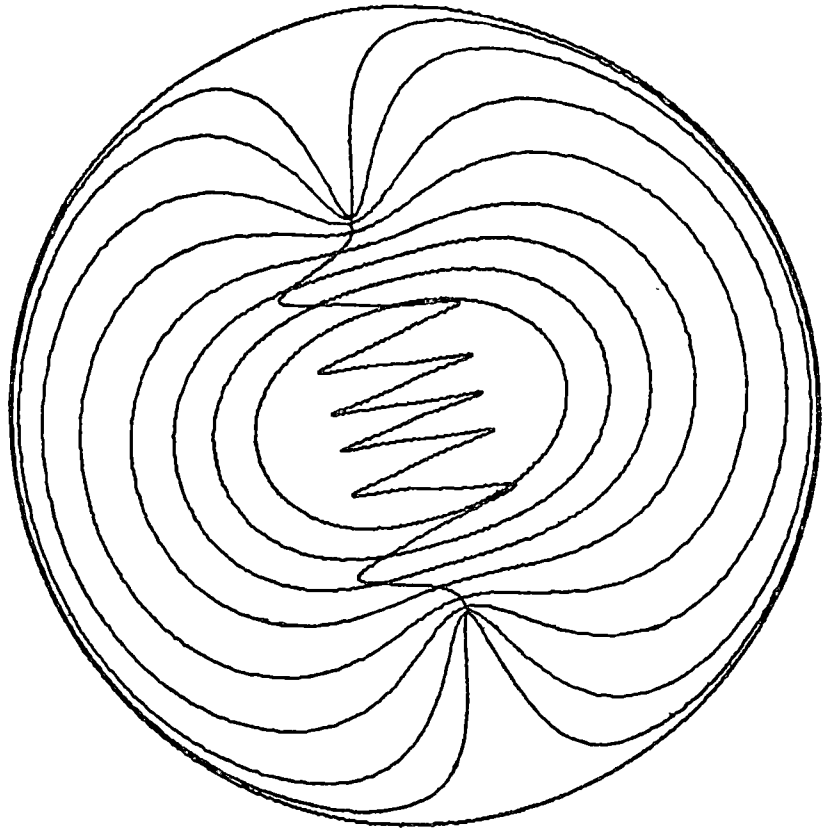

FIG.7.4 Trapped, returned Z ray. Frequency 4.225 MHz. Duct Width 3 km. $\Delta N/N = \pm 0.01$. Elevation angle of "transmission" 71.5^{o}.

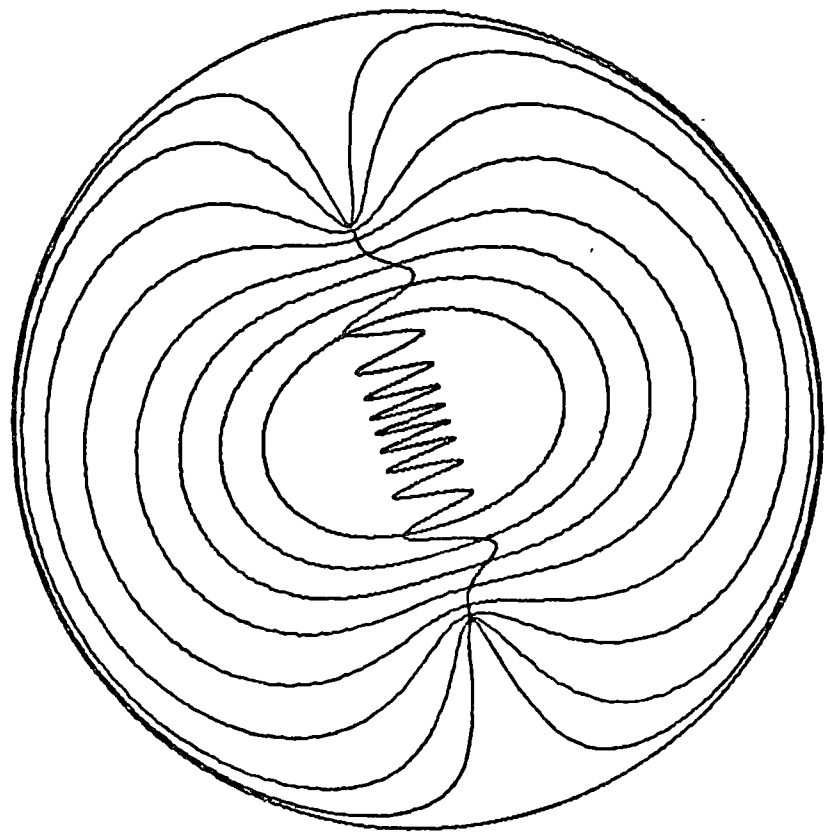

FIG.7.5 Trapped, returned Z ray. Frequency 4.225 MHz. Duct Width 3 km. $\Delta N/N = \pm 0.01$. Elevation angle of "transmission" 72.5^{o}.

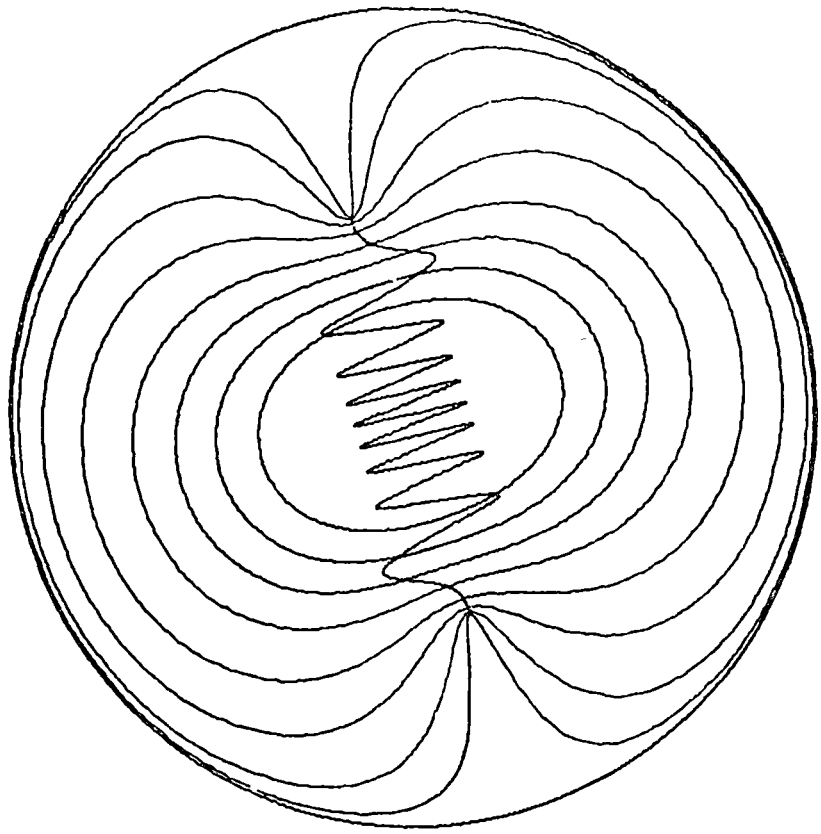

FIG.7.6 Trapped, returned Z ray. Frequency 4.225 MHz. Duct Width 3 km. $\Delta N/N = \pm 0.01$. Elevation angle of "transmission" 72^{o}.

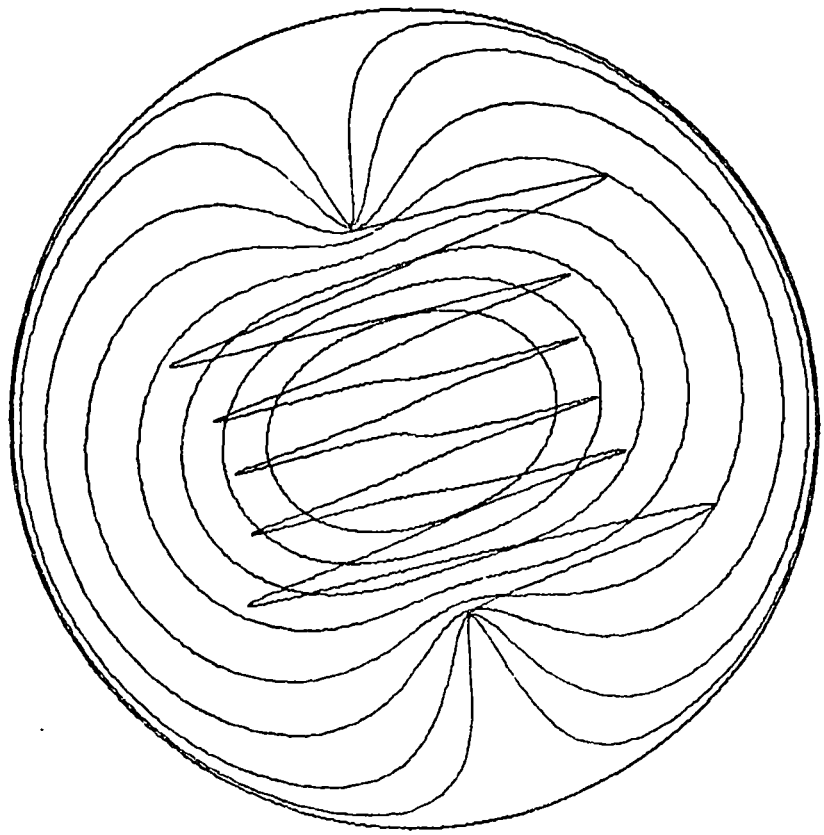

FIG.7.7 Trapped, returned Z ray. Frequency 4.225 MHz. Duct Width 4 km. $\Delta N/N = \pm 0.05$. Elevation angle of "transmission" 72^{o}.

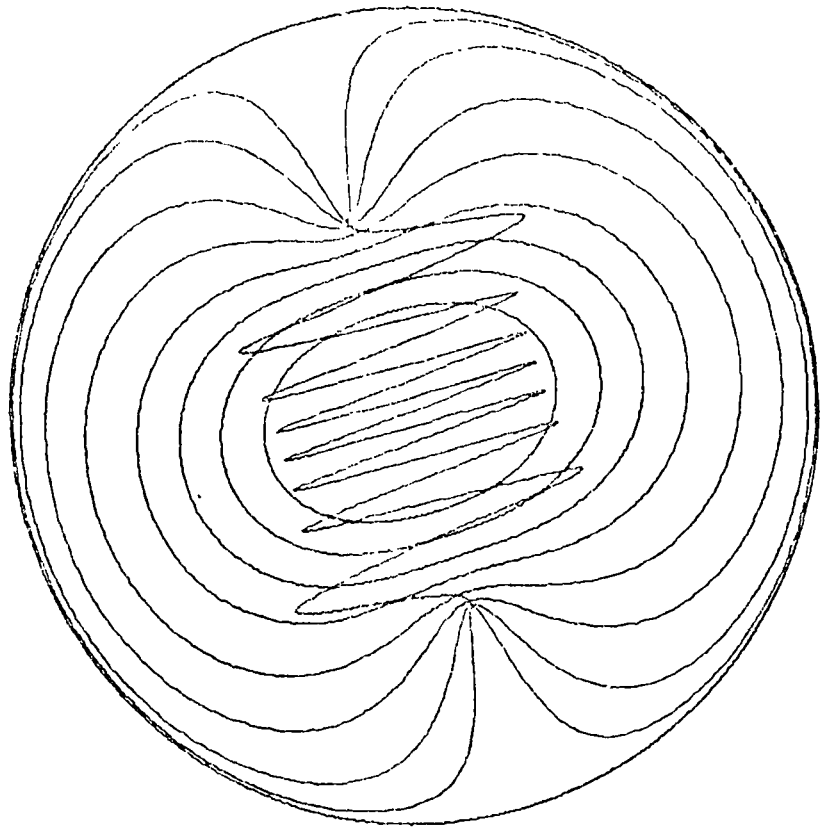

FIG.7.8 Trapped, returned Z ray. Frequency 4.225 MHz. Duct Width 7 km. $\Delta N/N = \pm 0.05$. Elevation angle of "transmission" 72°.

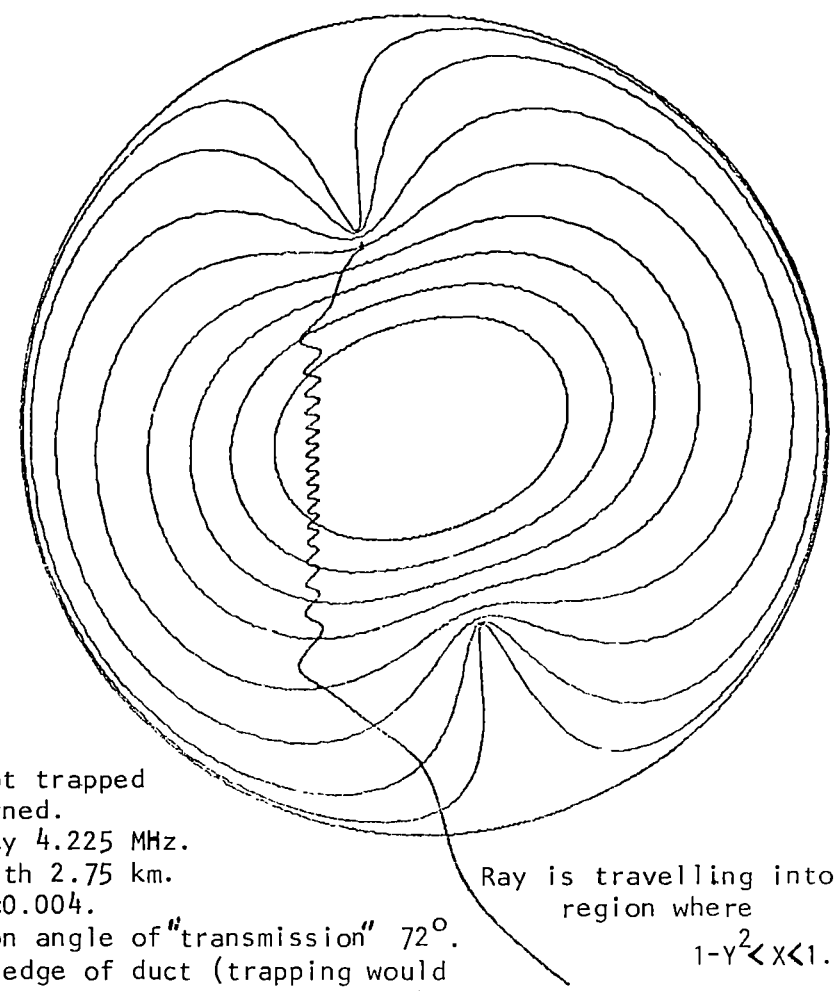

FIG.7.9 Z ray not trapped or returned.
Frequency 4.225 MHz.
Duct Width 2.75 km.
$\Delta N/N = \pm 0.004$.
Elevation angle of "transmission" 72°.
Ray started near edge of duct (trapping would take place if ray started near axis of duct).

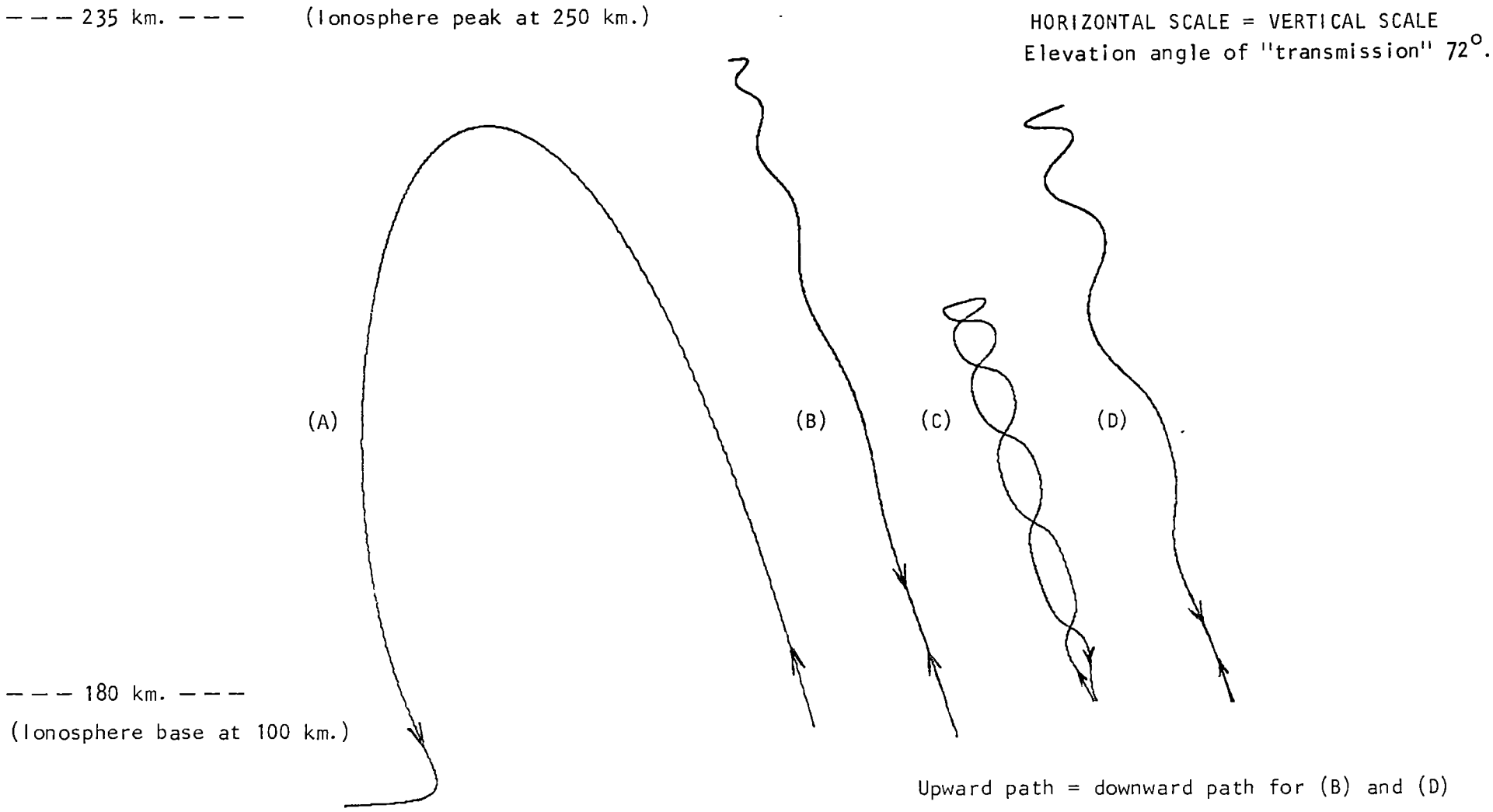

FIG.7.10 Physical ray paths corresponding to the ray paths of the Poeverlein plots. Frequency 4.225 MHz. (A) Z ray path in flat unperturbed ionosphere - Fig.7.1. (B) Z ray path in duct of width 3 km. and $\Delta N/N$ ±0.01 - Fig.7.6. (C) Z ray path in duct width 4 km. and $\Delta N/N$ ±0.05 - Fig.7.7. (D) Zray path in duct of width 7 km. and $\Delta N/N$ ±0.05 - Fig.7.8.

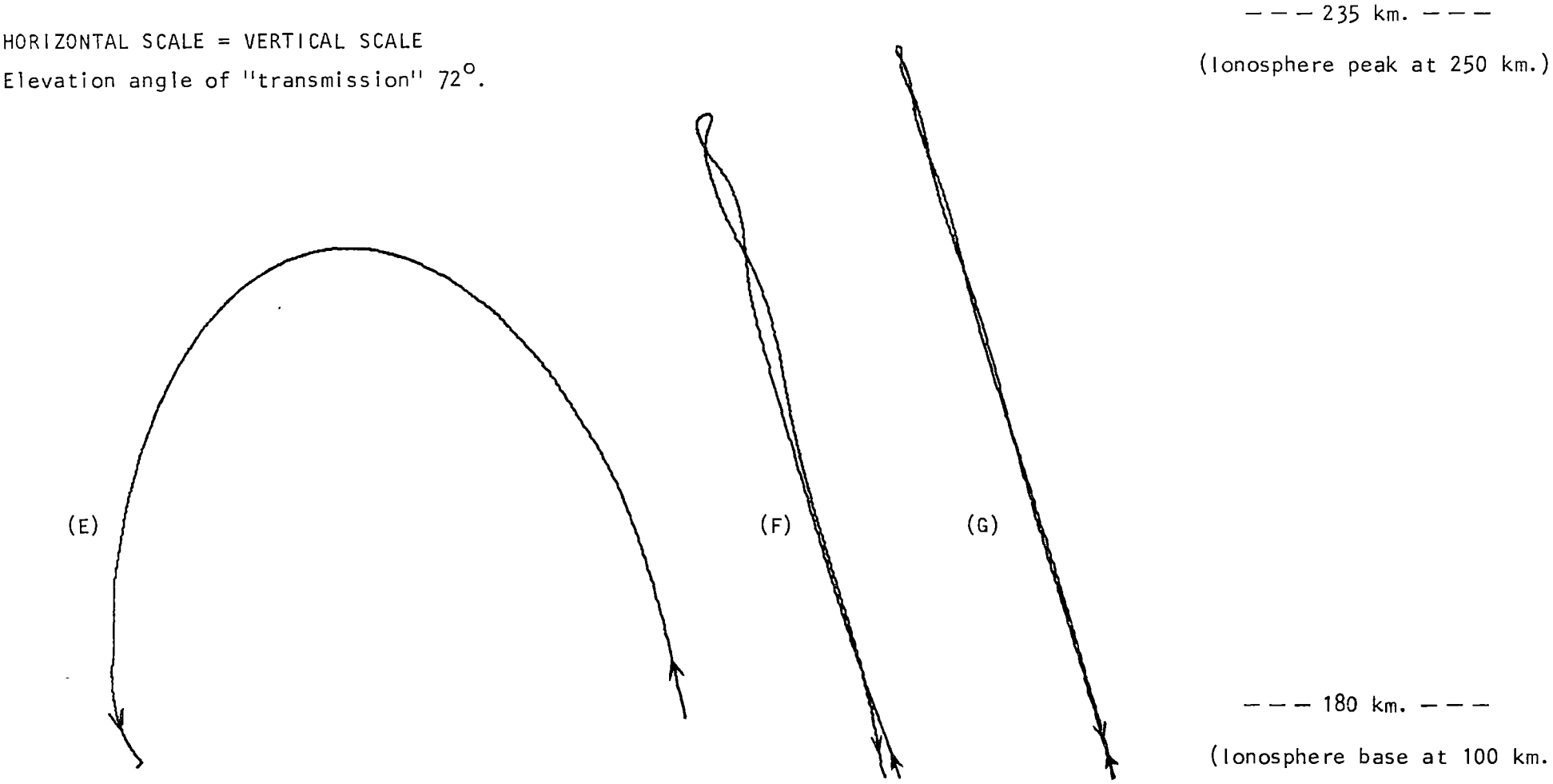

FIG.7.11 Physical ray paths corresponding to the ray paths of the Poeverlein plots. Frequency 4.225 MHz. (E) Z ray not trapped in ducting ionosphere (started near edge of duct). Duct width 2.75 km. and $\Delta N/N$ ±0.004 - Fig.7.9. (F) Z ray path in duct of width 2 km. and $\Delta N/N$ ±0.002 - Fig.7.3. (G) Z ray path in duct of width 1.5 km. and $\Delta N/N$ ±0.001 - Fig.7.2.

parameters as position of transmitter relative to duct axis, transmitter distance from the coupling region, width of the duct, strength of the duct etc. In the worst cases it was possible to achieve wild variations in the ray behaviour by small alterations to key parameters. Given such results it could be assumed either that the results are real or that the program is quasi-stable under trapping conditions. Circumstantial evidence all points strongly to quasi-stabilty. Although it is possible that there exists hitherto undetected fine and perhaps random structure in the Z echo neither experimental observations not theoretical investigations of the coupling region have ever given any hint of this. On the other hand, there are many indications that the program is suffering quasi-stabilty in this case. A significant percentage of rays failed to leave the transmitting region owing to the program suffering an illegal or indefinite arithmetic condition. Approximations in the model limit its fine detail resolution to a very much coarser scale than that on which the apparent variations occurred. As previously noted, the program was being operated in the fringe area of its reliability and its internal accuracy when tracing in a ducting ionosphere was often several orders of magnitude below that of more usual tracing applications. An increase in the internal accuracy requirements of the program sometimes overcame internal problems but seldom increased confidence in external accuracy and the increased expense of more "accurate" plots could thus not be justified. A further source of difficulty for the

program was the placing of the "transmitter" just above the coupling region. This meant forcing the wave to be "emitted" with wave normal and ray direction coincident in a region in which it is well known that marked differences may occur between the two directions. In order to obtain a rough estimate of the possible external accuracy of the program a test was conducted in which the program traced rays in a difficult but known situation. In a flat, unperturbed ionosphere an ordinary mode ray was transmitted at ground level (in free space) at oblique angles such that the O wave encountered or nearly encountered the coupling region from below and so that some of the waves displayed the "Spitze" effect. On the Poeverlein diagram the paths of the rays should have been at all times straight lines perpendicular to the ionospheric layers. The O mode wave was started at $\emptyset.1^{o}$ increments of elevation about the angle which would carry it to the coupling point in this ionosphere (Rays were traced at elevation angles 80.5^{o} to 82.9^{o} inclusive. Rays travelling at smaller elevation angles than the critical angle will not encounter the "Spitze" condition). The results indicated that the program is quasi-stable under such conditions. The program crashed at elevation angles 80.9^{o}, 81.0^{o} and 81.2^{o} to 81.6^{o} inclusive; the trace on the Poeverlein diagram was distorted from a straight line in the vicinity of the coupling region for elevation angles of 81.7^{o} to 82.2^{o} inclusive and 82.7^{o} to 82.9^{o} inclusive; the 81.1^{o} and 82.3^{o} to 82.6^{o} plots were so affected near the coupling region that the plotted values disappeared

from the Poeverlein diagram altogether, leaving a gap in the trace. In view of these results, it could well be that for ducts where the ray appeared to be trapped but failed the second requirement that such a duct would allow trapping in a real ionosphere.

7.4 Ionospheric Ducts

For over two decades magnetic field aligned irregularities have been postulated and observed in association with investigations of many ionospheric phenomena (e.g.whistlers, aurorae, spread-F, sporadic-E, scintillations) and in some cases trapping or ducting by these irregularities has been proposed. Depletion irregularities or ducts of interest to Z ray return include those classified by Muldrew (1980) as "MF (Medium Frequency) ducts". Characteristics of such ionization ducts observed above the F-layer peak by topside sounders are a diameter of one to a few kilometres and an electron density deviation from ambient of about 1%. This is in general agreement with characteristics of similar field aligned irregularities deduced from other data. For instance, Hajkowicz (1972) explained some scintillation observations in terms of a wavelike form of distribution of field aligned irregularities with wavelength mostly found in the 3-4 km. range, Hibberd (1970) studied ionospheric roughness and deduced the presence of field aligned irregularities of about 1%

electron density deviation and Lui and Yeh (1977) considered electron density fluctuations of 1% or so when explaining GHz scintillations but noted that values of about 20% had been proposed. Singleton and Lynch (1962,1962a) observed scintillations and interpreted the data in terms of field aligned irregularities with dimensions of the order of 1 km. occurring in patches with horizontal dimensions of 100 km. or more at heights around 200 to 600 km. As there are many such reports it can be seen that the dimensions, heights and strengths of the ducts required for Z mode return are not incompatible with existing postulates and observations of magnetic field aligned irregularities in the ionosphere.

Field aligned ducts extending below the F-layer peak are thought to be responsible for one of at least three generally recognized forms of spread-F. Pitteway and Cohen (1961) explained temperate latitude spread-F by presuming the spreading to be due to waveguide propagation along field aligned irregularities of transverse thickness greater than 250 metres. Muldrew (1963) explained certain topside ionograms by studying the propagation of radio waves guided along magnetic field aligned sheets of ionization. His sheets had an electron density gradient perpendicular to the magnetic field of about four times greater than that in the regular ionosphere, a thickness of about 1.2 km. and an electron density deviation from ambient of about 1%. He demonstrated that trapping of radio energy could take place and showed that a combination of

obliquely incident propagation followed by propagation along field aligned sheets may occur, the energy propagating along the sheet to the reflection point then returning essentially along its incident path. Muldrew carried out ray tracing in such sheets as that shown in Fig.7.12, and Figs.7.13 and 7.14 are a sample of his results. Fig.7.15 shows ducts which Muldrew modelled to fit an actual topside record and Fig.7.16 is a representation of Muldrew's proposed bottomside combination mode of propagation.

Calvert and Schmid (1964) qualitatively divided topside spread-F into three categories: aspect-sensitive scattering (e.g.Renau,1960; Calvert and Cohen,1961); ducted propagation along field aligned irregularities (e.g.Pitteway and Cohen,1961); refraction in large regions of reduced electron density (e.g.Booker,1961; Klemperer,1963). They examined large numbers of topside ionograms to determine the morphology of the three types of spread-F. Their observations were for northern winter for 75^{o} west longitude and were obtained near sunspot minimum. Fig.7.17 shows the percentage occurrence of aspect sensitive scattering and Fig.7.18 is as similar contour diagram for ducting. Calvert and Schmid note that aspect sensitive scattering on the ionograms may have obscured some ducting. The large scale electron density reductions were observed in about 1 per cent of the data examined and appeared to be related to the ducting irregularities. Spread-F was found on 54 per cent of the topside ionograms used in the study.

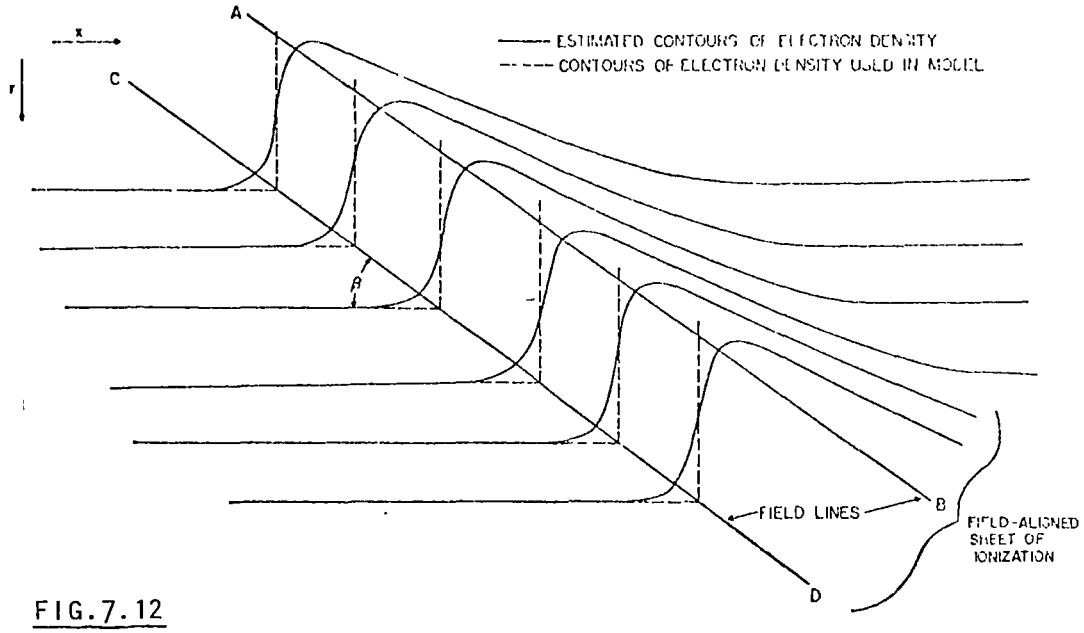

FIG.7.12

Cross section of model used for ray tracing in north-south magnetic plane.

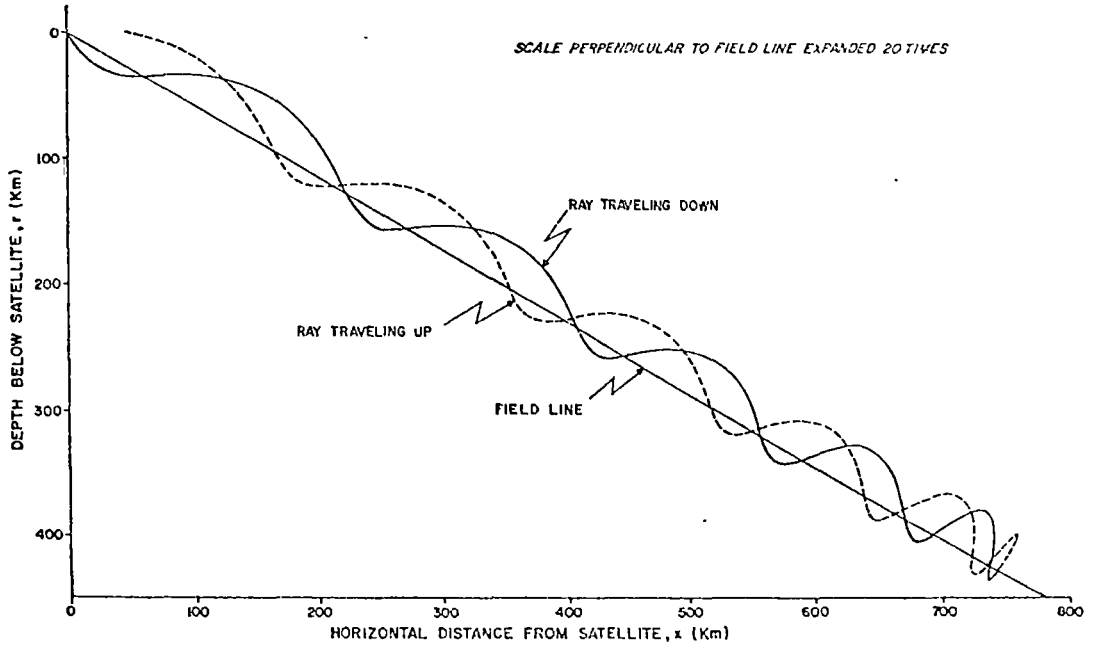

FIG.7.13

Ray path of extraordinary wave along model field-aligned sheet of ionization

(Figs.6 and 8a of Muldrew, 1963)

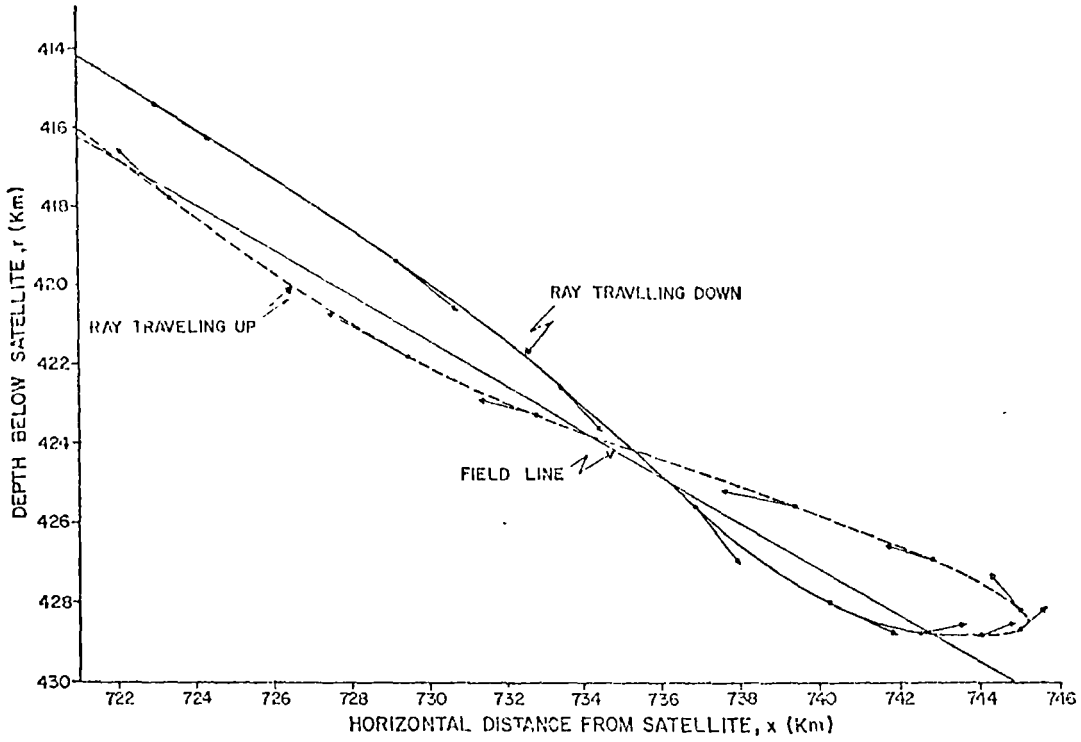

FIG. 7.14 Scale drawing of ray path in Figure 8a near the height of reflection. Arrows indicate the direction of the wave normal.

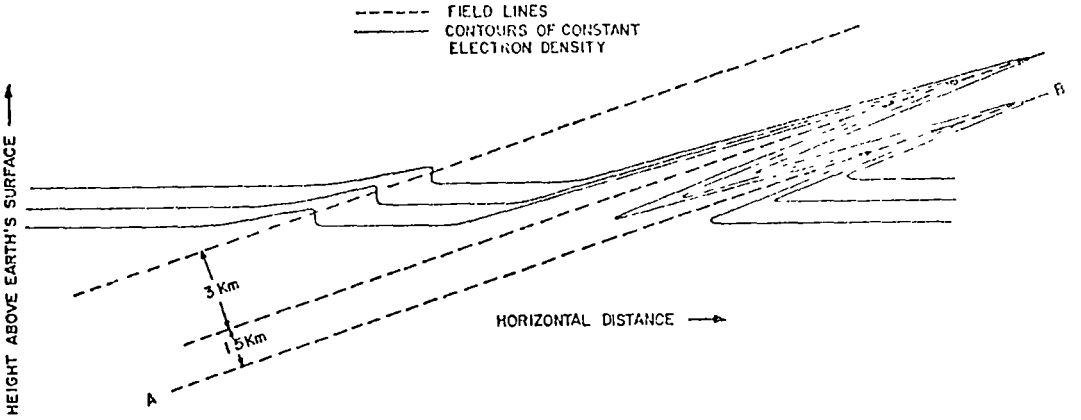

FIG. 7.15 Contours of constant electron density illustrating the approximate structure and distribution of the field-aligned sheets of ionization responsible for the traces of Figure 1(e) in the vertical plane.

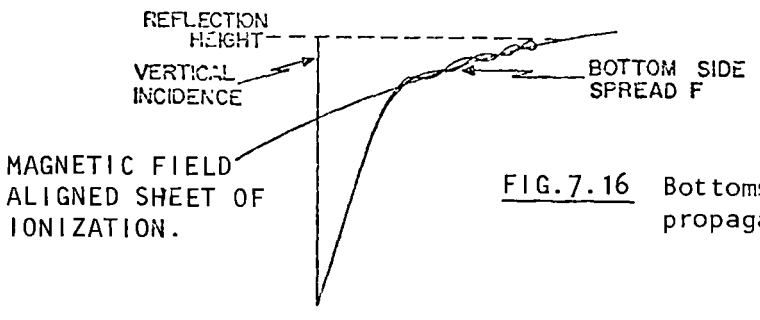

FIG. 7.16 Bottomside combination mode of propagation.

(Figs. 8b, 10 and 11(c) of Muldrew, 1963)

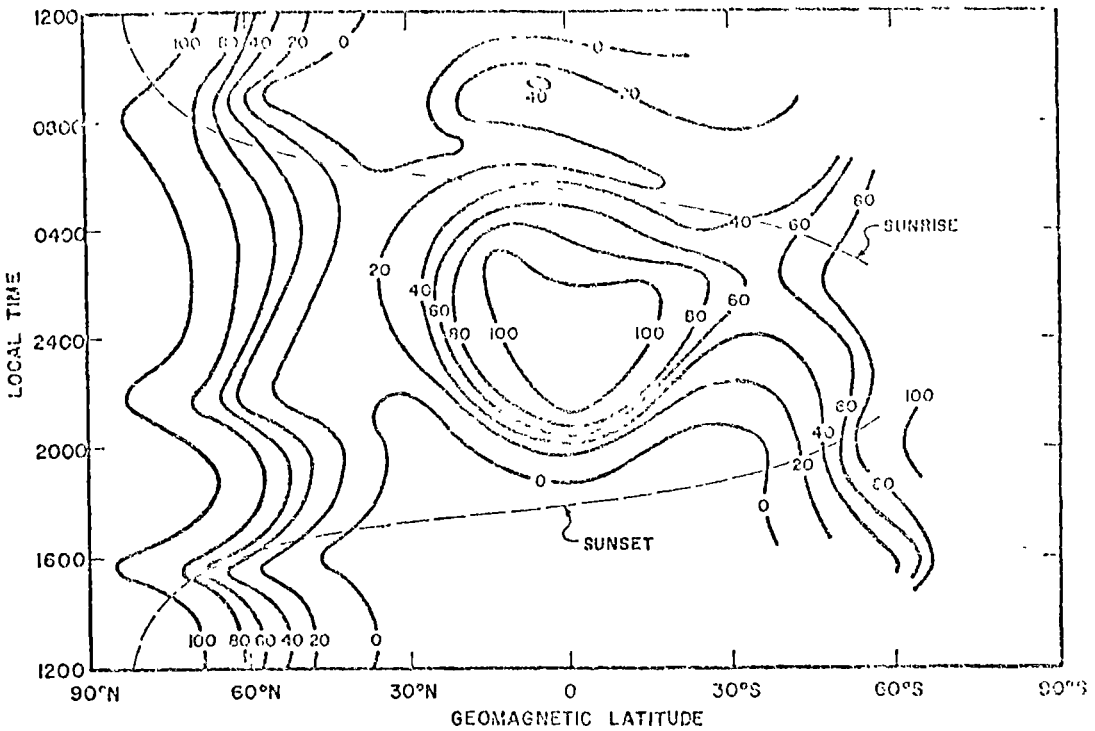

FIG.7.17 The percentage occurrence of aspect-sensitive scattering observed by the Alouette topside sounder satellite. Ground sunset and sunrise for the middle of the observation period, November 14, is indicated.

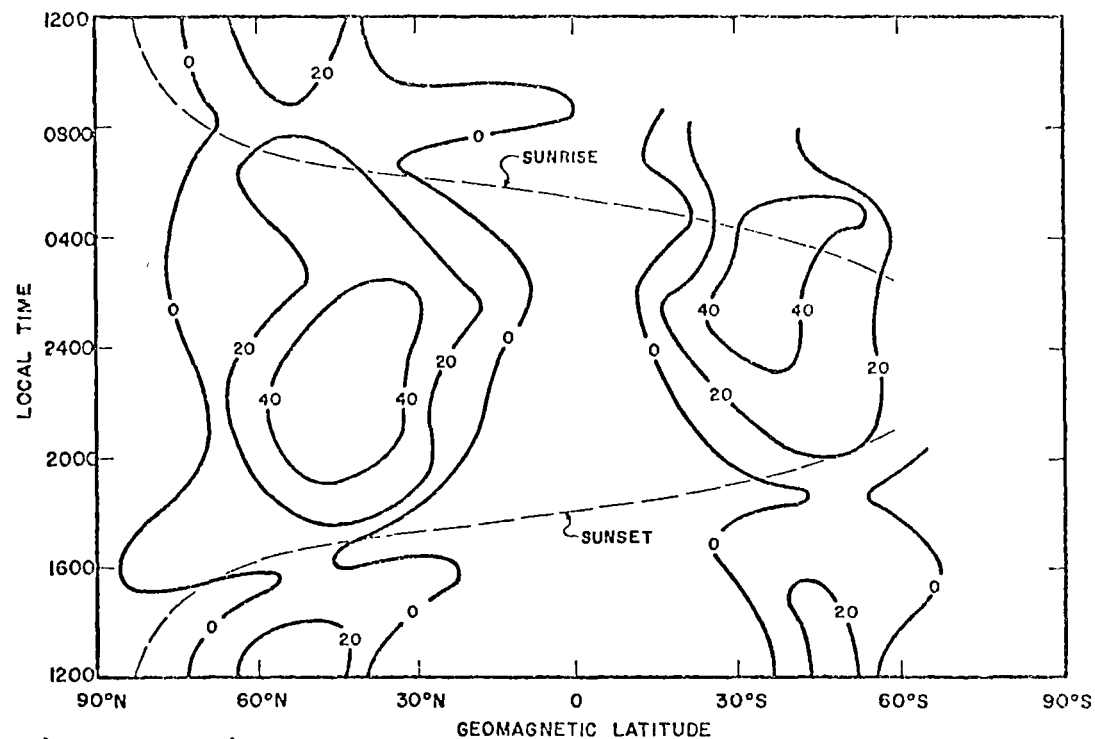

FIG.7.18 The percentage occurrence of ducting spread F on Alouette ionograms. November 11 ground sunset and sunrise are shown.

(Figs.6 and 13 of Calvert and Schmid, 1964)

7.5 Z Splitting

Explanation of Bowman's "z-ray duplication" in terms of either the backscatter or the tilt/wedge return mechanism is not easy and becomes exceptionally difficult when considering the Llanherne result that the 2+ echoes of Z splitting lie in the same narrow transmitting/receiving beam. The Z ducting mechanism, however, can offer a plausible explanation. In addition to the ray trapped in the duct mainly responsible for return of the Z ray there are at least three other additional ways in which a Z ray may be returned. A portion of the Z beam may escape at some point from the upper or lower side of the main trapping duct, travel obliquely both to the vertical and to the duct axis until becoming trapped in another duct on its downward path while approaching the coupling region; the Z beam may illuminate two adjacent ducts so that two Z rays are returned; a portion of the beam may escape through the upper side of the main trapping duct, travel quasi-vertically to and from its reflection point and re-enter the main trapping duct, or an adjacent duct, in a similar (though reverse) fashion to the way it escaped (Fig.7.19). There will also be cases intermediate between the oblique and quasi-vertical cases. Z rays which are returned after travelling some distance obliquely and untrapped would return to earth up to tens of kilometres from the transmitter/receiver and it is extremely

POEVERLEIN PLOT

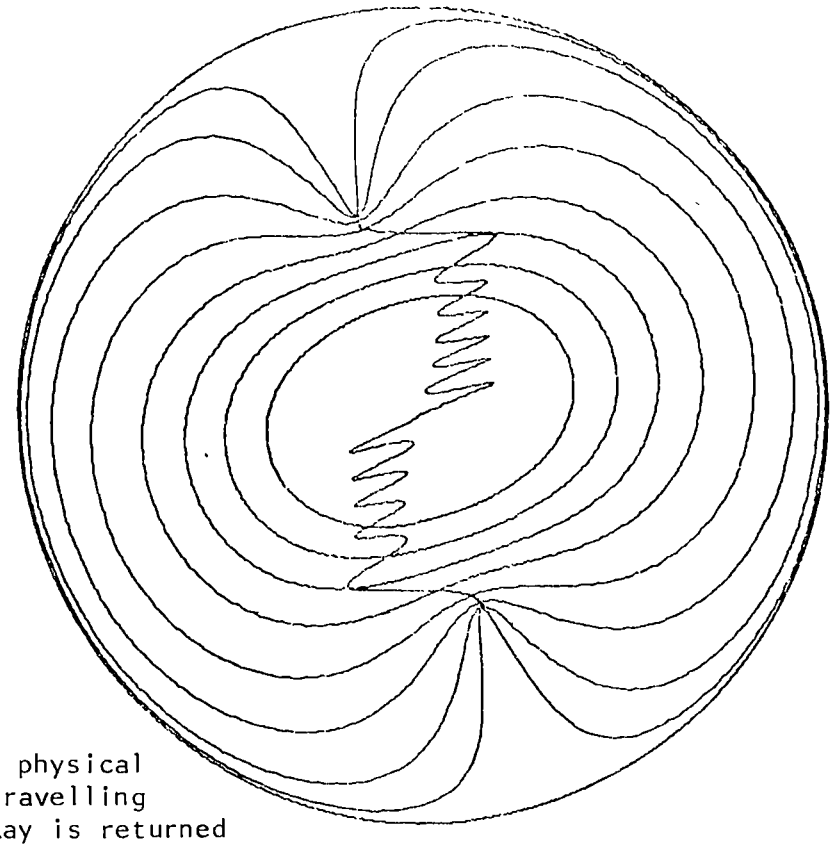

FIG.7.19

Poeverlein plot and physical ray path of Z ray travelling quasi-vertically. Ray is returned but not confined in the duct. Together with the ray which is returned and confined in the duct (Figs.7.6 and 7.10) it will produce "Z splitting". (The two rays start in different positions relative to the duct axis.) Frequency 4.225 MHz. Duct Width 3 km. N/N = ±0.01. Elevation angle of "transmission" 72°.

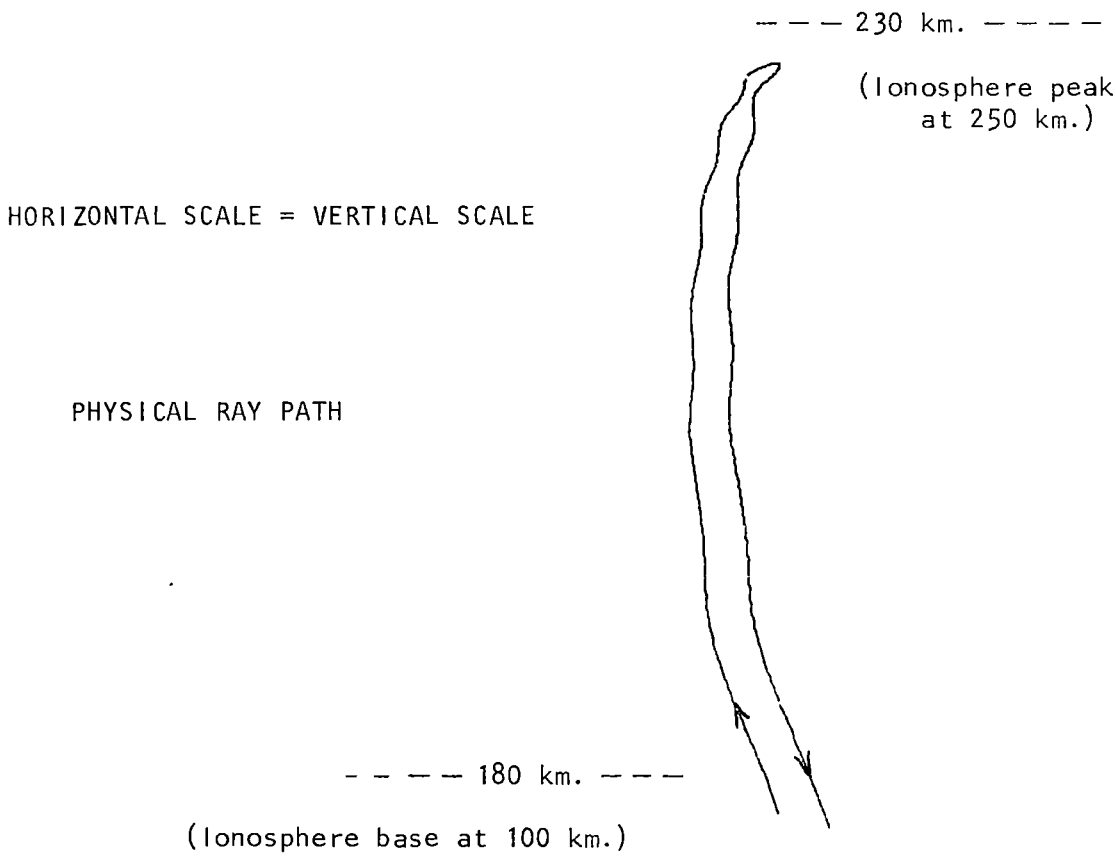

unlikely that detection would take place in the majority of these cases. Z rays which illuminated two ducts would both be detected. The degree of frequency separation of the two echoes would depend upon both the relative strengths of the ducts and also on the N-S horizontal gradient. In the case of the Z ray travelling quasi-vertically the frequency separation will again depend on both the duct strengths and the N-S horizontal gradient but in this case the horizontal gradient will be more important owing to the separation of the reflection points of the trapped and vertical Z rays. Muldrew's (1963) model fitted to an actual topside record (Fig.7.15) is an example of ducts which, if both illuminated by the Z beam, would produce Z splitting. The so called "diffuse" Z echo observed by Bowman on 16% of the September 1946 Hobart records ıe examined is probably a variation of the splitting situation where the frequency separation between traces is very small.

7.6 Discussion

The ray tracing model of the duct theory was unable to establish trapping criteria although it did establish that trapping could take place. We may, however, speculate on trapping criteria with qualified assistance from those results which were obtained from the models.

The trapped ray must travel through two different trapping

regions on its path from the coupling point to the reflection point and back down to the coupling point. The boundary of these regions may be taken on the Poeverlein diagram as the contour where the curves change from concave only to concave and convex as viewed from the centre point of the diagram. These regions will be referred to as the upper (or inner) and lower (or outer) trapping regions (Fig.7.1). On leaving the vicinity of the coupling point on the Poeverlein diagram the ray path on the Poeverlein diagram follows the direction of -grad.N. If the duct is too weak to trap the Z ray (the ionization contours are not sufficiently perturbed as to become perpendicular to the duct axis) then the path followed will be similar to that for a ductless ionosphere except that the straight line path will be rippled as the ray crosses successive ducts. If the duct is sufficiently strong to have ionization contours perpendicular to the magnetic field line (duct axis) but sufficiently weak that the contours do not deviate far from perpendicularity to the axis over a reasonable part of the duct width then trapping will be easily accomplished by the lower trapping region. A stronger duct will have less of its cross section nearly perpendicular to the duct axis and less of the duct will be available for easy trapping in the lower region. Furthermore, the ray may more quickly stray to less favourable contours so that the wave normal is at too great an angle for trapping when entering the upper region. Under these circumstances, an increase in the width of the duct will clearly increase trapping efficiency.

If the duct is very strong the Poeverlein ray path will approach perpendicularity to the field direction and the ray path may reach the concave section of the lower region curves without leaving the duct (such a path on this part of the Poeverlein diagram would be in a direction of slow increase of electron density which would facilitate reaching the desired part of the diagram while remaining in the duct) and trapping may again occur. In the upper trapping region trapping is much simpler: the steeper the duct sides, the easier the trapping (in that rays having larger wave normal angles with the axis may be trapped. Also the steeper the sides in the upper trapping region the more likely the trace will pass through the centre of the Poeverlein diagram or a point near the centre of the diagram so that the ray may trace a path to the lower coupling point).

The shape of the duct is determined by its width, its electron density deviation from ambient and the vertical ionospheric electron density gradient. If the first two parameters remain fixed throughout the duct then the shape of a particular electron density contour depends upon the vertical gradient at that level. For situations other than very strong ducts we prefer the duct to be shallow walled in the lower trapping region and steeper walled in the upper trapping region. There is a part of the ionosphere which provides these conditions very well: that is the part of the ionosphere below the peak where the vertical electron density gradient weakens

rapidly with height. If the coupling point is at an altitude where the vertical gradient is still steep but not far below where it begins its rapid decrease then in the lower coupling region the duct may be shallow sided with the sides becoming steeper as we progress upwards and into the upper coupling region. Strong duct trapping will also be assisted at altitudes near the layer peak as the duct sides will be steeper here. If our speculation is correct then the Z echo should often be seen on the critical part of its trace. This turns out to be the case for original records, although it is not necessarily so true of published Z echoes (authors have probably selected strong examples of the Z echo in preference to typical examples). As already noted in Section 3.3, Ellis (1954) found that there was an increase in the Z echo amplitude near the critical frequency on all four occasions on which he recorded the variation of echo amplitude with frequency. His results are shown in Fig.7.20. Ellis also noted that "It is characteristic of many P'f records of triple splitting that the Z trace appears strongest near the Z critical frequency". We futher note that two of Ellis's four observations show a second increase in amplitude at a slightly lower frequency. This may be seen on many n'f records as several maxima (e.g.Figs.3.16, 3.44, 5.24 to 5.26) and the Z trace sometimes takes on a "string of sausages" appearance. Again this is easy to explain in a ducting ionosphere. As the frequency changes, so do the critical incidence angle and the spatial coordinates of the coupling point. As the position of

the coupling point moves so may vary the trapping efficiency and with sufficient frequency change the coupling point may progress into an adjacent duct. The form of the amplitude peaks of the Z trace may reflect the structure of the ducts. Trapping efficiency in a given duct may also vary with frequency.

With regard to the physical path of the ray it can be seen from the Poeverlein diagram that except in the immediate vicinity of the coupling point the ray must stray well away from the axis (through the coupling points) of the diagram before the group directions deviate significantly from the magnetic field direction. Thus there would normally be no problem with the ray moving rapidly from a favourable to an unfavourable trapping environment.

Although spread-F correlates well with Z echoes on a seasonal and sunspot cycle variation there is not a diurnal correlation. In the case of Hobart the Z mode is predominantly a daytime phenomenon and is usually associated only with spreading which is weak. The major diurnal occurence of Z echo at Hobart occurs early in the daylight sector when spread-F (which has been evident during the night) is disappearing. It may be that the strong spread-F at night is associated with moderately strong ducts not favourable to Z ray trapping in the lower trapping region. The weakening of these ducts around dawn may facilitate Z ray trapping whilst producing only weak or

barely detectable spreading. It should be noted that Calvert and Schmid (1964) found the highest percentage occurence of ducting spread-F at latitudes roughly corresponding to those found by Bowman (1960) to show the greatest occurrence of Z echo (Figs.3.24 and 7.18). Examination of Fig.7.18 shows that within the belt of ducting spread-F the occurrence at night is greater than that in the daytime. However, if the night occurrence also represents stronger ducts which find Z ray trapping more difficult then the diurnal occurrence of Z echo would not follow the diurnal behaviour of Fig.7.18. If the ducts responsible for strong spreading become sufficiently strong for strong trapping in the lower trapping region then we will have Z echoes on records showing strong spreading and we might expect these Z echoes on average to exhibit an increase in echo amplitude and/or the spectral range of the Z echo. Z echos in association with strong spreading are seen quite often on Hobart night time records.

So far we have seen that ducting is a possible Z return mechanism and can fit the available evidence quite well. Despite this, we have not yet shown that there is any direct evidence of duct return of the Z ray. Fortunately there is a paper in the available literature which provides such evidence and we describe the experiment and results in the next section.

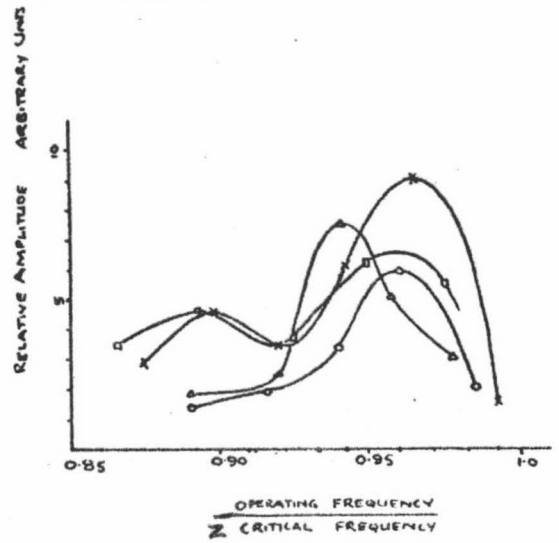

FIG.7.20

Variation in Z Echo Amplitude near the Critical Frequency.
(Fig.31 of Ellis,1954)

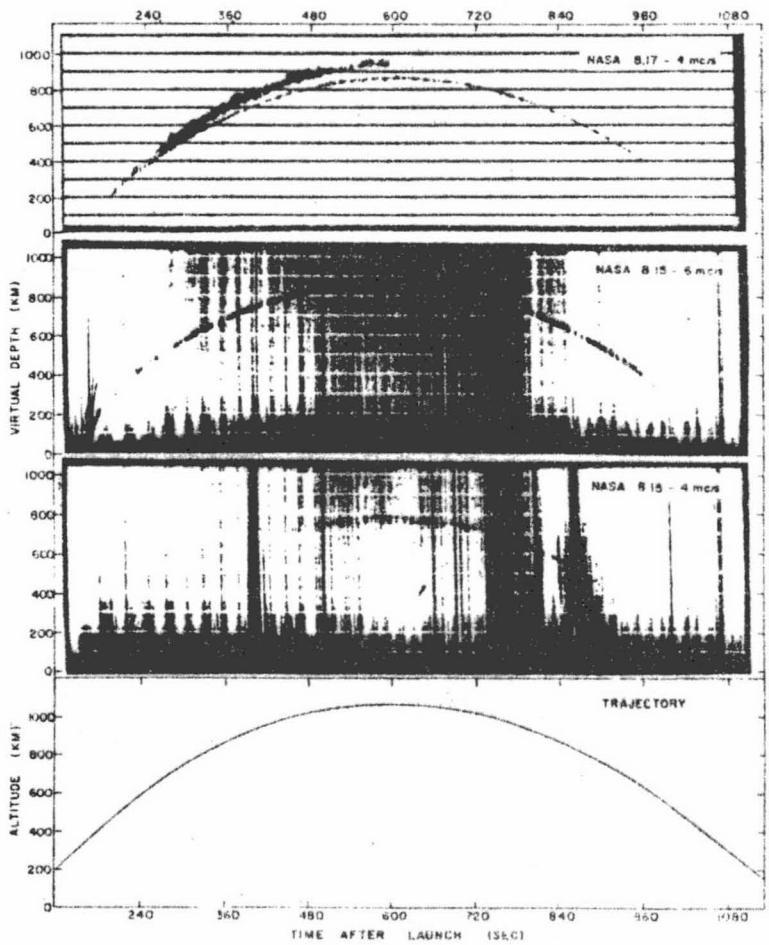

Ionospheric echoes obtained during the flights of topside sounder rockets.

FIG.7.21

(Fig.1 of Calvert et al.,1962)

7.7 Direct Evidence

In 1961 and 1962 three rocket flights were launched from Wallops Island, the payload in each case being a fixed frequency radio sounder. The 1962 flight was unsuccessful. The 1961 flights took place on 24th. June (Quiet day, 4.07 and 5.97 Mhz) and 13th. October (Disturbed night (spread-F), 4.07 Mhz). Calvert, VanZandt, Knecht and Goe (1962) reported that the flights confirmed the existence of field aligned ducts. The echoes from the two flights together with the trajectory common to the flights is shown in Fig.7.21. They reported that the existence of magnetic field aligned ducts was indicated by (1)strong multiple echoes during the exit on both flights, and (2)spread echoes during the first half of the 8.17 flight. They argued that propagation within the field aligned ducts should be almost longitudinal and reflections should occur only at the x and z levels, this being consistent with the fact that multiples of only x and z traces were observed.

Calvert et al found the ducted echoes to be up to 30-40 dB stronger than the normal echoes as shown in Fig.7.22 which is a superposition of A-scans during ducted propagation, the smaller echo to the left being the normal echo. They estimated the widths and spacings of the ducts intercepted during the 8.17 flight and their findings are shown in Figs.7.23 and 7.24. They found that the duct spacings did not appear to be periodic.

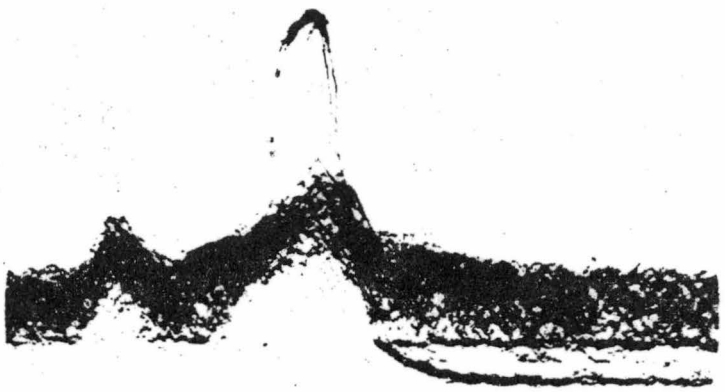

A superposition of the echoes received as the payload passed through a duct. Amplitude increases upwards and delay increases towards the right.

FIG. 7.22

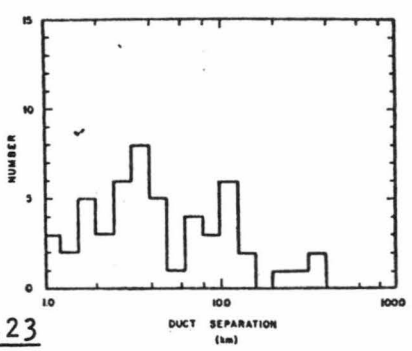

FIG. 7.23

The distribution of the measured separations between ducts.

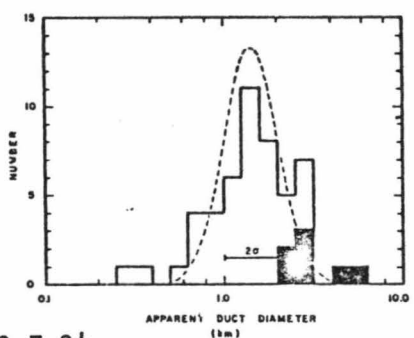

FIG. 7.24

The distribution of the measured chords across ducts. The strongest ducts are shown solid and the best-fitting logarithmic normal distribution is shown as a broken curve.

(Figs. 3, 5 and 6 of Calvert et al., 1962)

Singleton and Lynch (1962) found that the field aligned irregularities occur in patches and there is other evidence supporting this view. For instance, Calvert et al found Z ducting over only half the rocket trajectory and not at the lower latitudes. Given a patch of ducts with non periodic spacing, we have an excellent model to simulate the detailed occurrence patterns of the Z echo. As these ducts either drift, or dissolve and reform at non periodic intervals, we will have Z echoes which will appear and disappear in a non periodic fashion. The Z echoes will continue their intermittent presence for an indefinite period of time depending on how long the patch is in the vicinity of the ionosonde. This may be a matter of minutes or hours. This is exactly the observed behaviour of Z echoes (Figs.5.29 and 5.30).

NOTE ON POEVERLEIN PLOTS.

When (as is the case with the ionospheres described in this chapter) the magnetoplasma is not plane stratified then the method of Poeverlein as described in Section 2.4 may be no longer easily applied. Nevertheless, the principles expounded by Poeverlein may be utilised and the Poeverlein diagram is now treated as a refractive index space where the locus of the refractive index vector along the path of the ray can be drawn and the outward normal to a refractive index surface at its point of intersection with the locus gives the direction of the ray at the corresponding point in the medium. This application of the Poeverlein diagram has previously been employed as an aid in interpretating magnetospheric and solar radio wave ray tracing and is well described by Herring (1980).

CHAPTER EIGHT

CONCLUSIONS

8.1 Summary

Two alternative mechanisms postulated for return of the Z ray have been examined and experiments carried out to investigate which of the mechanisms is operating during the presence of the Z echo. The results of the experiments taken together with the results of previous experiments effectively demonstrate that neither the backscattering mechanism nor the tilt/wedge mechanism is a suitable explanation of Z ray return in the overwhelming majority of Z echo cases.

The duct mechanism of Z ray return has been proposed in an endeavour to overcome some difficulties encountered with the previous proposals. The duct mechanism is able to explain many features of Z echoes not easily accounted for by the other mechanisms; some ray tracing models have successfully returned the Z ray in a ducting ionosphere; and in addition to substantial circumstantial existing evidence favouring the duct model there is a report of two rocket flight sounding experiments which provides direct evidence of Z ducting at Z echo latitudes (Wallops Island dip angle is 70°). The Z duct model is the obvious choice of those mechanisms so far proposed to account for return of the Z ray.

8.2 Recommendations For Future Research

It is important that the criteria for trapping be established. This will probably require modelling using techniques such as full-wave analysis at least in the vicinity of the coupling region. Workers who have already carried out detailed modelling studies of the coupling region (e.g. Smith,1973; Budden,1980) may be well equipped to carry out such an investigation. Once trapping criteria are established it may be possible to obtain a great deal of information about the presence, type, structure and spacing of ducts from routine h'f ionograms. This in turn will assist spread-F (including artificially created spread-F) and other duct related studies and may have a bearing on the overall picture of ionosphere/plasmasphere and ionosphere/magnetosphere interactions. For instance, there is some similarity between the patterns of presence and strength ("fading" patterns, for want of a more appropriate term) of some micropulsations and the Z echo. Fraser-Smith (1981) recently reported on the occurrence of mid-latitude Pc 1 and there is in his plot (Fig.8.1) a suggestion of an inverse sunspot cycle relationship reminiscent of that found by Bowman (1960) for Z echo occurrence. It should be pointed out that Fraser-Smith did not find an eleven year periodicity in his data: nevertheless, the possibility of a link between Z ducts and micropulsations is

worth pursuing at this stage. There may also be a connection between Z ducts and those of whistlers. Andrews (1975) found similarities between whistler rates and the incidence of mid latitude spread-F in both time and space for the years 1963 to 1968. He noted that other workers had also found an association between whistler propagation and spread-F occurrence. Singleton (1961) noted reports of the dependence on geomagnetic latitude of whistler incidence. One worker reported a maximum at about 45^{o} geomagnetic latitude while another group put the maximum whistler occurrence at 50^{o} geomagnetic latitude but both reported a marked decrease in whistler activity at higher and lower latitudes. The latitude belt of whistler activity is similar to that found by Bowman (1960) for Z echo occurrence.

Z duct origins may possibly be found in the existing explanations for, and postulates of, other field aligned phenomena. For instance, in the existing literature are such suggestions as field aligned plasma interchange between ionosphere and plasmasphere (e.g.Carpenter and Park,1973; Park,1973); and growth of field aligned irregularities from ionospheric turbulence (e.g.Booker,1956). There have also been suggestions that atmospheric gravity waves dissipate energy through turbulence (e.g.Bretherton,1969) and so there may possibly be an indirect connection between TID's and Z ducts.

It is noted that the presence of the Z echo is not

currently recorded on a routine basis at ionospheric stations except at those stations where it is considered to be an unusual event. Since ducting is of importance to so many other ionospheric phenomena, the presence of an h'f trace which relies primarily on ducting (i.e. the Z trace) should be recorded as part of the routine scaling.

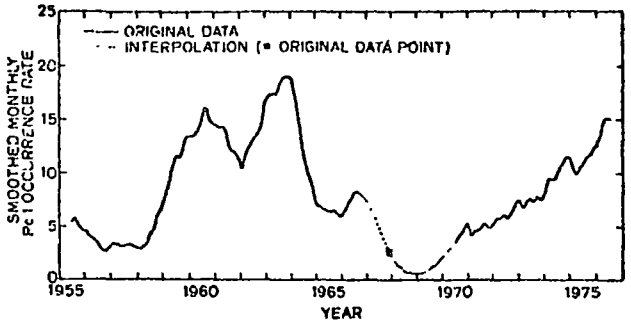

SMOOTHED MONTHLY OCCURRENCES OF Pc 1-ACTIVE DAYS IN CALIFORNIA.
The tick marks on the time axis indicate the month of January.

FIG.8.1 (Fig.1 of Fraser-Smith, 1981)

SELECTED BIBLIOGRAPHY

ANDREWS,M.K.: 1975, J.Atmos.Terr.Phys. 37, 1423.

BANERJI,R.B.: 1952, Ind.J.Phys. 26, 28.

BOOKER,H.G.: 1936, Proc.Roy.Soc. A155, 235.

BOOKER,H.G.: 1938, Phil.Trans.Roy.Soc. A237, 411.

BOOKER,H.G.: 1955, J.Atmos.Terr.Phys. 7, 343.

BOOKER,H.G.: 1956, J.Geophys.Res. 61, 673.

BOOKER,H.G.: 1961, J.Geophys.Res. 66, 1073.

BOWLES,K.L.: 1958, Phys.Rev.Letters 1, 454.

BOWMAN,G.G.: 1960, Planet.Space Sci. 2, 214.

BOWMAN,G.G.: 1960a, Planet.Space Sci. 2, 133.

BOWMAN,G.G.: 1960b, Planet.Space Sci. 2, 150.

BRETHERTON,F.P.: 1969, Radio Science 4, 1279.

BRIGGS,B.H. and PHILLIPS,G.J.: 1950, Proc.Phys.Soc. 63B, 907.

BUDDEN,K.G.: 1961, "Radio Waves in the Ionosphere", Cambridge Uni. Press, Cambridge.

BUDDEN,K.G.: 1964, "Lectures on Magnetoionic Theory", Gordon and Breach, New York.

BUDDEN,K.G.: 1980, J.Atmos.Terr.Phys. 42, 287.

CALVERT,W.and COHEN,R.: 1961, J.Geophys.Res. 66, 3125.

CALVERT,W. and SCHMID,C.W.: 1964, J.Geophys.Res. 69, 1839.

CARPENTER,D.L. and PARK,C.G.: 1973, Rev.Geophys.Space Phys. 11, 133.

DAVIES,K.: 1965, "Ionospheric Radio Propagation", National Bureau of Standards, Washington.

DIEMINGER,W. and MOLLER,H.G.: 1949, Die Naturwiss. 36, 56.

ECKERSLEY,T.L.: 1933, Proc.Roy.Soc. A141, 710.

ECKERSLEY,T.L.: 1950, Proc.Phys.Soc. 63B, 49.

ELLIS,G.R.A.: 1953a, Nature 171, 258.

ELLIS,G.R.A.: 1953b, J.Atmos.Terr.Phys. 3, 263.

ELLIS,G.R.A.: 1954, "The Magneto-ionic Triple Splitting of Ionospheric Echoes", Ph.D. Thesis, University of Tasmania.

ELLIS,G.R.A.: 1956, J.Atmos.Terr.Phys. 8, 43.

ELLIS,G.R.A.: 1957, J.Atmos.Terr.Phys. 11, 54.

ELLIS,G.R.A.: 1972, Proc.Astron.Soc.Aust. 2, 135.

FRASER-SMITH,A.C.: 1981, Planet.Space Sci. 29, 715.

HAJKOWICZ,L.A.: 1972, Can.Journ.Phys. 50, 2654.

HARANG,L.: 1936, Terr.Mag.Atmos.Elect. 41, 160.

HASELGROVE,J.: 1954, Rep.Conf.Phys.Ionosphere, p355, Phys. Soc.London, London.

HIBBERD,F.H.: 1971, J.Atmos.Terr.Phys. 33, 783.

HOGARTH,J.F.: 1951, Nature 167, 943.

JONES,R.M. and STEPHENSON,J.J.: 1975, "A Versatile Three Dimensional Ray Tracing Computer Program for Radio Waves in the Ionosphere", OT Report 75-76, Washington.

KLEMPERER,W.K.: 1963, J.Geophys.Res. 68, 3191.

LANDMARK,L.: 1952, J.Atmos.Terr.Phys. 2, 254.

LOCKWOOD,G.E.K.: 1962, Can.J.Phys. 40, 1840.

LUI,C.H. and YEH,K.C.: 1977, J.Atmos.Terr.Phys. 39, 149.

MEEK,J.H.: 1948, Nature 161, 597.

MILLINGTON,G.: 1954, Proc.Inst.Elec.Engrs. 101(Pt.4), 235.

MULDREW,D.B.: 1963, J.Geophys.Res. 68, 5355.

MULDREW,D.B.: 1980, J.Geophys.Res. 85, 613.

MUNRO,G.H.: 1950, Proc.Roy.Soc. A202, 208.

MUNRO,G.H.: 1953, Proc.Roy.Soc. A219, 447.

NEWSTEAD,G.: 1948, Nature 161, 312.

PAPAGIANNIS,M.D.: 1965, J.Atmos.Terr.Phys. 27, 1019.

PAPAGIANNIS,M.D.: 1972, "Space Physics and Space Astronomy", Gordon and Breach, London.

PAPAGIANNIS,M.D. and MILLER,D.L.: 1969, J.Atmos.Terr.Phys. 31, 155.

PARK,C.G.: 1973, J.Geophys.Res. 78, 672.

PITTEWAY,M.L.V.: 1958, Proc.Roy.Soc. A246, 556.

PITTEWAY,M.L.V.: 1959, Phil.Trans.Roy.Soc. A252, 53.

PITTEWAY,M.L.V. and COHEN,R.: 1961, J.Geophys.Res. 66, 3141.

POEVERLEIN,H: 1948, S.ber.Bayer.Akad., 175.

POEVERLEIN,H.: 1949, Z.angew.Phys 1, 517.

POEVERLEIN,H.: 1950, Z.angew.Phys. 2, 152.

RATCLIFFE,J.A.: 1962, "The Magneto-ionic Theory and its Applications to the Ionosphere", Camb.Uni.Press, London.

RATCLIFFE,J.A.: 1972, "An Introduction to the Ionosphere and Magnetosphere", Camb.Uni.Press, Cambridge.

RATCLIFFE,J.A. and WEEKES,K.: 1960, "Physics of the Upper Atmosphere", ed. J.A.Ratcliffe, Academic Press, New York.

REBER,G.: 1956, J.Geophys.Res. 61, 157.

RENAU,J.: 1959, J.Geophys.Res. 64, 971.

RENAU,J.: 1960, J.Geophys.Res. 65, 2269.

RIVAULT,R.: 1950, Proc.Phys.Soc . 63B, 126.

RYDBECK,O.E.H.: 1950, J.Appl.Phys. 21, 1205.

SATYANARAYANA,R., BAKRU,K. and KHASTGIR,S.R.: 1959, J.Atmos. Terr.Phys. 13, 201.

SCOTT,J.C.W.: 1950, J.Geophys.Res. 55, 65.

SCHMERLING,E.R.: 1958, J.Atmos.Terr.Phys. 12, 8.

SINGLETON,D.G.: 1961, Nature 189, 215.

SINGLETON,D.G. and LYNCH,G.J.E.: 1962, J.Atmos.Terr.Phys. 24, 353.

SINGLETON,D.G. and LYNCH,G.J.E.: 1962a, J.Atmos.Terr.Phys, 24, 363.

SMITH,M.S.: 1973, Nature Phys.Sci. 243, 29.

TAYLOR,M.: 1933, Proc.Phys.Soc. 45, 245.

TAYLOR,M.: 1934, Proc.Phys.Soc. 46, 408.

TOSHNIWAL,G.R.: 1935, Nature 135, 471.

YEH,K.C. and LUI,C.H.: 1972, "Theory of Ionospheric Waves", Academic Press, New York.

ADDITIONAL REFERENCES FOR CHAPTER SEVEN.

CALVERT, W. : 1981, J. GEOPHYS. RES. 86, 1609.

HERRING, R.N. : 1980, J. ATMOS. TERR. PHYS. 42, 885.

LESTER, M. & A.J.SMITH. : 1980, PLANET.SPACE SCI. 28, 645.

STRANGEWAYS, H.J. : 1981, J.ATMOS. TERR. PHYS. 43, 231.

STRANGEWAYS, H.J. & RYCROFT M.J. : 1980, J.ATMOS. TERR. PHYS. 42, 983.